PHD

Polymeric Facades
Advanced composites for retrofit

Gates, Peter

Award date:
2014

Awarding institution:
University of Bath

POLYMERIC FACADES:
ADVANCED COMPOSITES FOR RETROFIT

by

Pete Gates

A thesis submitted for the degree of
Doctor of Philosophy

University of Bath
Faculty of Engineering and Design
Department of Architecture and Civil Engineering

September 2013

Signature of Author ……..

ACKNOWLEDGEMENTS

I would like to thank Professor Tim Ibell, Dr Antony Darby and Dr Steve Lo at the University of Bath, for supervising the research reported in this thesis. I would also like to thank Dr Mikkel Kragh, the project's industry partner with Arup, for his guidance and support.

Grateful thanks are due to the sponsors of this research: Arup, and the Engineering and Physical Sciences Research Council (EPSRC). Both have provided generous sponsorship as part of an Industrial Collaborative Award in Science and Engineering (CASE).

I would like to thank Dr Stephen Ledbetter at the Centre for Window and Cladding Technology at Bath for his technical guidance. For valued insight into manufacturing practices I would like to thank Richard Irvine at Strongwell and Morten Gantriis Sørensen and Kristian Koldtoft at Fiberline.

For guidance and assistance with the practical work undertaken throughout the research project, I am indebted to Will Bazeley, Neil Price and Sophie Hayward in the Department of Architecture and Civil Engineering. I would also like to thank John Mitchels in the Microscopy and Analysis suite. At the BRE Centre for Fire Safety Engineering at the University of Edinburgh I would like to thank Dr Tim Stratford and Daryan Othman for assistance with the project pyrotechnics.

Finally, thank you to Marion, Phil, Celia, and Rory for your incredible support that has regularly proven so invaluable throughout the last few years.

ABSTRACT

Replacing a building's façade offers the prospect of improving the whole life performance of the building, in some instances as a favourable alternative to replacing the entire structure. This presents the opportunity to exploit the properties of advanced composite materials for maximum benefit. 'Upwards and outwards' retrofit, where extending floor slabs yields extra floor area, is permitted by a lightweight replacement façade, without the need to underpin foundations. For typical medium or high-rise office buildings, the extra let-able space obtained, and reduced heating and maintenance costs, can work to offset the expense of implementation.

The specific materials, manufacturing processes, and façade type, most appropriate for such a scheme have been investigated. A unitised façade of sandwich panels with foam cores and pultruded GFRP skins has formed the 'design platform' for research conducted.

It is paramount to resolve how the connections in such a façade system can meet the many requirements of an integrated building envelope. Structural integrity, enhanced environmental control, sustainability attributes, fire provisions, acoustic control, ease of manufacture, tolerance control, durability, lightness in weight, cost effectiveness and aesthetics must all be addressed simultaneously by any proposed design methodology.

Investigating suitable connections through prototype development and review reveals key issues requiring targeted research. The permanent action acting on light, self-supporting GFRP panels is small, however wind and occupancy loading impart significant imposed actions. Therefore, whilst creep deflection is often a significant consideration for structural GFRP design, quantifying fatigue performance is a higher priority for validating the ideology of polymeric facades.

The unidirectional nature of pultrusion reinforcement yields a scenario of principle stresses at the panel interfaces, occurring in the weaker, secondary fibre, direction. As a consequence a fatigue-testing programme is aimed at understanding the performance and characteristics of pultruded angles compatible with 'long-edge' panel connections.

The long-term performance of fibre-reinforced polymer (FRP) structures must be assessed if FRP is to win acceptance as a mainstream material for use in the construction industry. The environmental durability of wholly polymeric structures is often called in to question. In response, accelerated testing is usually undertaken on artificially aged FRP specimens; lack of genuine naturally aged material has previously hindered research and validation of material related design life. Case study investigation has permitted a full durability appraisal of naturally aged GFRP through laboratory testing campaign.

Retrofit of existing buildings as an activity makes up 50% of all building construction in the UK. This project aims to address the shortfall in industry-required design knowledge.

The tensile strength of pultruded naturally aged GFRP has been shown to reduce by only 0.65% over 17 years where natural exposure does not include UV irradiation, and by 13.1% where UV irradiation does occur as one element of exposure. The findings expose the degree of inaccuracy and fundamental flaws in existing predictive ageing models. The physical mechanisms of degradation do not match. A procedure to quantify the extent of polymer brittle hardening has been developed and applied as an analytical tool.

Mechanical testing campaign has pioneered the use of the RMS (Route Mean Square) procedure to present the performance of connection specimens as a continuous function throughout programmes of fatigue testing. Testing has shown that though a threshold strain for damage accumulation does exist in complex fatigue loading of connections, and for direct tension fatigue loading.

CONTENTS

1 INTRODUCTION 1

1.1 The solution to a nationwide problem 1

1.2 Material selection 1

1.3 Design issues 2

1.4 Panel design and GFRP fabrication 3

1.5 Performance of the building envelope 3

1.6 Research direction 4

1.7 Scope and research objectives 5

1.8 Summary 6

2 BACKGROUND AND LITERATURE REVIEW 7

2.1 FRP 7

2.1.1 Material properties 7

2.1.2 Composite properties 10

2.1.3 Fabrication and manufacturing 18

2.2 Environmental durability 19

2.2.1 UV radiation 20

2.2.2 Moisture coupled with temperature 26

2.2.3 Temperature in isolation 35

2.2.4 Chemical ageing 36

2.2.5 Testing of modern GFRP pultrusions 37

2.3 Foam and other core materials 41

2.3.1 Material properties 41

2.3.2 Manufacturing considerations for sandwich panels 45

2.4 Facades 46

2.4.1 Structural Integrity 46

2.4.2 Environmental control 54

2.4.3 Acoustic control 56

2.4.4 Sustainability 58
2.4.5 Fire provisions 63
2.4.6 Aesthetics 64
2.4.7 Further applications 65

2.5 Design methodologies 68

2.6 Fatigue in pultruded GFRP 70
2.6.1 Introduction 70
2.6.2 Damage accumulation 71
2.6.3 Testing methodology 72
2.6.4 Theoretical representation 75
2.6.5 Previous experimental findings 77
2.6.6 Potential to improve the fatigue performance of pultruded connections 80

2.7 Summary 81

3 DURABILITY: CASE STUDY TESTING AND RESULTS 83

3.1 Introduction 83

3.2 Severn Crossing Visitors' Centre 85
3.2.1 Introduction 85
3.2.2 Methodology 88
3.2.3 Results 99
3.2.4 Model for composite panel action 105
3.2.5 Assessment of polymer hardening 109
3.2.6 Discussion of the Second Severn Crossing Visitors' Centre case study 112

3.3 Mondial House 114
3.3.1 Introduction 114
3.3.2 Methodology 117
3.3.3 Results 126
3.3.4 Discussion of the Mondial House case study 138

3.4 Summary 139

4 DURABILITY: DISCUSSION AND CONCLUSIONS 141

4.1 Severn Crossing Visitors' Centre 141
4.1.1 Polymer matrix characteristics 141
4.1.2 Degradation 142

4.1.3 Relevant studies in accelerated ageing 143

4.2 Mondial House 152

4.3 Performance of aged material 157

4.4 Summary and implications 162

5 FATIGUE: LABORATORY TESTING PROGRAMME 165

5.1 Introduction 165

5.2 Methodology 167

5.2.1 Coupon preparation and testing procedure 167

5.2.2 Analysis of coupon test data 169

5.2.3 Preparation of angle sections and test rig set-up 169

5.2.4 Defining testing parameters for angle section fatigue programme 174

5.2.5 Data processing 178

5.2.6 Post fatigue inspection of angle section material by coupon extraction and testing 181

5.3 Results 182

5.3.1 Fatigue testing of coupons in tension 182

5.3.2 Preliminary angle section specimens 185

5.3.3 Post fatigue inspection of preliminary angle sections by coupon extraction and testing 189

5.3.4 Angle section specimens: main fatigue testing at ‘realistic strains’ 191

5.3.5 Angle section specimens: fatigue testing at ‘realistic loads’ 198

5.4 Conclusions 200

5.5 Summary 203

6 FATIGUE BEHAVIOUR OF ANGLE CONNECTIONS IN UD-GFRP 205

6.1 Response of pultruded angles to fatigue loading of connections 205

6.2 Distribution in the specimen’s response to cyclic load 207

6.3 Design limit for transverse strain at pultruded panel edge returns 210

6.4 Summary 215

7 CONCLUSIONS AND FURTHER WORK 217

7.1 Introduction 217

7.2 Research findings and implications 217

7.3 Recommendations for future research 221

7.4 Material meets application 223

8 REFERENCES 225

9 APPENDICES 233

9.1 Appendix A: Response of angle sections to monotonic loading in a plane stress state 233

9.1.1 Introduction 233

9.1.2 Methodology 234

9.1.3 Results 236

9.1.4 Discussion 237

LIST OF FIGURES

Figure 2.1 Stress block for FRP thin walled section 12
Figure 2.2 Bending stiffness of section as a function of the degree of compressive fibre contribution and principal fibre volume ratio 16
Figure 2.3 Bending stiffness of section as a function of the degree of compressive fibre contribution and matrix modulus 17
Figure 2.4 Bending stiffness of section as a function of the degree of compressive fibre contribution and overall section depth T 17
Figure 2.5 T_g of unsaturated polyester (UP) during QUV ageing from Cabral-Fonseca et al. (2012), data for vinylester (VE) also shown 22
Figure 2.6 Tensile strength of unsaturated polyester (UP) during QUV ageing from Cabral-Fonseca et al. (2012), data for vinylester (VE) also shown 23
Figure 2.7 Flexural strength of unsaturated polyester (UP) during QUV ageing from Cabral-Fonseca et al. (2012), data for vinylester (VE) also shown 23
Figure 2.8 Interlaminar shear strength of unsaturated polyester (UP) during QUV ageing from Cabral-Fonseca et al. (2012), data for vinylester (VE) also shown 23
Figure 2.9 Rockwell hardness for room temp cure and UV cure of vinylester resin from Compston and Dexter (2008) 25
Figure 2.10 Water uptake of vinylester resin matrix by Kotani et al. (2011) 28
Figure 2.11 Residual strength of unidirectional GFRP after hydrothermal ageing, replotted from Kotani et al. (2011) 28
Figure 2.12 Rupture strain of unidirectional GFRP after hydrothermal ageing, replotted from Kotani et al. (2011) 29
Figure 2.13 Stiffness of unidirectional GFRP after hydrothermal ageing, replotted from Kotani et al. (2011) 29
Figure 2.14 Predicted residual strength of UD GFRP after hydrothermal ageing from Kotani et al. (2011) 30
Figure 2.15 Comparison of tensile strength predictions by Chu et al. (2004) for both ageing in deionized water and in alkali solution (reconditioned and non-reconditioned are labelled as ‘dry’ and ‘wet’ in the plot) 32
Figure 2.16 Results of tensile tests. Variation of the tensile strength (a,c) and of the tensile elastic modulus (b,d), for fraction in 0^o (a,b) and 90^o (c,d) (Carra and Carvelli 2012) 38

Figure 2.17 Results of flexural tests. Variation of the flexural strength (a,c) and of the flexural elastic modulus (b,d), for bending in 0^o (a,b) and 90^o (c,d) (Carra and Carvelli 2012) 39
Figure 2.18 Results of inter-laminar shear tests. Variation of the inter-laminar shear strength in the 0^odirection (Carra and Carvelli 2012) 39
Figure 2.19 Vault enclosure featuring aerogel membrane at London Imperial War museum (pic. credit: Aspen aerogels) 44
Figure 2.20 Façade retrofit using aerogel mat for small scale domestic (pic. credit: Aspen aerogels) 45
Figure 2.21 Geometry of facade panel 47
Figure 2.22 Possible application in foam core sandwich technology 54
Figure 2.23 Multilayer fabric façade comprising a PCM layer (ILEK) 56
Figure 2.24 Farrell and Grimshaw's former Herman Miller premises in Bath 57
Figure 2.25 Hypothetical plot, for total structure potential against arbitrary displacement parameter or erection sequence in a deployable structure 67
Figure 2.26 Hypothetical prototype design (i) for panel mullion connection: 69
Figure 2.27 Hypothetical prototype design (ii) for panel mullion connection: 69
Figure 2.28 $\log N_f$ - σ_{peak} failure envelopes, showing influence of different matrix resins and fibre architectures. Cycling frequency 1Hz. From Harris (2003) 72
Figure 2.29 Effect of variability on the strength and fatigue life of the S-N curve. From Harris (2003) 73
Figure 2.30 Normalized residual strength curves for 0,90 laminates of various fibres in epoxy. The values for the exponents of the fitted curves are shown in brackets. From Adam et al. (1986) 76
Figure 2.31 S-N_{10} envelopes from results obtained by three-point bending fatigue tests, from Salvia et al (1997) 78
Figure 3.1 Left: Location of the four 'panel pairs' from the Visitors' Centre at the Severn crossing estuary. Right: Photo of the southerly elevation 87
Figure 3.2 Strongwell panel cross-section (Strongwell 2010) 88
Figure 3.3 Three-point loading test rig set-up 89
Figure 3.4 Graphical plot of Equation 3.1 for an East-facing panel. (Squares represent tests with external face up and diamonds represent tests with internal face up.) 90
Figure 3.5 Sample was ignited using Bunsen (left) then later placed into muffle furnace (right) 92

Figure 3.6 Principal fibres visible within the aged web coupon cross-section, after removal from furnace. Principal fibres are in the direction perpendicular to the page..94
Figure 3.7 Fibres from new material. Left: Surface veil over CSM Right: Principal fibres.....95
Figure 3.8 Coupon setup for compression test rig 96
Figure 3.9 Iosipescu shear rig set-up (all dimensions in mm). Schematic showing how loads on specimen are achieved and shear is derived at zero moment location 98
Figure 3.10 Flexural elastic modulus for each of the building panels, and the manufacturer's testing derived value of 25.3 GPa.....100
Figure 3.11 Flexural shear modulus G for each panel, as per original orientation on building, and nature of test and the manufacturer's testing derived value of 0.95 GPa 100
Figure 3.12 Tensile elastic modulus as a function of coupon origin 101
Figure 3.13 Stress-strain plots, for internal (left) and external (right) panel material .102
Figure 3.14 Maximum tensile strength of coupons.....103
Figure 3.15 Compressive modulus, E_c as a function of coupon origin.....104
Figure 3.16 Shear modulus as a function of coupon origin 105
Figure 3.17 Max compressive fibre stress at failure of whole panel in three-point bending.....108
Figure 3.18 Flexural testing of coupon 110
Figure 3.19 Mondial House.....114
Figure 3.20 Discarded façade sandwich panels 115
Figure 3.21 External and internal sandwich skin material, showing 'combed' ripple profile of outer gel coat.....115
Figure 3.22 Longitudinal coupon set up 118
Figure 3.23 Coupon surface integrity, external (left) and internal (right) 118
Figure 3.24 Straight sided coupons prepared for assessment of polymer brittle hardening.....119
Figure 3.25 Three-point simply supported span set-up for flexural testing.....120
Figure 3.26 Plate twist test rig set up to determine shear modulus.....121
Figure 3.27 Anticlastic (left) and single axis (undesired) flexural deformation (right) 122
Figure 3.28 Dynamic mechanical thermal analysis rig.....123
Figure 3.29 GFRP specimens set into epoxy resin pot for inspection of cross section;

steel mounts also visible 125
Figure 3.30 Specimen prepared by cold fracture before installing in scanning electron microscope (SEM) 125
Figure 3.31 Images for thresholding exercise on internal (left) and external (right) GFRP cross sections. Magnification is the same for both images.....126
Figure 3.32 BES image showing inferred fibre diameter of internal material (x2500)127
Figure 3.33 SEI output showing inferred fibre diameter of external material (x2500) 127
Figure 3.34 External polyester matrix produced using SEI on cold fracture 128
Figure 3.35 Internal polyester matrix produced using SEI on cold fracture 129
Figure 3.36 Thermal response of all coupons (T_g is the temp. at max value) 131
Figure 3.37 DMTA temperature-stiffness relationship for all coupons 132
Figure 3.38 Tensile elastic modulus as a function of coupon orientation and origin...132
Figure 3.39 Ultimate tensile strength as a function of coupon orientation and origin .133
Figure 3.40 Stress-strain plots to failure, for internal (left) and external (right) panel material in the 0^o direction.....134
Figure 3.41 Shear modulus G_{12}, of the four internal and four external coupons and average values.....136
Figure 4.1 Illustrative GFRP section showing fibre length, effective interfacial bond length with respect to tension in direction shown, and absence of voids 154
Figure 4.2 Illustrative GFRP section showing fibre length, effective interfacial bond length with respect to tension in direction shown, and voids 154
Figure 4.3 Illustrative GFRP section showing fibre length, reduced effective interfacial bond length with respect to tension in direction shown, attributed to shorter fibres, not voids.....155
Figure 4.4 Percentage retention of tensile strength of GFRP as per Chun et al. (2004) showing relative position of experimental data point for naturally aged material 161
Figure 5.1 Waisted coupon of transverse alignment to principal reinforcement.....167
Figure 5.2 Transverse coupon failure: cycled at peak load 75% of monotonic maximum 168
Figure 5.3 Angle section specimen sited in rig. (Crosshead and jaws moved up). Inset upper: custom welded adjustable clamp for point load application. Inset lower: protective steel tabs taped to specimen at load application point.....170
Figure 5.4 Schematic showing general arrangement of specimen bolted into rig, loading displacement direction and strain gauge orientation 171

Figure 5.5 Specimen dimensions: equal angle sections (root radii not shown) 172
Figure 5.6 Gauge offset parameter on prepared angle section specimen..... 173
Figure 5.7 Gripped length parameter on prepared angle section specimen 173
Figure 5.8 Typical response of connection to initial linear ramp (specimen S6) 178
Figure 5.9 Snapshot of small time-step behaviour response of specimen when sampling at 10Hz 179
Figure 5.10 Snapshot of small time-step behaviour response of specimen when sampling was triggered in the outer quartiles of displacement at 25Hz 179
Figure 5.11 Sinusoidal relationship and associated RMS value 180
Figure 5.12 Location of coupon extraction post fatigue programme, for large (100 mm angle) and small (75 mm angle) specimen sizes, left to right. All dimensions are in mm. 182
Figure 5.13 Plot for stiffness against cycles for transverse coupon at 75% of transverse material ultimate tensile strength, R = -0.2 183
Figure 5.14 Plot for stiffness against cycles for transverse coupon at 50% of transverse material ultimate tensile strength, R = -0.2 184
Figure 5.15 RMS load over duration of fatigue test on specimen P1 186
Figure 5.16 RMS strain over duration of fatigue test on specimen P1 187
Figure 5.17 RMS load over duration of fatigue test on specimen P2 188
Figure 5.18 RMS strain over duration of fatigue test on specimen P2 188
Figure 5.19 Typical response of connection to final linear ramp (specimen S6) 192
Figure 5.20 RMS load variation over fatigue programme for specimens S1-S4 193
Figure 5.21 Load displacement plot for initial linear ramp of specimen S3 194
Figure 5.22 RMS Strain profile over fatigue programme for specimen S1 195
Figure 5.23 Crack on specimen S1; opened for photos using bench vice..... 196
Figure 5.24 RMS strain profile over fatigue programme for specimen S5..... 197
Figure 5.25 Conducting tests with more intricate use of strain gauges to plot RMS strain across greater extent of specimen was abandoned 198
Figure 5.26 Load-displacement plot for initial linear ramp on specimen S7..... 199
Figure 5.27 Load-displacement plot for final linear ramp on specimen S7..... 199
Figure 6.1 Varation in transverse strain as a function of distance from connection load, shown for specimen S5 during greatest displacement of initial linear load ramp 208
Figure 6.2 Curve fitting (in black) of RMS load profiles for S1-S4 using a power relationship 210

Figure 6.3 Curve fitting (in black) of RMS load profiles for S1-S4 using a log law relationship 211
Figure 6.4 Φ and Ψ values, as a function of maximum imposed transverse strain 212
Figure 6.5 Ψ and maximum imposed transverse strain, as a function of Φ 213
Figure 6.6 Initial stress amplitude for number of cycles to failure, for pure flexure and combined with torsion. From El-Assal and Khashaba (2007).....214
Figure 9.1 Force-displacement plots for 6 identical equal angle sections in plane-stress prying set-up for opening mode failure from Turvey and Zhang (2007) 234
Figure 9.2 Illustration of laboratory test set-up for monotonic loading of short angle section.....234
Figure 9.3 Schematic representation of critical stress derivation at angle apex.....235
Figure 9.4 Stress-deflection plot for two identical equal angle sections in plane-stress prying set-up for opening mode failure 236

LIST OF TABLES

Table 2.1 Mechanical properties of FRP constituent parts (Bank 2006) 8
Table 2.2 Properties for common grades of glass fibre (Bank 2006) 8
Table 2.3 Neutral axis and bending stiffness relating to section in Figure 2.1 14
Table 2.4 Comparison in percentage regains of tensile strength due to reconditioning after exposure; extracted from table by Chu et al. (2004)..... 31
Table 2.5 Summary of properties variation exhibited by material after 18 months hydrothermal ageing. Extracted from Cabral-Fonseca et al. (2012)..... 34
Table 2.6 Properties of various core materials 41
Table 2.7 Carbon and energy costing for GFRP and Aluminum..... 61
Table 2.8 Comparison of embodied energy for FRP and aluminum functional units ... 62
Table 3.1 Panel geometric properties of both new and old panels from manufacturer's design literature (Strongwell 2010)..... 88
Table 3.2 Fibre volume fractions for the flanges and webs of new and old material 93
Table 3.3 GFRP material properties (Strongwell 2009) 99
Table 3.4 Composolite panel properties. Neutral axis depth and resistive moment per unit surface strain, as calculated theoretically..... 106
Table 3.5 Failure strain and stress, derived from load, test span and theoretical distribution of stress 107
Table 3.6 Compressive strain at failure for each panel and orientation, based on failure load and theoretical model, alongside average of two strain gauge measurements ('*' indicate where gauges peeled from the specimen or went off-scale prior to failure, and value represents single remaining gauge) 107
Table 3.7 Retention of coupon flexural stiffness post tensile straining: aged material. 110
Table 3.8 Retention of coupon flexural stiffness post tensile straining: new material. 111
Table 3.9 Comparison of fibre and voids areas as % of cross section 126
Table 3.10 Average T_g at maximum tan delta for internal and external material 130
Table 3.11 Retention of coupon flexural stiffness post tensile straining: internal material..... 137
Table 3.12 Retention of coupon flexural stiffness post tensile straining: external material..... 137
Table 9.1 Tensile strength reduction: comparison of experimental results with literature

sourced predictions 147
Table 4.2 Correlation of UV exposure in artificial ageing to that experienced over a period in service.....148
Table 5.1 Angle section design values for mechanical properties from manufacturer's literature.....172
Table 5.2 Specimen information for main 'realistic strain' tests 176
Table 5.3 Specimen information for 'realistic load' tests 177
Table 5.4 Stiffness retention of transverse coupons after 100,000 cylces in tension, ..185
Table 5.5 Influence of fatigue testing on the subsequent material primary axis tensile elastic modulus 190
Table 5.6 Specimen information for main 'realistic strain' tests 191
Table 5.7 Stiffness retention of 'connection' for 'realistic load' testing as per initial and final linear ramps 200
Table 6.1 Φ and Ψ values, for specimens S1-S4, S7 and S8 211

NOTATION

a,b	Specimen plate dimensions in x,y plane
a_s,b_s	Locally applied point loads inducing shear in coupon specimen
b_w	Web thickness for thin-walled cellular panel section
c	Connection spacing
c_{limit}	Limit of connection spacing for interference of adjacent connections
k	Thermal conductivity, equivalent to λ, also measured in W/mK
k_d	Diffusion co-efficient
k_0	Reference rate co-efficient of flaw growth rate
l	Element length or denoting location by longitudinal distance from an action
m, n	Positive integers that increase incrementally from unity in a series expansion
n_c	Cycle number
p,r	Cartesian co-ordinates for the location of an action on a plate
p_a,p_b	Material constants for residual strength curve
q	Out of plane loading as a UDL
r_g	Radius of gyration
s	Distance form a discrete point of connection
t	Time
t_f	Flange thickness
t_p	Plate thickness
w_f	Fibre weight fraction
w	Deflection in z-axis direction
x_{na}	Depth through section to neutral axis position
x,y	Co-ordinate axes in plane of plate
z	Co-ordinate axis in direction of plate thickness or displacement direction
A	Cross-sectional area
A_s	Shear area (effective cross section area resisting shear)
B	Web separation distance for thin-walled cellular panel section
C_v	Specific heat capacity
D	Plate stiffness coefficient
D_p	Length of diagonal between loading points
E_d	Activation energy of flaw growth rate

E_f Elastic Young's modulus of fibre reinforcement

E_{fc} Compressive Young's modulus of fibre reinforcement

E_{ft} Tensile Young's modulus of fibre reinforcement

E_m Elastic Young's modulus of polymer matrix

E_r Elastic Young's modulus of resulting composite material

E_{long} Elastic Young's modulus of resulting composite material in longitudinal direction

E_{trans} Elastic Young's modulus of resulting composite material in transverse direction

F Denotes a point load used to apply shear to a material coupon specimen

G Shear modulus

$\#_{flex}$ Subscript appearing with G or E indicating property relates to straining in flexure

I Second moment of area

I_r Irradiance, full solar spectrum or UV only as stated

K Geometric correction factor for plate twist method to determine shear modulus

M Bending moment

M_{xy} Torsional moment

M_n Minor's constant

N_f Number of cycles to failure

N_i Number of cycles in block i

P Point load, mid-span beam unless stated otherwise

Q Shear force across region of plate/panel

R Stress ratio

R_m Molar gas constant

S_p The measured mean span of plate according to ES ISO 15310

T_o Overall section depth for thin-walled cellular panel section

T Temperature

T_g Glass transition temperature

V Total structural potential (strain energy and potential energy)

V_f Fibre volume ratio

V_{pf} Fibre volume ratio for principle fibres only

α Inclination of strain gauge from principal fibre direction

α_n Fibre proportion, as a decimal, lying parallel in one direction

γ_{xy} Shear strain in plane xy

Δ Damage fraction

ε Strain

ε_{45} Strain measured at an angle of 45^{o} to a horizontal axis

η_{θ} Fibre efficiency factor

ν Poisson's ratio, in xy plane unless stated otherwise

ρ Density

σ Permissible stress

$\#_{r}, \#_{m}, \#_{f}$ Subscripts appearing immediately after ρ *and* σ to denote resulting composite, polymer matrix and fibre reinforcement, as for elastic Young's modulus above

$\#_{\#c}, \#_{\#t}$ Subscripts appearing with ρ *and* σ to denote compressive and tensile nature of property, as for elastic young's modulus above

σ_{t} Strength after ageing for time t

σ_{0} Initial strength before ageing

σ_{max} Maximum cyclic stress

σ_{min} Minimum cyclic stress

σ_{R} Residual monotonic stress following cycling

σ_{ult} Ultimate monotonic tensile strength

τ_{xy} Shear stress in plane xy

Φ material constant for equation describing fatigue performance curve

χ Ratio of span over permissible plate deflection at centre-span

Ψ material constant for equation describing fatigue performance curve

∇^{2} Laplace operator in two dimensions (hence, ∇^{4} signifies this expression squared)

1 Introduction

1.1 The solution to a nationwide problem

The urgency with which retrofit of building stock in the UK is required has been well described by the 'One building a minute' notion; a calculation explicated by Manning (2011) at the national conference for building services engineers this year. Meeting the 2050 carbon reduction targets in the UK is expected to require refurbishment of domestic and commercial premises at the rate of approximately one a minute. Commercial and non-domestic retrofit candidates could account for approximately 2 million of these cases.

Replacing a building's façade offers the prospect of improving the whole life performance of the building, in some instances as a favourable alternative to replacing the entire structure. 'Upwards and outwards' retrofit, where extending floor slabs yields extra floor area, is permitted by lightweight replacement façades, without the need to underpin foundations. For typical medium or high-rise office buildings, the extra let-able space obtained, and reduced heating and maintenance costs, can work to offset the expense of implementation.

It would therefore seem that a suitable course of action for structural engineers is very apparent. Assessing the practicality of adopting such practice however has required careful consideration of how the properties of suitable lightweight materials will impinge on meeting the structural and other functional requirements of an integrated façade scheme.

1.2 Material selection

Advanced composite materials comprise a structural skeleton of fibres, and a polymer matrix that acts to transfer stresses between fibres, bind them and protect them. The fibres, most commonly glass, carbon or aramid, are chiefly responsible for the mechanical properties of a composite (Bank 2006). The amount and arrangement of these fibres dictates the precise behaviour. Thermosetting resins such as polyester, vinylester or phenolic, can each impart unique qualities to the resulting material.

Constituent composite parts can be selected and tailored to yield a material innately suited to a particular structural function. However, cost effectiveness, enhanced environmental control, sustainability attributes, fire provisions, acoustic control, ease of manufacture, tolerance control, durability, lightness in weight, and aesthetics, are all qualities of a building envelope that must be addressed.

Polymeric façade panels, as secondary structural elements, can easily make use of glass fibre reinforcement, as do many primary structural elements today. Though ranking behind carbon fibres in some areas of mechanical performance, such as stiffness, glass fibres represent high functionality per pound spent on each square metre of façade. Thermal insulation, inherent to glass fibre reinforced polymer (GFRP) is clearly desirable here; the accompanying electrical insulation, too, might be explored to uncover some intriguing prospects. The idea of accommodating first-fix electrical installation within the skin of a building is appealing and could be vital in striving towards a truly integrated façade. Furthermore, there is the architecturally exciting possibility of including LED arrangements in a translucent façade panel (Tsoi 2010).

A polymer matrix of vinylester resin, whilst influenced by the exact chemistry and other fill materials present, can achieve a durable finish (Correia et al. 2006) that also transmits light. The fibre architecture enclosed by the matrix is visible within the structural skin, or can be masked by an opaque setting resin or other finish.

1.3 Design issues

Designing with GFRP requires careful consideration of the mechanical properties; linear elastic behaviour is known to be exhibited, but attention must be given to the differences in compressive and tensile axial strength and stiffness. Analytical studies have shown neutral axis position to deviate from the geometric centroid by significant margins in typical structural sections, as a consequence of this characteristic.

It is not the understanding of structural behaviour, but durability of composite materials, that is called into question most frequently (Busel 2002). A researcher's response is often to conduct investigation on GFRP samples that have first been subjected to

accelerated ageing procedures (Boinard et al. 2000; Wang et al. 2010). This practice however is open to some conjecture. Testing conducted on naturally aged GFRP investigates a trend for hardening of aged resin, whereas popular artificial ageing techniques inadvertently maintain resin plasticity (Liao 1999).

1.4 Panel design and GFRP fabrication

The processes by which GFRP elements are fabricated each possess unique advantages. For automated fabrication of panels to form modular units in a façade, pultrusion is likely to prove most appropriate. The width constraint imposed on panels produced using pultruded GFRP (1.2 - 1.5m) is of little consequence; façade panels are often limited in width to prevent a ripple appearing in the architectural aesthetic (Brookes and Meijs 2008). When wider expanses of a lightweight, flexible cladding are used, a phenomenon can occur whereby the perception of movement in the façade under wind loading is amplified. In highly reflective polymeric facades this must be avoided.

The principally uni-directional nature of fibre reinforcement in pultruded elements will influence panel and mullion arrangement in a unitised façade system. The corresponding connections employed exert effect on the structural integrity, thermal performance and constructability of the final scheme. They will also have specific implications for the end-of-life options of the GFRP (Halliwell 2010). Whilst mechanical connections are more facilitating for reuse, resin bonded connections would earmark retired panels for a composite recycling method, such as fuelling cement kilns. (In this process the polymer component burns to fulfil a fuelling function, whilst precipitated fibres ultimately contribute to reinforcement of concrete made using the resulting cement (Pickering 2009)). In this scenario any embedded metallic connections would encumber the process (Conroy et al. 2006). Basing research around mechanical connections, with scope to extend to non-metallic forms, is deemed to be a responsible approach.

1.5 Performance of the building envelope

The options available amongst modern insulation materials mean that suitable panel designs can easily surpass requirements if considering one-dimensional heat flow. An elemental value of 0.28 W/m^2K for walls, stipulated in building regulations part L2b

(for retrofit of buildings other than dwellings) can be met with sandwich panel constructions comprising a mere 100mm of PIR (polyisocyanurate) foam core (HMGovernment 2010).
It is the influence of connections and the associated three-dimensional heat flow that assumes far greater significance in the thermal performance of newly retrofitted façade systems. This is evidenced in part L2b by the far less stringent requirement of 1.8 W/m^2K for overall curtain wall performance.

Sandwich panel construction, or similar variants are expected to represent a large proportion of designs for GFRP retrofit façades. Provisions for panel replacement or enhanced envelope maintenance are present, along with design scope for alternative internal GFRP skins. Internal structural skins might consist of phenolic as opposed to vinylester resin, thus enhancing the fire safety attributes of an envelope system (Easby et al. 2007).

Invariably it is the connection design that will prove most critical to the performance of a replacement façade.

1.6 Research direction

The properties of GFRP most critical in the design of pultruded structural elements are fortuitously bypassed in façade application. Existing research into creep behaviour of GFRP is extensive, and has resulted in a large amount of design guidance sensitive to serviceability criteria (Russo 2001; Sa et al. 2011). For advanced composite facades however, the permanent action upon prospective panels could be very low, perhaps resulting from only the self-weight of the panels themselves.

The low Young's Modulus of GFRP (usually in the range of 17 – 23 GPa for pultruded sections (Bank 2006)), in comparison with steel, could, in some instances be an advantage. Cladding that is flexible in nature, which can deform elastically in-situ without fracturing or breaking free, is certainly safer than concrete cladding for use in seismically active regions. Because serviceability requirements, specifically deflection criteria, are usually most critical to the design of GFRP elements (Bank 2006), there is naturally a significant capacity for elastic deformation before failure occurs. This

resilience, and the reserve of strength exhibited, is very fitting within any performance-based design philosophy (Mottram 2011).

Fatigue behaviour however, a characteristic of pultruded GFRP that is rarely of much consequence to design, could be of greater concern in a cladding situation. Pultruded profile edges of prismatic GFRP units can assume forms that accommodate suitable connections. Such angled returns will require a fatigue resistance to withstand a lifetime of cyclic straining, due to the transient action of wind or occupancy loading (Salvia et al. 1997). Fatigue testing to an equivalent degree is therefore required to validate viable façade schemes. Much existing research focuses on fatigue when axial stresses are in the principal fibre direction (Salvia and Vincent 1996; Salvia et al. 1997; Tong 2002; El-Assal and Khashaba 2007). Deterministic approaches dominate, and damage is attributed to an accumulation of many cracks, unlike the damage propagation exhibited by steel (Tong 2001). By targeting the secondary-fibre direction at angled sections, data produced is directly transferrable to realistic connection designs.

Research investigating pultruded angles identifies the features of section geometry and fibre architecture that are most important. Variables to which the fatigue life of this type of composite component is most sensitive must be established and understood to assess the feasibility of prospective connection designs.

1.7 Scope and research objectives

The scope of this project is to reveal long term characteristic properties of GFRP pultrusions necessary for the design and application of polymeric façades in retrofit of buildings. Specifically addressing whole life performance, through:

- The development of a means to quantify design limits for material strain based on number of cycles, where fatigue loading will occur
- Investigating pertinent fatigue characteristics of pultruded connection assemblies
- Quantifying reduction in mechanical material property over service life
- Investigating the validity of existing predictive ageing models

1.8 Summary

GFRP is no longer a new material. Used in new systems however, it unfortunately shares some of the 'barriers to acceptance' commonly experienced by new materials in many sectors within engineering (Bakis et al. 2002). There are significant financial and carbon related incentives to embrace this technology.

To understand the fatigue life of pultruded angle connections in the secondary-fibre direction is one objective of research presented in this thesis. By enabling more informed design of connections, to meet the many demands placed upon them, it is intended that the properties of GFRP can be exploited for significant reward.
A parallel focus to validate durability attributes is pursued by case study investigation. Laboratory appraisal of the mechanical properties of naturally aged material permits comparison with existing work, and establishes characteristics which will impinge on design of new polymeric facades.

By conducting research of the type discussed above, as much as possible of the associated risk is removed, to ensure that this potential can be realized. It is understood that the GFRP material can be tailored to precisely suit the function required, whilst offering scope for further exciting prospects architecturally.

By consideration of the most likely FRP types and panel forms, the most urgently needed research areas have been identified. The issues associated with sandwich panels of pultruded GFRP structural skins have been explored, enabling a targeted programme of investigation to be formulated.

2 Background and Literature review

This chapter examines key issues concerning material properties and design considerations for polymeric façades touched on in Chapter 1. Material properties are examined in turn in relation to the prospective application. Appropriate design methodologies are then explored to reveal key areas to benefit from in-depth literature review of previous work in specific fields. Namely durability and fatigue.

2.1 FRP

2.1.1 Material properties

The constituted form of FRP offers can be tailored to meet specific requirements. Three principal types of fibre are briefly discussed below with their engineering attributes and corresponding resin components. FRP has a high strength to weight ratio, but a comparatively low stiffness when compared with steel.

Because GFRP possesses a propensity to creep, leading to the risk of creep fracture, design limitations as low as 60% of ultimate strength may be imposed for permissible stresses. However, as service-loading deformations are in any case most likely to dictate design, this is often of little consequence. To accommodate creep in long-term deflection criteria, the design value for Young's Modulus is reduced also, usually by dividing the short-term value by 1.8 (Bank 2006). For application in facades, permanent actions will be relatively low (or nothing), for out-of-plane panel loading, and wind and occupancy loads are transient actions.

Table 2.1 shows at a glance the mechanical properties and basic cost of the primary components of an FRP composite. Fibre filaments, which in glass might typically be 25μm in diameter, can be bundled into multifilament strands called 'rovings'. Carbon fibre strands called 'tows' are an equivalent product, of superior stiffness, and lower density, though far greater cost. For application in wholly polymeric structural facades tows would be uneconomical, or indeed any use outside of primary structural members or the strengthening of such members.

Table 2.1 Mechanical properties of FRP constituent parts (Bank 2006)

Material	Tensile Strength (GPa)	Young's Modulus (GPa)	Density (10^3 kg/m^3)	Cost (£/kg)
Fibre				
Aramid*	3.15 – 3.60	58 – 130	1.39 – 1.47	20
Basalt	3.00 - 4.84	79 - 93	2.5 – 2.9	5
Carbon	2.10 – 5.5	200 – 500	1.74 – 2.20	10 – 200
Glass	2.4 – 3.5	72 – 87	2.46 – 2.58	2.5
Resin				
Polyester	50 – 75	3.1 – 4.6	1.11 – 1.25	~ 2.5
Vinylester	~ 82	~ 3.5	1.11 – 1.25	~ 3
Epoxy	60 – 85	2.6 – 3.8	1.11 – 1.20	~ 5 – 10
Phenolic	60 – 80	3.0 – 4.0	1.00 – 1.25	~ 2.0

**not frequently used in construction*

Carbon fibres can, however, be used effectively in critical regions of structural sections as, for instance, a more economical means of increasing stiffness than would be achieved by a completely CFRP structural section. Properties for the different grades of glass fibre can be observed in Table 2.2. E-glass finds greatest application in polymeric structures. A borosilicate glass, it exhibits good strength and also electrical resistivity, affording the potential for developments in the way circuits and components may be contained within a building skin.

Table 2.2 Properties for common grades of glass fibre (Bank 2006)

Glass	Tensile Strength (GPa)	Young's Modulus (GPa)	Density (10^3 kg/m^3)	Max. Elongation (%)
E	3.40	72.5	2.57	2.5
A	2.76	73	2.46	2.5
C	2.35	74	2.46	2.5
S	4.60	88	2.47	3.0

C-glass, alkali/corrosion resistant glass finds specialized use in structural engineering whilst S-glass fibres are used mainly in the aerospace industry. Aramid fibres present good tenacity and toughness though perform poorly in compression and can tend towards high moisture absorption, as a result they find greater application in roles where energy dissipation is required such as in bullet proof vests or automotive crash attenuators (Bank 2006).

All fibres discussed in this section exhibit linear elastic behaviour to failure (as does the resulting FRP), though rather different properties are observed for thermal response. Thermal expansion in composites is dominated by the fibres, (where there exist fibres in that longitudinal direction) though the resin possesses markedly different properties. The coefficient of thermal expansion for an E-glass reinforced polyester or vinylester is approximately 5×10^{-6} K^{-1} and nearer 8×10^{-6} K^{-1} when part of a phenolic resin based FRP. Carbon fibre and sometimes aramid fibre FRPs can exhibit negative coefficients of thermal expansion. The absolute value for resin expansion coefficients is generally much larger (up to order of ten times greater), though the relatively low stiffness of the matrix permits the fibres to dominate.

Polymers are viscoelastic, semi-crystalline materials, with good thermal resistance. They are good thermal and electrical insulators provided that they have a low voids ratio; water in any voids will reduce insulative properties of the polymer (Bank 2006). Whilst epoxy resins are favoured for FRP strengthening schemes due to their good adhesive properties, it is an expensive option in other structural application. It does however present very good environmental durability and low shrinkage. Polyester is the cheapest and most versatile resin in Table 2.1. It can be easily pigmented and filled (inert fillers to permit economy of resin material in the matrix, often calcium chloride or clay minerals can be added).

Vinylester resin, boasting the same versatility as polyester, has the added benefit of increased environmental durability in alkaline environments. The glass transition temperature for both polymer resins is usually stated as being between 40 and 110°C. The range here is quite an important issue, because if by reaching 40°C on a building façade, which is entirely possible as a matter of course, properties are already

diminishing, this will have implications on the safe design of the elements. The glass transition temperature should be checked when procuring resin materials for use in structural applications.

Phenolic resin will feature later in this report relating to fire issues; it possesses the best fire resistance of any of the resins in the group, though presents problems relating to workability and curing. Industry feedback has allayed fears to this end, with phenolic mouldings attributing to significant tonnage yearly for the pultruding manufacturers surveyed. It is noted however that there is increased wear of the die used in the pultrusion process for these chemicals (so complex shapes are not desired), and the phenolic resin is also difficult to pigment, never changing appearance greatly from it's natural brownish colouring.

2.1.2 Composite properties

Mechanical properties for a resulting composite are dictated by the manufacturing process adopted, and the control of the chosen operation. This is discussed more in section 2.1.3. To assess basic properties for stiffness and strength of a tensile nature, in unidirectional reinforced elements it is usually assumed, for fibre volume ratios higher than 50%, the resin does not contribute, and Equation 2.1 and Equation 2.2 are adopted. Where E is the Young's Modulus, σ is permissible stress and V_f is the fiber volume ratio; subscripts r, f and m, refer to the resulting composite, fiber and matrix respectively.

$$E_r = E_f V_f \tag{2.1}$$

$$\sigma_r = \sigma_f V_f \tag{2.2}$$

Fibre orientation (in 2D plate like elements like façade panels for instance) can be considered by several possible means. Most easily by considering all fibres at greater than 45° to the main axis as contributing 10% of their stiffness and strength to the main direction, again, ignoring the contribution of the resin. More accurately, the contribution of each group of fibres of proportion α_n lying at angle θ to the applied

stress is presented as $\alpha_n cos^4\theta$ and sum to produce efficiency factor η_θ as shown by Equation 2.3.

$$\eta_\theta = \Sigma\alpha_n cos^4\theta \tag{2.3}$$

For stiffness and strength the equations are then as:

$$E_r = \eta_\theta E_f V_f \tag{2.4}$$

$$\sigma_c = \eta_\theta \sigma_f V_f \tag{2.5}$$

Defining accurate values for compressive properties of FRP is somewhat more difficult, and interesting. Under compression the flexural strength and stiffness of the resin becomes more important, as it is preventing the fibres from buckling and allowing them to contribute to the compressive axial stiffness. Of course this is not possible to the same extent as those in tension, and the full capacity in compression can never be realised. This can be illustrated by a brief study.

The issue is pertinent to the project as bearing in mind that for façade panels, where out-of-plane loading is most significant, the loading could be as likely in one direction as the other (external overpressure, or suction and occupancy loading), thus leading to symmetrical sections or sandwich constructions. As mentioned previously the flexural strength will not dominate in design, however the stiffness observed in tests conducted in the laboratory may be examined accordingly by this means. As a guide the compressive stiffness is usually taken to be in the region of 80% of the tensile stiffness and the compressive strength as about 55% of the tensile strength, but it is the stiffness that is examined below.

The stress block in Figure 2.1 illustrates an FRP section in its elastic range (before failure). An equation balancing the compressive and tensile forces across the section permits the deduction of the neutral axis position. If the fibre content is known, and the compressive stiffness of fibres relative to tensile modulus, the model can be used to determine theoretical surface strain on the flange in compression, when in an element undergoing bending.

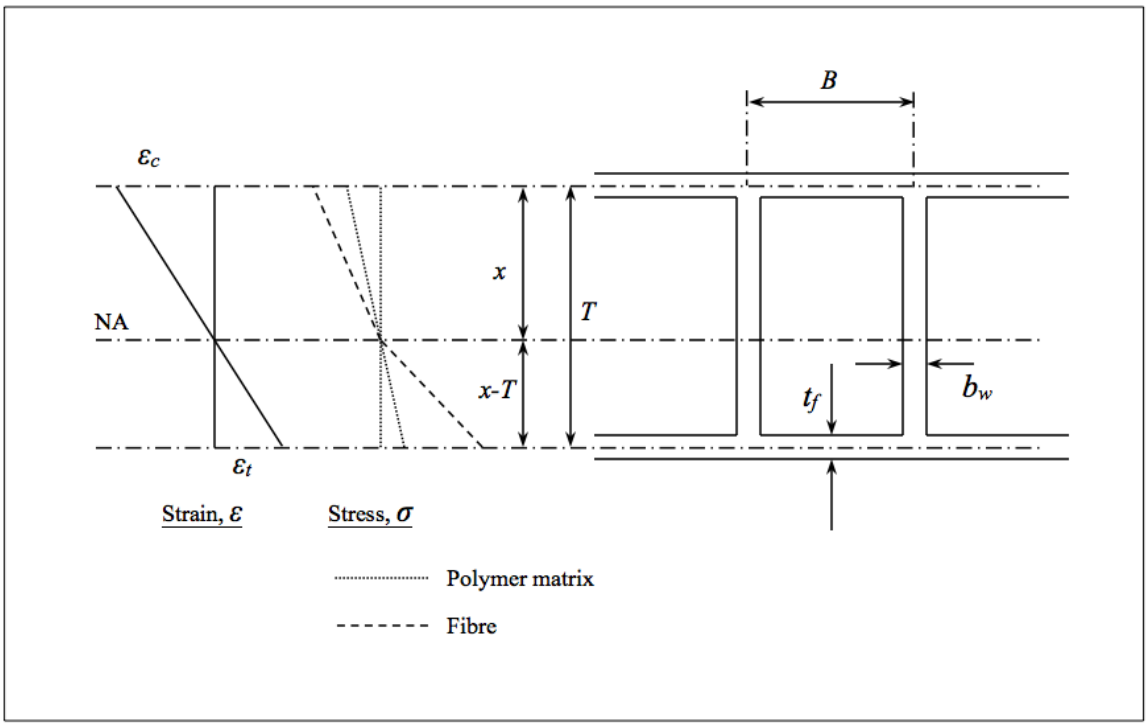

Figure 2.1 Stress block for FRP thin walled section

In the Figure 2.1 the cell dimensions of the section displayed are 'centre to centre' of the individual elements. The stress in the flanges is assumed to be of constant value through the thickness of the flange. Imposing an arbitrary strain at the top flange position allows the stresses through the section to be determined in general form. The assumption that plane faces remain plane in bending is adopted. For a cellular panel with slenderness ratio (l/T) typically exceeding 60, it is expected that axial strains will dominate and the assumption is deemed acceptable. It must be noted that relating this theory only applies to specimens of comparable slenderness.

The compressive strain at the top face is related to the tensile strain by the following:

$$\varepsilon_t = \varepsilon_c \left((T/x)-1\right) \tag{2.6}$$

Compressive force per unit width of panel in top flange, due to fibres:

$$E_{fc}\, \varepsilon_c\, t_f V_f \tag{2.7}$$

Compressive force per unit width of panel in top flange due to matrix:

$$E_m\, \varepsilon_c\, t_f (1-V_f) \tag{2.8}$$

Tensile force per unit width in the bottom flange due to fibres:

$$E_{ft}\,\varepsilon_c\,((T/x)\text{-}1)\,t_f\,V_f \tag{2.9}$$

Tensile force per unit width in the bottom flange due to matrix:

$$E_m\,\varepsilon_c\,((T/x)\text{-}1)\,t_f\,(1\text{-}V_f) \tag{2.10}$$

Aside note: for a sandwich panel, these expressions along with a shear component to represent deformation of the core material would be sufficient.

Compressive force per unit width of panel in webs, due to fibres:

$$E_{fc}\,\varepsilon_c\,(b_w/2B)\,x\,V_f \tag{2.11}$$

Compressive force per unit width of panel in webs, due to matrix:

$$E_m\,\varepsilon_c\,(b_w/2B)\,x\,(1\text{-}V_f) \tag{2.12}$$

Tensile force per unit width of panel in webs, due to fibres:

$$E_{ft}\,\varepsilon_c\,((T/x)\text{-}1)\,(b_w/2B)\,(T\text{-}x)\,V_f \tag{2.13}$$

Tensile force per unit width of panel in webs, due to matrix:

$$E_m\varepsilon_c\,((T/x)\text{-}1)\,(b_w/2B)\,(T\text{-}x)\,(1\text{-}V_f) \tag{2.14}$$

The value of x can be determined in general form by equating the compressive and tensile net forces across the section. The resulting expression for 'x' is a quadratic and does not simplify to a very good extent. It is shown below for completeness, and a spreadsheet was produced using the Newton-Raphson iterative method ('goal seek' in excel) to deduce values for x, and furthermore, an expression for a panel's section modulus, which is used with experimental data to find the compressive stiffness of fibres when in a composite undergoing bending.

$$x^2\left[E_{fc}\left(\frac{b_w}{2B}\right)V_f + E_m\left(\frac{b_w}{2B}\right)(1-V_f)\right] - (T-x)^2\left[E_{ft}\left(\frac{b_w}{2B}\right)V_f + E_m\left(\frac{b_w}{2B}\right)(1-V_f)\right]$$
$$+ (T-x)\left[E_{ft}t_fV_f + E_mt_f(1-V_f)\right] - x\left[E_{fc}t_fV_f + E_mt_f(1-V_f)\right] = 0$$

(2.15)

Table 2.3 illustrates the sensitivity of the neutral axis position with variable compressive fibre action and shows the implication this has on the resulting bending stiffness per surface strain per mm width. As such it can be used to check measured surface strains in the laboratory against resistive moment and corresponding theoretical strains. This table takes nominal values for fibre content volume ratio and matrix modulus.

Table 2.3 Neutral axis and bending stiffness relating to section in Figure 2.1

T (mm)	B (mm)	t_f (mm)	b_w (mm)	V_f	E_m (GPa)	E_{ft} (GPa)	E_{fc}/E_{ft}	E_{fc} (GPa)	x (mm)	M/ε/unit width (kNmm/mm)
100	100	4	3	0.6	3.5	80	1	80	50.0	1.98E+04
100	100	4	3	0.6	3.5	80	0.9	72	53.3	1.76E+04
100	100	4	3	0.6	3.5	80	0.8	64	57.0	1.55E+04
100	100	4	3	0.6	3.5	80	0.7	56	61.0	1.35E+04
100	100	4	3	0.6	3.5	80	0.6	48	65.3	1.16E+04
100	100	4	3	0.6	3.5	80	0.5	40	70.1	9.67E+03
100	100	4	3	0.6	3.5	80	0.4	32	75.2	7.83E+03
100	100	4	3	0.6	3.5	80	0.3	24	80.6	6.03E+03
100	100	4	3	0.6	3.5	80	0.2	16	86.3	4.24E+03
100	100	4	3	0.6	3.5	80	0.1	8	92.2	2.42E+03
100	100	4	3	0.6	3.5	80	0	0	98.2	5.58E+02

The neutral axis can be observed to follow a trend that indicates an accurate expression for x. It can be seen that when the compressive fibre modulus is equal to the tensile, the neutral axis is at mid-depth of the section, as expected. Results from this point are concerned with the section bending stiffness as calculated by the neutral axis position and the appropriate stress blocks and 'lever arms to centroids' as shown by Figure 2.1.

Figure 2.2, Figure 2.3 and Figure 2.4 represent the bending stiffness (in the primary direction) as a function of two variables. In each case the degree of compressive fibre modulus, expressed as a ratio of the typical tensile value, is one variable, and the behaviour of this variation is observed for different fibre content volume ratios, Figure 2.2, different matrix moduli, Figure 2.3, and different overall section depths (with other section geometry remaining constant), Figure 2.4.

Taking firstly Figure 2.2, it can be appreciated that the degree by which compressive fibres contribute to stiffness has a significant impact on the performance of the panel even at extremely low fibre contents (for pultrusions where V_f is equal to 0.3, and at high fibre contents even more so, not least because of the effective matrix area in compression also reduces. What is highlighted, is the role of the matrix strictly as a binder to transfer stress between fibres. The direct compressive and tensile properties appear to be of limited consequence.

Note that the numerical mechanics of the presentation in Figure 2.2 assumes that the extent by which compressive fibre stiffness if exhibited, and fibre content volume ratio, are independent variables of mutually exclusive effect. In the typical range of fibre contents used this is usually the case. However it is likely that at extreme values of fibre content, a 'packing factor' may exert an effect, resulting, at high v_f values for instance, in a reduced capacity for matrix to transfer force between fibres. This effect will not be represented by the graph in Figure 2.2, though one might expect to see a slight plateauing parallel to the V_f axis at only very high values.

To further examine the above findings regarding matrix action, Figure 2.3 represents a study observing the effect of compressive fibre action over a range of different matrix moduli. The importance of the compressive fibre action is observed in terms of the overall stiffness achieved at the range of matrix moduli presented. The matrix modulus has very little effect on the section stiffness.

The extent of linearity observed in all these graphs is surprising when looking at the mathematics of the applied mechanics involved. For almost any value of V_f and E_m the degree of compressive fibre action exerts effect in an almost linear proportional nature on the section bending stiffness.

Figure 2.4 has been produced to identify any size effects, often seen in stiffness to strength studies on structural sections, that may become evident in the way that the E_{fc}/E_{ft} ratio impinges on the stiffness. Particularly, it is to identify if such a linear relationship is still observed where the overall depth is small. As it can be appreciated by the graph in this figure the relationship remains linear through the test range.

With experimental test data for fibre content (by resin burn off technique) and panel stiffness in three point bending it will be revealed whether a compressive fibre contribution of 80% the tensile value is an accurate approximation.

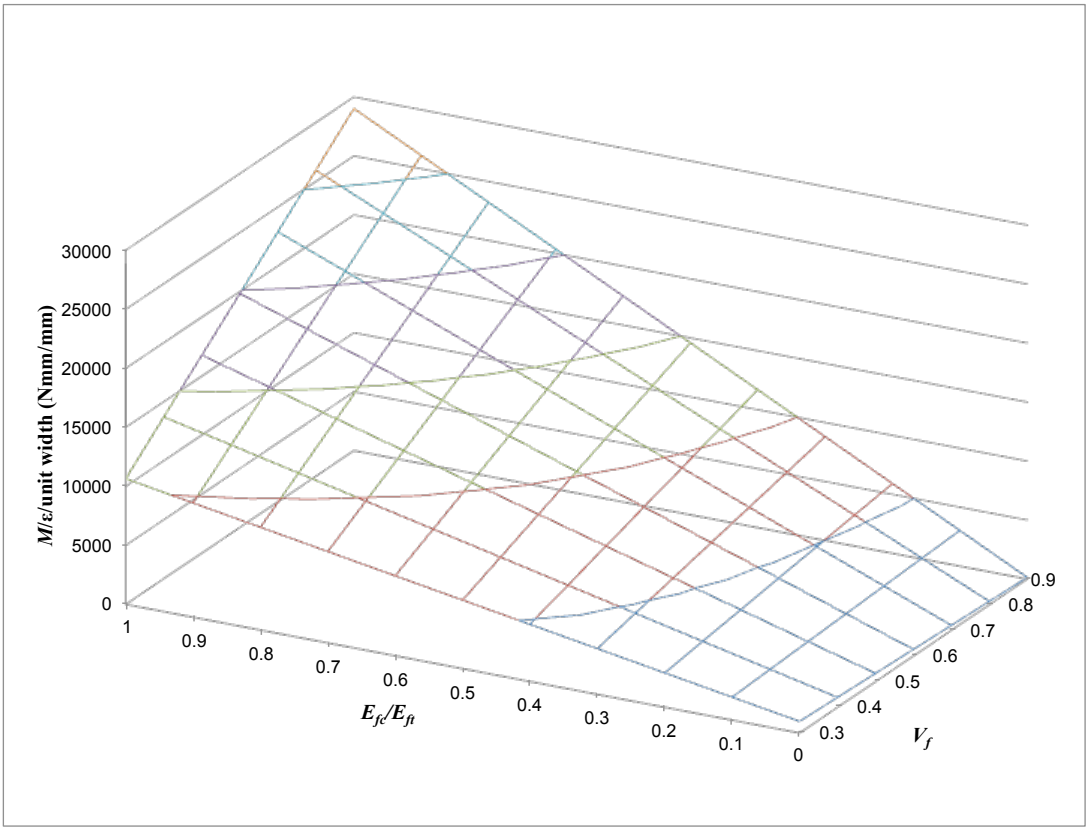

Figure 2.2 Bending stiffness of section as a function of the degree of compressive fibre contribution and principal fibre volume ratio

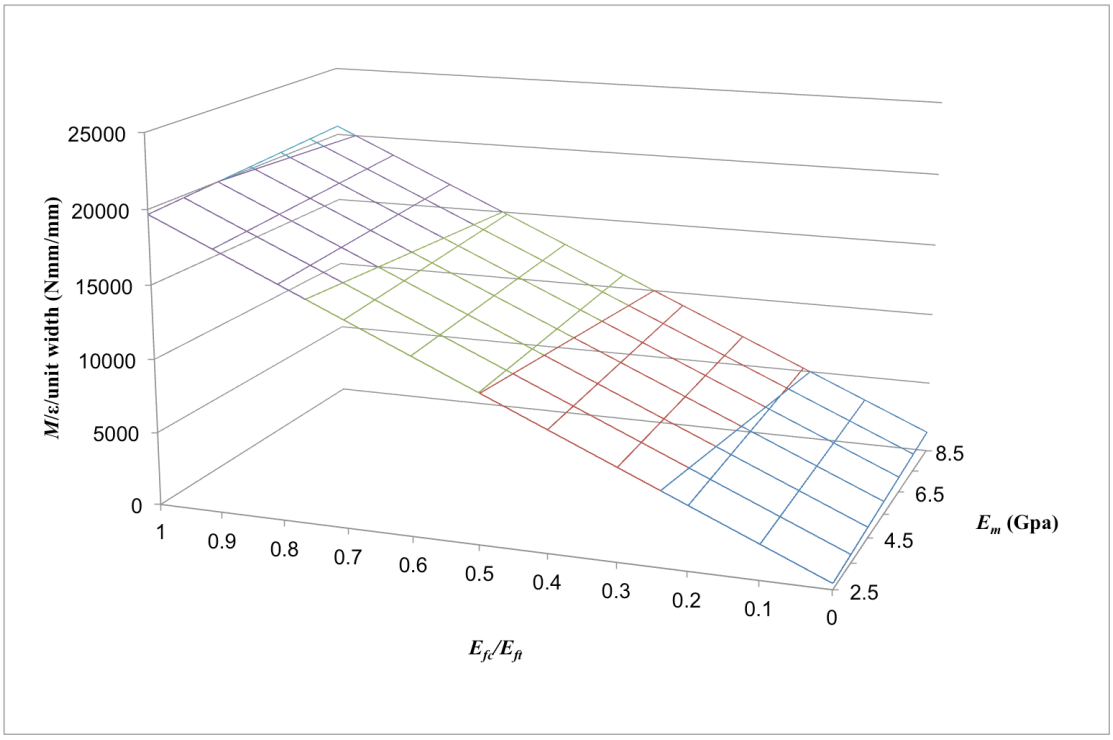

Figure 2.3 Bending stiffness of section as a function of the degree of compressive fibre contribution and matrix modulus

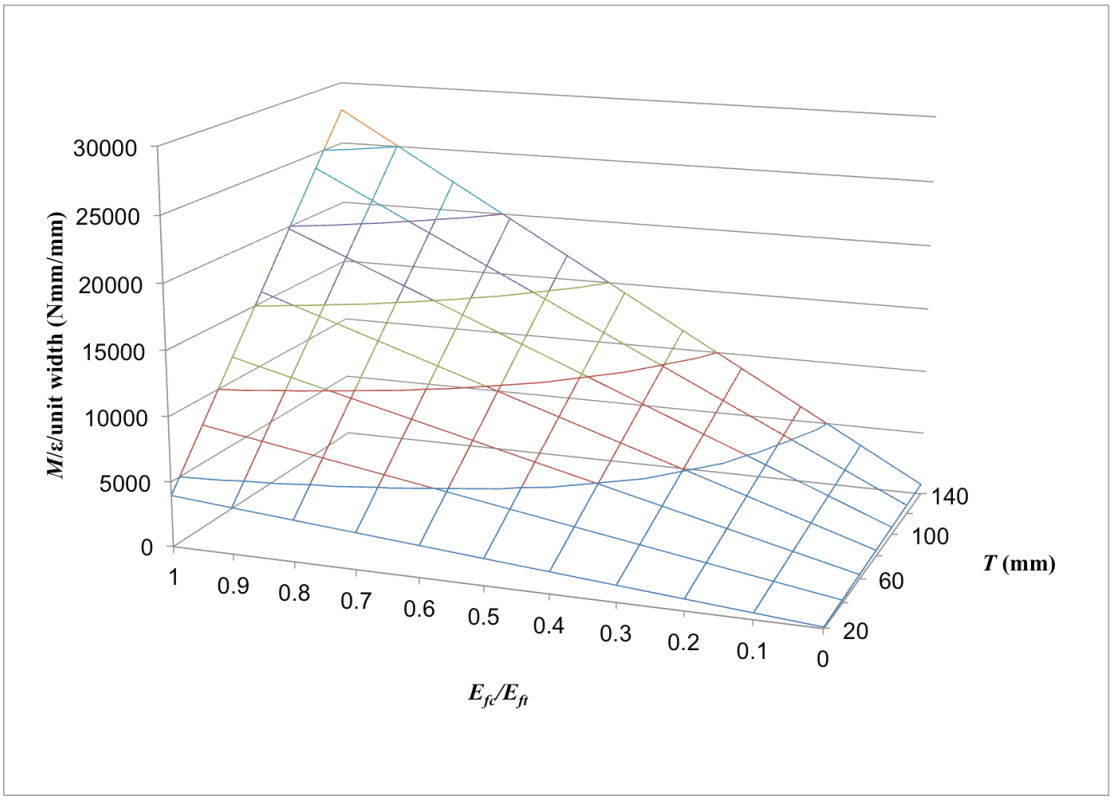

Figure 2.4 Bending stiffness of section as a function of the degree of compressive fibre contribution and overall section depth T

2.1.3 Fabrication and manufacturing

Three principal methods exist that are relevant to producing structural façade elements in FRP: hand lay-up, resin transfer moulding and pultrusion. Hand lay-up is typified by the skilled labour required, and the ability to produce bespoke or batch items specific to a particular mould, whilst pultrusion is synonymous with more linear-natured elements and automated processing. Resin transfer moudling (RTM) is becoming more popular in façade engineering. Like hand lay up, custom elements can be produced with desired mechanical properties tailored to suit in each surface direction. Any shape or curvature, which can be removed from a mould, can be produced, with almost unlimited scope for embedded metallic connections or cutouts. Whilst an area full of exciting prospects for façade application, it is to resolve obstacles to the application of pultrusions in retrofitted façades that is the focus of this project.

Pultrusion offers higher fibre contents, though the reinforcement is principally in one direction; the longer orthogonal dimension of the element. Pultrusion is the cheaper process and as such is more appropriate to a modular system of repeat units such as a unitised façade system to cover an office building of fairly regular geometries. Pultrusion offers the potential for achieving high fibre contents, which is desirable because not only does the strength and stiffness of the resulting element come from the fibre, but also because silica, the basic elemental unit, is an abundant material in the Earth's crust, and therefore to exploit this as opposed to the petrochemical-sourced polymer matrix makes sense.

Pultrusion cannot offer the same scope for wide elements as other fabrication techniques. However, manufacturers assure that widths up to 1.8 m are easily accommodated, and this is more than acceptable for application in facades. Often, façade panels, even if part of a larger unitized element, will not be more than 1.8 m in width as otherwise a ripple in the aesthetic can become prominent. It might also be anticipated that, for what could be expected to be a high gloss finish provided by an FRP façade, the reflection's movement character in windy conditions could be all the more undesirable due to a loss of perceived safety to those outside the structure.

Fibre 'architecture' in a pultruded element is, for the individual rovings, solely longitudinal in nature, however perpendicular and 'off zero' angle fibre contents are

made possible by the inclusion of fibre mats. Woven, random or stitched mats enable fibres to be pulled through the die as part of a mat, which will have some longitudinal fibre component to provide the necessary resistance to stretch and breakage that the pultrusion force imparts. The 'tightness' of the longitudinal fibres as they are drawn through the die provides superior mechanical properties and the fiber positioning process allows fiber content to be aggregated as desired through the section depth. Lightweight fabric or 'surface veils' of unwoven E-glass or polyester filament improve the aesthetic of the final element. Additionally, due to the higher resin volume fraction of this layer, a resin-rich surface is created similar to that achieved by a gel coat in hand lay-up, which yields greater corrosion and UV resistance (Bank 2006).

For any method of fabrication, at laminate level, the architecture of the fibre construction of the various laminates or individual fibre reinforcement bundles, (rovings,) has an impact on the mechanical properties achieved; there are possible interlaminar planes along which slip can occur.
Further to the organic fillers already mentioned, accelerators, UV stabilizers and polymerising agents may all be present in the matrix alongside the binding polymer, with the intention of creating a durable but easily fabricated product.

'Sizing' is a coating that serves to protect the fibres when they are formed into a bundle or a strand and contains coupling agents to enhance the fibre resin bond. As it will be specific to the polymer used, it must be remembered that if carbon fibres are to be used along with glass fibres, where additional stiffness is required, the sizing for those fibres must be selected accordingly (Bank 2006).

2.2 Environmental durability

Durability is a key aspect of specifying FRP materials. Chapter 3 and Chapter 4 provide details of durability studies undertaken on naturally-aged GFRP panels. The significance of these studies is that there are very few opportunities to assess the characteristics for GFRP from real structures aged in natural environments; testing must usually be undertaken on artificially-aged composite material, at a small scale; the calibration of the various ageing methods will impinge significantly on the conclusions drawn.

Weathering is claimed by many manufacturers/pultruders not to be a significant problem for GFRP, with durability in fact being one of its great virtues. The importance of gel coats and good quality control of surface finish must be stressed though, in order to achieve remarkable properties.

UV degradation, moisture absorption, alkalinity and aesthetic factors of colour fading and surface smoothness, are design life factors affected by gel coat application. Provision for easy replacement of damaged elements, parts or panels, of a unitised system can be extended to matching the design life of similar elements for convenient replacement when necessary as a planned occurrence. For instance neoprene gasket, of only 20 years in design life would not be sensibly placed in design, if to replace it meant having to remove a lot of other elements of much greater design life to grant access, whether these parts could be conveniently reinstated or not.

Environmental durability is considered under headings for the different factors that cause degradation or decomposition of the polymer, affecting performance of the resulting composite. 'Degradation' is loss of properties caused by a physical change in the polymer, which could be brought about by mechanical stress, heat or abrasion. 'Decomposition' occurs when the chemical structure of the polymer itself is changed by a particular stimulus. Factors such as heat, at high enough levels to cause breaking or changing of bonds in the polymer, can cause decomposition, as too can ultraviolet (UV) radiation, which can result in severe decomposition, either by chemical bond cleavage or by creating free-radical sites along the polymer backbone (Pochiraju et al. 2012).

It is known that cracking accelerates oxidation by providing increased surface area in contact with oxygen (Pochiraju et al. 2012), a combination of different factors culminate in enhancing the processes of degradation and decomposition.

2.2.1 UV radiation

UV radiation, even at sea level is very injurious to composites, however UV does not penetrate beyond the near surface layer, so paints and other coatings can provide adequate protection (Pochiraju et al. 2012). In the presence of oxygen, chain scission

tends to dominate and properties such as T_g and toughness decrease dramatically; Sasuga and Hagiwara (1987) demonstrated that gamma radiation in air reduced polyester elongation at failure from 88% to as low as 3%. Reduction in the elongation of the polymer matrix of a composite will result in an increased propensity to crack under mechanical stress. When cracking occurs weight loss of the polymer is observed due to oxidation and the larger surface area in contact with oxygen due to the cracks (Colin et al. 2005).

Since most polymers have bond dissociation energies on the order of the 290 to 400 nm wavelengths in the UV region, they are greatly affected by solar radiant flux incident with the Earth's surface, which contains frequencies of the same wavelength (Kharbhari et al. 2003). Qiu and Gu (2011) tested glass fibre reinforced polyester composites after various durations of exposure to UV radiation (from an artificial, lamp source) and measured the subsequent 'bending tenacity' which represents flexural stiffness, the ultimate tensile strength, and the elongation at failure, which is closely related to the resin plasticity. This study did not use pultruded specimens but employed vacuum assisted resin infusion (VARI) to fabricate the composite material. The specimens were fabricated freshly for testing, and as a result the ageing characteristic observed are consequence of only the UV irradiation. The manner in which Qiu and Gu (2011) reported the results for bending stiffness is by presenting the 'centre-span displacements' of three-point bending of coupons, for a specific load.

In summary Qiu and Gu (2011) found that with increasing time of UV exposure the tensile strength decreased, the flexural stiffness decreased, but % elongation at failure increased. The behaviour of polyester alone when irradiated with gamma radiation has been shown by Sasuga and Hagiwara (1987) to reduce % elongation significantly. It is therefore evident that the fibres present, despite the resin possessing greater sensitivity to radiation, influence the response of the UV aged composite to tensile loading. It is noted that the elongation at failure in tension is not a direct measure of plasticity or strain limit of rupture of the polymer matrix composite component. As previously stated, it is rupture of the polymer that is known to increase the rate of oxidation and degradation of the composite. The polymer is exposed to the environmental elements, though it is important to remember that the glass fibres are themselves very vulnerable to degradation in moist environments when unprotected (Chu et al. 2004).

Cabral-Fonseca et al. (2012) also conducted an investigation into artificial accelerated ageing thorough UV exposure, using pultruded polyester GFRP composite material. A quantified ultra-violet (QUV) irradiation chamber was used to irradiate specimens. Exposure cycles consisted of 4 hours UV radiation simulated with fluorescent lamps at 60^{o}C, and 4 hours of exposure to moisture caused by constant condensation of deionized water at 50^{o}C. The fluorescent lamps provided an irradiance of 0.77 W/m^{2}nm at 340 nm (i.e. Intensity of 262 W/m^{2}), which reproduces the most relevant part of the sun's spectrum between 290 and 350 nm (Cabral-Fonseca et al. 2012). Extending the studies discussed above, Cabral-Fonseca et al. (2012) investigated the influence of moisture and UV exposure as cyclic events, similar to realistic service environmental conditions. The control and uniformity of testing parameters, from study to study, makes comparison with the work of others very difficult to compare quantitatively. The findings are indicative, of the mechanisms of degradation that prevail. Data concerning the mechanical properties, glass transition temp T_g, and the mass variation of the specimens was collected at intervals of 1000, 2000, and 3000 hours.

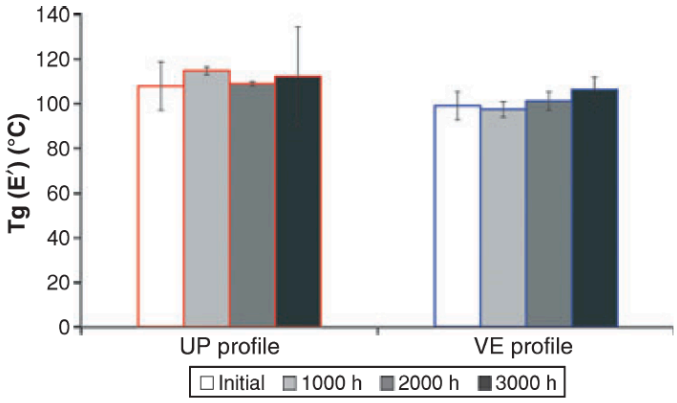

Figure 2.5 T_g of unsaturated polyester (UP) during QUV ageing from Cabral-Fonseca et al. (2012), data for vinylester (VE) also shown

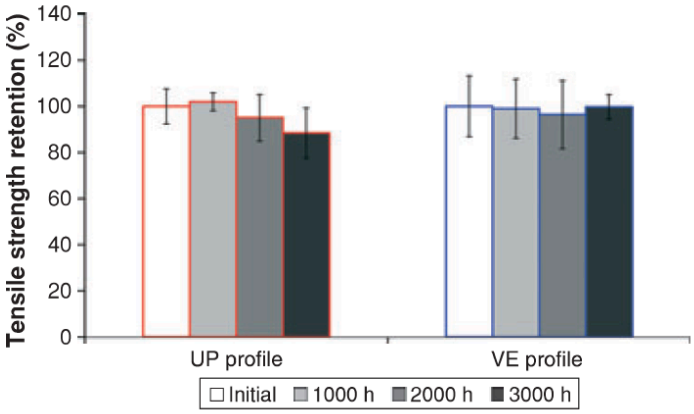

Figure 2.6 Tensile strength of unsaturated polyester (UP) during QUV ageing from Cabral-Fonseca et al. (2012), data for vinylester (VE) also shown

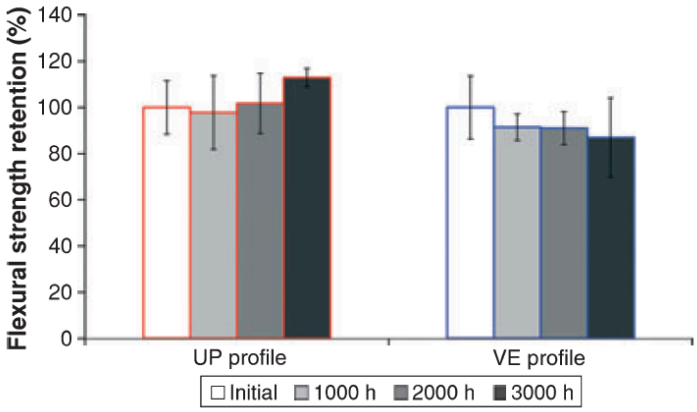

Figure 2.7 Flexural strength of unsaturated polyester (UP) during QUV ageing from Cabral-Fonseca et al. (2012), data for vinylester (VE) also shown

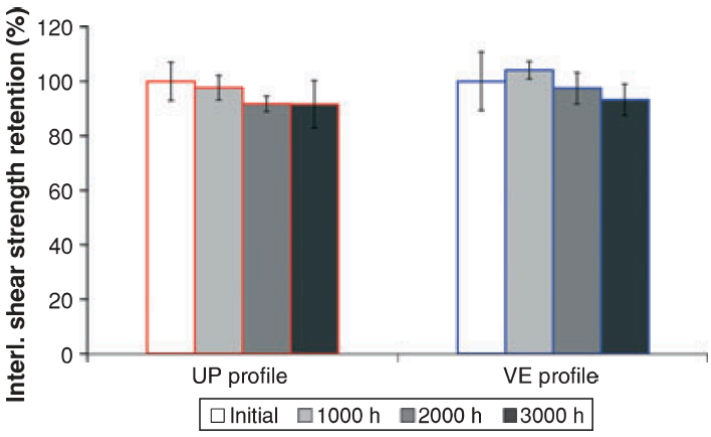

Figure 2.8 Interlaminar shear strength of unsaturated polyester (UP) during QUV ageing from Cabral-Fonseca et al. (2012), data for vinylester (VE) also shown

A slight (4%) increase in the T_g was observed for the PE material over the 3000 hour duration of ageing. The tensile strength and shear strength are shown to reduce over this time, however the flexural strength is shown to increase quite significantly. The flexural testing is evidencing an ageing related change in the material, not captured to the same degree by measurements of other mechanical properties. It is surprising to compare results for the flexural response of UV-aged polyester GFRP reported by Cabral-Fonseca et al. (2012) to those found by Qiu and Gu (2011). Qiu and Gu established a reduction in flexural stiffness (by almost 50%) with ageing under UV bulbs, whereas Cabral-Fonseca et al reported an increase in flexural strength. It can be noted that Qiu and Gu (2011) adopted as the subject of their investigation, a polyester matrix composite material, fabricated by resin infusion technique (VARI) as opposed to pultrusion. The authors report cracking to have occurred during flexural testing. The low initial straightness and 'toughtness' of fibres in a resin infused composite, the low fibre volume fraction, and the arrangement of fibres (mid depth, and present only in a single layer), could all explain why cracking was of such detriment to the flexural stiffness. The paper does not contain enough information about the strain levels encountered in such testing to make any quantifiable claims. Useful further work would establish at what strain level in the polymer composite such degradation of flexural properties was initiated.

Cabral-Fonseca et al. (2012) analysed the polyester material using Fourier Transformed Infrared Spectroscopy (FTIR). The chromatic profile pre and post irradiation was determined. Results were reported showing evidence of chemical change at only the surface of the material. Spectra disclosing the existence of silica revealed that some glass fibres had become more directly exposed as a result of the UV ageing. This is in contrast to earlier conclusions made by Correia et al. (2006) in a study that examined the effect of UV ageing on the chromatic profiles of pultruded GFRP polyester matrix based structural profiles. It was reported that although FTIR showed significant chemical degradation in the surface of the material after QUV and xenon arc experiments, the synergistic effects of exposure to UV irradiation, moisture and temperature on the mechanical properties were insignificant. Both studies, Correia et al. (2006), and Cabral-Fonseca et al. (2012) establish that the chromatic changes relate to the colour and gloss changes observed in the aesthetic of the material, and that for outdoor applications, protective coatings are vital.

Notable work concerning the use of UV irradiation to post-cure GFRP composite material has been undertaken by Compston et al. (2008) and Compston and Dexter (2008). These studies have focused on UV cured vinylester GFRP composites and how they compare with room temperature and thermally cured counterparts. It has been established above, as evident in Figure 2.5, Figure 2.6, Figure 2.7 and Figure 2.8, that unsaturated polyester responds to moisture and UV exposure as cyclic events differently to vinylester. The findings are notable as the resin hardness immediately after UV curing is increased by approximately 3-4 times. Figure 2.9 shows how the room temperature cure increases in hardness more gradually.

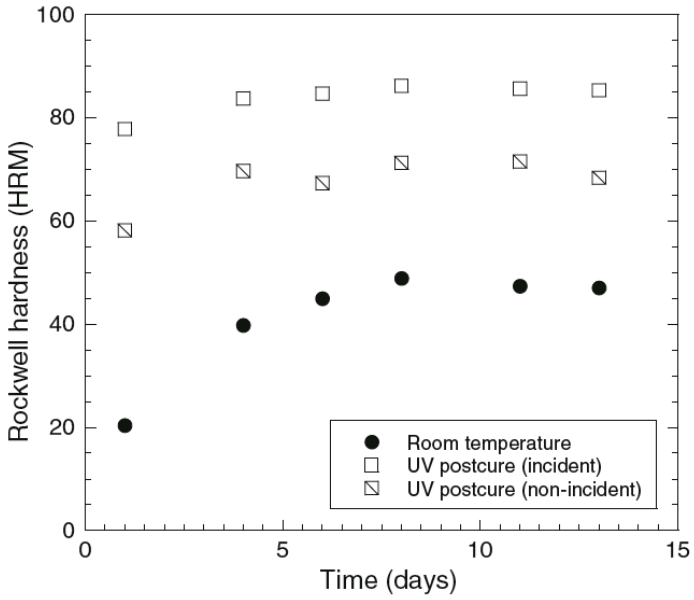

Figure 2.9 Rockwell hardness for room temp cure and UV cure of vinylester resin from Compston and Dexter (2008)

There are manufacturing and environmental benefits associated with using UV curing over thermal curing of resins. However, findings most relevant to the focus of this review concern the subsequent mechanical properties. It is reported that the interlaminar shear strength increased by 28% as a result of UV curing over room temperature curing (Compston et al. 2008). These studies are on vinylester not polyester, but they illustrate well the propensity of UV to harden thermosetting resins. It is interlaminar shear strength, closely related to the integrity of the interfacial bond, which is reported to be the mechanical property most enhanced.

2.2.2 Moisture coupled with temperature

Moisture plays a significant role in influencing the mechanical behaviour, and therefore the long-term durability of polymer matrix composites. Others have investigated the influence of damage and stress on moisture diffusion. The combined influence of temperature, strain gradient, relative humidity, and temperature on diffusion at the fibre-matrix interface, and how degradation of composites properties with is effected can all be considered (Pochiraju et al. 2012). Purnell et al. (2008) concluded that the correlation between moisture uptake and strength loss in GRP samples was poor. Though water uptake is known to cause plasticization in the short term and hydrolysis in the long term through attack of the Ester linkages (Cabral-Fonseca et al. 2012). Both of these phenomena induce higher levels of molecular mobility resulting in decreases in the glass transition temperature T_g (Pochiraju et al. 2012).

Hydrothermal ageing is a procedure used to artificially age polymer composites. The central tenet being that short periods of ageing at high temperature can be equated to longer periods at lower, service temperature (Purnell et al. 2008). To correlate the temperature dependent rate coefficients the Arrhenius relationship is used:

$$k_d = k_0 \cdot e^{-\frac{E_d}{R_m T}} \tag{2.16}$$

Where k_0 is a reference rate coefficient of the flaw growth rate, E_d is the activation energy of the flaw growth rate, T is the temperature at which the test is performed on a Kelvin scale, and R_m is the molar universal gas constant. The general influence of temperature on the diffusion co-efficient k_d can be understood from Equation 2.16.

Accelerated hydrothermal procedures have shown that ageing conducted whilst specimens are under stress can alter the uptake of moisture by weight from 0.408% to 0.556%, but that a threshold value for moisture uptake is exhibited by composites in most cases. The error in diffusivity is known to be large, however the eventual threshold value in the predicted maximum saturation level is less than 2% (Pochiraju et al. 2012). Berketis and Tzetzis (2009) examined the water absorption characteristics of GFRP after long-term exposure to a hydrothermal environment. Polyester matrix

laminates were immersed in deionized water baths for 2.5 years at temperatures of 43, 65 and 95^{o}C. The changes in the thermo-mechanical properties after water immersion were examined using dynamic mechanical thermal analysis (DMTA). Results revealed that the long-term water uptake profiles were highly sensitive to water temperature. The DMTA showed matrix plasticizing effects at 43^{o}C and some post curing effects at 65^{o}C and 93^{o}C. All specimens exhibited a decrease in storage modulus (related to mechanical stiffness) with increased time of immersion. T_g of the specimens increased with time of immersion (Berketis and Tzetzis 2009).

Kotani et al. (2011) developed a model to predict the strength of unidirectional GFRP after hydrothermal ageing. Like Purnell et al. (2008) before, Kotani et al. (2011) found that a threshold level of saturation in the composite existed, as shown by Figure 2.10, and classical Fickian behaviour in moisture gain and swelling strain were observed. The fibre strength and interfacial shear stress was evaluated experimentally using a single fibre composite (SFC). In addition the tensile strength, stiffness and strain at rupture, of the unidirectional GFRP were measured after hydrothermal ageing.

In the study of Kotani et al. (2011) the hydrothermal ageing was carried out in deionized water at 80^{o}C. Tests were conducted on vinylester composite. Figure 2.11, re-plotted from Kotani et al (2011) shows the residual strength as a function of ageing time. Figure 2.12 shows rupture strain and Figure 2.13 shows stiffness, both plots as a function of ageing time. It can be appreciated that the three variables presented in these plots as a function of ageing-time appear to plateau, or very nearly plateau over the longest immersion time investigated.

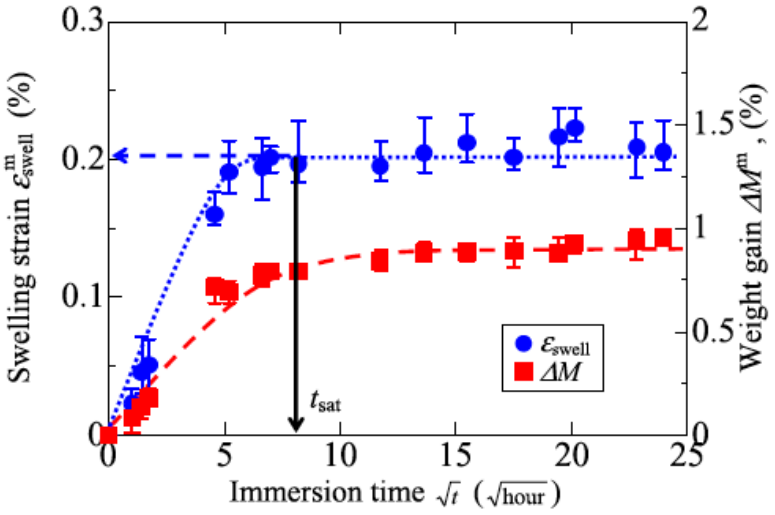

Figure 2.10 Water uptake of vinylester resin matrix by Kotani et al. (2011)

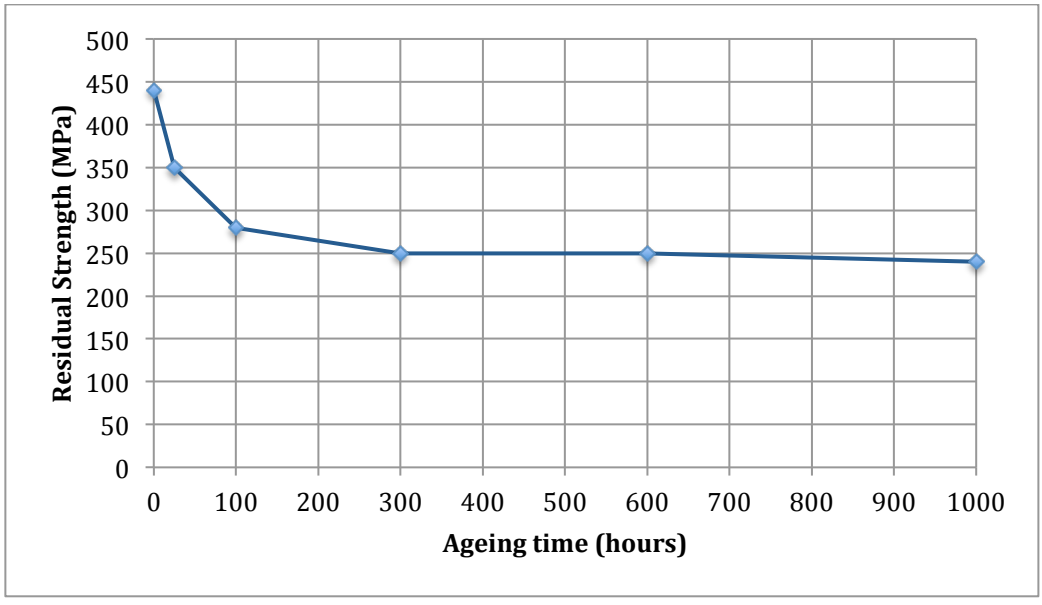

Figure 2.11 Residual strength of unidirectional GFRP after hydrothermal ageing, replotted from Kotani et al. (2011)

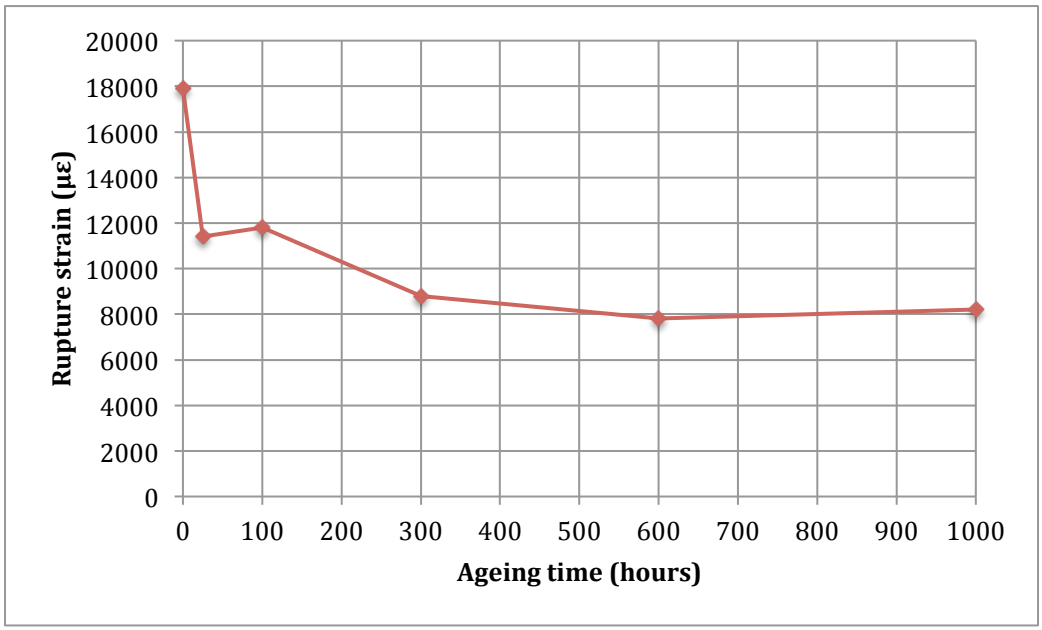

Figure 2.12 Rupture strain of unidirectional GFRP after hydrothermal ageing, replotted from Kotani et al. (2011)

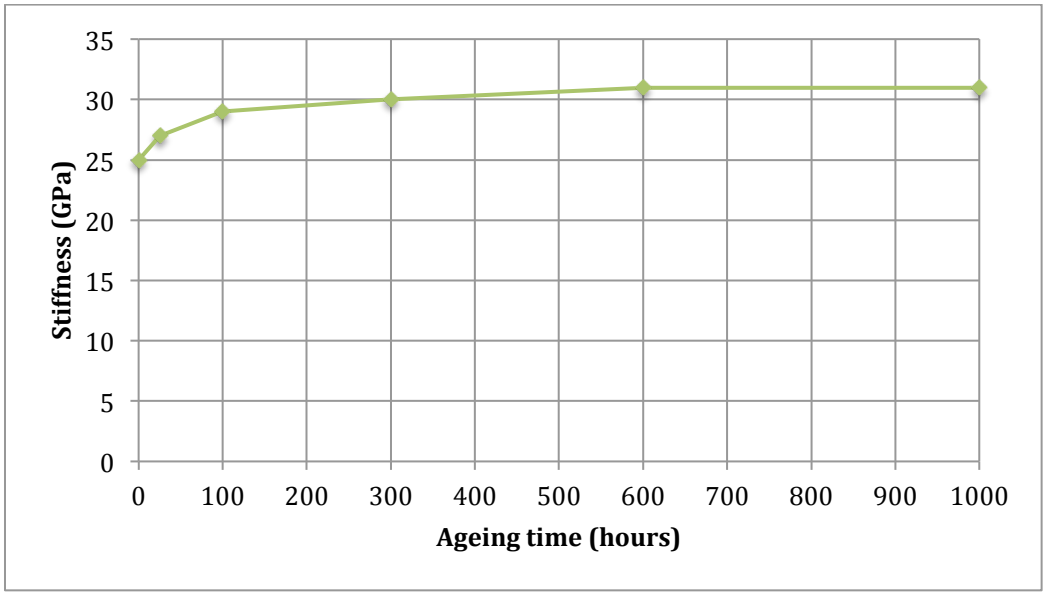

Figure 2.13 Stiffness of unidirectional GFRP after hydrothermal ageing, replotted from Kotani et al. (2011)

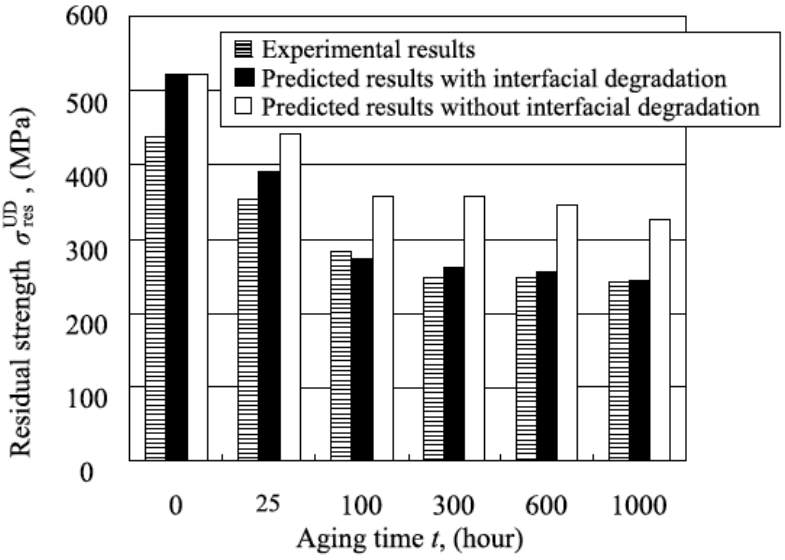

Figure 2.14 Predicted residual strength of UD GFRP after hydrothermal ageing from Kotani et al. (2011)

Figure 2.14 shows the residual strength found experimentally, and also the predicted strength (post ageing), using each of two theoretical models. It is evident the model accounting for interfacial degradation, developed by Kotani et al. (2011), better represents experimental findings. It is discussed later in chapter 6 how the interfacial zone is of paramount importance to the strength of a GFRP composite, though as illustrated by Figure 2.11 and Figure 2.13 it can have much less effect on the stiffness.

Thus far discussion has focussed on the mechanical properties of GFRP composite specimens as measured upon withdrawal from hydrothermal ageing environments. Chu et al (2004) have demonstrated however, that the properties of specimens recover to an extent upon 're-conditioning' after removal. 'Regain' of strength has been shown to occur according to Equation 2.8 where σ_0 is the unexposed strength, $(\sigma_t)_{wet}$ is the strength after immersion for time a in deionized water at the temperature under consideration, and $(\sigma_t)_{dry}$ is the strength of the same set but after re-conditioning at 23°C and 46% RH for 28 days (equal to the original period of conditioning in this study).

$$\%Regain = \left[\frac{(\sigma_t)_{dry} - (\sigma_t)_{wet}}{\sigma_0 - (\sigma_t)_{wet}}\right] \times 100 \tag{2.8}$$

Values for regain of specimens varied depending on the time period of ageing in hydrothermal bath and the temperature at which that ageing was conducted. Substantially less regain was observed after immersion in alkali solution, though the focus of this review will remain on non chemical ageing to address principles applicable to façades.

Table 2.4 Comparison in percentage regains of tensile strength due to reconditioning after exposure; extracted from table by Chu et al. (2004)

Hydrothermal ageing temperature for 75 week period (^{o}C)	%Regain after re-conditioning at 23^{o}C
23	33.1
40	12.1
60	6.0
80	2.7

After the longest period of immersion ageing (of 75 weeks), the reconditioning brought about regain in the composite of between 2.7 and 33.1% as shown by Table 2.4. As pointed out by Chu et al. (2004), specimens aged at higher temperatures, which represent longer ageing times, exhibit much smaller regain in strength, therefore greater irreversible degradation. Electron microscopy has verified that the fibres do indeed degrade more at higher temperatures and this is responsible for the lack of regain in such tests.

Chu et al. (2004) use the diffusion data for the four temperature levels to provide a linear fit to the Arrhenius relationship (in Equation 2.16) of the form shown in Equation 2.18. The activation energy is calculated to be 12.141 kJ/mol K. Since a linear fit is achieved, it is assumed in the published work that the material follows the same mechanisms of degradation, thereby allowing for use of the acceleration procedure proposed by Linderhand et al. (1981) and Proctor et al. (1982) wherein the results are used to predict service life at a given temperature (ambient temperature). This prediction of strength over a 50-year service life is illustrated in Figure 2.15.

$$\ln(k_d) = \ln(k_0) - \left(\frac{E_d}{R_m T}\right) \tag{2.18}$$

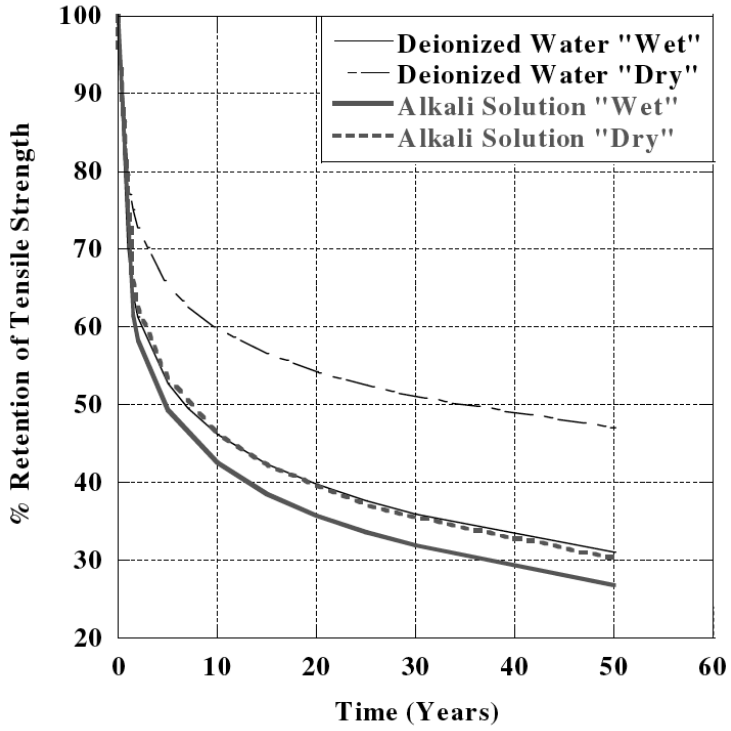

Figure 2.15 Comparison of tensile strength predictions by Chu et al. (2004) for both ageing in deionized water and in alkali solution (reconditioned and non-reconditioned are labelled as 'dry' and 'wet' in the plot)

The series of greatest interest regarding the focus of this review is the top line, which is formed from the diffusivity data relating to the reconditioned specimens after ageing in deionized water. Although this series, compared to the others presented, conveys material retaining a greater percentage of its tensile strength, it is predicted that the strength will drop by 50% after only 34 years. Initial loss of strength is predicted to be very rapid.

It is noted that there exists a shortage of literature concerning the effect of acidic conditions (acid rain) on the long-term environmental performance of GFRP. Alkali environments are the subject of a greater amount of testing, as they are used to emulate the conditions of GFRP rebar in concrete matrix, and the acidity is shown to influence the longevity of the material properties (Chu et al. 2004).

The studies of Chu et al. (2004) and Kotani et al. (2011) are both based on testing of glass/vinylester FRP composites. These studies present data from investigation using modern pultruded GFRP, and illustrate the principal effects and observable outcomes attributed to the various mechanisms of degradation. They also present the concepts of re-conditioning and regain, and results that consider the influence of this proven phenomenon. It is known that unsaturated polyester GFRP composite material does not exhibit durability performance as good as vinylester, which is generally only selected for fabrication of pultruded elements to serve in more aggressive or corrosive environments (Cabral-Fonseca et al. 2012).

Cabral-Fonseca et al. (2012) present a comparative study, measuring the durability performance of both pultruded vinylester and unsaturated polyester GFRP material following a variety of exposure conditions. The published study makes no prediction of how results would correlate with whole life performance over a realistic design life timescale, as Chu at al. (2004) does. Hydrothermal ageing (one of three means used by Chu at al. to perform accelerated ageing) was conducted in demineralized water, at several temperatures, and in salt water. Table 2.5 shows findings related to ageing by immersion in water, for both materials at various temperatures. The measures of subsequent performance are reported by results of mechanical assessment, the variation in T_g, and variation in mass over the 18-month duration of investigation. The two materials were also analised using Fourier Transformed Infrared Spectroscopy (FTIR). The specimens of new material were found initially to present very similar results. The intensity and localization of the peaks confirmed the presence of the ester group, as well as aromatic and aliphatic molecular structures, which are common in the chemical composition of both unsaturated polyester and vinylester. Post hydrothermal exposure, FTIR showed that no appreciable chemical degradation had occurred in either material. Degradation was attributed to mainly physical phenomena, namely plasticization (Cabral-Fonseca et al. 2012). In this respect the essential mechanisms of degradation for the two materials are of the same form.

Table 2.5 Summary of properties variation exhibited by material after 18 months hydrothermal ageing. Extracted from Cabral-Fonseca et al. (2012)

Properties	Unsaturated Polyester			Vinylester		
	Temperature of hydrothermal bath					
	20°C	40°C	60°C	20°C	40°C	60°C
Mass variation (%)	1.33	1.28	N.A	0.49	0.52	0.77
T_g Retention (%)	84	98	108	89	95	96
Strength retention (%)						
Tension	91	83	60	108	88	62
Flexure	95	82	69	82	87	58
Shear	87	72	58	101	77	59

It is observed from Table 2.5 that the mass (water) uptake of unsaturated polyester (UP) and vinylester (VE) are very different; for similar ageing conditions the VE material exhibited considerably lower uptake. (The PE specimens at 60°C was not reported by Cabral-Fonseca et al. (2012).)

The authors report an initial reduction in the T_g of the UP specimens, followed by a subsequent increase. It is concluded that this is caused by an initial onset of plasticization, but then offset over a longer period (to the max 18-month duration) by the occurrence of resin post-curing, particularly at higher temperatures, as evident in Table 2.5. These competing phenomena were less evident in the VE material.

Immersion in water at 20, 40 and 60°C significantly affected the mechanical properties of both materials. 'In general for the different types of loading, after a rapid strength decrease, a stabilization trend started to be observed' (Cabral-Fonseca et al. 2012). After the full 18-month duration observed, the strength of the UP and VE material was reduced to 60 and 62% in tension, 69 and 58% in bending, and 57 and 59% in shear. The study by Cabral-Fonseca et al. (2012) did not measure properties of the VE and UP materials related to mechanical stiffness. Considering the increase in T_g observed for the UP at longer durations, the influence that post-curing of the resin (the cause attributed,) could have on the composite would be a useful further finding.

Upon inspection of Table 2.5 it can be seen that at lower temperatures the VE outperforms the UP in terms of mechanical strength, though at higher temperatures,

representative of longer term ageing, the PE is performing to a similar standard in strength in tension and shear as VE, and surpassing VE in flexure. An increased capacity in flexure could be accounted for by increased post curing of the PE matrix, evidenced by the increased T_g. Flexure is the only test where a significant portion of the matrix is working in compression, where fracture of the polymer matrix is avoided.

Purnell at al. (2008) predicted that the half-life (the time taken for strength to be reduced to half of its original value) of GRP samples would be approximately 80 years at 20^{o}C. The study targets a number of GRP and GRC composites. It concludes however that the broad range of activation energies derived suggest each composite must be modelled separately. The model for GFRP samples aged under combined strain and hydrothermal loading, does however yield the outcome that a threshold value for strain exists between 30% and 45% of ultimate capacity (Purnell at al. 2008). The shortage of studies reporting experimental verification of this type of ageing hinders validation.

The Canadian research network: Intelligent Sensing for innovative Structures (ISIS), has produced notable works which do report on FRP naturally aged over 20 years. The majority of this research however is concerned with CFRP for retrofit and strengthening of RC structures, for instance the work of McCuiag et al. (2010), or the durability of GFRP reinforcement within the environment of concrete matrix (Robert and Benmokrane 2010). The Canadian federal Interest in FRP (Heffernan 2002) highlighted these areas as of importance to regenerate a waning infrastructure. Though whilst significant research was conducted in response, the influence of UV on naturally-aged wholly polymeric elements remains less well understood.

2.2.3 Temperature in isolation

The fundamental nature of the glassy material (inc. polyester) is that it conserves a state of liquid-like disorder but with solid-like properties. This is the result of the vitrification process occurring from either a supercooled liquid state in materials that can crystalize but do not in the specific conditions of interest, or from an equilibrium liquid state in the case of materials that cannot crystalize, as is the case for many polymers.

In high performance applications the properties of polymers may be constantly evolving because they are generally used at high fractions of their glass transition temperature, T_g. Even at ambient conditions of 25°C (298 K), this leads to the material being used at greater than 70% of its T_g, and hence temperature variations around this ambient value cause physical changes (Pochiraju et al. 2012).

Accelerated ageing programmes impose freeze-thaw cycles, as well as cycles in subjecting material to UV and varying conditions of moisture, to replicate the combined factors which cause the polymer composite to age in service (Wu and Yan 2011; Carra and Carvelli 2012). The work of Carra and Carvelli (2012), where freeze thaw cycles are incorporated in to a programme exploring the synergistic effects of exposure to UV irradiation, moisture and temperature on the mechanical properties. The authors did not report the pH of the ageing environment.

2.2.4 Chemical ageing

Much research exists addressing the response of polymer composites to conditions replicating service where the material is in contact with de-icing salts, or the alkaline environment experienced by concrete reinforcement bars. Chu et al. (2004) demonstrated how hydrothermal ageing in an alkali environment was more detrimental to mechanical properties measured on withdrawal of specimens, and also that the 'regain' exhibited by the material upon 're-conditioning' did not occur to the same extent. Cabral-Fonseca et al. (2012) established that demineralized water was more aggressive than salt-water solution because of the enhanced osmotic effects; as demineralized water is free of solute ions, its molecules can diffuse faster through the GFRP material.

Because the application in facades will not result in the material coming into significant contact with either of these environments, focus has been placed elsewhere, on models for damage that consider mechanisms of degradation influenced by the other factors listed.

2.2.5 Testing of modern GFRP pultrusions

Due to advances in manufacturing techniques of composite materials, newer GFRP products are far superior to those produced 7-10 years ago with respect to mechanical properties and durability. In addition, durability test techniques lack standardization, thus subjecting the material to environmental conditions far more extreme than will ever be encountered under actual field conditions. Therefore earlier durability research serves to understand the degradation mechanisms, while recent research identifies more meaningful material behaviour under realistic field conditions (Pochiraju et al. 2012).

Carra and Caravelli (2012) present a study using modern pultruded GFRP exploring the synergistic effects of exposure to UV irradiation, moisture and temperature fluctuations on the mechanical properties. This work incorporates replication of a continental freeze-thaw environment into the ageing programme by temperature fluctuation. It does not however, as with previous work reviewed above, investigate the influence of an applied stress throughout the ageing process. For a material that exhibits a propensity to creep, this is assessed as vital further work in this field.

Carra and Carvelli (2012) describe a climatic chamber that generates warm cycles, between 20 and 60^{o}C that complete over 8-hour periods, and cold cycles between -20 and 20^{o}C. These cycles are run alternately for 21 times (one week) each, for a total of 8 weeks (168 cycles). The relative humidity is held at 80% during the warm cycles and 90% during the cold cycles. UV irradiation was incident at 350 nm wavelength, at 40 W/m^{2} intensity. Lamps were switched on, then off, alternating in 12-hour intervals, throughout the duration of the test.

The subsequent material properties have been determined by conducting mechanical testing, measuring the tensile strength and stiffness, the flexural strength and stiffness and interlaminar shear strength. Furthermore, results have been obtained for the material in both the principal (0^{o}) direction, and in the direction perpendicular to main fibres (90^{o}).

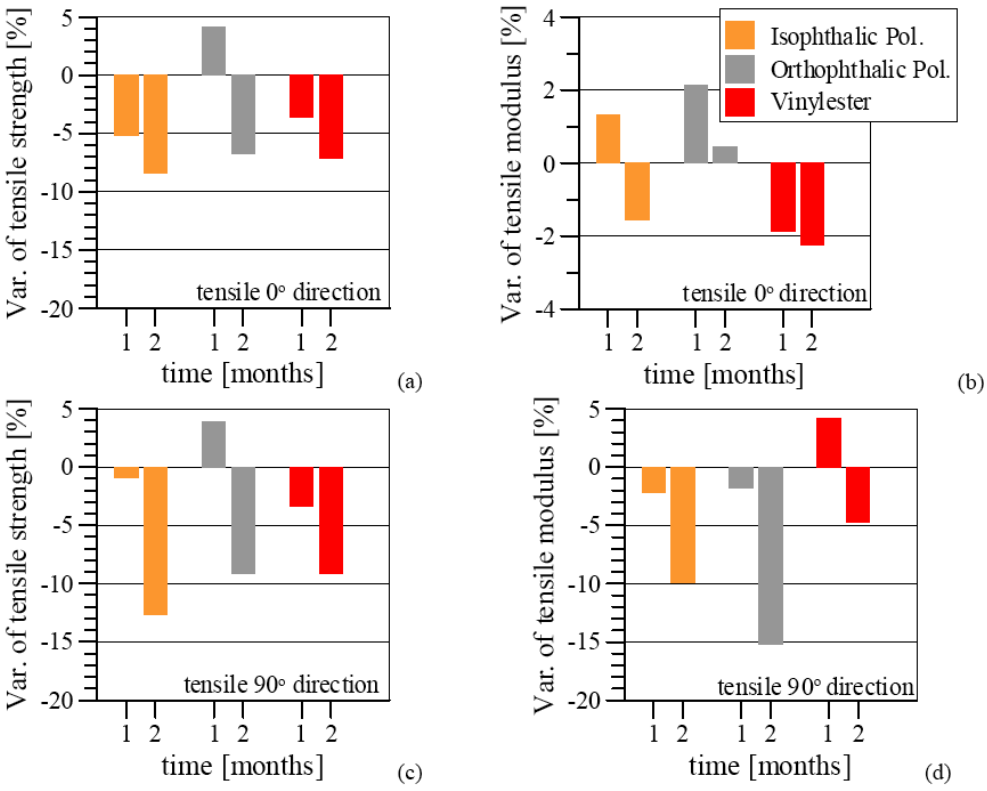

Figure 2.16 Results of tensile tests. Variation of the tensile strength (a,c) and of the tensile elastic modulus (b,d), for fraction in 0^o (a,b) and 90^o (c,d) (Carra and Carvelli 2012)

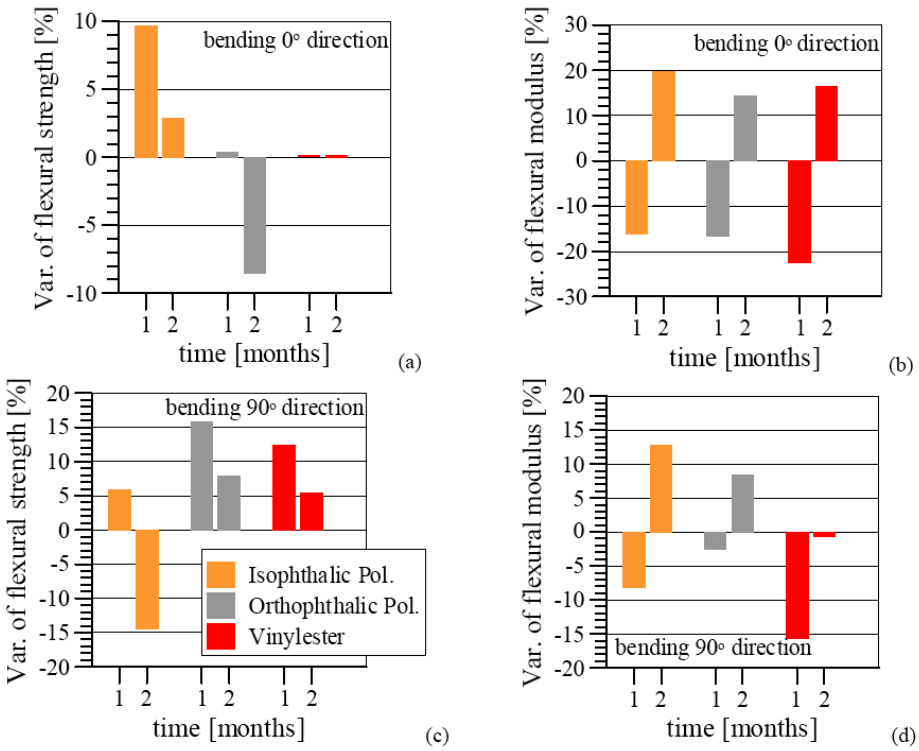

Figure 2.17 Results of flexural tests. Variation of the flexural strength (a,c) and of the flexural elastic modulus (b,d), for bending in 0° (a,b) and 90° (c,d) (Carra and Carvelli 2012)

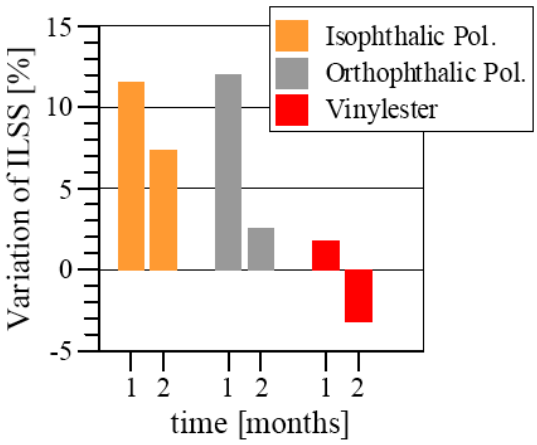

Figure 2.18 Results of inter-laminar shear tests. Variation of the inter-laminar shear strength in the 0°direction (Carra and Carvelli 2012)

The orange bars in the bar charts above represent the performance of GFRP composite pultruded using unsaturated polyester isophthalic resin. This material will be the focus of review. After two months of ageing induced by the cyclic factors described above, it can be seen in Figure 2.16 that the tensile strength and modulus of the material has

decreased. An 8.5% reduction in tensile strength of the material when tested in the principal fibre direction is a significant reduction. As detailed above, both Qiu and Gu (2011) and Cabral-Fonseca et al. (2012) reported a reduction in the ultimate tensile strength of polyester GFRP specimens as a consequence on UV irradiation alone. Cabral-Fonseca et al. (2012) also reported a reduction in tensile strength as attributed to only hydrothermal ageing, at 60^{o}C over an 18-month period, of 40%, as presented in Table 2.5 in Subsection 2.2.2.

Carra and Carvelli (2012) found that the strength in the transverse direction decreased by a larger amount, though the resin contributed to a larger proportion of the strength in this direction initially anyway, so a larger reduction is expected.

In the principal direction Carra and Carvelli (2012) discovered stiffness to be only slightly diminished, exhibiting less than a 2% reduction. Reduction in tensile stiffness, as attributed to solely UV influence, has not been reported by any of the above studies. However, Kotani et al. (2011) have reported a small increase in tensile stiffness following 1000 hours of hydrothermal ageing, though this was for vinylester resin.

The results of flexural tests are shown in Figure 2.17. After two months artificial ageing the characteristics relating to flexural performance have shown better retention than those of purely tensile nature. In the principle direction, the strength has shown to increase slightly (3%), but the modulus increased by 20%. In the weaker secondary fibre direction however, a small increase in modulus was observed, but a much larger decrease in flexural strength. These findings support an earlier discovery in Subsections 2.2.1 and 2.2.2, that flexural testing picks up an ageing-related change in the material, not captured to the same degree by measurements of other mechanical properties. This is seen in the chart from Cabral-Fonseca et al. (2012) presented in Figure 2.7, where UV irradiation is shown to cause an increase in flexural stiffness of the polyester composite, whilst the tensile strength and inter-laminar shear strength are seen to reduce.

Carra and Carvelli (2012) found the inter-laminar shear strength to have increased by 7% after 2 months of artificial ageing. Cabral-Fonseca et al. (2012) reported a decrease in inter-laminar shear strength of 10% after 3000 of UV exposure, but a quite severe

reduction in shear strength, of 42% at 60°C, after 18 months hydrothermal ageing.

Carra and Carvelli (2012) is a preliminary report on a longer term durability study; the paper makes no attempt to correlate the initial findings, after 2 months of ageing, to real life performance of the material over a number of years in service.

2.3 Foam and other core materials

2.3.1 Material properties

Table 2.6 Properties of various core materials

Material			k-value (W/mK)	C_v (J/(kg.K))	ρ (kg/m^3)	Manufacturer/ brand name
Function	Name	abbrv.				
Structural skin	*glass FRP (vinylester)*	GFRP	0.25	1880	2020	Fiberline
Foam Cores	*polyurethane*	PU	0.022	1400	40-55	Baxenden
	polyetherimide	PEI	all vary too widely			
	styrene acrylonitrile	SAN	all vary too widely			Gurit Corecell
	exp. polystyrene	EPS	0.035	1400	25	
	extr. Polystyrene	XPS	0.035	1500	28-45	
	polymethacrylimide	PMI				EKM Plastics
	polyvinylchloride	PVC	0.033	1600	60-150	Diab
	polyisocyanurate	PIR	0.022	1450	35-65	Celotex, Dow, Bayer
	phenolic foam	P	0.04	1400	80-160	
Wood Cores	*balsa*	B	0.05	2900	90-220	Alcan Baltek
Honeycombs	*polypropylene*	PP	0.102		64	
PCMs for thermal inertia	*sodium silicate*	SS	0.8	3830	1450-1600	Palusol
Aerogels for insulation	silicon dioxide nanostructure	AG	0.016	700-1150	70-90	Cabot

Different foam chemistries can be further divided into many different densities, each produced with properties as required by design. This can make determining the most suitable foam type for sandwich panel application very difficult, as there are many options available that can be produced to result in a product with the desired characteristics. The most economical foam is not always explicitly clear; the increased tonnage of the material will, in a heavy use application such as façade sandwich panels drive down costs, especially for products which are not currently as widely used.

Table 2.6 shows a range of possible core materials used in sandwich panels with the pertinent material properties information alongside, for those relevant to selection in

FRP building façade application. Nominal values are shown where a range is not given. PIR foam has emerged as a suitable candidate. Its k-value is about half that for a generic rock wool insulation and mechanical properties can be achieved as required within a reasonable range of densities. PIR has the benefits of PU but with lower flammability. PIR foam has clear benefits over established systems, especially in terms of the smoke it develops when burnt. Metal-faced panels tested according to the DIN EN 13823 Single Burning Item test have been shown to achieve a B-s0, d1 classification, representing the lowest class of smoke toxicity that is produced and no flaming droplets. Good shear resistance at the interface with a structural FRP sheet can be achieved by self-adhesion upon foaming action and setting of the PIR chemical compound.

Some worthwhile observations can be made with respect to Table 2.6. Firstly it can be noted that the density of FRP shown is for a 60% fibre volume content. More importantly, though, are the merits of the different foam core materials. Polyurethane is a suitable foam for sandwich panel construction though it is highly combustible. Whilst the polystyrene products exhibit better mechanical properties, the thermal transmission coefficient cannot compete with PIR. They do have good fire performance characteristics, and DIN 4132 accreditation can be awarded to XPS, as hardly flammable at all.

Two high-performance foam cores used mainly in aviation and specialist applications are PUR and SAN. Though SAN finds some application in the Civil/Structural sector, it does remain an expensive option, and the mechanical properties offered could not justify use in façade sandwich panel application. The strength and shear stiffness is not as good as PU.

PMI foam can achieve very good mechanical properties, but expense limits use in civil/structural application. PVC foam is used in the sector, though it is not a very environmentally friendly material, and has already attracted attention from environmentalists in the past when proposed as the membrane envelope for the Millennium Dome project in London. Although a favourable material concerning mechanical capabilities, acceptance in mainstream office building retrofit is unlikely because the density-to-thermal-performance ratio still cannot compete with PIR. Other

core materials, balsa and polypropylene honeycomb are included in Table 2.6 for reference though not examined further.

Phase Change Materials, or PCMs, possess extraordinary properties capable of enhancing the thermal performance of a building envelope, principally by virtue of their impressive specific heat capacity in relation to their density. One drawback of many of these materials is that they are highly combustible. However, this is not so for sodium silicate, which in fact finds its main application in buildings as an intumescing layer or strip. Palusol, a brand name for a sodium silicate panel, manufactured by BASF, has a specific heat capacity of more than double that of GFRP, though with a density of only about two thirds. The intumescing compound is supported in a mesh of textile-glass fabric and requires support, which is offered by a different panel layer, for instance by stapling the board/fabric to chipboard. Due to the existing common use of Palusol as a powerful intumescent, there are critical challenges facing transfer to design use for improving thermal inertia. Currently the products are manufactured with up to 4.2 mm in thickness, but will expand perpendicular to the panel face by 6 times upon fire heat activation. The possible pressure that can be exerted during this phenomenon may be up to 1.5 MPa. Consideration of this effect on structural integrity would therefore be necessary before incorporating the fabric/board into a composite façade panel.

Aerogels are another innovation in material development attracting attention amongst building environmental engineers. The appeal here is the thermal insulation to density ratio. Derived from silica gel by moisture extraction, the result is a compound of silica dioxide. Cabot's 'nanogel aerogel' holds a Silver 'Cradle to Cradle' certification from McDonough Braungart Design Chemistry, claiming that their product, which is derived in a closed loop process, has little to no environmental impact. A host of other applications are proposed for the product/material though there are plentiful examples of current use as insulation in both pioneering and mainstream buildings. Expense and fragility have proven problematic for the development and acceptance of the technology. The insulation is still an expensive option, though by casting the silica gel around polyester fibres, a reinforcing skeleton is offered to the brittle silica dioxide compound.

Globally, incorporation of aerogels into composite panels is observed to be nearly always where daylighting is required, with the panels concerned used almost in a glazing role. Full replication for use as glazing in the traditional sense is prevented due to the fragility of the material. It is still of great interest to the façade engineer to admit diffuse daylight yet afford excellent insulation. A range of GFRP panels filled with aerogels are marketed and a resulting k-value of 0.02 W/mK is yielded.

Examples of aerogel matting products can be seen below. Figure 2.19 shows the scheme to improve the u-value of a vaulted gridshell structure. The 20 mm thick product used has minimum impact on the overall envelope thickness. Self-supporting panels are also seen in industry though take the form of matting adhered to plasterboard, chipboard, ply or fermacell. (A plasterboard substitute used where thickness is critical.) Figure 2.20 shows a façade undergoing retrofit by installing 10 mm thickness fabric aerogel matting. Note that in this 'overclad' retrofit application, the supplier specifies that natural breathable plasterboard and internal finishes were necessary to allow entrapped vapour to breath through the wall. (Aerogel is hydrophobic and will not permit transport of moisture in the outwards direction as modern building felts are now designed to do).

Figure 2.19 Vault enclosure featuring aerogel membrane at London Imperial War museum (pic. credit: Aspen aerogels)

Figure 2.20 Façade retrofit using aerogel mat for small scale domestic (pic. credit: Aspen aerogels)

2.3.2 Manufacturing considerations for sandwich panels

With the reasoning behind maintaining a focus on pultruded FRP sheets already stated, there are some sandwich panel fabrication methods that can be immediately discounted. The use of through-thickness fibre 'pins' (sometimes called 3D or Z Pins) is only possible with hand lay-up panels, so it is not within the scope concerned with utilizing pultruded sheets. The design features of such 'pins' have been researched in their capacity to provide additional shear stiffness in an otherwise flexible foam core. A brief summary of the findings follows.

Some work involving the pin reinforcement concepts seems to address design properties that might be of less importance to façade application. For instance, an improvement in through-thickness compressive strength offered by carbon fibre and titanium pins has been verified and explained (Cartie and Fleck 2003) whilst other studies have explored the properties of a composite element where pins are included as a constituent part to combat delamination (Reis and Rizkalla 2008). It has been demonstrated that carbon fibre pins do successfully improve some properties of foam core sandwich panels, however increase in shear collapse load is only slight (Long et al. 2008) and they are an expensive feature.

Injection into GFRP sheets, held apart at chosen panel thicknesses, or bonding GFRP sheets to preset foam cores are two conflicting ideologies that remain for panel production. Working with pultruded GFRP sheets, the styrene resistance of the foam is less of an issue, especially in the case of foam injection, but true also for resin bonding to the core material. A resin can be selected that is appropriate to the foam without impinging on choice of polymer within the GFRP sheet, i.e. vinylester or phenolic resin. Capacity for self-adhesion of PIR foam upon foaming action has been researched through efforts to address the capabilities of water blown PIR, in relation to the more commonly used, but less environmentally friendly HCFC-141b variety (Naruse et al. 2002). It has been shown that adhesion strength higher than that seen in CFC blown foams can be accomplished with water blown foams though a very slight drop in thermal resistance is observed in the resulting foam block.

2.4 Facades

2.4.1 Structural Integrity

Some principal properties of the GFRP material allude to problems with structural applications where the composite might be taking a high permanent action (i.e. gravity loading). The susceptibility of GFRP to creep, and to stress relaxation of friction-based connections remains problematic, restricting many options for point-fixing methods.

In assessing the structural integrity of existing facades and novel façade systems in prototype, the following study has proven useful. To determine internal actions in a unitised curtain wall façade element, the need arises to develop a means to acquire data on structural properties without full knowledge of the materials used, and without access to advanced analysis software akin to that used for the original design.

Using the Navier solution for plate bending, a group of material, and geometrical variables of the ‘plate’, can be determined in a ‘fuzzy’ fashion. Assuming the initial design specification for deflection of the unitised façade panel and the appropriate loading achieves this. This ‘calibration’ yields an expression for plate stiffness. Classical plate theory is then applied from first principles to calculate the actions and internal stresses out of plane at various locations in the unitised façade panel.

The concept of assigning a value to a group of variables, where no absolute value can be determined for any one variable can be considered analogous to imaginary numbers, where i can be used to generate real results without ever being defined in any more precise terms than as the square root of negative one.

Methods exist to determine the stresses around small openings in plates under uniform loading out of plane. This is one application of this theory as it might be in such locations that stresses are critical. It is envisaged that this method will serve to assess stresses transferred between constituent composite sandwich panels. Additional benefits offered by the approach outlined, include the option to apply it easily anywhere in the panel, and on panels were exact properties are not known, or even, where the properties cannot be determined in the manner necessary for use in classical plate theory for homogenous cross sections. That is, in attempting to accommodate the analysis of composite foam core sandwich panels for instance, it can be appreciated that in much classical theory, for each of the constants of v, t_p and E and G there can be no meaningful single value assigned because the panel is not made of homogenous isotropic material of thickness t_p, but a series of layers of different materials.

The design check chosen for the purpose of illustrating this method is for shearing at the boundary marked in Figure 2.21, a region tolerating high torsion.

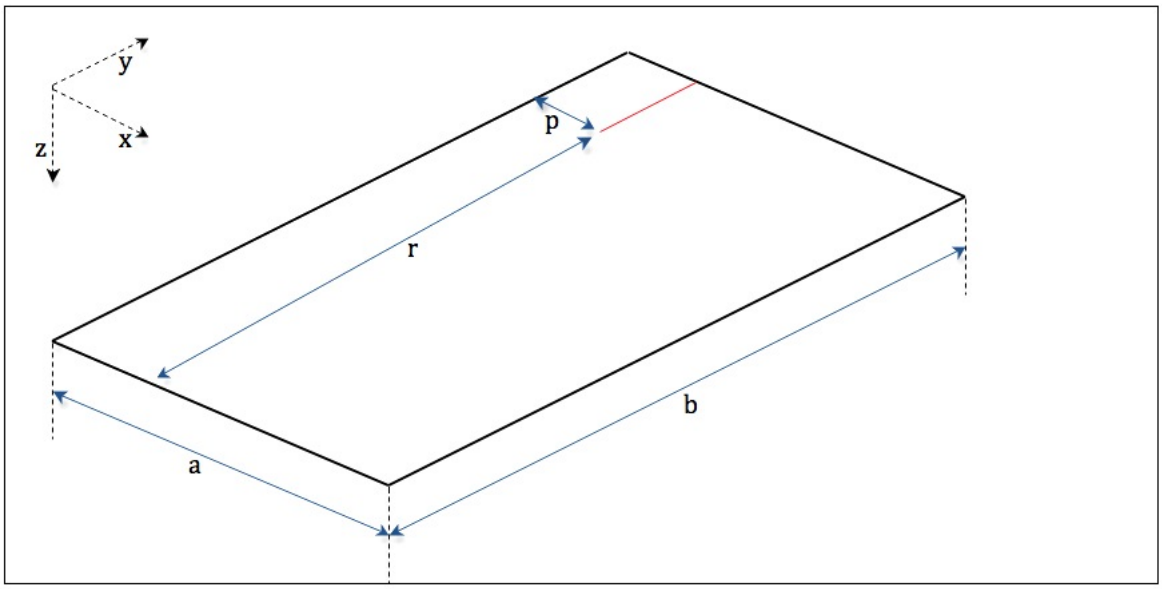

Figure 2.21 Geometry of facade panel

The panel shown in Figure 2.21 is to be treated as an entire plate; where by loading is taken across the entire panel area and internal stresses are such as for a plate of continuous stiffness. (I.e. the provisos noted above should be observed.)

2.4.1.1 Torsion across critical location

The required value can be expressed initially by Equation 2.19 (Chandrashekhara 2001).

$$\int_r^b M_{xy}\Big|_{x=p} dy = \int_r^b D(1-v)\frac{\partial^2 w}{\partial x \partial y} dy\Big|_{x=p} \tag{2.19}$$

The variable for stiffness of our panel is the parameter *D* as defined by classical plate theory (Chandrashekhara 2001), however it is not possible to assign meaningful values to the variables *v*, *t* and *E* and *G*. Thus Equation 2.20 is not useful, and the value of *D* must be approximated by some other means. The method by which *D* is defined below can be described more accurately as a 'calibration', using original design constraints for deflection imposed by codes of practice and typical design loading.

$$D = \frac{Et^3}{12(1-v^2)} \tag{2.20}$$

Using deflection limit criteria (along with typical factored design loading *q*) to calibrate the value for *D*, is considered appropriate for this type of construction because it will usually be this design check that is limiting to the overall unitised panel design, as opposed to ultimate strength. The expression above for D is only true for a rectangular cross section.

2.4.1.2 Using the Navier solution to determine 'fuzzy' *D*

Inherently the values of *E, t* and *v* are also fuzzy but never of any concern to the methodology. Equation 2.21 shows the solution in general form when the 'plate' is simply supported on all four edges and sides of length *a* and *b* are used for consistency.

A façade panel supported on four edges will experience a degree of moment resistance at connections. Thought as explained in Chapter 5 the stiffness of connections decreases over the life of the element and a simply supported state is a closer approximation, and a conservative means by which to assess internal actions in the panel

$$\nabla^4 w = \frac{q}{D} \tag{2.21}$$

Assuming the deflected shape of the plate as a sine curve for a simply supported case, i.e:

$$w(x,y) = w_{centre} \cdot \sin\left(\frac{\pi x}{a}\right) \cdot \sin\left(\frac{\pi y}{b}\right) \tag{2.22}$$

It can be shown that D is related to central deflection by (derivation of this result is not included in this report):

$$w = \frac{q \cdot \sin\left(\frac{m\pi x}{a}\right) \cdot \sin\left(\frac{n\pi y}{b}\right)}{D\pi^4\left(\frac{m^2}{a^2} + \frac{n^2}{b^2}\right)^2} \tag{2.23}$$

The first mode, where m and n are equal to 1 is chosen to reflect the first mode shape, which is appropriate for the simply supported deflection seen under lateral loading. This can be further simplified for central deflection by substituting x and y as equal to $a/2$ and $b/2$ respectively. Thus resulting in Equation 2.24 shown below:

$$w_{centre} = \frac{q}{D\pi^4\left(\frac{1}{a^2} + \frac{1}{b^2}\right)^2} \tag{2.24}$$

Making D the subject of the formula, and expressing the central defection in terms of the limit stipulated by codes of practice (largest dimension, b, over 175, for instance), Equation 2.25 is produced. Note that the afore-mentioned calibration taking place, to yield 'fuzzy D', is done so in this step, but to remain operating in general terms for the purpose of this paper, a constant χ will be utilised to express the part of the ratio of deflection, of the longest orthogonal dimension permissible. (i.e. the value 175 suggested above.)

$$\tilde{D} = \frac{q_{factored} \cdot \chi}{b\pi^4 \left(\frac{1}{a^2} + \frac{1}{b^2} \right)^2} \tag{2.25}$$

Where $q_{factored}$ is the design factored loading in kN/m^2.

An expression for fuzzy D given by Equation 2.25, and the required partial differentiation performed on Equation 2.22, can be substituted into Equation 2.19. Remembering that the central maximum deflection is now to be expressed in terms of b, and χ (which in the step below, cancels out).

$$\int_r^b M_{xy}\Big|_{x=p} dy = \int_r^b D(1-\nu) \frac{w_{central}\pi^2}{ab} \cdot \cos\left(\frac{\pi x}{a}\right) \cdot \cos\left(\frac{\pi y}{b}\right) dy \Bigg|_{x=p} \tag{2.26}$$

is shown to reduce to:

$$\int_r^b M_{xy}\Big|_{x=p} dy = \int_r^b \frac{q(1-\nu)}{ab\pi^2 \left(\frac{1}{a^2} + \frac{1}{b^2} \right)^2} \cdot \cos\left(\frac{\pi x}{a}\right) \cdot \cos\left(\frac{\pi y}{b}\right) dy \Bigg|_{x=p} \tag{2.27}$$

Performing the integration results in obtaining the following:

$$\int_r^b M_{xy}\Big|_{x=p} dy = \left[\frac{q(1-\nu)}{a\pi^3 \left(\frac{1}{a^2} + \frac{1}{b^2} \right)^2} \cdot \cos\left(\frac{\pi x}{a}\right) \cdot \sin\left(\frac{\pi y}{b}\right) \right]_{y=r}^{y=b} \Bigg|_{x=p} \tag{2.28}$$

It can be seen that maintaining a generalised approach has illustrated the role of the design deflection of the unitised façade element. For this methodology to be relevant the critical design criteria for the façade must be large span deflection, though the absolute value of the deflection constraint, represented by χ, is of no consequence to the results it yields.

Equation 2.28 can be considered a general result as far as the internal action of torsion is concerned, across a *y*-direction boundary where the cumulative extent of the torsion observed is proceeding for some point at $y=r$ to the edge of the plate (with higher *y* value). For sake of completeness, the corresponding equation for torsion across an *x*-direction boundary is shown below by Equation 2.29.

$$\int_{p}^{a} M_{xy}\Big|_{y=r} dx = \left[\frac{q(1-\nu)}{b\pi^3 \left(\frac{1}{a^2} + \frac{1}{b^2} \right)^2} \cdot \sin\left(\frac{\pi x}{a} \right) \cdot \cos\left(\frac{\pi y}{b} \right) \right]_{x=p}^{x=a}\Bigg|_{y=r} \tag{2.29}$$

It can be seen by Equation 2.20 that *v*, along with *t* and *E* are related to *D*, and as such are also fuzzy. It is suggested, for composite sandwich panels, and thus adopted for the purpose of the numerical example presented simultaneously with the general mathematics in this paper, that the Poisson ratio used is that for the foam. This is justifiable on two premises: (i) a lower *v* is more critical for the end result. (ii) Although the influence of *v* is generally greater near the through-thickness extents of a plate, regarding in-plane stresses, and overall plate stiffness, (which has already been determined,) the torsion and shear strains will be dictated more by the effect of the section as a complete composite, encompassing the foam as a significant part.

The total torsion across the marked boundary is determined using Equation 2.19 and taking *v* to be 0.1 (typical average value for PIR foam). It is not only shear due to torsion along the marked boundary that a connection located here will need to withstand. The direct shear borne by the connection must be considered too. It must be

noted, importantly, that both actions/effects must be considered and summed; The shear force calculated below is not related to the shear from the torsional moment found above by $S=dM/dl$, as direct shear in the plane examined and associated with the marked boundary is exhibited as a result of the variation in moment in the perpendicular orthogonal direction.

2.4.1.3 Direct shear across critical location

The required value can be expressed initially by Equation 2.30.

$$\int_r^b Q_x \Big|_{x=p} dy = \int_r^b -\tilde{D}\left[\frac{\partial^3 w}{\partial x^3} + \frac{\partial^3 w}{\partial x \partial x^2}\right] dy \Big|_{x=p} \tag{2.30}$$

The expression for Shear Q in this equation is derived from free body equilibrium of a plate in the same manner as Equation 2.10 and is not derived in this work. By performing the necessary partial differentiations on Equation 2.22, which defines the deflected shape, the direct shear across the critical location can be expressed thus.

$$\int_r^b Q_x \Big|_{x=p} dy = \int_r^b \frac{\tilde{D} w_{centre} \pi^3}{a} \cdot \cos\left(\frac{\pi x}{a}\right) \cdot \sin\left(\frac{\pi y}{b}\right)\left[\frac{1}{a^2} + \frac{1}{b^2}\right] dy \Big|_{x=p} \tag{2.31}$$

Again, substituting expression for fuzzy D and w_{centre}, the following general equation is produced. Note that cancelling of χ occurs together with a single set of the brackets from Equation 2.25.

$$\int_r^b Q_x \Big|_{x=p} dy = \int_r^b \frac{q}{a\pi\left(\frac{1}{a^2} + \frac{1}{b^2}\right)} \cdot \cos\left(\frac{\pi x}{a}\right) \cdot \sin\left(\frac{\pi y}{b}\right) dy \Big|_{x=p} \tag{2.32}$$

Performing the integration results in obtaining the following.

$$\int_{r}^{b} Q_x\Big|_{x=p} dy = \left[-\frac{qb}{a\pi^2\left(\frac{1}{a^2}+\frac{1}{b^2}\right)} \cdot \cos\left(\frac{\pi x}{a}\right) \cdot \cos\left(\frac{\pi y}{b}\right) \right]_{y=r}^{y=b}\Bigg|_{x=p} \tag{2.33}$$

Equation 2.33 can be considered a general result as far as shear is concerned across a *y*-direction boundary where the cumulative extent of the shear observed is proceeding from some point at which *y=r* to a point with *y=b*, in this case the edge of the plate. For sake of completeness, the corresponding equation for direct shear across an x-direction boundary is shown below by Equation 2.34.

$$\int_{p}^{a} Q_y\Big|_{y=r} dx = \left[-\frac{qa}{b\pi^2\left(\frac{1}{a^2}+\frac{1}{b^2}\right)} \cdot \cos\left(\frac{\pi x}{a}\right) \cdot \cos\left(\frac{\pi y}{b}\right) \right]_{x=p}^{x=a}\Bigg|_{y=r} \tag{2.34}$$

As for the case in Equation 2.17 and Equation 2.18, it must be observed that the sum of the action deduced across this boundary is not evenly distributed. Consideration must be given to this in deciding over what size increment to perform the analysis (i.e. it could be broken up into smaller integrations.) The distribution of direct shear across the boundary marked in Figure 2.21 for instance could be conservatively assumed as linear regarding stress at the inner most point calculated from the total force transferred.

2.4.1.4 Prospective application

As routine, classical plate theory carries many stipulations, but the fundamental reasons for its use, are that one may consider an element spanning in two orthogonal directions, and account for the interaction of stress and strain at material level in those two perpendicular axis, and the influence this bears to stiffness.

FRP skin/foam core sandwich panels can span in two directions, and for application of the procedure in this study would need to be of the same material cross section and modulus in those two directions also entirely possible. The interaction of strains at material level in plate bending is less easily represented by the mathematics, though by assuming some information about the original design of the façade, a perfectly workable value for *D* (plate stiffness) can be recognised.

It can be appreciated that even at serviceability limit state the foam core of composite sandwich panels may require some retrospective assessment regarding out-of-plane shear, in panels formed by aluminum or FRP sheets bonded to an array of preset foam cores; either in the foam itself or at interfaces.

One could for instance shed light on material properties for a foam core found to have experienced crushing, when cited as part of a facade subject to high winds. (High out-of-plane service loads.) Or, if the size of preset foam core internal elements became limiting to the design of a large unitized façade panel, such checks at the interface of foam blocks, as illustrated by Figure 2.22, could prove vital.

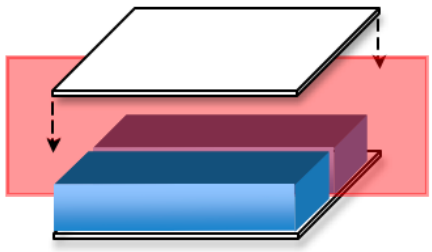

Figure 2.22 Possible application in foam core sandwich technology

2.4.2 Environmental control

Favourable u-values can be obtained using GFRP elements far more economically than good thermal inertia as this competes directly with a lightweight FRP solution. The Second Severn Crossing Visitors' Centre, a focus of study in Chapters 3 and 4, highlighted this as a problem, gaining too much heat in the summer months. One role of gel coats on FRP panels is in creating a reflective surface to combat solar heat gain, along with additional benefits of increased durability and aesthetic quality.

Any lightweight structure will require more controlled ventilation to maintain comfort than a corresponding heavyweight structure. Double skin envelopes have been implemented in the past to address the fluctuation of temperature in lightweight structures, though in retrofit of more heavyweight structures this is generally not called for, as there is sufficient thermal mass within the building.

The expense of sodium silicate or other PCM, specifically to reap significant rewards in retrofit for improving thermal inertia is therefore questionable. Palusol is currently only manufactured in thin sheets, because as previously mentioned, it is marketed as an intrumescent. Some current prototype applications for offering thermal inertia to building facades are being witnessed in the area of multilayer fabric facades. The fabric façade shown in Figure 2.23, developed by the Institute for Lightweight Structures and Conceptual Design – ILEK at the University of Stuttgart, comprises a PCM layer beneath an opaque element with pneumatic opening internally, and is enveloped by an insulative layer and weather resistant screen layer externally.

To ensure the heat sink (or what traditionally might be called the thermal mass) of the PCM is accessible, internal aesthetic finishes must ventilate or conduct internal office heat to this element to avoid ‘false ceiling syndrome’ – something that can make even heavyweight buildings behave in a very over-responsive manner.

Figure 2.23 Multilayer fabric façade comprising a PCM layer (ILEK)

With increase in the u-value of a panel, the arrangement of fixture becomes more significant regarding the thermal performance, where cold bridges would be of greater detriment. With increased thickness of panel (foam core sandwich for instance) it also becomes more difficult to fix the panels to a frame without inadvertently providing cold bridging. The thermal conductivity of GFRP is typically 0.2 W/mK, compared to 200 W/mK for aluminium.

2.4.3 Acoustic control

The concept of 'mass wall derived' sound enclosure would not be something desired in an office building, and not attainable by a lightweight façade in any case. Sound transmission, which by its very nature can shift the problem of a noisy environment whilst only alleviating ambient noise in the vicinity of the source, is also not desired where ingress of external, street and traffic noise is a problem.

To truly attenuate noise, the sound wave energy must be dissipated by viscous damping, usually achieved by interaction of the airwaves with open cell foam, and perhaps additional means to optimise this process such as Helmholtz cells. Of course, other strategies such as external reflectance, attention to reflectance angles around window

openings, and internal profiles that avoid focus points and standing waves, could all assume vital roles for the acoustic façade engineer.

Implications for GFRP skin / foam core sandwich unitized facade can be summarized as follows:

- Orthogonal panel dimensions and stiffness must not permit significant façade resonance at traffic noise frequencies.
- The option to include acoustic damping material internally, to dissipate and attenuate office noise, could be offered over the internal sandwich skin. But this must not effect on fire performance and thermal response.
- Any horizontally spanning elements above openings, typically possible at storey levels, must not act as reflectors directing street noise into offices.

An interesting concept discovered in a building survey, was found in the composite sandwich panels of a protected industrial building in Bath, - Farrell and Grimshaw's former Herman Miller factory - an industrial premises sited on the banks of the River Avon.

Figure 2.24 Farrell and Grimshaw's former Herman Miller premises in Bath

The construction detail of the sandwich panels on this structure is found to consist of two foam-filled regions separated by an air filled void in between. One of the air/foam boundaries is delimited by an internal FRP sheet, though the other has open cell foam

directly adjacent to the void. This design has the potential to attenuate noise in the same way as a Helmholtz resonator. Standing waves in the void will be brought past the open cell foam repeatedly, dissipating the airwave energy in cycles.

New super efficient sandwich panels developed in the aviation industry use a similar approach to afford good sound insulation, but in this application, as factory buildings, there is a more prescribed set of wavelengths to attenuate emanating from machinery of known operation frequency.

The application of a similar principle in retrofitted facades for medium/high rise office buildings is small however, as the thermal performance will be paramount to justifying the scheme, and connections, and sandwich construction may not be able to cater to such design intent; the clamped, panel housing connections in this industrial building would have facilitated resonance of the internal 'portion' under heavy vibration from within the factory environment. The panels in Figure 2.24 taper to single ply thickness (~5mm) at the edges and the neoprene gasket is not shielded from UV.

2.4.4 Sustainability

It has been concluded that until the waste flow of composite materials increases, as the materials become more mainstream in the civil/structural sector, the technology required to perform efficient recycling and safe disposal is being developed with only minimal incentive for progress (Goodship 2010).

Close reference to the recycling hierarchy must be observed as follows (Pickering 2009):

- Prevent waste
- Reuse product
- Recycle material
- Incinerate
    - With material and energy recovery
    - With energy recovery
    - Without recovery
- Landfill

Using advanced composites for retrofit, is, as a philosophy, inherently in accordance with the first choice item above by preventing the demolition and complete replacement of existing inefficient structures, and building in a prolonged design life at low environmental impact for an improved whole life performance. A unitised curtain wall system is also modular and has potential to find direct reuse in the same application if the building it enveloped became redundant.

Attention must be given to the recycling options that are available for FRP. Thermosetting plastics cannot be remolded, and the mixture of materials, especially with long fibres present, yields an additional difficulty. Firstly mechanical recycling can be considered. The processes of crushing by twin-screw shredders and hammer milling are intended to create fibre-rich recyclate, the hammer milling is labour intensive though provides scope for using evolved fibres as reinforcement in lower grade composites, and polymer matrix as powdered filler.

Thermal recycling is typified by two aims: to separate the constituent parts of a composite, and to recover energy in the process. Normally the methods employed follow on from some means of mechanical shredding to improve handling and increase surface area.
It is noteworthy that most current research in this area is researching the use of carbon fibre recycling methods, as there is greater financial incentive, though compatibility of GFRP as a fuel for cement kilns is a pleasing coincidence. Disposing of GFRP in this way provides glass fibres and fillers to contribute to the cement whilst the burning polymer fuels the kiln energy demand.

The simplest means of obtaining clean fibres, separated from the polymer, is by burning in the presence of air. The fluidised bed process is one possible option that is very tolerant of contamination/mixed materials but is currently only feasible for CFRP, as a consequence of carbon's higher melting temperature.

Pyrolysis processes, which heat in the absence of air, must avoid char on fibres by controlled atmosphere and subjection of the chamber contents to microwave radiation. Thermal-Fluid Processes introduce the scrap FRP into the chamber with a supercritical fluid (propanol). After expelling the fibres the resulting fluid is used for an array of

chemical products, and fibres are clean and of high grade. Developments in this area are once again only for CFRP.

The main issues with all the thermal methods concern the retention of tensile strength. The modulus is relatively unchanged, which for structures is the more critical part, with serviceability often dictating design. Some retention of fibre architecture is achievable using continuous pyrolysis processes, but otherwise fibres are generally short, (of fluffy bunched character,) and of variable length distribution.

In the development of composites in construction, there needs to be bespoke applications developed with specific waste available (Pickering 2009). Currently recyclate from the mechanical processes is commonly used for acoustic insulation and plastic timber reinforcement (George et al. 2000), and fibers liberated by thermal processes are suitable for surfacing veils, and for carbon fibre only, as electro-magnetic shielding material application forming faraday cages.

The UK FRP industry produces 240,000 tonnes of products a year with 11% of this for the construction industry (Conroy et al. 2006). 'The UK highway engineering industry shows a willingness to adopt alternative sources of material for use in road construction and thereby promote sustainable development. As road construction consumes vast quantities of natural materials, it has the potential to provide a suitable end-use for waste materials such as FRP. A project is aiming to improve the recyclability of composite building products by incorporating GRP waste composites into highway materials and conducting tests to ascertain whether they have a detrimental effect on the material performance. Preliminary findings have shown that the addition of shredded GRP off-cuts at 1% has had minimal effect on the performance properties of 20 mm dense bitumen macadam. The research is continuing, using higher proportions of shredded composite material.' (Conroy et al. 2006). A brief observation regarding design with end of life in mind is that resin bonding of elements is bound to antagonise a philosophy of reuse, as opposed to demountable mechanical connections. However, embedded metal fixings, used when resin bonding might be more appropriate makes it very inefficient to recycle, as these would need to be removed. Thus illustrated is the need mentioned above of developing facades with the intended end of life option for each component borne in mind at the time of design conception.

The Carbon Economy Britain enters in 2016 will result in further ever-present incentive and legislation to put sustainability at the forefront of any significant Civil works. In order to compare the carbon credentials of different materials, some important factors must be addressed: it is inappropriate for instance to compare figures for embodied energy on a kg for kg basis. Functional units relevant to the amount of material required to perform the set function should be used, and the design life of each material with maintenance required throughout its life also considered (Hammond and Jones 2008). For this reason Aluminum can provide a simpler comparison with FRP as compared to concrete, because in relation to concrete facades at least, the functional units are similar. Despite this however there remains an issue regarding 'feedstock energy'. Polymers, being petrochemical based materials, represent energy being used as a material and not as a fuel. The figures quoted below, as for all those in the Inventory of Carbon and Energy produced by Hammond and Jones (2008), are 'Cradle-to-Gate values'. The implication of which is that the feedstock energy of the polymer in FRP will exert greater impact on the resulting percentage difference, as energy/carbon attributable to transport, handling on site, and through design life to 'grave' are not included.

With reference to the values in Table 2.7, it should be noted that the higher feedstock energy possessed by FRP is of merit, as this embodied energy will never be realized as CO_2 in the atmosphere, but is locked into the material. This is not the case is the material is burned as part of a recycling method.

Table 2.7 Carbon and energy costing for GFRP and Aluminum

Material		Embodied Criteria	Units	Use-weighted Average	Virgin	Recycled	Comment
Rolled Aluminium		Energy	MJ/kg	155	217	27.8	-
		Feedstock contribution		13.8	20.6	0	
		Carbon	kg CO_2/kg	8.26	11.5	1.67	
GFRP constituents	Polyester	Energy	MJ/kg	103.83	all	none	no data for vinylester
		Feedstock contribution		45.7			feedstock of 44% assumed (average plastic ratio)
		Carbon	kg CO_2/kg	no data			-
	Glass Fiber	Energy	MJ/kg	28	no data		whilst there is scope to recylcle the glass for use in composites, in high end application, there is no known use of recycled glass in pultrusion
		Feedstock contribution		0			
		Carbon	kg CO_2/kg	1.53			
GFRP as per V_f = 0.7		Energy	MJ/kg	40.8911	-		When volume fiber fraction, V_f = 0.7, the weight fraction, w_f = 0.83, which is the ratio found from *equation 2.22*, which must be used to generate the use weighted average in the cells left. (and IS the ratio used here!)
		Feedstock contribution		7.769			
		Carbon	kg CO_2/kg	-			
GFRP as per ICE		Energy	MJ/kg	100	no data		not pultruded data, but 'traditional' fiberglass (lower glass content)
		Feedstock contribution		no data			
		Carbon	kg CO_2/kg	8.1			

Whilst the data in the table is for polyester as opposed to vinylester, it is thought that this is a reasonable substitution to make in the light of available data, as the materials are very similar in process and chemical pathway. Polyester only requires a small amount of engineering to turn it into vinylester at a late stage of material production.
A further calculation regarding functional units can be performed for the sake of achieving accurate embodied carbon comparison. By calculating the volume (thickness) of sheets required, for each material, to achieve the same bending stiffness for two foam core sandwich panels of equal stiffness, the mass of FRP relative to aluminum can be determined and embodied carbon compared for equivalent functional units. Table 2.8 illustrates this procedure. Regarding the Table 2.8 it can be noted that simple method of mixtures is used to determine the density of GFRP by Equation 2.35.

$$\rho_r = v_f \rho_f + v_m \rho_m \tag{2.35}$$

It can also be explained at this stage how one might convert between fibre volume fraction v_f and fiber weight fraction w_f.

$$w_f = v_f \frac{\rho_f}{\rho_c} \tag{2.36}$$

Table 2.8 Comparison of embodied energy for FRP and aluminum functional units

Material	Embodied energy as per *table 2.5* (MJ/kg)	Young's modulus, E (GPa)	Density, ρ (kg/m^3)	Embodied energy per functinal unit (MJ/m^3/GPa)	Normalised ratio	Disregarding functional units
Rolled Aluminium	155	75	2700	5580	3.2	3.8
GFRP where V_f = 0.7	41	51	2159	1736	1	1

The embodied energy of GFRP sheet per 'unit stiffness' of sandwich panel is seen to be less than one third that of aluminum. It should be noted that in the above Table 2.8, the energy total for GFRP is for production of each material, glass and polymer, separately. One might expect forming the polymer around the fibers in a pultrusion process to incur further carbon cost.

2.4.5 Fire provisions

The means to address fire provisions lies partly with materials selection; use of sodium silicate (an intumescent PCM), phenolic resin and foam, and more recently PIR foam, all present fire-conscious choices for sandwich panel core material. Aerogel products may also find application in schemes considerate to fire risk. Aspen aerogels 'Spaceloft' has received a C rating in the Euroclass fire test, and a class A rating in the ASTM E 84 fire test (flame spread of less than 25). It is the reinforcing fibre that is critical to the fire performance, so there may exist scope to 'cast' the nanogel around other substrates, or use as a fill to improve its fire resistant attributes.

In designing a façade to meet and surpass the fire building regulations, phenolic pultrusions of both sheet type faces, and moldings to form edge connections, could certainly provide the necessary components. The pigmentation issue for phenolics may not be so much of a concern because in the foam core sandwich scheme chosen, the construction has scope to adopt internal and external faces of different polymer materials. A phenolic sheet forming the internal face of a foam core sandwich could be covered from view possibly with additional fire lag material such as a sodium silicate PCM or acoustic dissipative material where necessary. The phenolic polymer is an economical option and could alleviate the need for other fire retardant materials to be incorporated at certain locations in the building envelope. Celotex, a manufacturer of PIR foam claims that long strands of glass fibre reinforcement can be easily accommodated in the foam, leading to improved structural endurance in a fire.

Whilst flame spread and fume toxicity are explicitly covered by regulations, the time-dependent structural response of GFRP in any polymer form is a more complex issue and remains the subject of a great deal of research. The mechanical property degradation observed in the temperature range below the glass transition temperature has been investigated by analytical means (Gu and Asaro 2005). Continuous gradient theory permits the application of an approach using a varying degree of material stiffness across the through thickness FRP skin dimension. Alternatively a transformed section can be used. Global, or overall, panel stiffness and buckling load can then be calculated. Verification using finite element analysis (Ramroth et al. 2006) accounts for arbitrary reorientations of the laminate and testing that is conducted using combined mechanical and thermal modeling.

The outcome of this work is an understanding of the structural behaviour of panels in the time before glass transition temperature is reached; this will depend entirely on the level to which other protective measures are employed.

ATH (aluminum tri-hydrate) can be used as a polymer filler to improve fire retardence, but both fillers and additives in a polymer matrix will generally decrease corrosion resistant properties (Vaughan et al. 2006). Internally, where durability may not be a concern, the FRP sheets could be tailored in their chemistry in respect of this, but it may be more economical and enhance performance by using phenolic GFRP sheets if fire issues are pertinent.

2.4.6 Aesthetics

As explained in Subsection 2.1.3, the limitation of pultrusion to provide prismatic or sheet panel widths up to 1.5m, but also it is explained that this is more than acceptable for application in facades. Often façade panels, even as part of larger unitized element, will not be more than 1.5m in width as otherwise a ripple in the aesthetic can become prominent.

Constraining design to a scheme built around prismatic panel parameters can of course be considered a significant limitation, though the ease with which complex, yet repeated, prismatic profiles can be produced means that not only can panel connections be weather tight and perform well structurally, but further, they can be innovative expressions of architectural form. These may choose to embrace fluidity or concepts involving tighter return angles observed as possessions of the building skin. Compatibility with more complex prismatic panel shapes is a significant advantage of applying thermal insulation foam by injection method.

Form and finish are terms that would usually suffice to describe the aesthetic of a surface, but find additional variable counterparts when FRP is concerned. Translucency, and incorporation of light emitting devices, identifies some novel possibilities, and ties strongly with the emerging concept of ‘multimedia facades’. At the 2nd Symposium in Advanced Façade Engineering and Technology in Hong Kong 2010, an architect from Arup presented the functional objectives of such multimedia

facades, and offered evaluation of examples in use (Tsoi 2010).

Whilst not all aspects of light, sound and image generation detailed in the referenced conference paper may be relevant to FRP retrofitted facades, the material certainly offers new possibilities in the translucency of structural skin and the potential to accommodate the necessary electrics and diodes for emitting light within the FRP skin itself. For instance it is possible that copper wires, for at least principal cabling, could be pultruded into an FRP sheet, whilst FRP housing for diodes and more complex arrays of wiring could be specially constructed. Design concepts whereby arrangements of diodes and bulbs are merely covered by a translucent FRP skin are also possible of course, though the issue of foam core insulation in such areas might become an issue, and for the purpose of illustrating the electrical insulation of GFRP, the former concept is perhaps a more exciting notion of a prototype.

Note that whilst vinylester or polyester seems tailored to this function, there would be problems presented in the form of copper corrosion in zones of either phenolic foam or matrix. The European Phenolic Foam Association claims however that there is no additional risk in comparison to other foam materials as long as other environmental factors can be controlled, for example, the presence of oxygen, water, salt, and pollution. ‘The advancement in LED technology allows potential for the modern day’s façade to exhibit multiple appearances and atmosphere creation for different commercial and operational function usages… in both day form and night form appearances’ (Tsoi 2010).

2.4.7 Further applications

Whilst prospective applications of FRP and composite materials form a large share of conference proceedings in the topic today, the application of FRP facades is only now being realised in the extent of benefits and payback available. As a result, some space is spared in this section to consider the advantages of FRP facades not implied by the brief/introduction to this report, and to speculate on uses of FRP outside the remit of this project.

2.4.7.1 Retrofit as seismic repair

Many structures exhibit safer behaviour under earthquake loading as a result of modern seismic design, the RC façade panel system often employed results in a high frequency of brittle failures, causing damage and death to vehicles and persons in the vicinity of the building.

A sophisticated system of composite façade panels would reduce the likelihood of failures in the building envelope due to their inherent flexibility and resilience. Whilst energy absorption is more significant for the superstructure, lightweight secondary structure, including such panels, would yield a lower damage count in the event of a panel falling from a building, and flexible, resilient panels will also be less likely to break free. Lightweight panels will also reduce the carbon cost through transportation of materials.

Lightweight buildings have traditionally been constructed in the tropics, and the modern affinity to RC façades is often not needed in terms of obtaining thermal inertia, if there is no clear sky to which heat is radiated at night. The durability characteristics possessed by FRP is a further benefit for panels that will experience extreme rain cycles intermittent with intense UV radiation. These environmental factors have prevented the lightweight alternatives of metal cladding in the past from seeing application in such tropical seismic regions.

For the composite panel manufacturers of Northern Europe, there does exist the potential for trade and supply to Central and South Americas West Coast, via the newly widened Panama Canal, developed with a view to accommodating ever more shipping from Europe.

2.4.7.2 Deployable structures in FRP

As an application that can exploit not only the durability material properties of FRP, but the mechanical characteristics too, deployable, gridshell type structures with in-situ gin-poles and cable-winch opening sequences built in, could provide effective, eye catching and functional structures, that are quickly erected and inherently durable.

The specific properties of FRP targeted by this application are lightness in weight and resilience. Low stiffness with high strength is desired and the linear behaviour exhibited up to failure is not the disadvantage that it would be in many other structural applications. High strength and low stiffness results in the potential to strain a structure sufficiently to create a suitable, desired shape, though being sufficiently far enough away from failure to exhibit additional resilience under variable, accidental and transient actions.

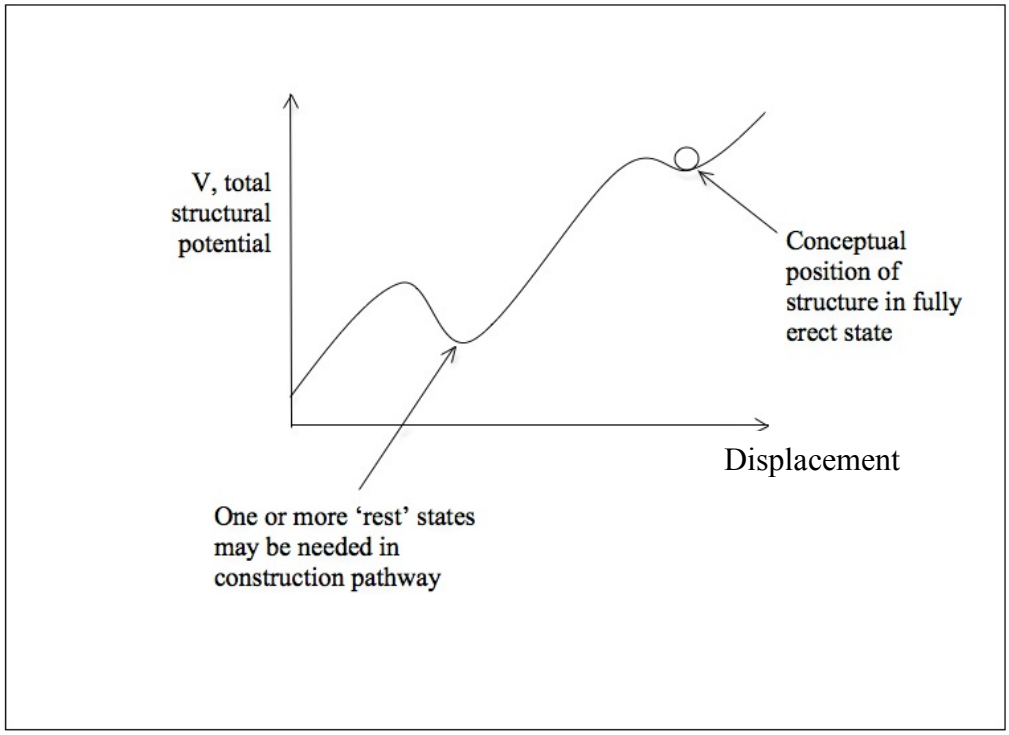

Figure 2.25 Hypothetical plot, for total structure potential against arbitrary displacement parameter or erection sequence in a deployable structure

It is an option, but not necessarily a necessity for a fabric/membrane enclosure of such a deployable, expo-type structure to contribute to the 'restraining part' of the structural potential. The degree to which the membrane contributes in this way could be to any desired amount dependent on the type of membrane.

The 'rest' states are properties of the structural mechanism and can be afforded easily by either 'mobile nodes' - nodes moveable under strain designed safely into the scheme, or by provision of multiple straining mechanisms to be used in a designed sequence. Incidentally it is these same two means that permit the first-derivative of a potential

plot, like that in Figure 2.25, to be tailored to increase in magnitude in regions proceeding and following the final and rest structural positions relating to *x*. (i.e. the steepness of the slopes where the conceptual 'ball' will sit in a firm equilibrium.)

2.5 Design methodologies

Understanding the fatigue life of pultruded angle connections in the secondary-fibre direction to enable more informed design of connections, and to validate durability attributes by case study investigation is intended to facilitate the uptake of the polymeric façade retrofit concept.

By consideration of literature presented above, the most likely FRP types and panel forms can be identified. The issues associated with sandwich panels of pultruded GFRP structural skins have been explored.

More specifically the work in Subsection 2.1.1 on the fundamental principles of composite action (and determining mechanical material properties) serves to explain the mechanical behaviour of cellular building panels; the focus of study in Section 3.2. In the same way the work in Subsection 2.4.1 on plate theory as a tool for structural analysis, serves to inform the testing parameters associated with fatigue studies presented in Subsection 5.2.4.

Figure 2.26 and Figure 2.27 show hypothetical prototype designs that satisfy the design conflicts revealed by the proceeding scoping exercise. The purpose of developing these was to reveal and understand key issues problematic to design, which would be unavoidable and benefit from targeted research. Something evident in Figure 2.26 and Figure 2.27 is the abundance of pultruded return angles, where the prying force at connections will induce stresses, at the angle root locations, in the weaker secondary fibre direction. These locations will experience a lifetime fatigue loading of this nature. Testing reported in Chapter 5 explores the nature of this phenomenon and establishes characteristics that are vital for the informed design of polymeric façade connections.

Equipped with background in the material properties of GFRP composites, and understanding of composite behaviour, the durability characteristics of the material can

be assessed from a point of authority. Doubts relating to the degree of durability offered by GFRP will only be dispelled if testing using genuine, naturally-aged material can validate the performance of material after a life in service. Testing reported in Chapter 3 aims to do precisely this.

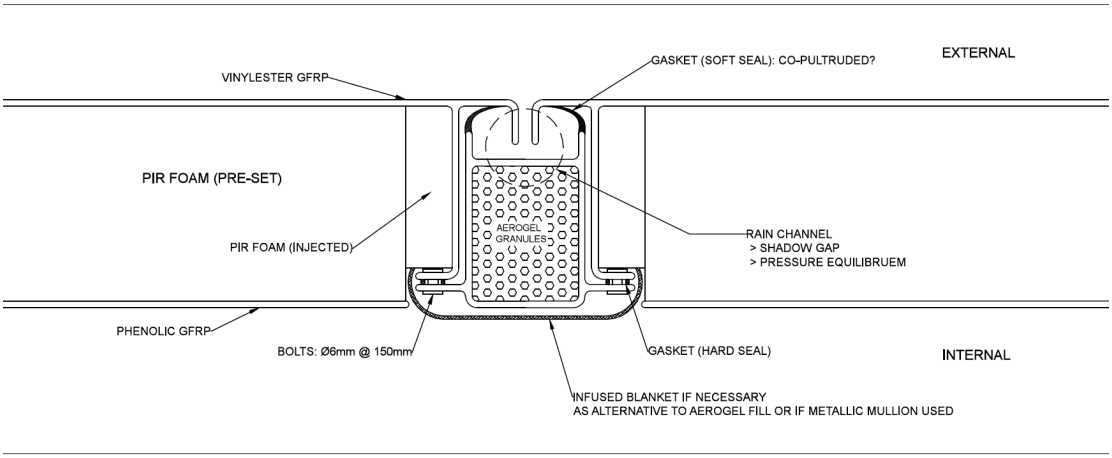

Figure 2.26 Hypothetical prototype design (i) for panel mullion connection: discrete mechanical connection

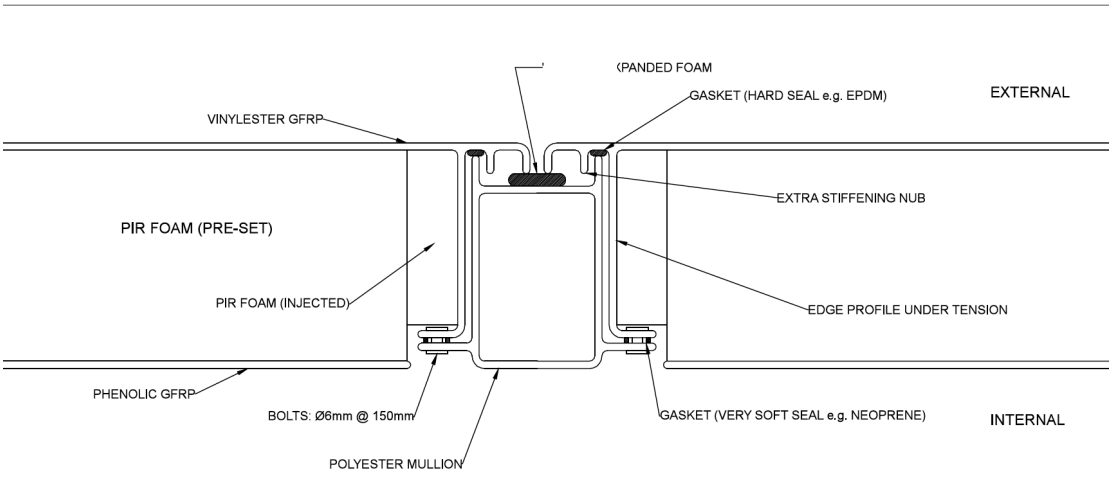

Figure 2.27 Hypothetical prototype design (ii) for panel mullion connection: discrete mechanical connection

2.6 Fatigue in pultruded GFRP

2.6.1 Introduction

'The engineer's perception of fatigue is so closely linked with the behaviour of homogenous, isotropic, metallic materials that there has often been the tendency to treat modern fibre composites as though they were metals. Fatigue in metals often progresses by initiation of a single crack and its intermittent propagation until catastrophic failure, which occurs with little warning. The usual effect in metals of fatigue at low tresses is simply to harden the metal slightly. Generally speaking a stronger material will have a higher fatigue resistance, the fatigue ratio (fatigue limit divided by tensile strength) to be roughly constant. Since anisotropy is a characteristic of composites that we accept and must design for, a stress system that develops only a small working strain in the main fibre direction may nevertheless cause strains normal to the fibres or at the fibre resin interface which are high enough to cause the kind of degradation that we call fatigue damage' (Harris 2003).

Composites accumulate damage in a general rather than a localized fashion, and failure does not always occur by propagation of a single macroscopic crack. The microstructural mechanisms of damage accumulation, including fibre breakage and matrix cracking, de-bonding, transverse ply cracking, and delamination, occur sometimes independently and sometimes interactively, and the predominance of one or the other may be strongly affected by the material variables and testing conditions (Harris 2003). It is claimed that failure models should address the influence of complex stresses and should have criterion addressing each possible failure mechanism (Hart-Smith 1998). Hart-Smith (1998) agues that homogenization methods, that are incapable of distinguishing between fibre and resin failure, are not appropriate.

It is fortunate that targeted experimental testing of GFRP elements in fatigue permits an understanding of the type of failure mechanism or mechanisms by which damage occurs and failure is brought about, for a specific combination of loading parameters, material, and element variability. A testing campaign of pultruded elements is reported in chapter 6. It has long been recognized that the variety of composite types available reduces the applicability of unified life prediction models. It is shown that experimental validation for specific connections/elements is vital, especially in a complex

element/multi axis 3D stress problem such as that presented by a façade connection scheme. The virtues of unified life prediction models incorporating both microstructural and micromechanical aspects of composite response have been presented by Petermann and Plumtree (2001). It was recommended that incorporation of compressive failure mechanisms should be the next challenge since tension and compression are governed by different failure mechanisms and do not contribute equal parts to damage development.

Life prediction methods that are based on mechanistic models of material's degradation under load have, in the past, always been the preferred approach of materials scientists. However, no generally applicable model has yet been able to supplant the only perceived acceptable alternative; that is the carrying out of a full fatigue test programme (Harris 2003).

A study by Turvey and Zhang (2007) that reports on the behavior of pultruded GFRP angle leg junctions when subjected to monotonic prying loads is examined later in this chapter. Literature describing the response of pultruded GFRP angles or indeed any structural section or element in the weaker secondary fibre direction is scarce. Commonly adopted principles of measuring and quantifying fatigue performance of composite materials are reviewed with an objective to determine a means of applying material parameters to the type of 3D stress scenario presented by a façade connection.

2.6.2 Damage accumulation

At low levels of stress, in early life during cyclic loading, most types of composite sustain damage. This damage is distributed thought the stressed region, and although it does not immediately reduce the strength it does reduce the stiffness (Harris 2003). The amount of damage accumulated in some regions of the composite may become so great that the residual strength of the specimen falls to the maximum stress imposed by the fatigue cycle, σ_{max}, and failure ensues. This process may occur gradually when it is termed degradation, or catastrophically when it is termed 'sudden death' (Harris 2003). Damage is well represented by reduction in stiffness. Yang et al. (1992) monitored damage through fatigue modulus degradation. The model developed was shown to correlate well with experimental results. The study pertained to matrix-dominated

fatigue of composite laminates. El Mahi et al. (1995) also presented a model employing stiffness degradation to predict composite life. A linear relationship between stiffness reduction and crack area was reported, indicating the proportionality between stiffness degradation and energy release rate.

The direct measurement of damage as the surface density of micro-defects (the crack area on representative volume element (RVE), in the specimen cross section) is difficult to perform. It is easier to take advantage of the coupling between damage and elasticity (Lemaitre and Desmorat 2005).

2.6.3 Testing methodology

Fatigue testing of coupon material is most commonly conducted under load control.
A reliable S-N fatigue curve obtained from a large sample population is the prerequisite to fatigue design (Petermann and Plumtree 2001). When the log for the number of cycles to failure is taken a linear relationship of the type shown in Figure 2.28 is yielded. The linearity of such graphs is often complicated by the significant rise in temperature that is not easily dissipated by the non-conducting constituents, results in a lower tensile strength. By cycling at frequencies no greater than 2 Hz the effects of autogenic heating can be mitigated (Harris 2003).

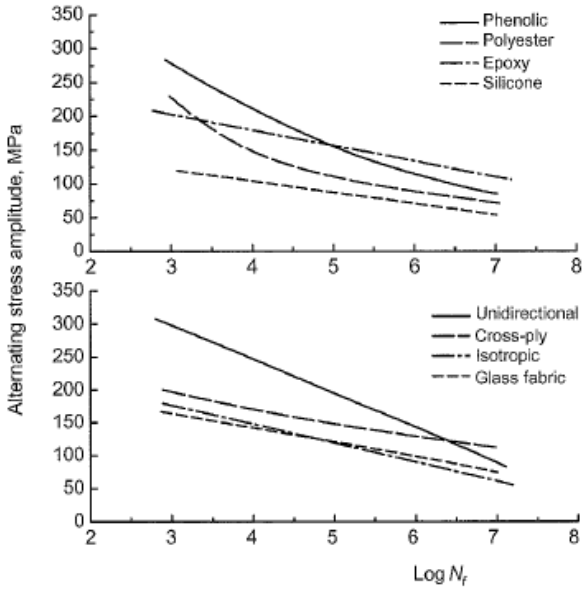

Figure 2.28 logN_f - σ_{peak} failure envelopes, showing influence of different matrix resins and fibre architectures. Cycling frequency 1Hz. From Harris (2003)

The variability in the fatigue response of composites is greater than that associated with metallic materials. Stress life data may be obtained by testing single samples at many different stress levels, or by carrying our replicate tests at fewer levels. The plot in Figure 2.29 illustrates the effect of variability. One of the problems encountered is to know how many replicate tests should be done at each level given the cost of fatigue testing programmes (Harris 2003). It is often expected that 20 replicate tests, at each replicate stress, may be necessary before the user can have confidence in a statistical analysis of the results (Lee et al. 1997). It is understood that due to the time and resources required for such a programme of fatigue testing, the validation of a particular prototype connection, comprising GFRP material, pultrusion form and connection design, cannot be an objective of this research. The aim is to investigate the general behaviour and response of such a connection scheme and demonstrate how over a longer duration testing campaign; further data could be acquired to eventually attain statistical confidence. In undertaking such an exercise, the predominant type of failure/damage mechanism can be established, and the rate of degradation in stiffness measured as a means to monitor the accumulation of damage. Parameters relating to appropriate threshold design values for loading and design combination can be investigated.

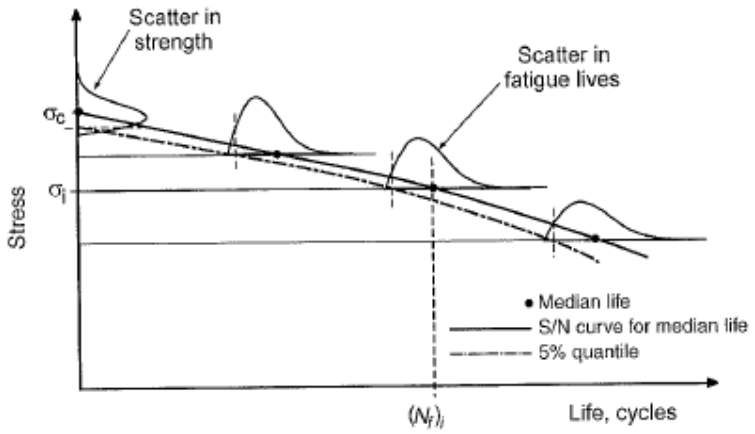

Figure 2.29 Effect of variability on the strength and fatigue life of the S-N curve. From Harris (2003)

The low elastic modulus of GFRP in comparison to other metallic materials results in a larger cyclic displacement. A cycling frequency of only 1 or 2 Hz facilitates smooth application of load from the test rig, without undue noise in the data.

The majority of fatigue testing undertaken is in the simplest form: constant-stress testing, in repeated tension, and subsequently at different *R*-values. The stress ratio *R* is defined as $\sigma_{min}/\sigma_{max}$. It follows that for cycling between a maximum stress and zero, R=0, which is the most common starting point (Harris 2003). It is evident that this type of testing is usually done under load control because R is normally constant. Many theoretical models, and damage accumulation models are reported on the premise of load control testing. Tensile testing of coupon specimens is easily conducted under load control in the laboratory, however component testing, especially where the reaction stiffness is comparatively low, (and displacements are high) is sometimes only possible under displacement control owing to limitation of the test rig employed.

Under displacement control testing, the stiffness (which had been verified as a suitable index by which to measure damage and energy release from the composite (Elmahi et al. 1995)) reduces and hence the maximum cyclic stress σ_{max}, also reduces. There does exist scope to represent σ_{max} as a continually changing variable in the models of some published reports. It is also possible to represent the max stress changing in finite steps, consisting of a certain number of cycles at a certain stress. This is possible due to Miner's rule, illustrated by Equation 2.37, which is said to hold true for 'all tension' cycling. To use Miner's Rule, damage is postulated to be linear with number of cycles, according the Palmgren-Miner linear damage rule expressed: $\Delta = n/N_f$. Where Δ represents the fraction of catastrophic damage sustained after n cycles (where $n < N_f$) so that at failure $n = N_f$ and $\Delta = 1$ (Harris 2003).

$$\frac{n_1}{m(N_1)} + \frac{n_2}{m(N_2)} + \frac{n_3}{m(N_3)} + \frac{n_4}{m(N_4)} = M_n \tag{2.37}$$

In Equation 2.37, n_i is the number of cycles in the unit and $m(N_i)$ is the median life at that particular stress level. If Minor's rule is followed, and M_n were 0.2 for instance, the block of cycling portrayed could be repeated 5 times before failure. This is true for an

all-tension series, (eg TTTT), however if the series were TTCT for instance then Miner's law is no longer obeyed (Harris 2003). It is seen that if the number of cycles at each stress (n_i) reduces, and the number of terms in Miner's equation increases, a closer approximation of damage for a continually changing σ_{max} could be attained.

2.6.4 Theoretical representation

It has been established that stiffness acts as a good means by which to monitor damage accumulation, through being a representative index, as validated by the work of others (Yang et al. 1992; Elmahi et al. 1995), and of practical compatibility with continuous measurement throughout testing.

Talreja et al. (1981) identified three mechanisms that control fatigue failure: At high stress levels fibre breakage within the normal monotonic tensile failure scatterband occurs. At lower cyclic stress levels, although statistical fibre breakage still occurs, it does not occur so rapidly to form composite destruction such as other mechanisms. Matrix cracking, and interfacial shear cracking, can then influence the overall damage state providing the composite damage working strain is sufficiently high. Talreja et al (1981) speculates whether plots of the type shown in Figure 2.28 plateau completely at very low stresses, indicating the existence of a fatigue limit (or 'threshold') below which damage accumulation will diminish and not subsist. (A significant hypothesis for any structural application of composites.) This historic paper related primarily to composite laminates and does not specifically address characteristics of pultrusions. It does make transferable conclusions; reiterating that the fatigue performance of composites regarding tensile stresses in their longitudinal fibre direction is very good, though for other stresses and orientations the problem is very complex.

Adam et al. (1986) studied the residual strength of different FRP specimens (carbon, aramid, and glass fibres, in a common epoxy resin), which had been cycled for various durations, to develop an interaction curve, which can be used to solve for the number of cycles to failure, N_f. Alternatively the residual strength, σ_R can be determined for a given fatigue stress, σ_{max}. Like most damage accumulation models, the model of Adam et al. (1986) is formed on the premise of load control, where σ_{max} is unchanging.

Two parameters are defined in order to plot the relationship described by the model: a cycle ratio, *t*, shown by Equation 2.38, and a normalized residual strength ratio, *s*, shown by Equation 2.39. σ_{ult} is the ultimate monotonic tensile strength.

$$t = \frac{\log n - \log 0.5}{\log N_f - \log 0.5} \tag{2.38}$$

$$s = \frac{\sigma_R - \sigma_{max}}{\sigma_{ult} - \sigma_{max}} \tag{2.39}$$

The parameters for each of the materials mentioned can be represented by an interaction curve of the form shown in Figure 2.30, which illustrates the governing relationship shown by Equation 2.40.

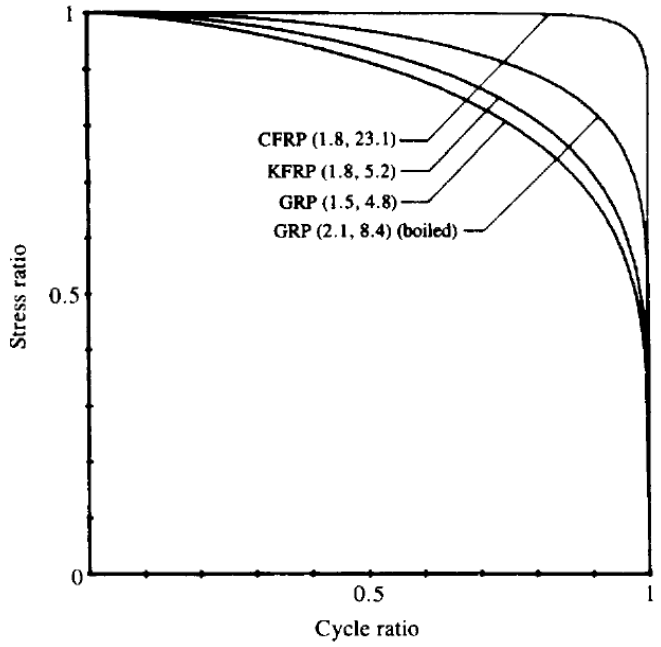

Figure 2.30 Normalized residual strength curves for 0,90 laminates of various fibres in epoxy. The values for the exponents of the fitted curves are shown in brackets. From Adam et al. (1986)

$$t^{p_a} + s^{p_b} = 1 \tag{2.40}$$

With exponents p_a and p_b established for a certain material as per Figure 2.30, the residual strength for any fatigue stress can be evaluated according to Equation 2.41.

$$\sigma_R = (\sigma_{ult} - \sigma_{max})(1 - t^{p_a})^{\frac{1}{p_b}} + \sigma_{max} \tag{2.41}$$

Adam et al. (1986) explains that this model will require validation for each system of interest – material, fabrication, and stress system. It is also pointed out though that specific calibration curves, of the type shown by Figure 2.30, can be deduced from relatively few data sets, unlike the S-N fatigue plots of the type shown in Figure 2.28.

In assessing this model Harris (2003) points out that despite the damage mechanism, and damage development being structure dependent, with a single generated model, predicting both gradual wear out and sudden death behaviour can be accommodated.

Harris (2003) states that the hierarchy of 'structural scales' relevant to coupon testing, element testing and structural interactions, require portrayal by damage mechanics, continuum mechanics, and fracture mechanics respectively. With a completely constrained design, continuum mechanics based approaches greatly reduce the number of experiments needed, and is greatly conducive with simple optimization, though bearing a higher degree of empiricism. Continuum strategies will contain no information about specific mechanisms of failure. Micro-mechanical (physical) models are rarely precise enough to be of much use to an engineer, they can find use in applying limits to the values of physical constants that enter them, and suggest the form and limitations of continuum models developed.

2.6.5 Previous experimental findings

Salvia et al. (1997) present findings from more than 1000 medium and long-term tests investigating the behaviour of unidirectional GFRP, of which pultrusions represent a significant portion. The study is based around epoxy glass fibre systems, though the means by which damage was measured and how the batches of material were profiled is of significance. The evolution of stiffness was recorded to portray the accumulation of damage in the specimens, and the fatigue life was conventionally defined by the

number of cycles required to yield a 10% reduction in stiffness, N_{10}. The concept of an envelope, like the failure envelopes in Figure 2.29, but for a certain stiffness reduction, is an important consideration regarding presenting the material performance in a range that is conscious of serviceability requirements.

The plot in Figure 2.31 shows that the linear (on a log scale) relationship is still observed for stiffness reduction limits, as it is for failure envelopes. The testing conducted to form this plot was undertaken by performing three-point bending fatigue tests, under displacement control. The displacement limits selected are correlated to maximum applied strains, and the results are presented using this parameter. It is evident that for the maximum strains imposed, the vast majority of specimens underwent more than 100,000 cycles before reaching a 10% reduction in stiffness.

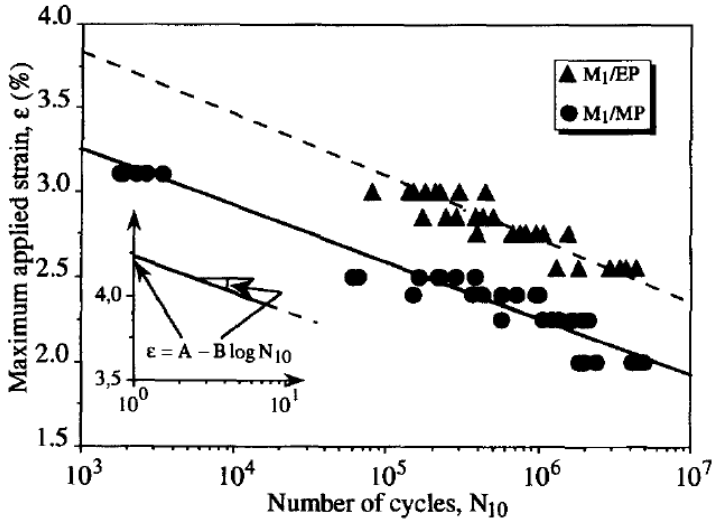

Figure 2.31 S-N_{10} envelopes from results obtained by three-point bending fatigue tests, from Salvia et al (1997)

The two data series shown on the plot in Figure 2.31 represent specimens of material with different types of glass fibre sizing, but both pultruded with fibre volume fractions, V_f of approximately 0.5, and using the same epoxy resin polymer matrix (Salvia et al. 1997). In fatigue tests to failure, the peak cyclic stress is often presented as a percentage of the ultimate stress achieved in a monotonic test to failure. Salvia et al. (1997) instead present extrapolated values that correspond to a 10% reduction in stiffness after one cycle, but the failure strain, under monotonic loading, of the material in the test described is not reported.

Salvia et al. (1997) explain that, although from a mechanical point of view, the results of axial tests appear easier to analyse, there are many benefits to adopting flexural fatigue testing. Because of the high resistance at failure, the use of straight-sided tabbed specimens leads to scattered results in tension fatigue tests. This is associated with debonding of aluminium tabs, or gripping problems at the jaws of the test rig at higher loads. It was reported by Salvia et al. (1997) that the scatter for flexural tests was greatly reduced. A span to depth ratio for coupon specimens was chosen to be 20 in order to minimise shear effects and nucleate failure on the tension side. (This was analysed using microscopy in the study.)

It can be noted that the imposed deflection of coupons was always in the same direction. The implication of this being that the coupon material experienced either only tension cycles or only compression cycles across the through section thickness, with the stress ratio, R, close to zero. In fact, the authors report that an R-value of 0.1 was adopted to ensure that 'drawback' didn't occur when passing at zero stress level. In other words, to ensure the coupon was not inadvertently flexed in the opposite nature for any tests, which would yield a negative R-value and skew results. Salvia et al. (1997) did not investigate the influence of negative R-values or compressive-tensile block alternations (i.e. TTCT effects, as described in Subsection 2.6.3).

Salvia and Vincent (1996) presented prior, a model to describe the kinetics of stiffness loss as a function of the number of cycles within a large applied strain range, for this precise type of flexural fatigue testing described above. They concluded that although the model successfully achieved this, it was not possible to relate the parameters of the model with the properties of the elementary components. It was found, that the number of cycles resulting in the first sign of surface damage on the tension face of specimens, and the number of cycles necessary to inflict a 10% reduction in stiffness, remained in a constant ratio of the total number to failure.

These findings led to the work of Salvia et al. (1997) that explore different types of fabrication and glass fibre sizing by experimental means. The finding also suggests that developing a model based around damage mechanics, for a specific pultruded element and connection arrangement would not be possible. A continuum based mechanistic model would be possible though.

The 2D plane stress behaviour of flexed angle sections has been investigated by Turvey and Zhang (2007), who investigated the 'opening mode failure' of GRP angle leg junctions, cut to 30, 45 and 60 mm in length. The specimens were 102 × 6.4 mm in size (leg length and element thickness respectively). It was found that when subjected to monotonic prying loads, in a state of plane stress, the specimen response was linear elastic up to approximately 60% of the ultimate failure load. Testing of this type only addresses flexural behaviour and no literature exists pertaining to fatigue testing of pultruded angles in this way. The stresses occurring in a pultruded façade panel connection could be better replicated more accurately by a loading action that incorporates bending and torsion. Analysis of the fatigue performance of pultruded rods under torsional loading has been investigated by Khashaba (2003) and El-Assal and Khashaba (2007). It was concluded that unidirectional glass fibre reinforced polyester composites have a poor torsional fatigue strength compared with the results of pure bending fatigue strength. Endurance limit values (calculated at $N=10^7$ cycles) of specimens tested in combined bending and torsion gave a strength half that compared to specimens subjected to pure bending.

2.6.6 Potential to improve the fatigue performance of pultruded connections

Interleaving is the concept of introducing soft regions into the composite to provide barriers to crack growth and to raise the intrinsic toughness of a particular zone in the element. Kim and Mai (1998) explore the possibilities of engineered interfaces in FRP composites, and have established that extra toughness can be obtained, which has potential to improve fatigue resistance. Franke and Schurmann (2010) also explored the characteristics and benefits of crack arresting layers. It was found that specimens including layers of polyacrylonitrile (PAN) fleece, and polyethylenterephthalate (PET) fleece, possessed a better fatigue performance than for laminates of purely glass fibres. This was found to be especially true for specimens with a fibre volume fraction higher than 0.6, applicable to the common range of fibre fractions in pultruded elements.

Whilst this is a notable prospect regarding application in polymeric facades, the objectives of testing (reported in chapter 6) and this thesis is to explore the behaviour of pultruded return angles, as explained in Chapter 1.

2.7 Summary

The many favourable properties of GFRP rendering it an appealing material candidate for polymeric facades are also quite well understood in industry and in the research community. These include environmental control, good thermal and electrical insulation, basic structural properties including good stiffness to weight ratio, and good strength in general. The values for embodied carbon also assume an encouraging attribute.

Of the negative attributes of GFRP concerning application in polymeric facades some are well understood. Acoustic and fire performance are good examples of this where design of a structures is sensitive to use of composite material in these respects. Designing for protection, or considering the suitability of application. End of life options are also limited but understood to be developed with time and increased use of the material. The literature reports no great barrier to developing the existing options available.

The well understood characteristics of composites can be broadly related to the qualities it possesses when manufactured, at ‘day zero’. The case for developing composite materials at all, it largely the attain scope to tailor materials to possess desired properties. Tolerance control, appearance, and mechanical properties on day zero can be well defined.

Long-term characteristics, relating to whole life performance are far less well understood. Creep, fatigue and durability present barriers to acceptance of GFRP in the construction industry, as well as areas of uncertainty in design of structural elements. For lightweight façade panels, creep is surpassed in importance by long-term environmental performance (durability), and long-term mechanical performance (fatigue character). Accurate means to measure and quantify these properties either do not exist or have yet to be corroborated. Sufficient and accessible testing methodologies are limited. There exists little robust design guidance for long-term performance.

3 Durability: case study testing and results

3.1 Introduction

This chapter presents findings from two case studies. Laboratory testing has allowed investigation of the performance of GFRP panels naturally aged in service. Façade panels of GFRP material, 17 and 30 years old, have provided a means to appraise the durability characteristics of the material. Experimental data provides a realistic profile of the material and highlights where characteristics of accelerated ageing techniques commonly adopted are not representative.

For each case study, information about the panels is presented first. The case study investigating GFRP panel material from the second Severn Crossing Visitors' Centre incorporated whole panel testing and coupon testing. The whole panel testing is presented first with the aim to assess environmental degradation of panels from different aspects of the building façade. Further information about the nature of degradation has been obtained by testing the panels in different orientations in the test rig.

A range of mechanical tests has been performed on coupons extracted from these panels. Proceeding the findings from these tests, however, is a report on the fibre properties of the panel material, which was accomplished by performing resin burn-off. This has provided an insight into the extent to which the variability observed in performance mechanically is attributed to environmental degradation and not merely differing fibre contents. The mechanical tests performed have assessed the influence of façade aspect, and provided comparison between internal (shielded environment) or external panel material. This has been invaluable in terms of investigating environmental degradation where 'base case' data for panel mechanical properties was not known.

Results from the mechanical tests conducted to determine compressive and tensile elastic modulus of the material, prompted further investigation into the behaviour of the polymer resin matrix. This was conducted by a methodology designed specifically for the purpose of assessing brittle hardening, a key ageing characteristic expected to be a

major issue. The practice devised is presented and findings concerning pertinent characteristics of the aged resin are reported.

The model describing composite action of the cellular building panels introduced in Subsection 2.1.1 has been employed with the intension of comparing failure stresses for each of the panels, and also to compare the theoretical flexural response of panels according to a compressive/tensile modulus ratio from literature, with a measured experimental response. Results are presented that indicate whether environmental exposure has influenced ultimate collapse load of panels from different aspects of the original building façade.

The case study investigating GFRP panel material from Mondial House does not incorporate full panel testing. Details of the panel construction are given with information about the building. For this case study mechanical tests undertaken differ to those adopted previously. In the case of shear testing, the test chosen better suits the nature of the coupons extracted, and for tensile testing coupon preparation is altered accordingly to suit the coupon properties. Tensile testing explores the nature of fibre reinforcement in these panels, which were fabricated using a different technique to those in the first case study.

Mechanical testing, microscopy, and dynamic mechanical thermal analysis (DMTA) has aimed to examine the degree of degradation for external material compared to internal material that was shielded from environmental factors that cause degradation. Material from different aspects of the building façade was not available to incorporate in this case study. The fibre content of internal and external material has been compared in this case study using microscopy. As with the previous case study, this has aimed to verify the extent to which variation in mechanical performance observed is attributed to environmental degradation and how much is due to fabrication variability.

The methodology developed previously to assess brittle hardening of the aged polymer was adopted to establish whether the phenomenon had occurred, and to quantify this characteristic of ageing as for the GFRP material in first case study.

Environmental durability of the GFRP material is assessed as a function of material

origin and exposure, age and fabrication technique. Characteristics of aged GFRP that have been revealed through testing presented are noted, and discussed in detail in the following Chapter.

3.2 Severn Crossing Visitors' Centre

Presented here are the findings of a durability study undertaken on pultruded GFRP building panels. Sourced, at demolition, from the Second Severn Crossing Visitors' Centre building, these panels offer the rare opportunity to assess the characteristics of naturally aged composite material. Mechanical properties have been determined and compared to the properties of new, equivalent material. The phenomenon of polymer hardening, typified by a reduction in material strain limit over time has also been investigated by further mechanical testing procedures. By contrasting the properties as found for panels taken from each of the four external walls of the building, factors concerning environmental exposure, and factors relating to original fabrication condition have been investigated. It will investigated whether UV exposure causes a hardening of the resin component of the composite, resulting in an increase in compressive elastic modulus, but a reduction in the threshold of brittle fracture of the matrix in tension.

3.2.1 Introduction

A quantitative study assessing the mechanical material properties of panels salvaged from the Severn Crossing Visitors' Centre is intended to address the shortfall in knowledge relating to naturally aged GFRP. The pultruded panels have been tested whole, in flexure, and cut to produce coupons of material for performing a range of mechanical tests. The results produce a profile of the material as a function of both its location within the section (internal flange, web, or external flange), and the aspect of the original location on the Visitors' Centre building. Coupon testing using new, equivalent sample material, has provided a means to assess the mechanical property degradation attributed to exposure in a natural environment. Despite an exhaustive literature search no 'base case' test data could be recovered to accurately describe the mechanical properties of the aged at the time of manufacture. It was therefore impossible to measure environmental degradation in this way. Resin burn-off has been conducted on the new and aged panel material to aid verification of the extent to which

variation observed between these two types is attributed to environmental degradation.

Maunsell Structural Plastics produced the eight panels tested in this investigation for application as bridge enclosure panels. Leftover panels, described as 'factory seconds' by the manufacturer, were used to build a site office in 1993, which was later converted into the Visitors' Centre in June 1998, located in an exposed position near the Severn estuary (see Figure 3.1). Two panels from each of the four principal facades were salvaged for testing upon demolition in May 2009. N, E, S and W (north, east, south and west) denote the elevations from which the panels were taken. Tested in 2010, the results express an account of pultruded GFRP panels naturally aged over 17 years.

3.2.1.1 Panel construction

The prismatic cellular panels (that are now produced by Strongwell Ltd.) are symmetrical in section (as shown in Figure 3.2) with an injected foam fill. The fill, which serves to provide a degree of thermal insulation, was applied as an afterthought to improve the environmental performance of the building and is not deemed to enhance structural function. The polymer forming the matrix of the material is polyester unsaturated isophthalic resin. The panel geometric properties, as specified by the manufacturer for both the new and aged panels alike (these specifications have not changed), are shown in Table 3.1. It has been established, by conducting resin burn-off, that glass fibre content (e-glass fibres) are present in new panels with fibre volume fraction, V_f, of approximately 0.36. Full details of fibre volume fractions for the flanges and webs of new and old material are presented in Table 3.2. The volume fraction of fibres that act as principal longitudinal reinforcement is also shown in Subsection 3.2.2.2.

It should be noted that specific design information from the manufacturer, concerning details of: principle, secondary, CSM (chopped strand mat), and surface veil fibre volume fractions was not available. This information in considered confidential by pultrusion manufactures.

Environmental factors that can cause degradation of the composite include UV irradiation, moisture absorption and thermal fatigue from both diurnal and annual cyclic

variations (Karbhari et al. 2003; Compston et al. 2008). South facing panels (see Figure 3.1) will have experienced the greatest solar irradiation, whilst panels on the north facing façade are expected to have endured the dampest conditions. Panels were missing surface veils (a component present in new panels, responsible for creating a resin rich surface layer during the pultrusion process, to improve aesthetics and durability) on the external face, thus decreasing the expected longevity mechanical performance of this material. This concurs with reports that these panels were earmarked as factory seconds and not used for the primary design purpose in bridge enclosure. A comparative study using internal, external, and web material from each of the façade elevations has been carried out to establish the influence of environmental exposure on the mechanical performance of GFRP pultrusions.

The value of the elastic modulus, E, when defined in the field of composites, can be $E_{tensile}$, $E_{compressive}$ or $E_{flexural}$ (Tolf and Clarin 1984). This is essentially due to the difference between the tensile and compressive moduli of the constituent materials. In this study all forms of the elastic modulus of the aged material have been determined by coupon tests. This allows further exploration of the time dependent properties of the constituent composite parts. Inspecting the results for these relative moduli has prompted further investigation into the occurrence of polymer hardening.

Figure 3.1 Left: Location of the four 'panel pairs' from the Visitors' Centre at the Severn crossing estuary. Right: Photo of the southerly elevation

3.2.2 Methodology

The methodology used to investigate whole panels is presented first. This is followed by the methodology used for calculation of theoretical strengths and stiffnesses for material at coupon level, followed by coupon testing procedures. The results of the laboratory investigations are then presented in the next Subsection.

3.2.2.1 Whole panel testing

It was hypothesised that the differing degrees of environmental exposure (in UV irradiation for instance) on the four building facades would yield different reductions in mechanical properties. The properties pursued for comparison were the flexural elastic modulus E_{flex} and flexural shear modulus G_{flex}. By establishing values of these properties for each of the panels, the extent of any mechanical deterioration attributed to exposure aspect can be assessed. Table 3.1 shows sectional geometric properties of the panels, which were tested in flexure to determine E_{flex} and G_{flex}.

Table 3.1 Panel geometric properties of both new and old panels from manufacturer's design literature (Strongwell 2010)

Second moment of area, I		6620000 mm^4
Area, A		5740 mm^2
Shear Area, A_s		1790 mm^2
Section depth, T		80.3 mm
Radius of gyration, r_y		33.8 mm
Panel width		605 mm

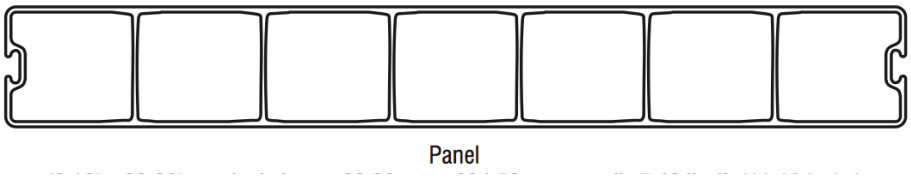

Figure 3.2 Strongwell panel cross-section (Strongwell 2010)

A test rig for three-point bending was constructed, as shown in Figure 3.3. Strain gauges were attached to the panel faces at an offset of 150 mm from the central axis of the loading beam. Two gauges on each face (spaced at approximately quarter-width

points, with one gauge over a web junction and one between two web locations) were applied to measure an average compressive and tensile strain across the width of the flanges. Three transducers were set up across the panel width to measure the average mid span deflection. Readings from all instrumentation were recorded every second. Three bearing plates, all 150 mm wide, spanned the entire panel width; one under a pinned loading plate beneath the central loading ram, and one at each end, consisting of a pin and roller support plate, forming the simply supported ends of the set-up, as shown in Figure 3.3.

To determine the flexural elastic modulus and shear modulus, E_{flex} and G_{flex}, a graphical method based on the Timoshenko Beam Theory for thin walled sections (Bank 1989) has been adopted. Each panel was tested over three different spans consecutively before turning over to repeat testing. Timoshenko's Beam Equation can be re-arranged to produce the following relationship:

$$\frac{4Aw}{Pl} = \frac{1}{12E_{flex}}\left(\frac{l}{r}\right)^2 + \frac{1}{G_{flex}} \tag{3.1}$$

where l is the span length, P is the load applied, w is the mid span deflection, and the other variables are as per Table 3.1. Each load deflection result can be plotted on a graph of the type shown in Figure 3.4.

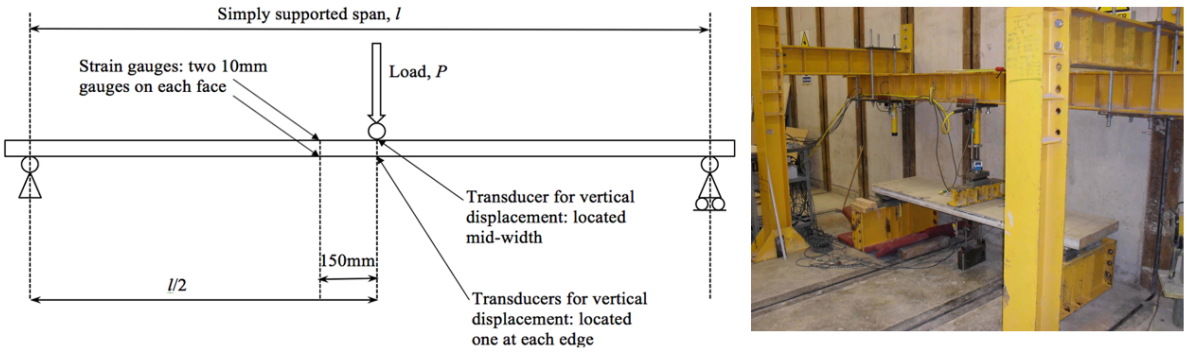

Figure 3.3 Three-point loading test rig set-up

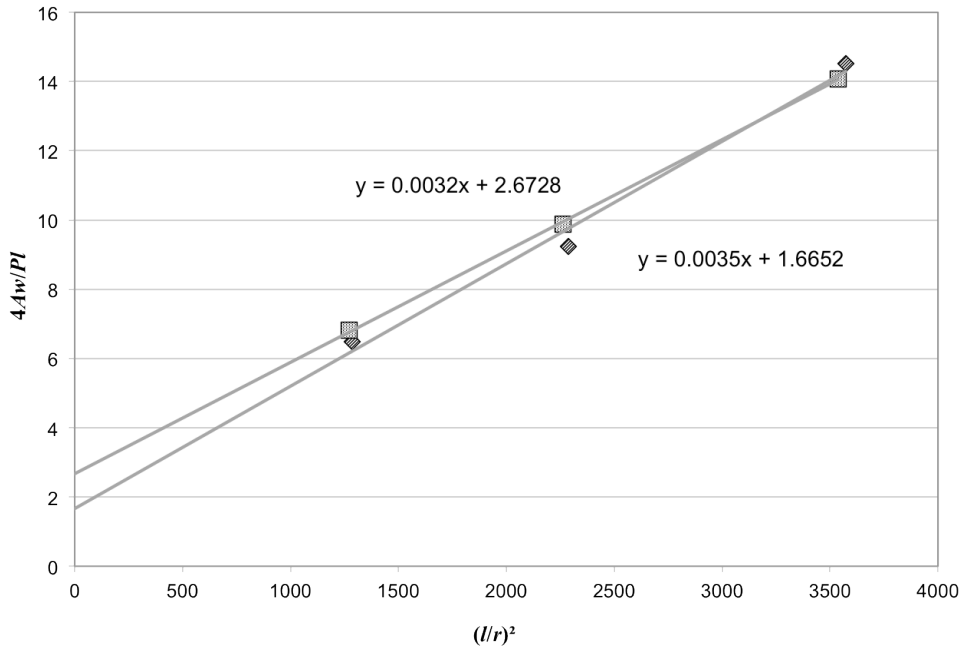

Figure 3.4 Graphical plot of Equation 3.1 for an East-facing panel. (Squares represent tests with external face up and diamonds represent tests with internal face up.)

A three-point bending set up is used because it means a great proportion of the resulting displacement is attributed to shear deflection, and as a consequence the accuracy of the value obtained for shear modulus is improved.

The flexural elastic modulus and flexural shear modulus can then be inferred graphically from the gradient and vertical axis intercept respectively. Panels were testing in both orientations (with each face uppermost) to investigate whether the resulting mechanical properties of the weathered external face influenced a different mechanical performance, dependent on whether that face was in tension of compression.

Panel length dictated the maximum span for three-point testing to be 2.1 m with subsequent span reductions of 80% and 60%. Testing over these spans permitted formation of plots like that shown in Figure 3.4, producing three well spread data points that were used to define the position of a line of best fit. The gradient of this line is equal in value to $1/12E_{flex}$ and the y-axis intercept is equal in value to $1/G_{flex}$. Hence, the values of the flexural elastic modulus and flexural shear modulus are obtained.

Following the flexural tests detailed above the panels were loaded to failure, using the longest of the three simply supported spans described previously. Panel pairs from each façade orientation were tested in alternate orientations in the test rig (one with the weathered external face uppermost and one with this face down-facing in tension, to observe the anticipated lower failure load when this face was in tension).

3.2.2.2 Determining relative theoretical mechanical properties by resin burn-off

Stiffness and strength of pultruded GFRP is closely related to fibre content. By establishing the fibre content of material from different parts of the panel cross section, and finding out if there is any inter panel variation in the material fibre content, the relative performance of the coupons can be predicted in mechanical tests. Specimens for testing were cut from webs and flanges of each of the panels. The specimens were 25mm square in size, and sourced at location away from the flange-web junctions of the cellular panels.

For both the aged and new material, resin burn-off to establish fibre weight fraction has been conducted according to ASTM code D 2584-02. After weighing to find the initial mass of each of the 25 mm square samples, each sample was ignited by heating in a crucible over a Bunsen flame and left until the volatiles had cleared (once the smoke had stopped) and only the fibres, ash and carbon remained. Each sample, in its own crucible, was then placed in a muffle furnace at 565^{o}C until all the carbonaceous material had disappeared (see Figure 3.5.) Six hours was sufficient for this. Re-weighing of the remaining fibres yielded the fibre weight fraction, and using values for the fibre and matrix density, (2570 and 1200 kg/m^3 respectively (Bank 2006),) the volume fractions could then be determined.

Figure 3.5 Sample was ignited using Bunsen (left) then later placed into muffle furnace (right)

Principal fibres, chopped strand mat, and surface veils (present on only new composolite panel material) were separated to enable more accurate calculation of volume fractions and subsequent theoretical mechanical properties, as others have recommended (Ye et al. 1995). Fillers have not been removed however as this entails procedures of chemical washing and then drying, such that the chopped strand matt (CSM) fibre fractions are known to be overestimates.

Three samples were subjected to resin burn-off for each of the locations specified in the first column of Table 3.2. 'Int' denotes internal flange material, which relates to the orientation of panel and material from the interior facing surface. In the same vein 'Ext' refers to flange material that was taken from the exterior face of the panel.

Not all façade aspects are represented in this testing, but the aged panels were all manufactured to the same specification. Whilst the degree of variation observed between material from facades of different aspect and panel location (internal or external) is revealed, it is the average fibre content values for flange and web material, of the new and aged panels, that was required to establish the desired theoretical properties of relative mechanical performance.

The volume fractions presented in Table 3.2 are mean values derived from the results of three coupon specimens. The results from coupons taken from the north facing

façade web elements (highlighted in grey in Table 3.2) are not included in the averages for aged webs owing to the large standard deviation in those results. The distribution of principal fibres in many of the web elements tested was not uniform, but as illustrated by Figure 3.6, it can be seen that the principle fibres (seen as darker fibres in the image) in the web are lying in bunches. Samples for testing taken from these webs capture various amounts of these fibres, rendering a reduced confidence in the average value yielded. This was especially true for web samples taken from panels originally on the north facing façade.

Table 3.2 Fibre volume fractions for the flanges and webs of new and old material

Coupon location	Total fibre volume fraction, V_f	Principal fibre volume fraction, V_{pf}	Standard deviation
Int flange E	0.40	0.24	0.014
Int flange S	0.38	0.26	0.024
Int flange W	0.40	0.24	0.046
Ext flange E	0.37	0.21	0.012
Ext flange S	0.40	0.26	0.015
Ext flange W	0.36	0.22	0.008
Ext flange N	0.38	0.24	0.003
	Aged flange average	**0.24**	
Web E	0.39	0.18	0.003
Web S	0.29	0.09	0.016
Web N	0.38	0.16	0.087
	Aged web average	**0.14**	
Flange new	0.36	0.25	0.041
Web new	0.34	0.24	0.026

New composolite panels appear to be fabricated with a similar proportion of principal fibres in the flange and the web elements. The aged panels, although possessing a similar fibre content in the flanges, exhibited reduced fibre fraction in the webs. Thus, the stiffness and strength predicted for the aged webs is approximately 67% that of the aged flanges. (Which is indicative of how they were manufactured.) It should be noted that a reduced amount of principal fibres were found to exist in the web elements from the southern façade panel tested, and as with other webs examined the distribution was not uniform, but as illustrated by Figure 3.6. This illustrates a high degree of inter-panel variation in the manufacturing of the webs in the aged panels, as well as intra-panel variation.

The resin burn-off results verify that variation in mechanical performance observed between new and aged flanges can be observed chiefly as a consequence of ageing rather than differing fibre contents. One large manufacturing difference is evident. In Figure 3.7 the additional layer (surface veil) present in the new material can be distinguished easily by eye, from the CSM and the principal fibres, once removed from the furnace. The surface veil was known to be present in the original composolite panel design to create a resin rich surface layer to enhance environmental durability. It was not found in the aged panels however that are understood to be factory seconds, and hence not used for the intended application of bridge enclosure.

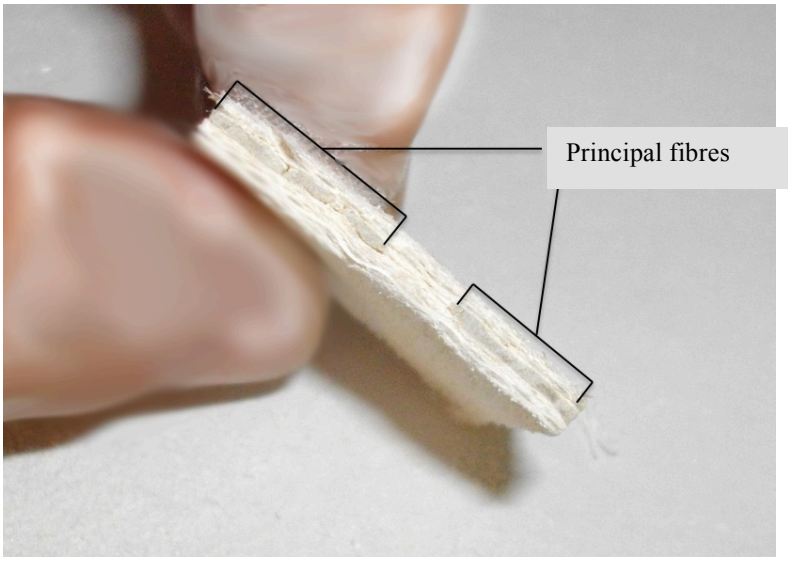

Figure 3.6 Principal fibres visible within the aged web coupon cross-section, after removal from furnace. Principal fibres are in the direction perpendicular to the page.

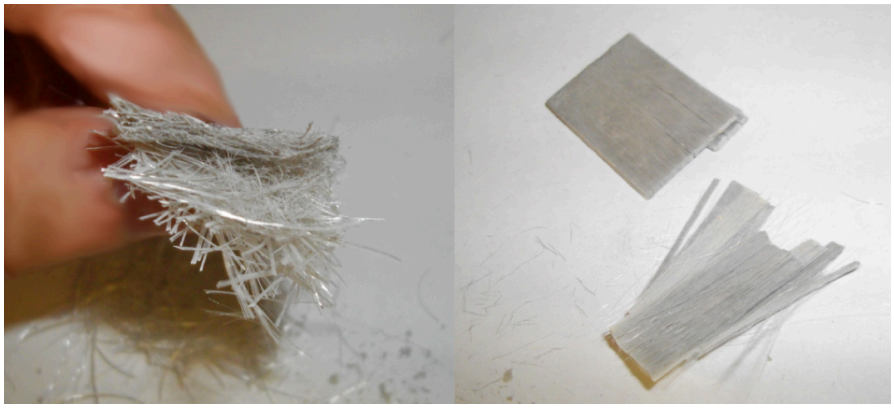

Figure 3.7 Fibres from new material. Left: Surface veil over CSM Right: Principal fibres

3.2.2.3 Tensile testing of coupons

To compare the mechanical properties of material from different panel locations, and compare new and old material the axial tensile strength and modulus were two properties determined by fabricating and testing coupons in tension. These properties are influenced mainly by the fibre component.

Three coupons representing each of the internal and external flange material, and web material, for each façade aspect, were cut from near the panel ends, which had not experienced significant bending stresses from the previous whole panel testing (less than 20 MPa; ~ 10% of the ultimate tensile strength from Strongwell (2010) literature.) The average thickness for flange coupons was 3.15 mm, and for the web coupons, 2.66 mm. The precise cross sectional geometry of each coupon was measured using Vernier calipers. Coupons were sized at 25 mm wide × 250 mm long according to BS EN ISO 527 (BSi 2009), with the pultruded fibres (0 degree fibres) aligned along the coupon length. Aluminum tabs of 1.5 mm thickness and 50 mm length were bonded to the coupon ends (in the area in contact with the test rig jaws) using epoxy resin. A single 10 mm strain gauge was attached centrally on each face of the coupon, orientated in the direction of the applied load. Testing was conducted under displacement control at 1 mm/min, in line with both manufacturer testing and the code-based approach adopted. Coupons extracted from a new, equivalent panels, manufactured by Strongwell, were also tested for comparison.

3.2.2.4 Compressive testing of coupons

To further compare the mechanical properties of the various categories of material (as described above) the axial compressive modulus was determined. This property is influenced more by the resin component than tensile properties are, and so permits the opportunity to assess environmental degradation of the resin.

A test rig used to clamp the ends of the coupons was fabricated to prevent rotation whilst loading the sample through its ends, as shown in Figure 3.8. For testing in compression, overall coupon length was 165 mm (again, aligned such that the pultruded fibres were aligned along the coupon length) and 10 mm width, with 70 mm of each

end clamped in the rig, and 25 mm left clear. Strain gauges were attached using cyanoacrylate cement, a single component room-temperature curing adhesive, one to each face of the coupon in this free region. Testing was again conducted under 1 mm/min displacement control. Results for ultimate compressive stress are not included, only compressive elastic modulus, because buckling prevented the determination of accurate material compressive strength. Shorter specimens would have enabled ultimate compressive stress to be established, however they would require smaller gauges that would not be accurate in determining the elastic modulus. Further tests would be required to achieve this.

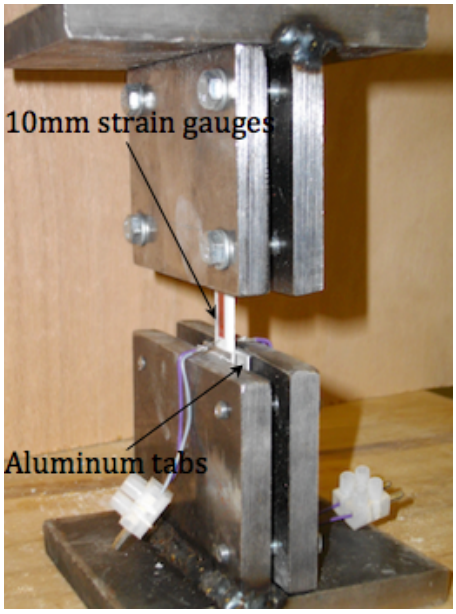

Figure 3.8 Coupon setup for compression test rig

3.2.2.5 Shear testing of coupons

Shear testing is a resin dominated mechanical test of the composite material. The Iosipescu Shear Test (Vishay 2008) procedure was adopted to perform testing. A custom rig was designed to accommodate suitable coupon sizes and apply shear force in line with the Iosipescu methodology as shown in Figure 3.9. Principal (0 degree) fibres were once again aligned parallel with the longitudinal specimen direction (perpendicular to the load direction). Two steel plates provided out of plane stability to the test specimen. The specimens were 20 mm wide × 100 mm long. Top and bottom steel loading bars, together with a pin arrangement, enabled loading to be applied to produce maximum shear and zero moment at the centre point of the test coupon. An

observation window cut-out allowed strain gauges to be located effectively. The pins were located within long slotted holes to guide them, avoiding the need to notch the sample at the pin locations, which could otherwise cause unwanted stress concentrations due to the notch inhibiting lateral movement of the pin across the surface upon flexure. The specimen was loaded by means of a mass hanger and weights with the load applied through the top pin of the rig. Loading was limited to 80 kg by the strength of the loading system, and it was found that this could be applied accurately without damaging the rig, using the mass hanger and weights. The geometry of the loading arrangement results in a shear force, in the measured region, of 80% of the applied load, as shown by Equation 3.2 and illustrated in Figure 3.9.

$$\text{Shear} = b_s - a_s = 0.9F - 0.1F = 0.8F \tag{3.2}$$

Where a_s and b_s are locally applied point loads inducing shear in the specimen.

Readings from two perpendicular 45° strain gauges were recorded and the shear modulus G_{xy} calculated according to Equation 3.3. This equation is true for any inclination of shear plane in the specimen (as a result of variation in the specimen depth), providing the gauges are centred at mid depth at the point of contra flexure of the specimen.

$$G_{xy} = \tau_{xy}/(\varepsilon_1 - \varepsilon_2) \tag{3.3}$$

Where ε_1 and ε_2 are strains from the two perpendicular gauges inclined at 45° to the horizontal, and τ_{xy} is the shear stress at mid depth of the section found from the section dimensions, and the shear force as per Figure 3.9. Equation 3.4 is taken from a technical note for use of strain rosettes in preforming Iosipescu tests (Vishay 2008) and accounts for the influence of the vertical compressive strain when using gauges inclined at 45° to determine shear strain, γ_{xy}; where α is the inclination angle of the gauge. Thus explaining why γ_{xy} is represented as $(\varepsilon_1 - \varepsilon_2)$ in Equation 3.3.

$$\gamma_{xy} = (\varepsilon_1 - \varepsilon_1)/\sin 2\alpha \tag{3.4}$$

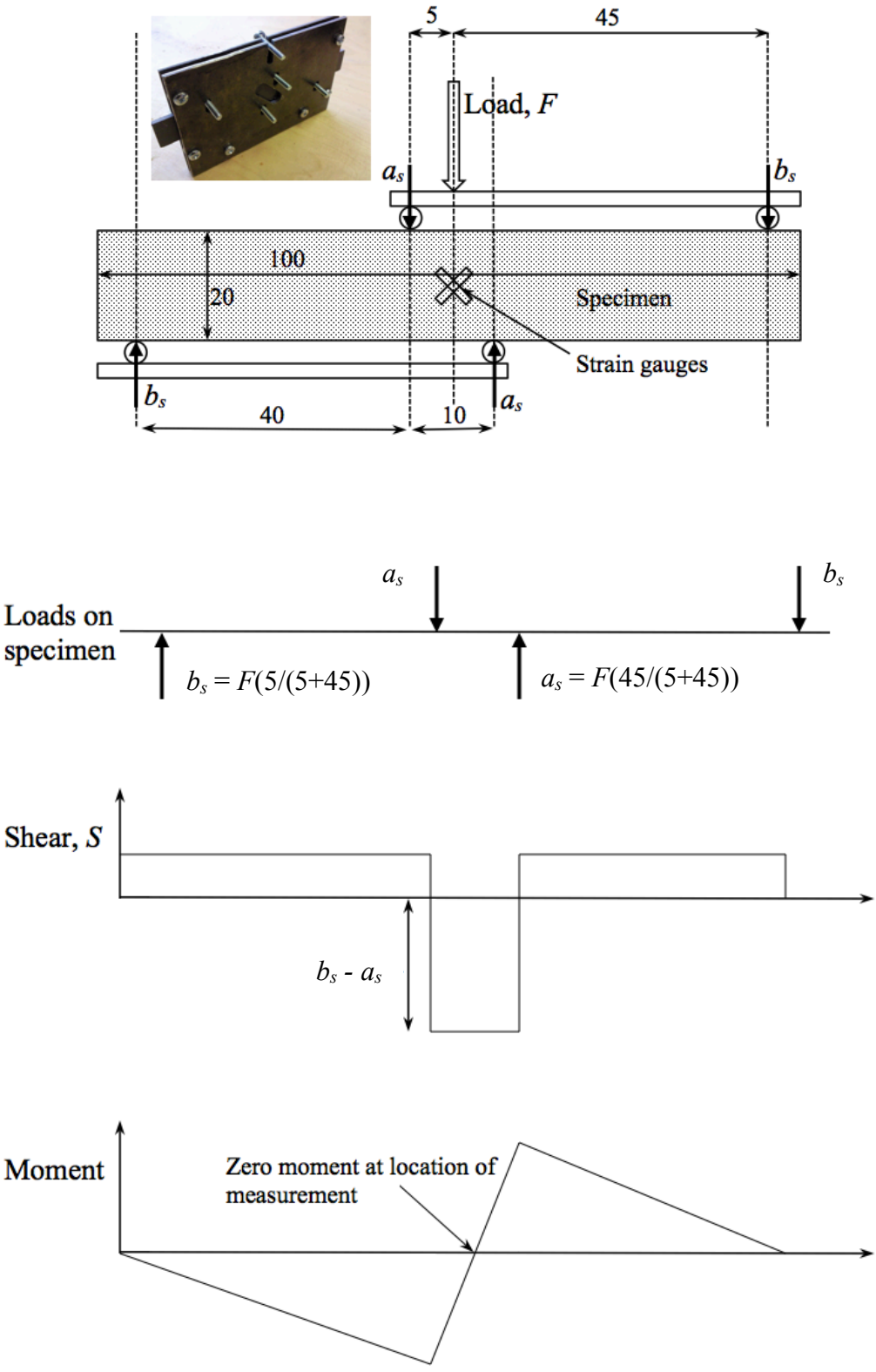

Figure 3.9 Iosipescu shear rig set-up (all dimensions in mm). Schematic showing how loads on specimen are achieved and shear is derived at zero moment location

3.2.3 Results

3.2.3.1 Design values for new composolite panel properties

Design values for the Composolite panels, as manufactured today, are stated in the Strongwell design literature (Strongwell 2009). Table 3.3 shows values related to stiffness and strength. Also obtained from the manufacturer's literature are the results of three-point bending tests performed on complete panels, equivalent to the testing undertaken on the aged panels. By performing the graphical method describing Timoshenko Beam Theory on these results, further values (also included in Table 3.3) have been established for comparison.

Table 3.3 GFRP material properties (Strongwell 2009)

Strongwell design literature (min value)		
Tensile elastic modulus, E		17.1 GPa
Ultimate tensile strength		214 MPa
E_{flex} and G_{flex} inferred by graphical method from Strongwell's in-house load-deflection test results		
Flexural elastic modulus, E_{flex}		25.3 GPa
Flexural shear modulus, G_{flex}		0.95 GPa

3.2.3.2 Whole panel testing: flexural elastic modulus

Figure 3.10 and Figure 3.11 provide a summary of results concerned with flexural stiffness. Each bar represents the value for a single panel. A single panel from each façade elevation has been tested over three spans in three point bending, with the exposed face in tension, and then again with the exposed face in compression, according to the procedure described in Subsection 3.2.2.1.

Figure 3.10 shows panels that have experienced direct UV irradiation (on the east, south and west facing building elevations,) exhibit a lower stiffness when tested in bending with the exposed external face in tension. The north facing panels do not show this behavior. This suggests that degradation attributed to UV exposure, or cyclic wetting and drying, is of greater detriment to material stiffness when compared to damp conditions alone. It also suggests that in tension the matrix is compromised however in compression it is not.

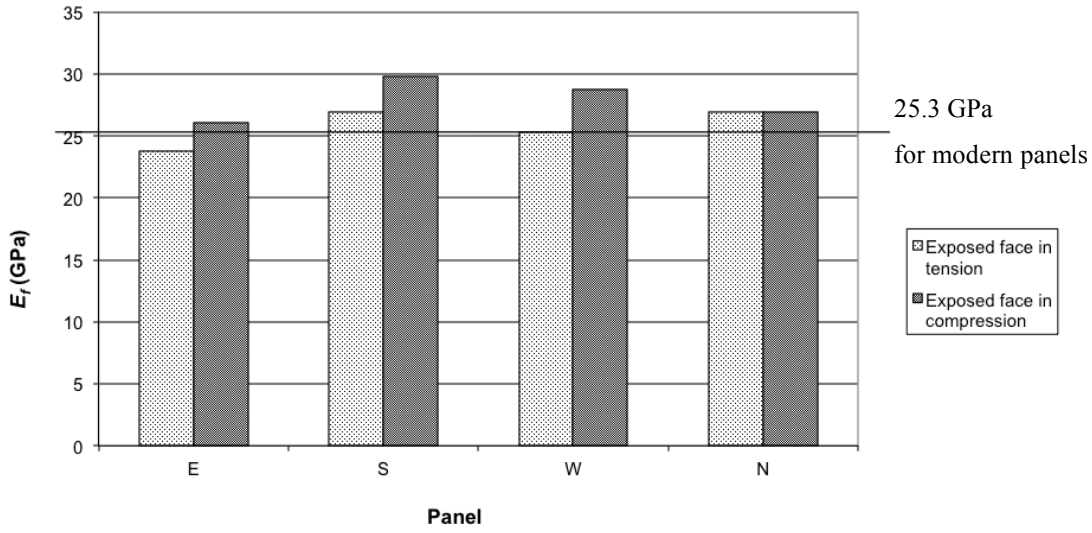

Figure 3.10 Flexural elastic modulus for each of the building panels, and the manufacturer's testing derived value of 25.3 GPa

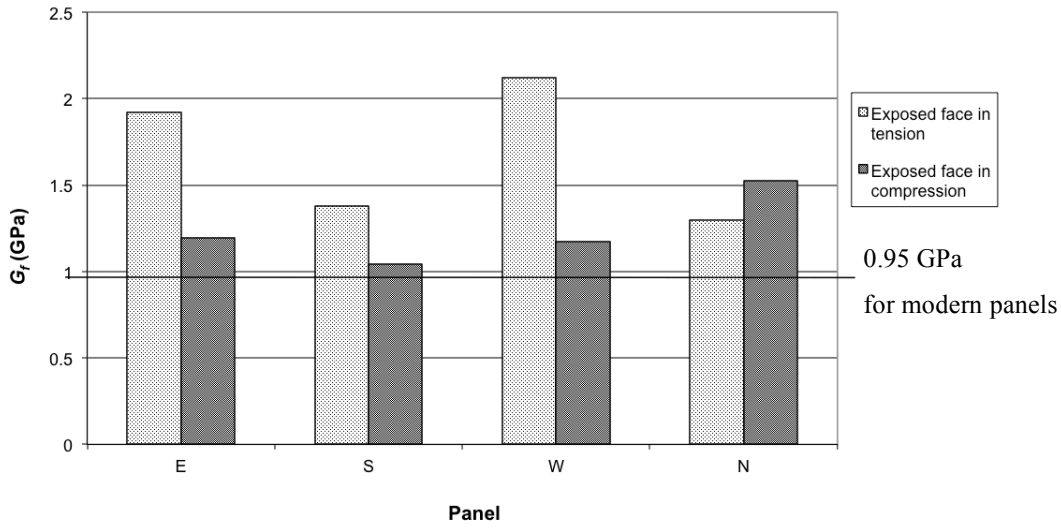

Figure 3.11 Flexural shear modulus G for each panel, as per original orientation on building, and nature of test and the manufacturer's testing derived value of 0.95 GPa

Examining the results of Figure 3.11, the calculated flexural shear modulus appears to be sensitive to the nature of testing of the panel (inverted or not). However, it has previously been documented (Tolf and Clarin 1984) that the shear modulus values derived using the graphical method employed are sensitive to small changes in the fit of the regression line. Considered mathematically, the adopted Timoshenko equation for

beam bending produces a solution for flexural shear modulus that is highly sensitive to small changes in the input variables, due to the small contribution of shear deformation to the total deflection. The average shear modulus measured does appear to meet that of the manufacturer's value for modern panels. See Figure 3.11.

3.2.3.3 Coupon testing: tensile modulus

Figure 3.12 shows the results of coupons taken from the panels and tested in tension. The web material of the aged panels appears to have a lower tensile modulus compared to flanges, though this difference is not evident in the new material. This is as predicted by resin burn off and hand calculation. The lowest value of tensile elastic modulus established during testing was 15 GPa (for the south facing panel web coupons). This correlates well to the established reduction in fibre content of these elements as illustrated in Table 3.2. Coupons of internal material out-perform those of external material from both south and west facing panels, subjected to the prevailing estuary wind. Coupons from north and east facing panels do not exhibit this trend. A large variance across tests is observed, particularly for the webs (as already discussed) and external material, prompting further investigation. Each result represents an average from three coupon tests.

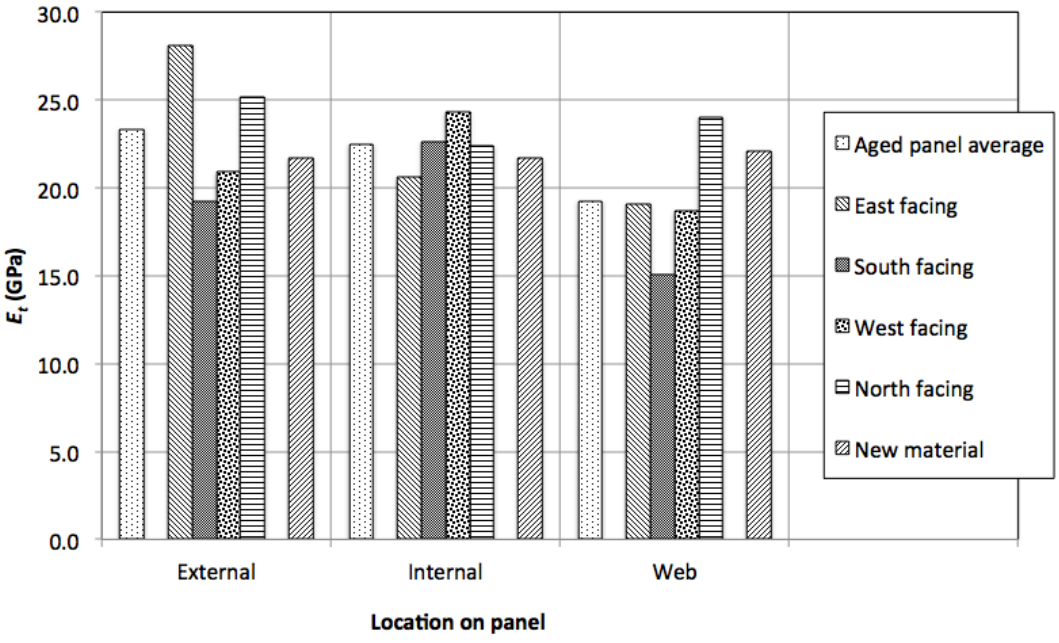

Figure 3.12 Tensile elastic modulus as a function of coupon origin

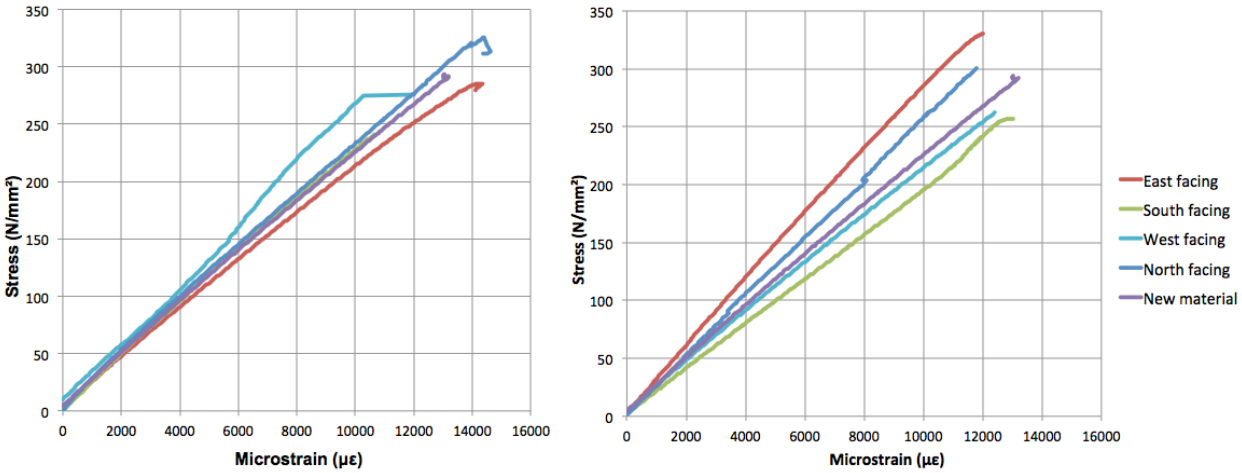

Figure 3.13 Stress-strain plots, for internal (left) and external (right) panel material

Figure 3.13 shows that a high degree of linearity to failure in the stress-strain response of the pultruded GFRP to axial tensile load. It should be noted that not all of the plots presented in this figure represent the material to failure due to strain gauges going off-scale or breaking from the specimen before this, and tensile elastic modulus was calculated over strains up to 2000 με. Figure 3.14 portrays the strength of material from different panel origins.

3.2.3.4 Coupon testing: tensile strength

Figure 3.14 shows coupons of external flange material exhibited a lower strength when compared to internal ones, indicative of environmental degradation. Material that was exposed on the south facing building façade shows the biggest reduction in strength. This material has been subjected to the most UV irradiation. Each result represents an average from three coupon tests.

As also found in the tests measuring tensile elastic modulus, webs from the south facing panels tested gave a low result, equal to the manufacturers design value (214 MPa), which again, correlates well with the reduced fibre content of these elements established by resin burn-off.

Tensile strength and modulus exhibit similar trends indicating that perhaps fibre volume is responsible for the variation, rather than degradation. Table 3.2 shows that this is probably not the case, and that environmental degradation is responsible. The

south facing external flange material that was subjected to rein burn-off possessed the highest fibre content.

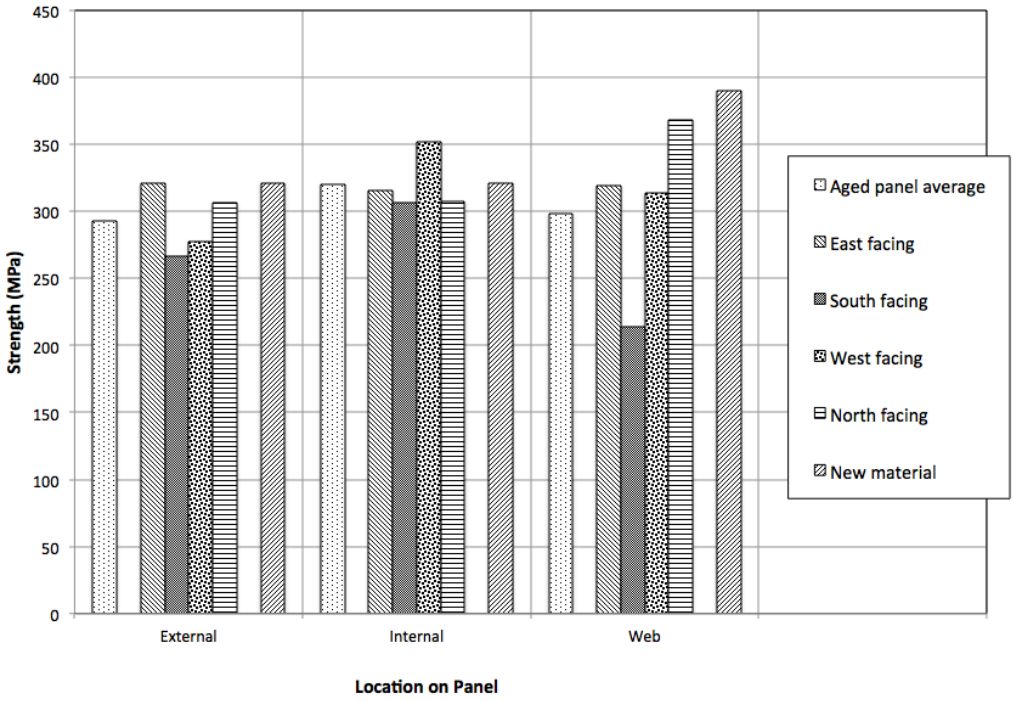

Figure 3.14 Maximum tensile strength of coupons

3.2.3.5 Coupon testing: compressive modulus, E_c

The compression modulus data presented in Figure 3.15 is the minimum value determined from the two coupons tested to establish each data point. A high level of variation was shown between the two coupons tested for south facing panel webs (41.9 GPa and 15.5 GPa, resulting in a standard deviation of 18.7 GPa). This supports the existence of a non-uniform distribution of principal fibres in the web material of the south facing panels (the next largest standard deviation of only 3.7 GPa was for web coupons from the east facing panels.) The fabrication variability in this web material, attributed to the reduced quality control, (they were 'seconds',) is seen to impinge on the mechanical properties. The limited width of coupons extracted (10 mm for compressive testing), and the distribution of fibres in the webs, as shown in Figure 3.6, is understood to permit large variations in the amount of fibre 'captured' in the prepared test specimen. Thus the degree of variability exhibited in results for web specimens is amplified.

The overall average compressive elastic modulus of 26.8 GPa was 17.5% higher than the tensile modulus determined in Subsection 3.2.3.3. It is more usual that compressive modulus is lower than tensile modulus for FRP materials (Bank 2006), so this suggests that, in this case, the resin is playing an important part in the behaviour. The resin component, which would not contribute much to the measured modulus in new material, could be contributing to compressive stiffness to a greater extent than tensile stiffness, owing to physical change with age. A hypothesis explaining this outcome is presented and tested in Subsection 3.2.5.

No new material was available by the stage of compression testing for comparison. A standard deviation of 2.1 GPa was found for average results relating to panels on different facades, in both tensile, and compressive testing for elastic modulus. In tension, however, the panel webs displayed a lower average stiffness compared to the panel flanges, which is not evident in results for compressive testing. This suggests that the resin is of greater influence on the compressive modulus measured than the tensile modulus. The compressive strength was not measured due to test limitations resulting in premature buckling of the specimens.

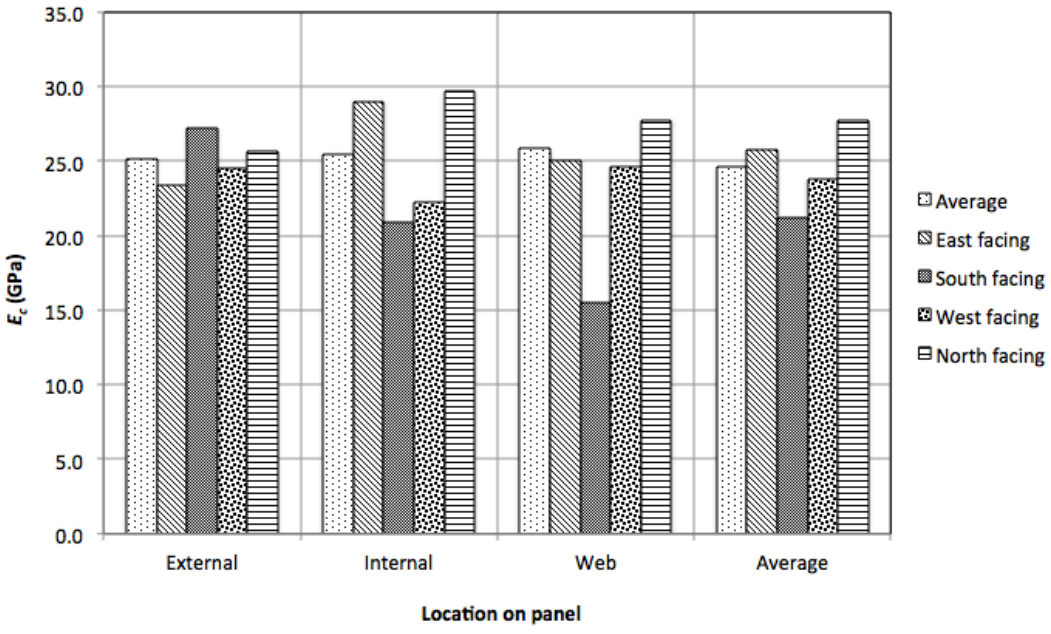

Figure 3.15 Compressive modulus, E_c as a function of coupon origin

3.2.3.6 Coupon testing: shear modulus

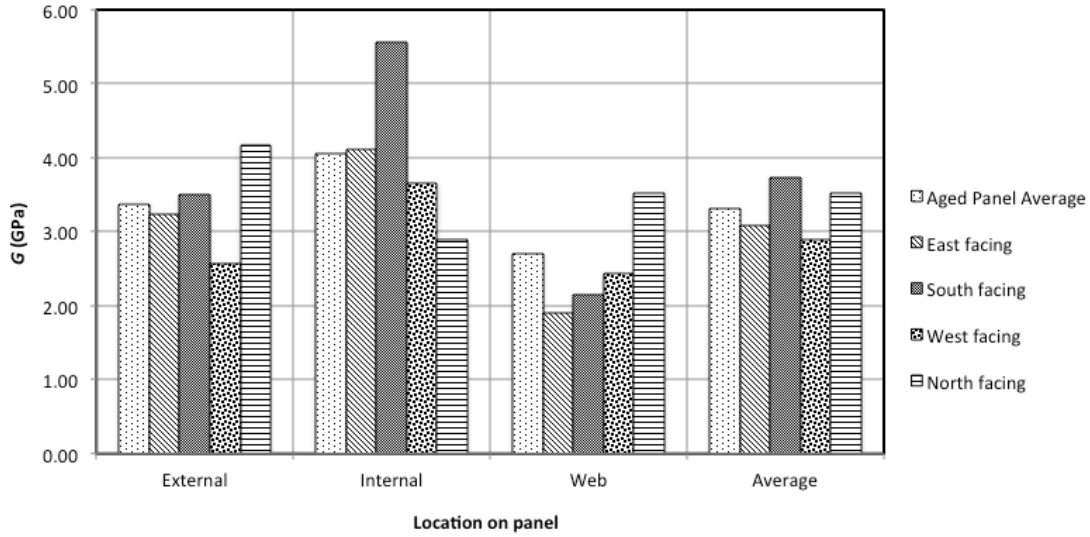

Figure 3.16 Shear modulus as a function of coupon origin

Figure 3.16 shows the results of the shear modulus coupon tests. It can be seen that the west facing panels exhibit the lowest average shear modulus. The lack of stiffness of webs in this panel is not likely to be attributed to deterioration with age, as the exterior material has maintained good integrity. Internal coupons were observed to be stiffer than external coupons by 17%, although the averages displayed are affected by the result for the internal coupons from South facing panels.

3.2.4 Model for composite panel action

In Subsection 2.1.1 a model was derived, from first principles, for the bending stiffness of cellular panels (of the type investigated above in section 3.2). Previous studies have reported that the axial compressive stiffness is typically 80% that of tensile stiffness (Bank 2006), and the model takes into account this ratio of differing compressive and tensile axial elastic modulus of the fibres in the GFRP. It has been demonstrated in Section 3.2 that the aged resin influences the relative compressive and tensile elastic moduli to an extent where the fibre behaviour does not yield a similar effect on stiffness. This section details work undertaken with the intention of comparing failure

stresses for each of the panels, and also comparing the theoretical flexural response of panels according to a compressive/tensile modulus ratio from literature, with a measured experimental response. This second objective was not possible, for reasons explained below. It has been shown that the model developed to describe the stress and strain in the composite section is useful in comparing the performance of panels from each façade orientation, to observe whether environmental exposure has influenced ultimate collapse load.

Table 3.4 shows values relating to the properties of the Composolite building panels that are necessary to determine the neutral axis depth and resistive moment per unit surface strain according to Equation 2.15 and the stress distribution in Figure 2.1. The resulting value of 9,800 kNmm/mm was used together with the 3-point test span, and failure load found experimentally for each panel, to provide an expected strain at failure on the compressive upper panel face. Note that the figure 9,800 kNmm/mm is a moment per unit width, Per unit strain on the surface in compression. Table 3.5 shows how this was used to determine failure strain and stress: the values in the column for compressive strain are found from the moment per unit width of panel divided by the value 9,800 kNmm/mm, the moment per unit width, Per unit strain on the surface in compression.

The model developed in Subsection 2.1.1 allows comparison of theoretical values for surface strain with measured values in the laboratory. Table 3.6 shows this expected strain at failure, alongside average measured strain at failure from the two gauges present on the upper surface of each panel.

Table 3.4 Composolite panel properties. Neutral axis depth and resistive moment per unit surface strain, as calculated theoretically.

T (mm)	B (mm)	t_f (mm)	b_w (mm)	V_f	E_m (GPa)	E_{ft} (GPa)	E_{fc}/E_{ft}	E_{fc} (GPa)	x (mm)	M/ε/unit width (kNmm/mm)
77.1	85	3.15	2.66	0.67	3.6	75	0.8	60	44.0	9.80E+03

Table 3.5 Failure strain and stress, derived from load, test span and theoretical distribution of stress

Panel façade	Nature/orientation	Failure load (kN)	Length of span (mm)	Moment per unit width Nmm/mm	Compressive strain (as per table 3.4) (microstrain)	Comp. fibre stress (as per E_{fc} = 60GPa) (MPa)
E	Int. in comp.	36.8	2010	30571	3120	187
	Ext. in comp.	52.1	2010	43282	4417	265
S	Int. in comp.	49.5	2090	42815	4369	262
	Ext. in comp.	40.5	2100	35200	3592	216
W	Int. in comp.	34.5	2090	29810	3042	183
	Ext. in comp.	43.0	2110	37499	3826	230
N	Int. in comp.	37.1	2560	39259	4006	240
	Ext. in comp.	32.4	2550	34182	3488	209
					average:	224

Table 3.6 Compressive strain at failure for each panel and orientation, based on failure load and theoretical model, alongside average of two strain gauge measurements ('' indicate where gauges peeled from the specimen or went off-scale prior to failure, and value represents single remaining gauge)*

Panel	Strain at failure (με)			
	Internal face up		External face up	
	Predicted from model	Measured	Predicted from model	Measured
E	3120	2510*	4420	4010*
S	4370	3840*	3590	3120*
W	3040	2870	3830	3540*
N	4010	-	3490	3100

It can be seen from Table 3.6 that the measured strains are below those predicted from the theoretical model. This implies that the neutral axis position was closer to the compressive face than expected at (or just before) failure.

To quantitatively assess the extent to which the neutral axis had migrated from it's expected position more accurate strain gauge readings would be required. It is concluded that the work above cannot verify this. However the findings do seem to

align with previous results indicating that the GFRP polymer matrix was susceptible to brittle fracture in tension (causing the neutral axis to be closer to the compressive face than expected).

The results obtained for failure strain using the theoretical model are of much greater use to compare stress in the panels at failure; relying not on strain gauges, but on measured load, and panel and testing geometries. Figure 3.17 shows the data inferred by the failure load and the model.

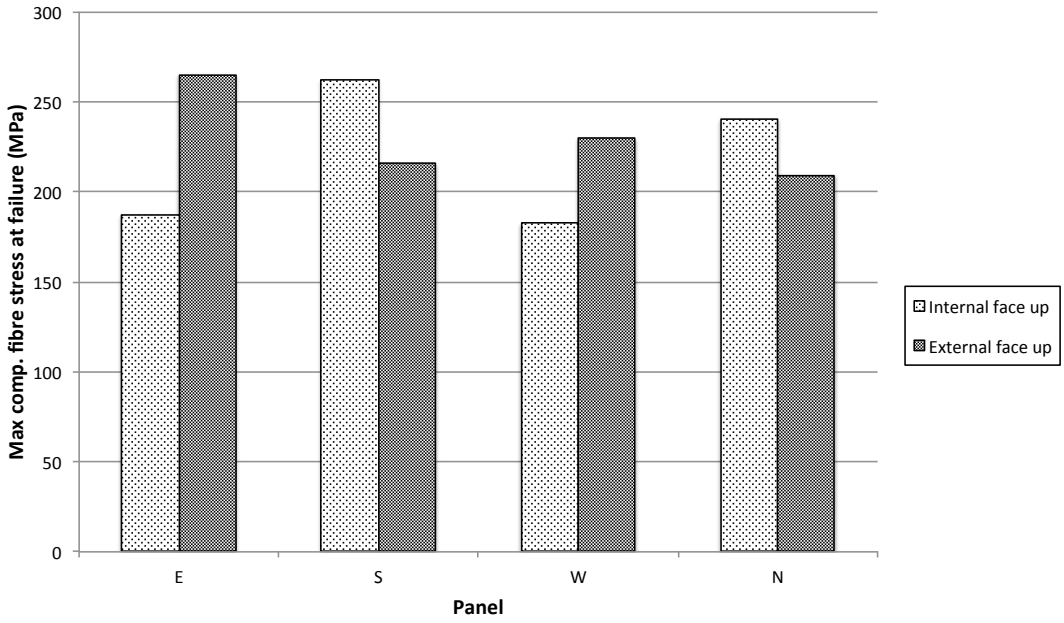

Figure 3.17 Max compressive fibre stress at failure of whole panel in three-point bending

The strength of the panels does not appear to be affected by the original aspect or orientation of testing as seen with the stiffness of whole panels. However it should be noted that failure of the panels was by flange buckling with accompanying tearing of the flange web junction. This type of failure is very unstable and sensitive to a large number of variables. The large scatter in results attributed to this means that a larger number of panels would need to be tested to destruction to make the same kind of conclusions regarding the influence of environmental exposure as could be made regarding the stiffness of the whole panels.

3.2.5 Assessment of polymer hardening

3.2.5.1 Introduction

Brittle hardening of the polymer resin is expected to be something of great significance in the whole life performance of GFRP. It is not a phenomenon that has been documented as being of great significance, in this context, in existing literature.

Upon inspection of the results from the coupon testing, the *compressive* elastic modulus measured (26.6 GPa mean value) was found to be higher than the *tensile* modulus found for the material (22.1 GPa mean value). An entirely opposite relationship had been expected, since micro-buckling of fibres typically reduces elastic modulus in compression; a value in compression of approximately 80% that of the tensile modulus is more typical (Bank 2006). It was hypothesised that brittle hardening of resin over time may be responsible. The external material from the south facing panels, which had experienced a higher degree of UV irradiation, exhibited the highest modulus. Hardening of the resin with age, and with UV exposure, could explain a higher modulus when working in compression. Such hardening could result in a reduced stiffness in tension due to early onset of brittle facture in the resin, whereas in compression no such fracture occurs. To investigate this hypothesis, further experimental work was undertaken.

3.2.5.2 Procedure for assessment of polymer hardening

Three coupons of aged GFRP external flange material, from south facing panels, and five coupons of new GFRP Composolite panel flange material, were subjected to two identical flexural tests (see Figure 3.18), each with intervening tensile loading. The tensile loading was undertaken in accordance with the method described previously in Subsection 3.2.2.3, but with samples 330 mm in overall length. The tensile strain to which each coupon was subjected was varied according to values indicated in Table 3.7 and Table 3.8. The influence of the direct axial tensile strain could be observed by changes in the response of subsequent flexural tests, i.e. if resin plasticity was preserved there should be no fracture of the resin and the initial and final flexural tests should correspond to identical flexural moduli. If UV degradation of the resin over the material lifetime had caused a brittle hardening, and the strain limit of tensile fracture

of the resin was exceeded then a variation between the two flexural responses (pre and post tensile test) would be evident.

These flexural tests were conducted over a 200 mm span such that the strain in all material remained below 4000 με, which corresponds to a stress of 87 MPa (41% of the 214 MPa design ultimate strength). Using the second moment of area of the coupon cross-section, and the applied load, the stress at the strain gauge location was derived. The corresponding strain recorded on the surface of the coupon at this same position (20 mm from the centre of the specimen) was then used to establish the flexural elastic modulus of the sample.

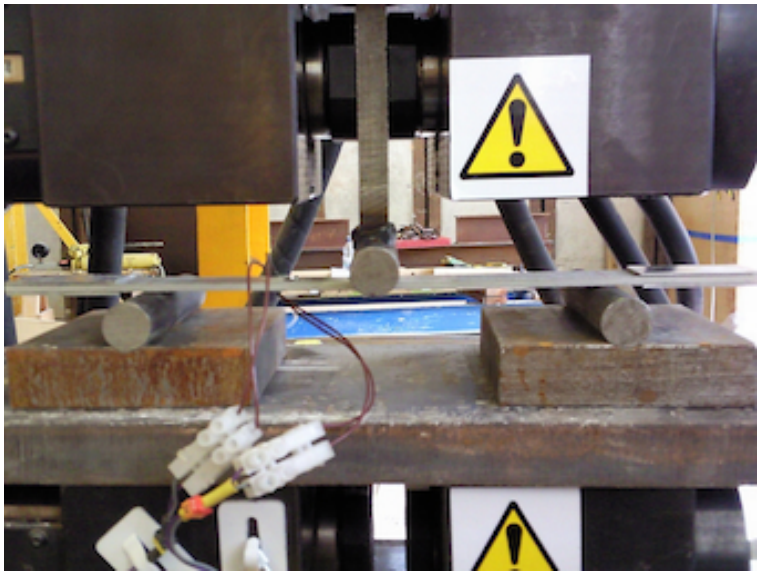

Figure 3.18 Flexural testing of coupon

3.2.5.3 Results

Table 3.7 Retention of coupon flexural stiffness post tensile straining: aged material.

Sample	Initial E_{flex} (GPa)	Tensile strain to which sample is subjected (με)	Subsequent E_{flex} (GPa)	% original stiffness retained
1	18.4	6000	19.6	106
2	21.5	9000	10.0	46
3	21.3	10000	5.8	27

The initial stiffness of the three coupons of aged panel material in Table 3.7 are seen to be very similar. The subsequent stiffnesses vary, depending on the axial tensile strain to which the specimens were subjected before being re-tested in flexure.

It can be seen that a tensile strain of 6,000 με has no detrimental effect on the residual flexural stiffness of the sample, however by imposing 9,000 με the subsequent stiffness is almost halved. Sample 3 was strained to 10,000 με and the subsequent stiffness was shown to be very low. A reduction in stiffness this large would appear at first glance to be attributable to more than resin fracture, as the resin area in cross section is only 30% of the total area. Indeed in the case of Sample 3 some fibre breakage could be heard. This did not occur during straining of Sample 2. Attributing such reductions in stiffness to the resin alone could be explained, and accounted for, by considering fibre distribution in the coupon. It was known that fibre distribution in the cross-section of pultruded GFRP elements is not uniform; the outer ply regions are more resin rich and the central lamina more fibrous. It could therefore be understood how flexural tests might be more sensitive to resin integrity, as the resin is more abundant in the regions more highly strained during flexure.

Table 3.8 Retention of coupon flexural stiffness post tensile straining: new material.

Sample	Initial E_{flex} (GPa)	Tensile strain to which sample is subjected (microstrain)	Subsequent E_{flex} (GPa)	% of original stiffness retained
1	12.5	4000	13.4	107
2	18.7	6000	20.4	109
3	18.7	6000	19.7	105
4	15.0	9000	14.7	98
5	19.4	10000	19.3	100

Further tests on new composite material, presented in Table 3.8, were necessary to demonstrate that the phenomenon of brittle polymer hardening, as characterised by a reduction in strain limit of resin fracture which is age dependent. Flexural tests both

before and after an intervening tensile loading yielded very similar results. The fact that the direct axial tensile stress did not affect flexural stiffness indicates that the resin was not affected in coupons of the new material. Coupons of new GFRP do not exhibit a reduction in flexural stiffness when subjected to previous axial tensile strains, up to values of 10,000 με. The conclusion that a reduction in strain limit of resin fracture is age dependent, and to a degree of such great mechanical significance, is an important finding. It confirms that design factors of safety, that should consider this limit, must account for the way in which this limit will change with age.

The initial flexural stiffness of some specimens (S1 of the aged material, and S1-S3 of the new material) was observed to be slightly lower than that found after straining. The stiffness of these specimens could not really increase of course, and the tolerance of the test is revealed to be as much as 10%. Variation between new and old material greater than 10% was deemed to be significant and occurring as a consequence of physical chance in the material with ageing.

With the application of material partial safety factors, the design strength used for design of structural elements in GFRP is typically 60% of the characteristic strength (Bank 2006). The ultimate tensile strength of the FRP, as defined by Strongwell, is 214 MPa. The useable design strength would therefore be around 0.6×214 = 128 MPa. Using an elastic modulus value of 21.7 MPa (the average tensile modulus from tests presented in Figure 3.12), this corresponds to a maximum design strain of 5900 με. This is lower than the strain of 6000 με at which no degradation in stiffness due to polymer hardening was observed and therefore the typical material partial safety factors seem appropriate. It should be noted that in their application as building panels for a site office and visitors centre, (not the intended bridge enclosure application,) the panel material tested will have experienced an estimated maximum strain no greater than 1000 με in service. This has been verified by structural design check accounting for both wind and occupancy actions at ultimate limit state on the structural facades.

3.2.6 Discussion of the Second Severn Crossing Visitors' Centre case study

A program of mechanical testing of naturally aged composite, taken from the Severn Bridge Visitors' Centre, has assessed the durability of pultruded GFRP. In 17 years the

mechanical material properties do not appear to have significantly diminished below design values, despite aesthetic quality suffering due to lack of maintenance.

Coupons of internal material from panels on the south and west-facing façades outperformed those of the weathered external material, in terms of tensile strength, tensile modulus and shear modulus. These elevations are those exposed to the prevailing estuary wind and rain, and those South-facing especially, to a higher degree of UV exposure. Degradation does not appear to have infiltrated the GFRP to a degree that significantly affects 'whole panel' behavior, and design values therefore appear to be appropriate. East, South and West facing panels, which have experienced direct UV irradiation, all exhibited a slightly reduced stiffness when tested whole with the weathered external face in tension, as opposed to the internal face in tension.

Coupon testing has demonstrated that the tensile elastic modulus of aged material, on average, meets that of new material. However the tensile strength of the aged material is lower than that of new material. This can partly be accounted for by the observed deficit in fibre content. The comparison afforded between new and old is qualitative, owing to fabrication and material variability remaining unknown factors despite fibre volume fractions being accounted for.

It was apparent that for all old (weathered) panel materials the tensile modulus was lower than the compressive modulus, contrary to most reports in current research. It was hypothesized that 'polymer hardening' had occurred leading to a brittle strain limit for the aged resin. A tensile strain of 9000 με caused severe cracking in the matrix such that subsequent flexural stiffness was reduced by half. However, this phenomenon does not completely explain the relationship between tensile and compressive modulus, because below 6000 με (the region in which the modulus was calculated) the onset of matrix cracking would probably not have been reached. The strong influence of polymer hardening on the stiffness of the composite, is very evident, and how this might improve resistance to micro-buckling of fibres in compression is the subject of further research. A reduction in the strain limit of resin fracture with age was observed.

3.3 Mondial House

This Section reports on a programme of testing on panels from Mondial House. In contrast to the panels tested from the Second Severn Crossing Visitor's Centre the panels from Mondial House were fabricated by hand lay up technique and had experienced a lifetime in service of 30 years.

Glass fibre reinforced polymer (GFRP) material from naturally-aged sandwich panels has been examined through a campaign of mechanical, thermal and microscopic analysis. The façade panels were salvaged from Mondial house upon its demolition. They offer the opportunity to test GFRP material incorporated in secondary structural elements after a 30-year life in service. The performance of this naturally-aged material has been examined by comparing properties as found for both internal and external structural GFRP sandwich skins. The influence of UV and weathering on the aged characteristics has been investigated. The phenomenon of brittle resin hardening has also been examined.

3.3.1 Introduction

Until August 2006 Monidal House occupied a position on the River Thames in London (Figure 3.19). The building was designed by Hubbard, Ford and Partners, and completed in 1975. Mondial House boasts 30-year old material, fabricated by hand lay up, in contrast to the pultruded material of the Visitors Centre panels that were 17 years in service.

Figure 3.19 Mondial House

The panels, shown during the building demolition in Figure 3.20, were designed by Peter Hodge Associates and fabricated by Anmac Ltd. and Brensal Plastics Ltd. (Brookes and Meijs 2008). They incorporated polyester resin GFRP structural skins. The outer skin included a gel coat that used isophthalic resin, pigmented white, with an ultraviolet stabilizer (see Figure 3.21.) The glass fibre reinforcement consisted of a 9 ounce per square foot CSM (chopped strand matt), and the gel coat itself used an underlying 3-ounce per square foot CSM reinforcement. A foam core of rigid polyurethane provided thermal insulation and some degree of panel stiffness (Domone and Illstone 2010). The internal lay up fibre construction details are unknown.

Figure 3.20 Discarded façade sandwich panels

Figure 3.21 External and internal sandwich skin material, showing 'combed' ripple profile of outer gel coat

Scott Bader and The University of Surrey inspected the structure in 1994 and the degradation was found to be minimal. The University of Surrey conducted further investigation into the mechanical properties since the demolition. Conclusions concerning the intra- and inter-panel variation of mechanical properties were made and models developed representing the probabilistic distribution of these properties in GFRP using CSM reinforcement (Sriramula and Chryssanthopoulas 2009). However there was no comparative study undertaken, between internal and external sandwich skin GFRP material. As such, the influence of UV and weathering on the outer skin was not investigated.

In this study, coupons cut from internal and external GFRP structural skins have formed part of an investigation into the influence of UV and weathering on the material. The lack of 'base case' data has prohibited a percentage reduction in mechanical properties over this period from being established. However a comparison of the material profiles for internal and external, exposed material has been undertaken. An assessment of how comparable the sandwich skins were originally has also been undertaken. The effect of exposure to UV and weather has been observed by three means: mechanical testing, dynamic mechanical thermal analysis (DMTA), and micro-analytical study using electron microscopy. The analytical study undertaken using microscopy is qualitative regarding observations concerning degradation of the polymer matrix. Microscopic analysis of the fibre reinforcement was vital to establish the fibre volume ratio of the internal composite skin of the panels, and to verify the extent to which a comparison against external skins is viable, with or without calibration of results to account for any difference in the amount of reinforcement.

The phenomenon of brittle resin hardening has also been investigated, in an attempt to verify previous findings presented in 3.2.5. A similar method of two flexural tests with an intervening tensile loading has been adopted to establish whether a reduced strain limit before matrix fracture in tension is observed for the resin of the external and the internal sandwich skin material.

3.3.2 Methodology

3.3.2.1 Mechanical testing: tensile

Tensile testing of coupons extracted from the panel faces was undertaken to compare the mechanical performance of the internal (shielded) material with external (exposed) material by determining the elastic modulus and the tensile strength for the GFRP material from each face. By extracting coupons at different orientations on the panel faces, these tests were also used to assess whether the panel hand lay up fabrication had an influence on the mechanical properties along certain axes.

In-situ the façade panel elements had an external GFRP skin which possessed a gel coat on the outer face, and a rigid polyurethane foam core to the inner side. The structural skins were firstly pried from the foam core, and the remaining foam cleaned from the GFRP by mechanical means. The composite material was made uniform, such that the through-thickness properties were not unevenly distributed and coupons could accommodate resin-bonded aluminum tabs necessary to perform tensile loading (see Figure 3.22). This was achieved by removing the gel coat and accompanying 3 ounce per square foot CSM with a belt sander. Each surface of the resulting element and each surface of the internal GFRP coupons were sanded to achieve uniform smoothness, such that cross section dimensions could be accurately determined. (Microscopy was later used to confirm equivalence of fibre contents.)

Coupons for tensile testing were prepared as per BS EN 2747:1998 (BSi 1998). These coupons were produced in a ‘waisted’ profile for tensile loading to permit the low grip pressure desired in the jaws of the test rig, and to allow the measurement of an even strain distribution in the composite material (in which the CSM reinforcement is multidirectional). Coupons were cut with longitudinal alignment of 0^o, 45^o and 90^o to the vertical panel orientation in situ as a façade, thus enabling verification of the random, multidirectional nature of the CSM reinforcement. Aluminum tabs of 1.5 mm thickness and 50 mm length were bonded to the coupon ends (in the area in contact with the test rig jaws) using epoxy resin. One 10 mm strain gauge was attached centrally on each face of the coupon, orientated in the direction of the applied load. Testing was conducted under displacement control at 1 mm/min. Coupon cross sectional dimensions were determined using a micrometer, accurate to 0.01 mm. It

should be noted however that the thickness of the internal coupons once sanded to smooth even profiles was very small but, despite this, significant pits and divots remained in the specimen as shown in Figure 3.23.

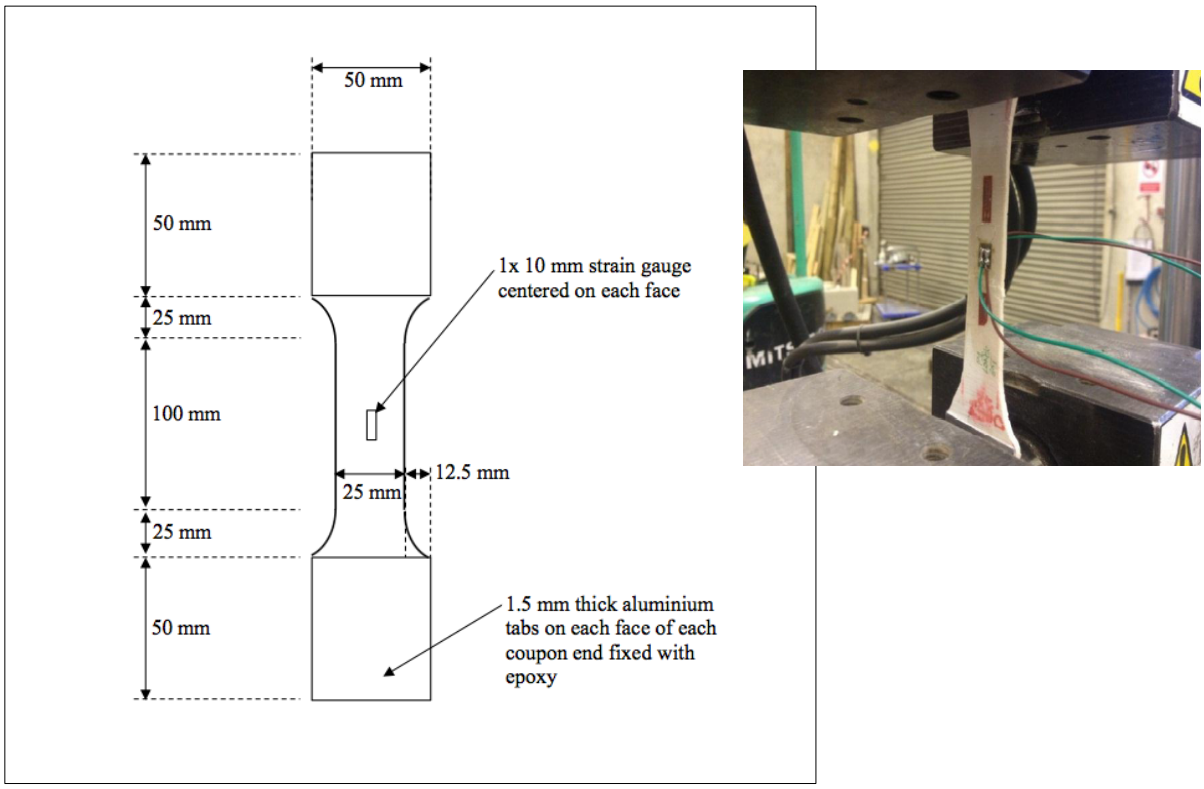

Figure 3.22 Longitudinal coupon set up

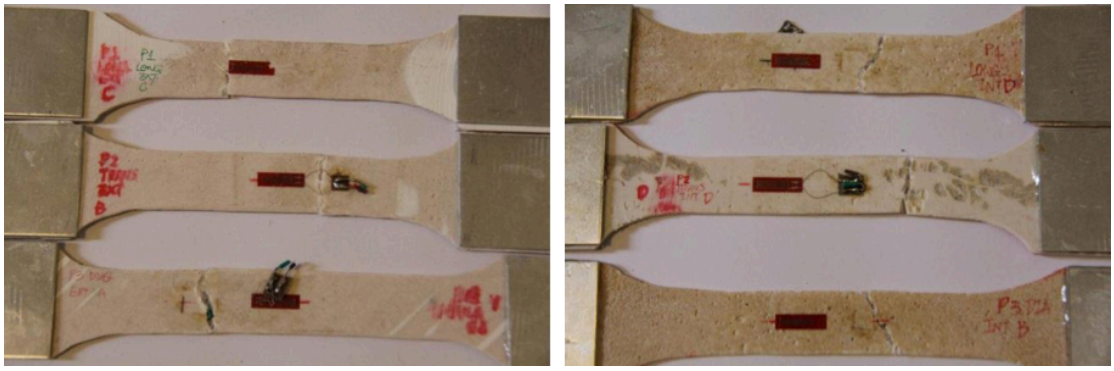

Figure 3.23 Coupon surface integrity, external (left) and internal (right)

3.3.2.2 Assessment of polymer brittle hardening

It was of interest whether the aged resin from the Mondial house panels had experienced hardening, and associated reduced limit of brittle fracture in tension, as observed for the Severn Crossing Visitors' Centre panel material. To test this, material from each panel face was subjected to the assessment methodology conducted previously: coupons were prepared and subjected to two identical flexural tests with an intervening tensile loading, as described in Subsection 3.2.5.2. The coupons were straight sided (to yield the constant bending stiffness desired for the flexural part of the test) and of 25 mm width as shown in Figure 3.24. Six coupons for each of internal and external material were prepared and tested. The tensile loading was conducted as explained in Subsection 3.3.2.1, and preparation of the specimens undertaken in the same manner whereby the gel coat with 3 ounce per square foot CSM was once again removed. The tensile strain to which each of the coupons was subjected is presented in Table 3.11 and Table 3.12 and ranged between 4000 and 8000 με. The upper limit of 8000 με was chosen due to the threshold of failure observed in the coupons. (The ultimate tensile strain of the GFRP material in this case study varied between 7500 and 9000 με.) The lower end of 4000 με corresponds to a typical design limit for strain, relating to an elastic modulus, E of 8 GPa, an ultimate tensile stress of 54 MPa (both values revealed from proceeding experimental findings) and a material partial factor of safety of 0.6 (Bank 2006).

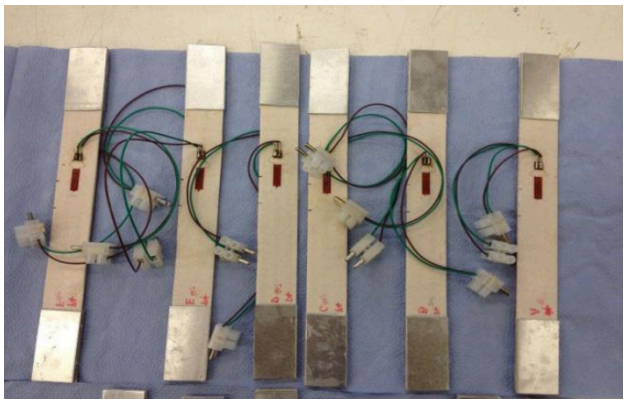

Figure 3.24 Straight sided coupons prepared for assessment of polymer brittle hardening

Flexural tests were undertaken as illustrated in Figure 3.25. It was ensured that during flexural tests the material remained below 40% of its ultimate tensile strength. For a

typical internal coupon of 1.5 mm thickness (and width 25 mm) the second moment of area I is 7.03 mm^4. Using a modulus of 8 GPa the limiting strain corresponding to 40% of the ultimate strength is 2,700 με. To impose loading on the flexural coupons to this limiting value was found to require the following parameters: a simply supported span of 100 mm, and a point load of 1 kg. Predicted deflections were approximately 3.7 mm, easily measurable with displacement transducer. This arrangement can be seen in Figure 3.25. A mass hanger (included in the 1 kg applied load) was suspended by a piece of wire looped over the specimen. Three-point bending was used as opposed to four-point because of the limited size of the specimens and to mitigate the influence of local defects on the coupon length, which caused uneven deflected shapes when loaded on a four-point rig.

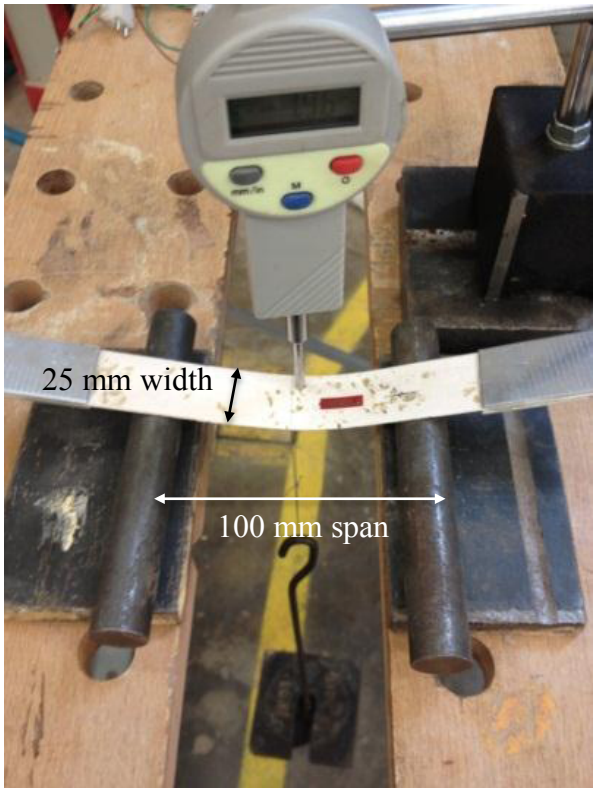

Figure 3.25 Three-point simply supported span set-up for flexural testing

3.3.2.3 Mechanical testing: shear

To perform a comparative study on the matrix of the internal and external composite material, the in-plane shear modulus, G_{xy}, has been determined, as further means by which to assess mechanical performance. The plate twist method for fibre reinforced

plastics has been used. Testing of the type described in 3.2.2.5, using the Iosipescu test rig, was not possible in this instance due to the weakness and small thickness of the material. These factors are both attributed to a higher than acceptable bearing stress being imparted by the steel pin on GFRP material, when installed in the rig shown in Figure 3.9. Hence viable results could not be achieved using the iosipescu method. Instead the plate twist method was adopted, and conducted according to BS EN ISO 15310:2005 (BSi 2005). Four specimens from each of internal and external panel faces were sanded as per the method described in Subsection 3.3.2.1, to produce smooth specimens of uniform thickness, and with the gel coat of the external material removed. The specimens were cut to squares of side length 150 mm. No strain gauging was required. The specimens were installed in the test rig as illustrated in Figure 3.26.

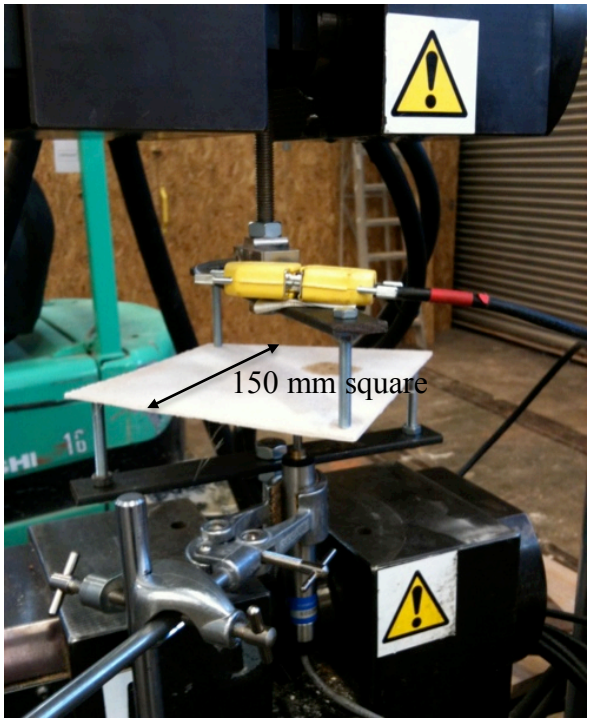

Figure 3.26 Plate twist test rig set up to determine shear modulus

Equation 3.5 to Equation 3.8 shows how G_{xy} is established, where a is the specimen edge dimension in mm, t is the specimen thickness in mm, K is a geometric correction factor, w_1 and w_2 are the deflections in mm ($w_1 = 0.1t$, $w_2 = 0.3t$), and F_1 and F_2 are the corresponding loads in Newtons. D_p is the length of the diagonal of the plate and S_p is the diagonal span of the loading pins. These equations are taken from BS EN ISO 15310:2005 (BSi 2005).

$$G_{xy} = \frac{3}{4} \times \frac{\Delta \times a^2 \times K}{100t^3} \tag{3.5}$$

$$\Delta = \frac{F_2 - F_1}{w_2 - w_1} \tag{3.6}$$

$$K = 3s^2 - 2s - 2(1-s)^2 \ln(1-s) \tag{3.7}$$

$$s = \frac{S_p}{D_p} \tag{3.8}$$

Tests were conducted under displacement control at 1 mm/min. Due to the small specimen thickness the maximum displacement over which G_{xy} can be determined as permitted by the code (BSi 2005), to get an accurate result for in plane shear modulus, was very small. This meant that to remain in accordance with the code of practice, a very low calibrated load was required. To address this, a 500 N load cell was incorporated into the load transfer set up. In addition a secondary displacement transducer was installed at the quarter span loading point (see Figure 3.26). This enabled tests to be run to larger displacements, whilst monitoring that the deformation exhibited was sufficiently anticlastic and had not reverted to simple flexural bending about a single axis. (See Figure 3.27.)

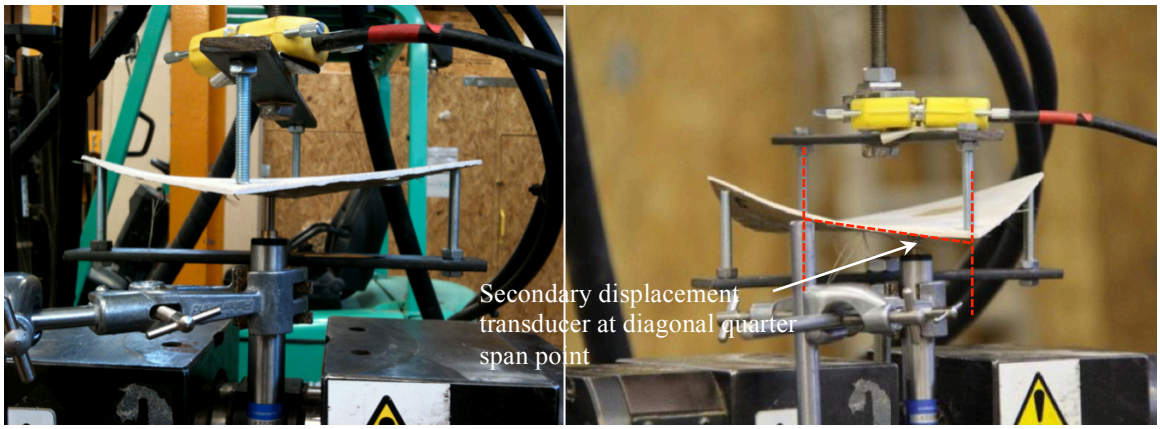

Figure 3.27 Anticlastic (left) and single axis (undesired) flexural deformation (right)

3.3.2.4 Dynamic Mechanical Thermal Analysis

Dynamic mechanical thermal analysis (DMTA) was conducted on specimens of internal and external GFRP panel material, according to code of practice ASTM D7028 - 07e1 Standard Test Method for Glass Transition Temperature T_g of Polymer Matrix Composites by Dynamic Mechanical Analysis (ASTM 2007). Environmental exposure is known to alter the T_g of polymer resins (Pochiraju et al. 2012). By comparing the relative values of T_g found for internal and external material it could be established how effectively gel coat on the external face protected the polymer against the effects of UV radiation.

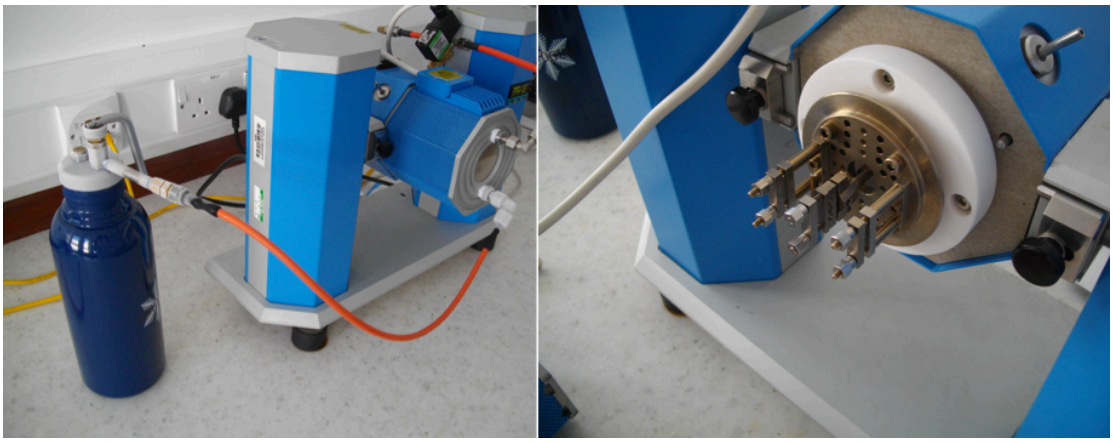

Figure 3.28 Dynamic mechanical thermal analysis rig

A total of twelve tests were analysed using the rig shown in Figure 3.28. Specimens were prepared from the sanded, smoothed GFRP, with the gel coat removed as before. Three specimens were taken from each of four different panel locations, two external skin locations and two internal locations. Average T_g is presented in Subsection 3.3.3.2 for each location and for internal and external material. Coupon dimensions were approximately 15 mm × 5 mm × 3 mm. Single cantilever bending was used to determine the Glass Transition Temperature T_g of specimens. Coupons were clamped into the centre and right hand side clips of the mounting shown in Figure 3.28, which imposed cycles of flexural displacement upon the specimen with increasing temperature, whilst recording the resistive load. The T_g is then inferred from the relationship between modulus and temperature.

3.3.2.5 Microscopy

Scanning electron microscopy (SEM) has been used to establish the fibre content and CSM distribution of each of the internal and external GFRP sandwich skins, by establishing the fibre area as a ratio in the material cross-section. The material was first sanded smooth and the gel coat of the external skin was removed as before. Square specimens of side 25 mm, produced to investigate the fibre architecture of the GFRP, were set into resin pots as shown in Figure 3.29. This enabled the specimen to be held in an orientation suitable to observe the cross section. The resin pots provided the image contrast necessary to differentiate voids in the original GFRP (which became filled with the epoxy resin), and also provided a surface that could undergo the polishing process necessary to obtain high quality images. Backscatter Electron Composition Imaging (BEC) was used to generate images on which to perform a thresholding analysis. This is a graphical process that was undertaken to determine which parts of the image represented the fibre cross sections. Only 40× magnification was necessary to produce suitable images of the material cross-section for this purpose. Software (ImageJ) was used to perform the thresholding that enabled fibres and voids to be located. Two specimens for each of internal and external cross sections were prepared and observed. Results for void ratio and fibre ratio are presented in Table 3.9.

Further analysis attempted to establish the proportion of the fibre cross sections bisected in the plane of the image at various angles. By performing a thresholding on the measured amount of light reflected from different parts of the cross section image, over a greater number of narrower intervals, it was hypothesised that the proportion of fibres at different angles to the cut surface plane would be established (as they will be more reflective if perpendicular to the cut section and decrease in reflectiveness as the angle decreases), and a more accurate set of the theoretical values for stiffness and strength determined according to literature (Bank 2006). However, some of the fibre edge surfaces had become highly polished during sample preparation, and the reflective nature of these meant that they contributed to the fibre volume fraction found, skewing the result. It was not possible to differentiate fibre edge from cut end of fibres, but the values established were sufficient to serve as a comparison.

Figure 3.29 GFRP specimens set into epoxy resin pot for inspection of cross section; steel mounts also visible

Secondary Electron Imaging (SEI) was used to perform analysis where high detailing (specifically shape) of surface features was necessary. This enabled comparison, or verification, of relative sizes of fibre reinforcement internally and externally and a general qualitative comparison of the polyester's appearance at high resolution: 2500× magnification. Specimens suitable for SEI were prepared using liquid nitrogen cold fracture, and gold coating. See Figure 3.30. Scanning using Backscattered Electron Shadow Imaging (BES) was also performed on the fractured specimens to reveal further topographical details of the interfacial (fibre edge – resin bond) failure of the broken parts. This proved more fruitful than scanning of the 'in plane' samples mounted in resin pots using BEC imaging, by demonstrating the characteristics of fracture in response to stress of both the internal and external material.

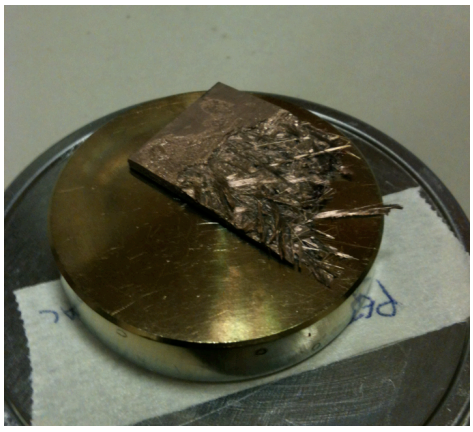

Figure 3.30 Specimen prepared by cold fracture before installing in scanning electron microscope (SEM)

3.3.3 Results

3.3.3.1 Microscopy

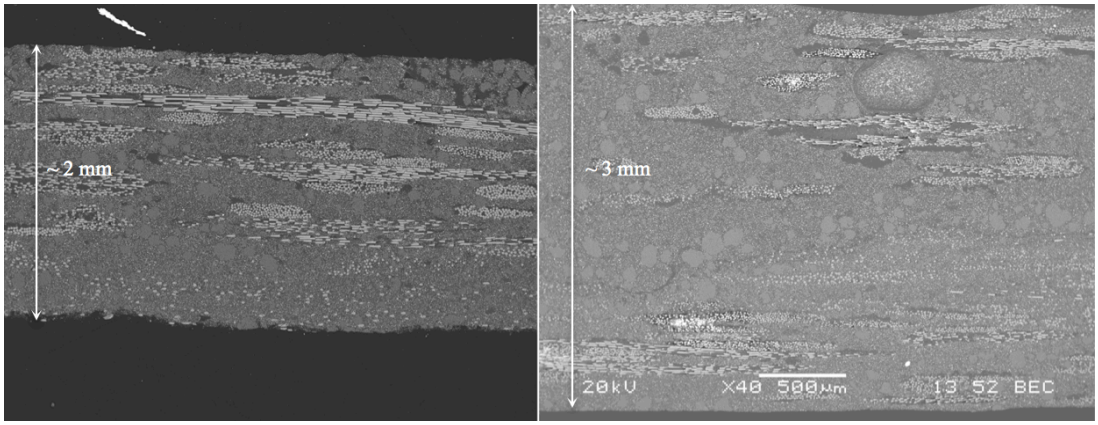

Figure 3.31 Images for thresholding exercise on internal (left) and external (right) GFRP cross sections. Magnification is the same for both images

Figure 3.31 shows two of the images upon which thresholding was used to compare the fibre content and amount of voids between internal and external material, presented in Table 3.9. The darkest areas of the image represent voids (filled with epoxy mounting resin), and the lightest are the fibres. It can be seen that the fibres are lying predominantly in parallel bunches. These data serve as a comparison of fabrication detail between inner and outer sandwich skins, but not accurate fibre volume ratios. This is due to the manner in which the fibre edges showing in these images impinge on the determined area of fibre cross-section, and to the limited number of results.

Table 3.9 Comparison of fibre and voids areas as % of cross section

Location	Specimen	Fibre area %	Void area %
External	1	9.86	15.30
	2	9.64	14.30
	Average	**9.75**	**14.80**
Internal	1	9.40	20.70
	2	9.53	21.10
	Average	**9.47**	**20.90**

It can be seen from Table 3.9 that the fibre content of internal and external material appears similar. However, the void content is larger in the internal material. This suggests variation in workmanship, rather than relating to degradation with age. (Presence of voids is indicative of insufficient wetting of fibres during the hand lay-up process.)

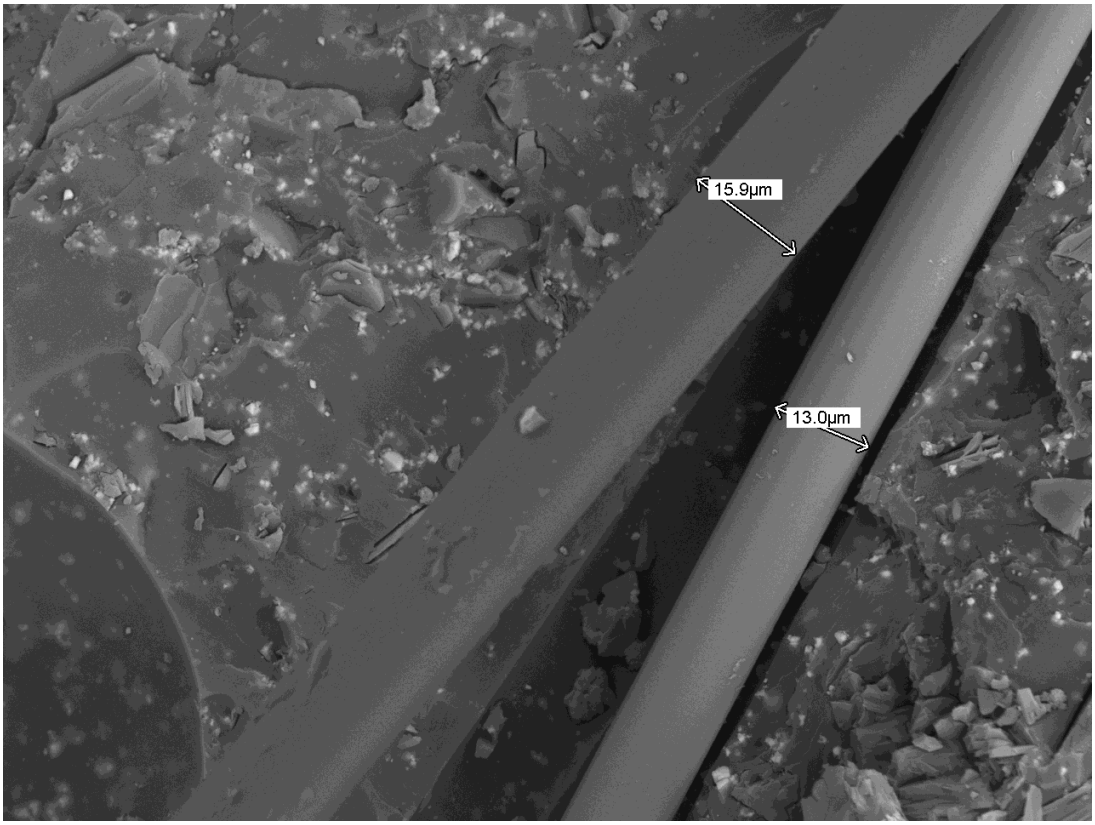

Figure 3.32 BES image showing inferred fibre diameter of internal material (x2500)

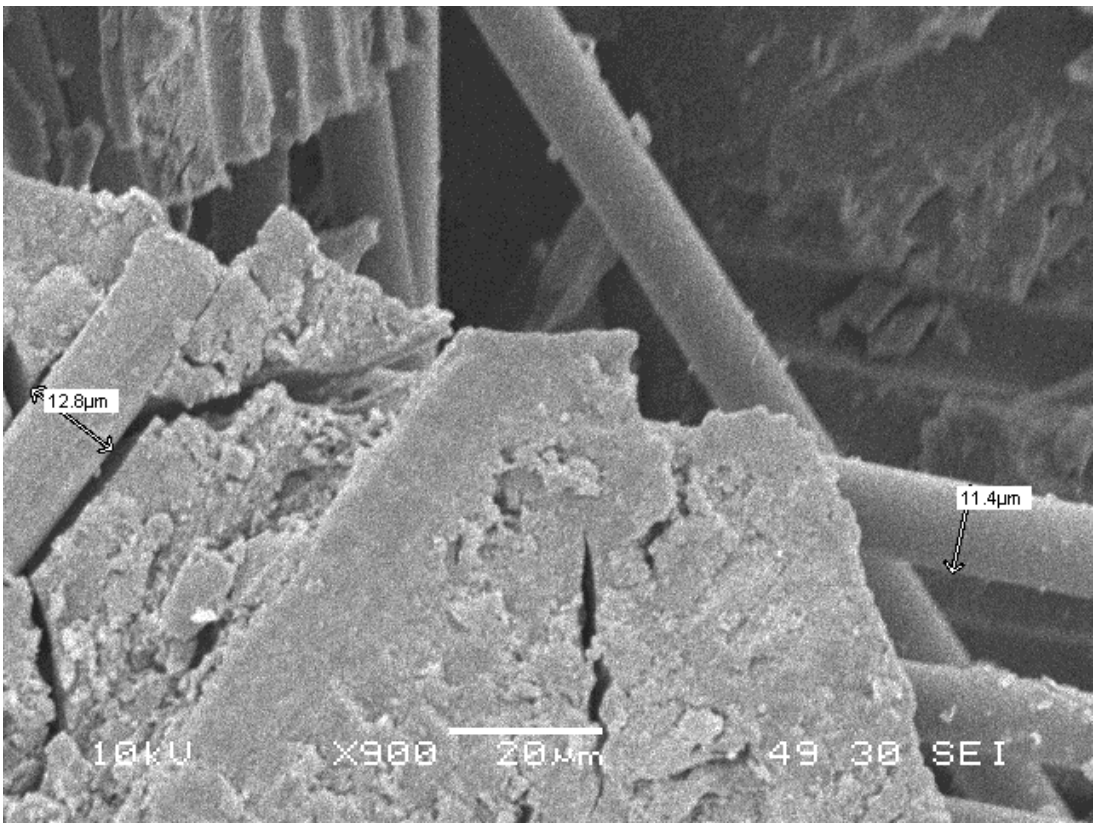

Figure 3.33 SEI output showing inferred fibre diameter of external material (x2500)

Figure 3.32 and Figure 3.33 are two examples of images used to determine the fibre diameter of internal and external material. Results vary for each set of images, internally and externally, between 10 and 16 μm. No difference in fibre architecture is evident. The BES image demonstrates accurate and smooth representation of topography, and was most useful for accurately determining fibre diameters. What can also be seen is the filler material, Aluminium Tri-hydrate (ATH); elemental analysis confirmed this material using energy dispersive spectroscopy. The filler is found in both internal and external material in approximately equal amounts. Added to improve fire performance, ATH is known to reduce environmental durability (Mansour 2000) as higher water absorption is observed (Tawfik et al. 2004).

At the highest magnification observed, (scanning at 2500× magnification,) the polyester matrix of the cold fractured surfaces of the external and internal material can be compared in Figure 3.34 and Figure 3.35 respectively. The external polyester matrix appears to have crumbled a lot more upon fracture. Larger crystals of glassy appearance, closer in character to what would be expected from new material, are shown in the internal sandwich skin specimen.

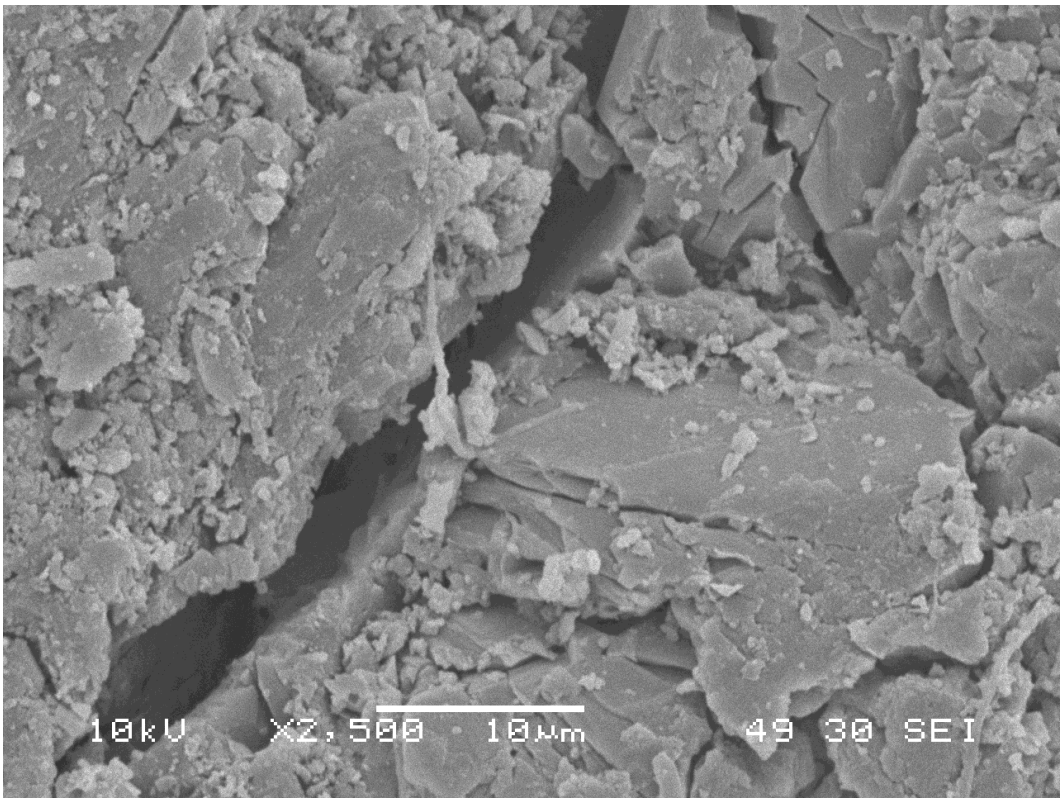

Figure 3.34 External polyester matrix produced using SEI on cold fracture

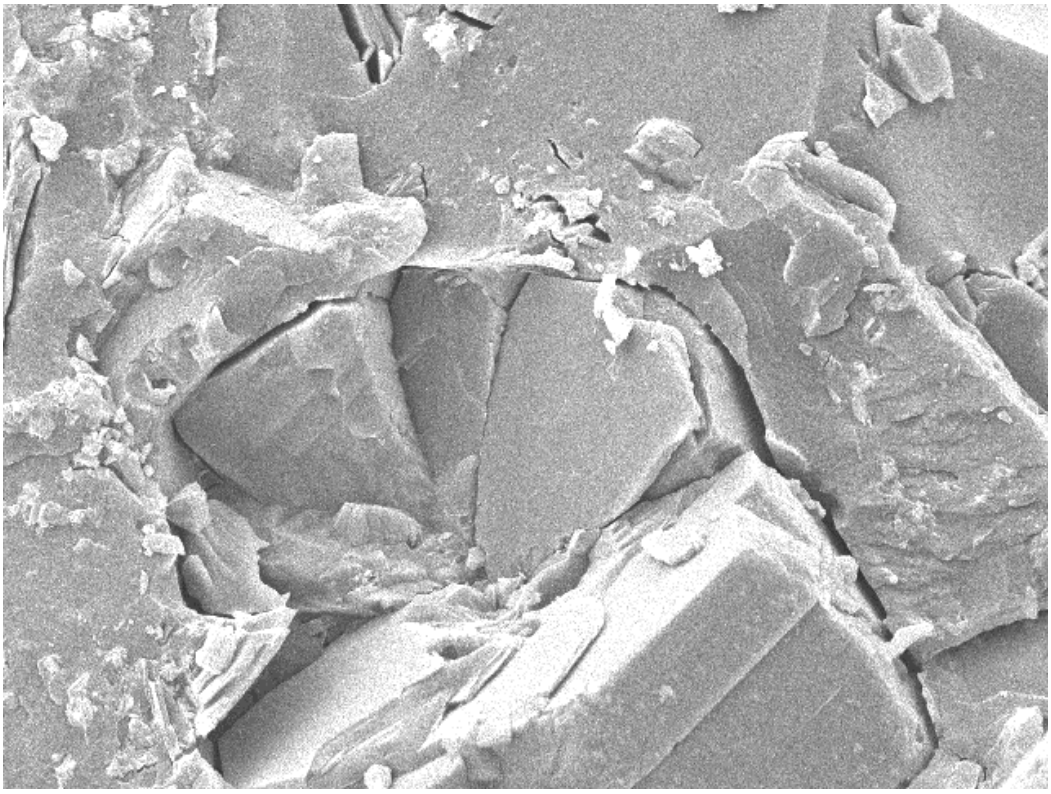

Figure 3.35 Internal polyester matrix produced using SEI on cold fracture

3.3.3.2 Dynamic Mechanical Thermal Analysis

It has been established that the fibre content of the internal and external (once the gel coat with 3 ounce per square foot is removed) GFRP material is comparable in fibre size, quantity and distribution. Some physiological differences in the appearance of the resin, and the amount of voids present in the polymer matrix, have been highlighted by the study using microscopy. Dynamic mechanical thermal analysis (DMTA) has then been used to determine the Glass transition temperature T_g of the internal and external material, which is a characteristic related to the resin component. These results are presented in Table 3.10, and provide one further measure in understanding differences in the material of the two sandwich skins before structural mechanical properties are considered. Locations A and B correspond to two panel locations. A is at the top quarter of the panel and B is at the bottom quarter, both mid-width.

The locations A and B are marked in Table 3.10 with Ext for external, and Int for internal, locations. Three coupons from each of these locations were tested. Results are segregated in to the different regions of panels such that the degree of intra-panel variation can be appreciated.

The terms in Table 3.10 'max loss modulus', 'onset of storage modulus' and 'max tan delta' relate to parts of the specimen modulus-temperature profile generated in testing. These three terms, that are those most commonly presented in literature (to report on glass transition behaviour) are included for completeness. Max tan delta is the principal of these, and can be described as the point at which the rate of elastic energy being lost starts to decrease.

It is observed that the values of T_g for the internal and external material are almost identical. This is surprising considering the degree of variation observed using microscopy, as appreciated qualitatively in Figure 3.34 and Figure 3.35.

Table 3.10 Average T_g at maximum tan delta for internal and external material

Coupon location	T_g at Max Loss Modulus/^{o}C	T_g at onset Storage Modulus/^{o}C	T_g at Max Tan Delta/^{o}C	T_g at Max Loss Modulus overall average/^{o}C
Ext A.1	83.9	70.3	99.7	
Ext A.2	79.4	65.6	101	
Ext A.3	85.9	71.8	103	
Average Ext A	83.1	69.2	101	
Ext B.1	79.9	65.9	98.4	
Ext B.2	84.6	71.6	101	
Ext B.3	82.8	68.4	101	**External Average**
Average Ext B	82.4	68.6	100	101
Int A.1	77.9	62.4	98.1	
Int A.2	76.4	61.0	100	
Int A.3	78.0	62.7	101	
Average Int A	77.4	62.0	99.8	
Int B.1	78.5	64.0	101	
Int B.2	76.3	62.3	98.8	
Int B.3	77.0	63.9	97.6	**Internal Average**
Average Int B	77.3	63.4	99.3	100

Figure 3.36 shows that very similar thermal response behaviour was exhibited by all DMTA coupons prepared, despite varying values of initial stiffness as shown in Figure 3.37. This variation in initial stiffness is attributed to variation in specimen; although specimen width and thickness is always the same (to within manufacturing tolerances), the number and orientation of fibres 'captured' in the coupon taken varies. The close agreement of thermal response behaviour shown in Figure 3.36 is valuable verification

that the DMTA testing targets the polymer matrix component of the composite. The vertical axis 'Tan Delta' values observed in Figure 3.36 denote an index derived mathematically from the rate of change of stiffness with temperature, according to the code of practice ASTM D7028 - 07e1. The T_g is specified as the temperature at which this value is a maximum (ASTM 2007).

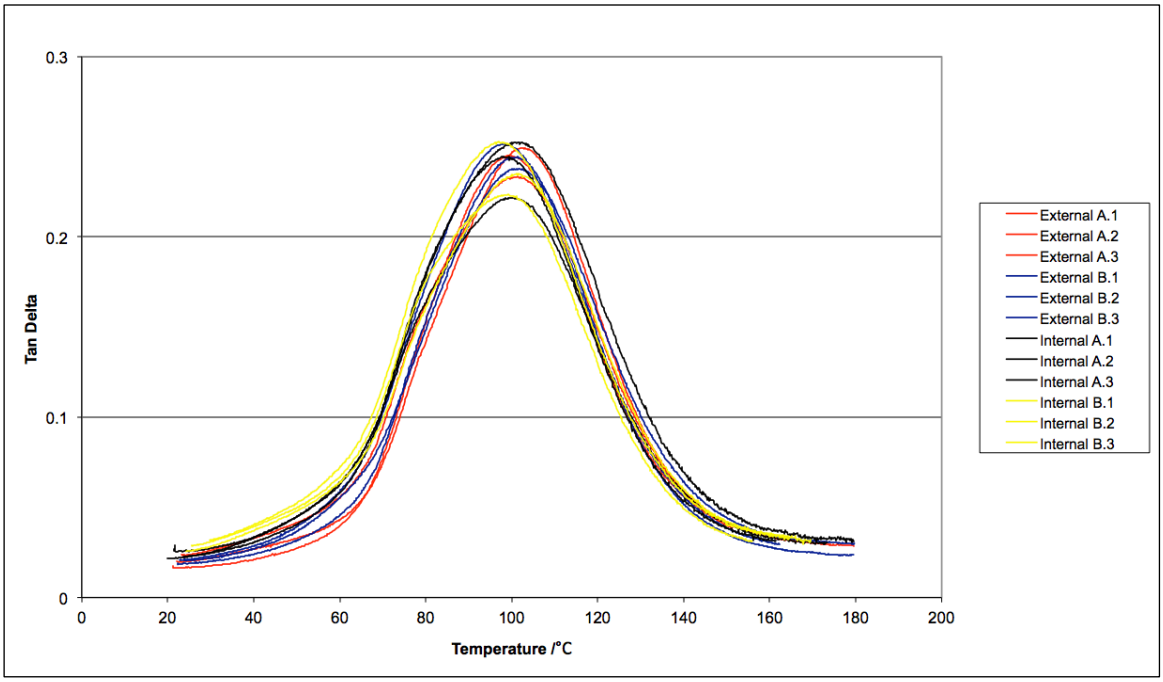

Figure 3.36 Thermal response of all coupons (T_g is the temp. at max value)

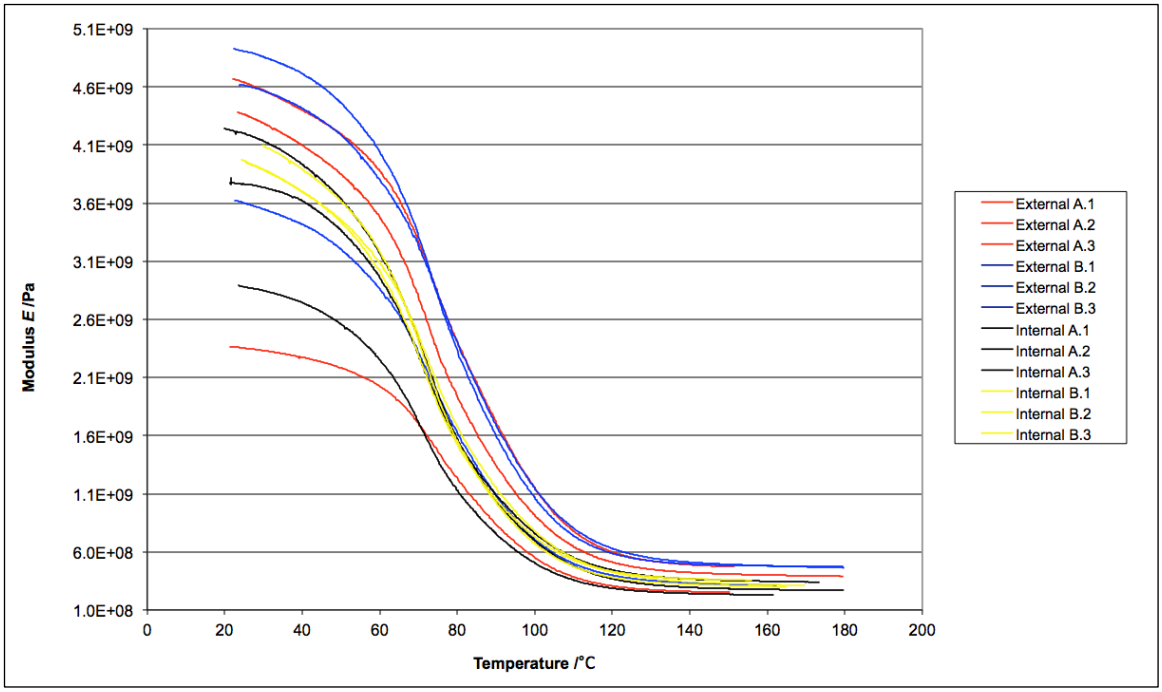

Figure 3.37 DMTA temperature-stiffness relationship for all coupons

3.3.3.3 Mechanical testing: tensile

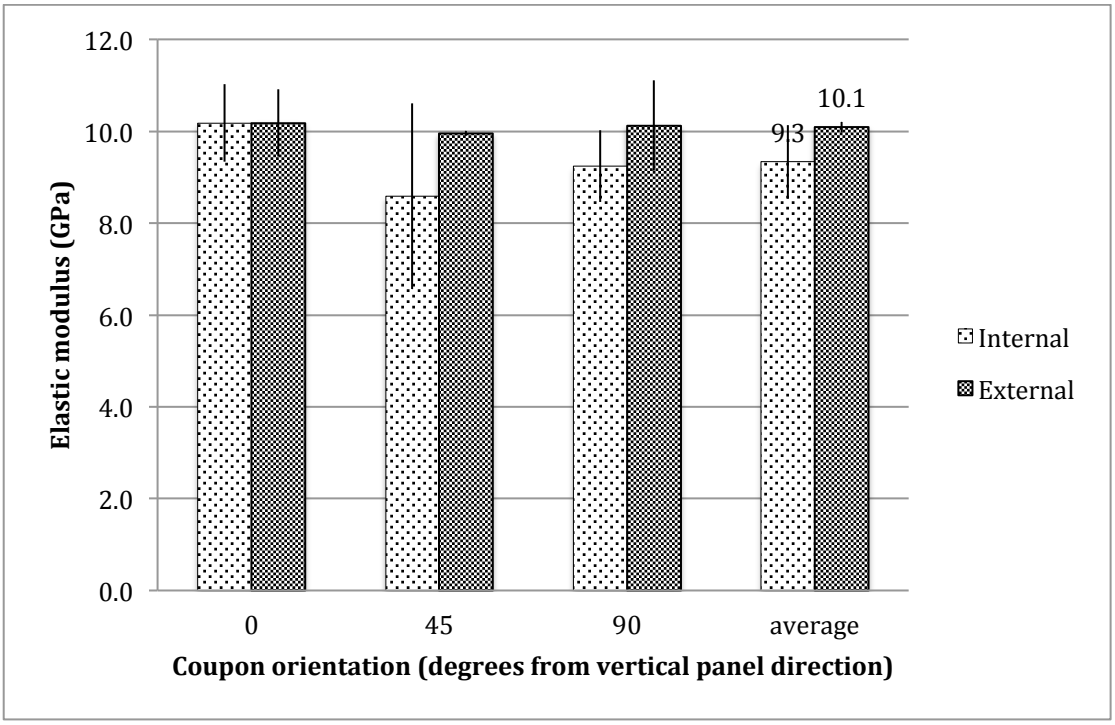

Figure 3.38 Tensile elastic modulus as a function of coupon orientation and origin

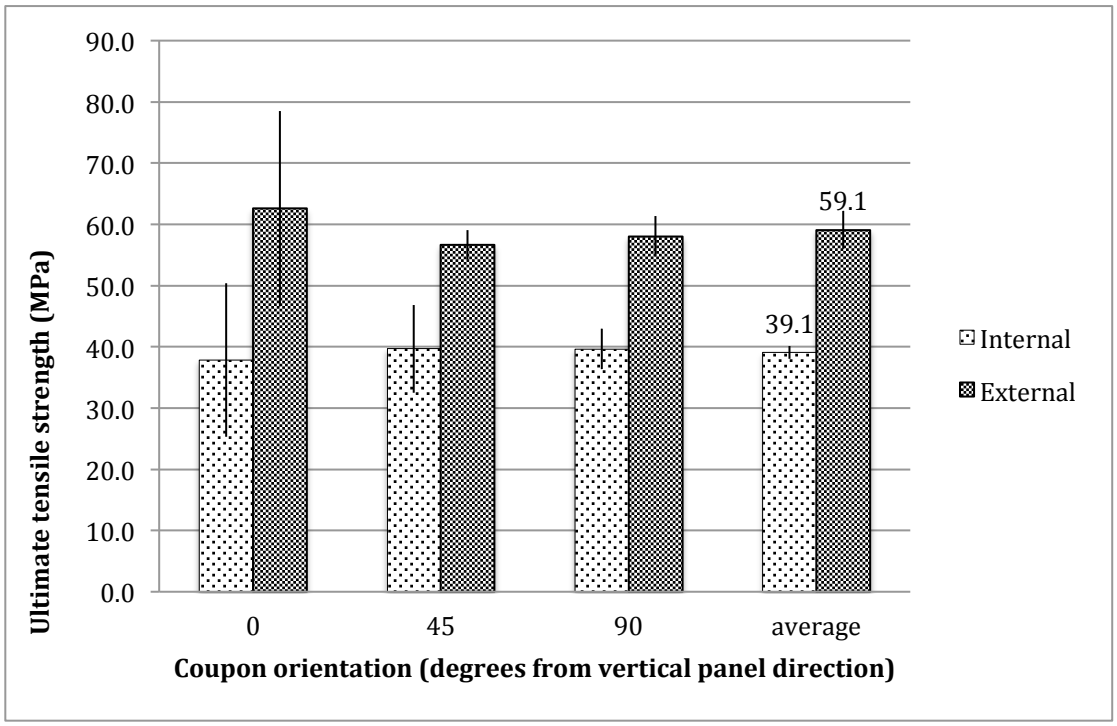

Figure 3.39 Ultimate tensile strength as a function of coupon orientation and origin

The tensile elastic modulus and tensile strength is presented for each of internal and external panel faces and for different orientations on the panel faces. Each bar in Figure 3.38 and Figure 3.39 represents an average value derived from the testing of four individual coupons, prepared as described in Subsection 3.3.2.1. The error bars represent plus or minus one standard deviation from the mean.

Both Figure 3.38 and Figure 3.39 agree with literature that the CSM reinforcement is truly random multidirectional, with no biased axis evident. Figure 3.38 shows the external material to be very slightly stiffer: 10.1 GPa compared to 9.3 GPa internally. More prominent, is the significantly lower ultimate tensile strength of the internal material compared to the external material: 39.1 GPa compared to 59.1 GPa, a difference of 33.8% (but with +/- 15%variation in some tests on some samples).

The values derived for ultimate tensile strength in the 0^o (longitudinal, or vertical) direction show a greater spread in the results, compared to other orientations in Figure 3.39. The stress strain plots generated for these coupons are shown in Figure 3.40, for both internal and external material. The area of panel from which these coupons were

taken was near a free edge. It is thought that intra panel variation, as a consequence of manufacturing variability, could be responsible for this outcome. The non-linear behavior observed here can be noted, and is discussed later in Chapter 5.

The increased number of voids occurring in the internal material could account for such a reduced capacity in tensile strength. It must be explained however as to why the variation in number of voids could impinge so greatly on the tensile strength of the composite, though yield such little effect on the stiffness.

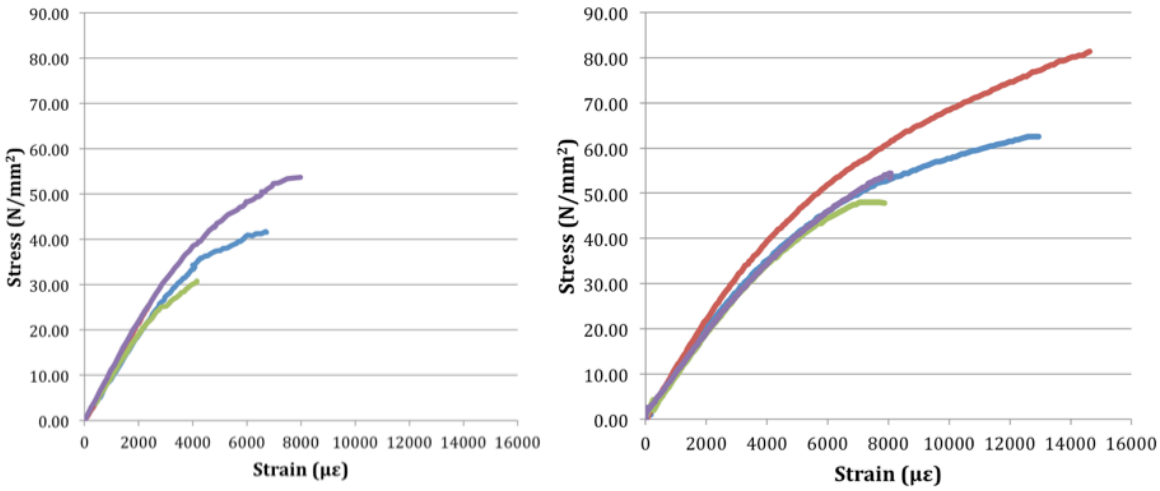

Figure 3.40 Stress-strain plots to failure, for internal (left) and external (right) panel material in the 0^o direction

The proportion of voids differs by approximately 5% (20.91% internally to 14.81% externally). It has been reported by others that voids occur most frequently at the fibre resin interface zones (Lambert et al. 2012; Schmidt et al. 2012). Fibres of the chopped strand mat present are known to lie in bunches, as observed by microscopy and presented in Subsection 3.3.3.1. This is in line with previous findings of others relating to the intra panel variation of mechanical properties of these panels (Sriramula and Chryssanthopoulos 2009).

It is entirely possible therefore, for a 5% difference in the proportion of voids present to exert significant effect on the mechanical properties of the composite, owing to the location of these voids and how they interfere with the interfacial bond region of a large proportion of the fibre reinforcement. This is especially true where the fibre volume

ratio is small, such as in a hand lay up composite of this type. It is demonstrated that the ultimate tensile capacity of the composite is far more sensitive to the interfacial bond length of the fibre than is the stiffness. This phenomenon/relationship is equivalent to that of how mechanical properties are affected by fibre length, which is a glass fibre polymer matrix composite characteristic that has been established by others (Thomason et al. 1996; Thomason and Vlug 1996). This hypothesis is explained further in section 4.2.

It is a significant finding therefore, that the deficit of internal GFRP composite strength observed in this study occurs as a consequence of fabrication, and not degradation with age.

3.3.3.4 Mechanical testing: shear

By determining the shear modulus of the GFRP material it is possible to measure resin performance in a selective manner, because it is not influenced as much by fibre properties as tensile tests are. This further explores the integrity of the polymer matrix. Four specimens from each panel face were prepared and tested as per Subsection 3.3.2.3. Figure 3.41 shows the average values of in plane shear modulus G_{12} for internal and external coupons. The shear modulus was calculated the initial displacement range (over values for displacement between 10 and 30% of the section thickness). This is as per the code of practice BS EN ISO 15310:2005 (BSi 2005). At larger displacements the secondary displacement transducer at the quarter diagonal span point confirmed that bending had reverted to single axis flexure.

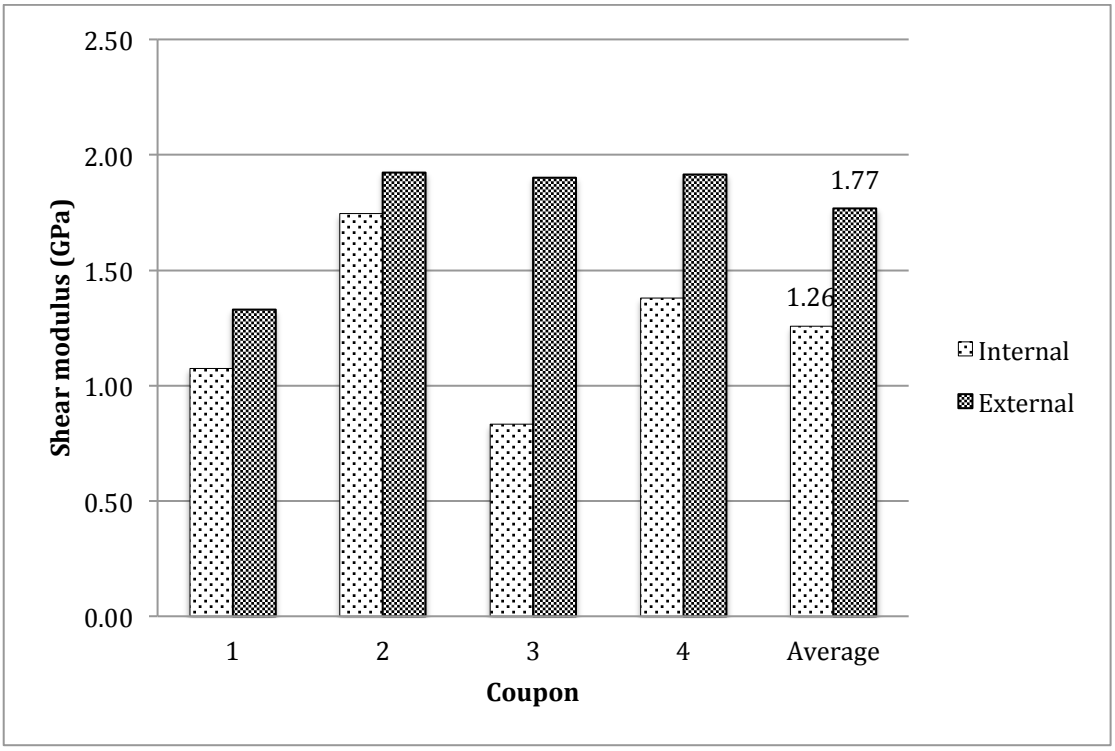

Figure 3.41 Shear modulus G_{12}, of the four internal and four external coupons and average values

It can be seen that the external coupons consistently surpass the internal coupons in shear modulus and therefore in performance of the polymer matrix. The 28.8% deficit in overall average performance of the internal coupons in shear concurs with the previous findings indicating that the internal GFRP skin possesses an increased amount of voids.

3.3.3.5 Assessment of polymer hardening

Previous findings using the pultruded GFRP of 17 years natural ageing in service of the Severn Crossing Visitors' Centre panels revealed that 6000 με in tension had no detrimental effect on the subsequent flexural stiffness (no cracking of resin evident), whilst 9,000 με yielded a reduction in subsequent tensile stiffness by approximately half. New material was shown to retain full flexural stiffness even with intervening strains up to 10,000 με for the Strongwell panel material.

The ultimate tensile strain capacity of the Mondial House panel material prevented the influence of strains greater than 8,000 με from being investigated. Table 3.11 and Table 3.12 show results for the stiffness retention (related to retention of polymer matrix

integrity) as a function of the maximum strain to which the coupon was subjected during the intervening tensile test.

There appears to be a only a very small difference in the response of the internal and the external material. The findings correspond with information that a UV barrier was present in the outer sandwich skin gel coat (Brookes and Meijs 2008; Domone and Illstone 2010) and this seems to have prevented brittle hardening of the resin.

Table 3.11 Retention of coupon flexural stiffness post tensile straining: internal material

Sample	Initial E_f (GPa)	Tensile strain to which specimen is subjected (με)	Subsequent E_f (GPa)	% original stiffness retained
1	5.37	4000	5.79	108
2	6.32	4000	6.51	103
3	4.08	6000	4.23	104
4	7.52	6000	damage	-
5	6.15	8000	5.17	84
6	6.48	8000	4.72	73

Table 3.12 Retention of coupon flexural stiffness post tensile straining: external material

Sample	Initial E_f (GPa)	Tensile strain to which specimen is subjected (με)	Subsequent E_f (GPa)	% original stiffness retained
1	8.60	4000	8.51	99
2	7.15	4000	7.03	98
3	7.67	6000	6.97	91
4	7.46	6000	7.03	94
5	7.57	8000	6.73	89
6	8.06	8000	failure	-

One of the internal coupons experienced damage during tensile straining at the test rig jaws and was unable to be retested in flexure, though the other coupon showed that full stiffness was retained to 6,000 με. In the Second Severn Crossing Visitors' Centre case study, investigating pultruded material aged 17 years in service, the stiffness of external material was also retained to 6,000 με. External material from Mondial house seems to be behaving similairy, retaining on average 93% at 6,000 με. Comparing the stiffness retained by the Mondial House material with that retained by the Second Severn Crossing Visitors' Centre material, following a tensile strain value of 6,000 με, is a stringent critique of the Mondial House material because the ultimate tensile stress is far lower that that of the Second Severn Crossing Visitors' Centre.

Tensile strains of 8,000 με yield further reductions in stiffness for both inner and outer Mondial House material, retaining 84 and 89% respectively. This could be due to fibre breakage or loosening or fibre anchorage in the resin at large strains, by compromised interfacial zones, and not necessarily rupture in the resin.

3.3.4 Discussion of the Mondial House case study

The influence of UV on the properties of GFRP fabricated by hand layup technique and naturally aged over 30 years in service, has been investigated by case study laboratory investigation comparing internal and external sandwich skins of façade panels from Mondial House.

The phenomenon of brittle resin hardening observed in the previous case study, in section 3.2.5, and typified by a reduced strain limit of brittle fracture for the matrix component in tension, has not been clearly observed in this case study. Mondial house panels possessed a gel coat containing a UV barrier, which appears to have protected against brittle hardening of the resin; at 8000με the GFRP retained 89% of its original stiffness. The performance of the internal material in this respect was not perfect either, and retained an average of 79% of its original stiffness. Results are consistent with a UV barrier that was responsible for the retention of mechanical properties, though testing to confirm this at higher strains in the polymer matrix is not possible, due to the low fibre content and ultimate strength of the GFRP composite.

Mechanical tensile testing and microscopy have confirmed the random multidirectional nature of the chopped strand mat fibre reinforcement. Microscopy also confirmed that the inner and outer fibre volume ratios, fibre size, and arrangement of internal and external principal reinforcements were equivalent, once the outer gel coat had been removed.

Microscopic analysis has also revealed an increased abundance of voids internally within the composite compared to the external material. Located at the interfacial (fibre resin interface) zones, around the CSM fibre bundles they have been shown to impinge on the ultimate tensile strength of the composite and the shear modulus of the composite. The voids are attributed to variation in fabrication quality control between internal and external sandwich skins, and are not related to degradation with age. The voids are shown to exert only a small effect on the tensile modulus of the resulting composite material, but a large effect on the tensile strength. A hypothesis has been formulated comparing this trend (occurring with void frequency) to a trend observed where fibre length is reduced, corresponds with the work of others (Thomason et al. 1996; Thomason and Vlug 1996) that has shown strength to be more sensitive to fibre length than modulus. In both cases, the increased voids or the reduced fibre length reduces the interfacial bonded length of fibres and the strength is greatly reduced. The analogy is explored in Section 4.2.

Qualitatively, the physiological appearance of the external resin appeared more degraded upon microscopic inspection at very high magnification, however the glass transition temperatures, T_g of the resins internally and externally were found to be identical, and supported by repeat tests in close agreement. Agreement in values for T_g is indicative of no difference in environmental degradation of the resin components.

3.4 Summary

A life in service of 17 years appears not to have significantly diminished the properties of the GFRP composite examined from the Second Severn Crossing Visitors' Centre. Material subjected to UV however does show a reduction in mechanical performance associated with brittle hardening of the polymer matrix. A threshold strain value of

6,000 με for the onset of this brittle fracture, and the ensuing properties, has been established for a particular resin matrix. It is understood from review of existing literature that accelerated ageing techniques maintain resin plasticity, whereas the opposite has been shown to occur by the testing undertaken. The next chapter examines the work of others in generating artificially aged GFRP coupons. Drawing on findings presented in this chapter permits an informed critique of the accelerated techniques. The role of protective gel coats, with UV barrier, has been illustrated by the second case study, where the resin hardening observed and quantified in the first case study was not evident. Differences in the fabrication of the inner and outer GFRP skins, the subject of the second case study, have been observed and the consequences on the mechanical properties quantified. Other analytical means and published work of others have explained how the presence of voids in some parts of the composite may impinge on its performance, and explains how environmental degradation is not responsible for these particular observed differences. This is explained further in the next chapter.

4 Durability: discussion and conclusions

Chapter 3 presented findings from a campaign of testing using naturally-aged GFRP material after a period of service as an element forming a real building. The behaviour exhibited by this material, as quantified by the experimental testing undertaken, is compared in this chapter against existing knowledge and the published work of others for predicting the rate of degradation of mechanical properties. The literature introduced in Section 2.2 is recalled to highlight where important findings of the testing campaign have filled in gaps in existing knowledge, or revealed behaviour that is contradictory to published findings for accelerated artificial ageing procedures. Literature is also used to better explain some phenomena encountered during testing of the naturally aged material.

4.1 Severn Crossing Visitors' Centre

The lack of 'base case' data (data relating to mechanical properties of the precise panels tested when new) proved a hindrance to establishing quantifiable loss of mechanical performance. What the testing yielded is a collection, or profile of properties, relating to particular conditions of exposure over the service lifetime of 17 years. Existing literature documents specific types of physiological and chemical changes, in unsaturated isophthalic polyester pultruded GFRP composite material, and in polymer composites in general, attributed to certain types of exposure. The Severn Crossing Visitors' Centre has permitted material testing on specimens taken from internal locations (low moisture, zero UV environments), and external locations (where the conditions of moisture variation and UV exposure vary as a function of aspect) to compare against experimental findings of others.

4.1.1 Polymer matrix characteristics

The measurement of elongation at failure is not in itself an informative measure of the strain limit before fracture of the resin component of a composite, as established in Subsection 2.2.1. Qiu and Gu (2011) demonstrated that the elongation at failure of GFRP composite increases after UV irradiation, whereas Sasuga and Hagiwara (1987) showed that high wavelength radiation decreases the elongation at failure of a pure

polymer matrix. The literature review has revealed that flexural testing can reveal a character of mechanical performance not picked up by other tests that relates to hardening of the resin component. Following UV ageing procedures by Cabral Fonseca et al. (2012) (see Figure 2.7 in Subsection 2.2.1) flexural testing showed the strength of specimen material to increase, whereas tensile strength and shear strength decreased. Flexural strength was not investigated using the naturally aged material, and it was found that the resin rich outer layer of specimens did influence the flexural stiffness. This is discussed in Subsection 4.1.3.

The procedure to quantify resin hardening, presented in Subsection 3.2.5, draws on findings relating to both, elongation of resin matrix at fracture, and behaviour of specimens during flexural tests. A hypothesis that resin hardening increased elastic modulus in compression, but decreased tensile performance by resin fracturing prematurely at lower than expected strains, and thus influenced flexural or compressive tests in this way, was formulated and tested. This methodology signifies a large step forward in revealing a phenomenon that occurs naturally in the resin as a result of the synergistic effects of environmental factors. The work in Subsection 3.2.5 has also served to show how a limit of brittle resin fracture in tension can be quantified for GFRP composite material.

4.1.2 Degradation

Some of the basic material mechanical properties, determined through testing of the Visitors' Centre panel material and new equivalent material, showed no degradation, although, as explained, only a qualitative comparison was possible. In some cases, an enhanced value was found for the specific property measured when compared with new equivalent material. For instance, whole panel stiffness (as reported in Subsection 3.2.3.2) shows a small increase. Coupon tensile strength, as reported in Subsection 3.2.3.4, reduced. This indicates that some environmental factors may trigger mechanisms that increase a mechanical property and some that bring about a decrease in it, impinging on the resulting measurement by varying proportions in a conflicting nature.

It has been stated in Subsection 3.2.6 that the comparison afforded between new and

old material is a qualitative one. Establishing the fibre content has improved the degree to which a comparison can attribute variation observed, between new and old material, to environmental factors. However, fabrication practices and variation in the precise material specification render a lower confidence in conclusions based on quantitative comparisons. Fortunately, it is possible to appraise the characteristics of aged material by comparing GFRP after a lifetime exposure with that which has been shielded from harsh conditions, to explore the influence exerted by the type of exposure: degree of moisture or UV exposure.

Figure 3.12 in Subsection 3.2.3.3 shows that coupons of pultruded polyester GFRP from internal locations on the original building panel outperform those of external material, on both the south and west facing façades with respect to their tensile modulus, and the south facing external material has the lowest value of all external flange material. It cannot be categorically stated which factor is more responsible: the UV irradiation, known to be a maximum on the south facing façade, or the enhanced degree to which the material is wetted and dried on these elevations. Of course the material could simply be very variable as per Mondial House (this material was not subjected to microscopic analysis). The pattern, in results shown, is consistent with one that might be expected due to weathering. The prevailing wind is most frequently from the southwest, at the building's former location, meaning that these façade aspects will have experienced greater wetting during rain.

4.1.3 Relevant studies in accelerated ageing

The only data presented in Section 2.2 concerning mechanical tensile elastic modulus following hydrothermal ageing relate to testing of vinylester by Kotani et al. (2011). The data show an increase in stiffness of 24% over 1,000 hours of hydrothermal ageing at 80^{o}C. See Figure 2.13. The initial increase plateaus, as with many variables dependent on hydrothermal ageing, such as moisture uptake, as shown in Figure 2.10. However, as has been demonstrated by Chu et al. (2004), some of this increase could be lost after a period of re-conditioning, which is a practice not carried out by Kotani et al. (2011). Just as Chu et al. (2004) show properties which diminish during hydrothermal ageing can then be restored with reconditioning, some of the increase in stiffness could be lost if reconditioning of specimens was undertaken. It is examined later whether

artificial ageing that incorporates reconditioning better represents natural ageing.

To account for such a large loss of tensile modulus on southerly facing external panel material of the Visitors' Centre, it could be that UV ageing is responsible, and, thus, artificial ageing by UV would show a similar reduction in tensile elastic modulus. Cabral-Fonseca et al. (2012) show polyester GFRP to reduce in axial tensile strength by 12% after 3000 hours UV irradiation at intensity 77 W/m^2 (see Figure 2.6). Carra and Carvelli (2012) have shown that a test programme incorporating both UV irradiation and cycles of temperature variation and high moisture exposure causes the elastic tensile modulus of pultruded polyester GFRP to decrease by 1.5% after 2 months (see Figure 2.16b).

Whilst the literature certainly points to the UV irradiation on the southerly façade of the Visitors' Centre being responsible for the reduction in tensile elastic modulus, no quantitative comparison can be made. Little literature exists relating to the serviceability of GFRP following artificial ageing practices. Literature presented in Section 2.2 is more useful in explaining the ageing character of the Visitors' Centre panel material concerning tensile strength. Cabral-Fonseca et al. (2012) present data on the flexural strength retention of pultruded unsaturated polyester GFRP composite, after artificial ageing by both UV irradiation, and by immersion in hydrothermal bath. Carra and Carvelli (2012) present data describing the axial tensile strength of pultruded GFRP of unsaturated isophthalic polyester resin after a programme of ageing incorporating both of these factors together with cycles of extreme cold, to observe the synergistic effects.

Results from the programme of testing on material from the Visitors' Centre panels relating to tensile strength can be aggregated into the following categories: internal material (which has been aged without direct contact to moisture and UV), external southerly facing material (which has experienced intense UV irradiation and cyclic wetting and drying), and lastly, external material from the northward facing façade (which has endured minimum UV exposure and the dampest conditions). The panel fabrication is such that the panels are symmetrical about their neutral axis; i.e. the internal flange material is identical to external flange material in new panels (although the neutral axis of flexure will move upon loading and not remain central). This has

been verified by comparison of fibre content, established by resin burn off and presented in Table 3.2 in Subsection 3.2.2.2.

Test data relating to these categories can be used firstly to ascribe the most accurately fitting data set from Cabral-Fonseca et al. (2012) concerning hydrothermal test parameters. The authors present results of testing at each of three temperatures of water bath immersion, as shown in Table 2.5, over an 18-month period. The value derived from the Visitors Centre case study, for reduction of tensile strength due only to moisture exposure is a negligible 0.65%. This is found using data from testing of internal and external flange material from north facing panels, which will have experienced minimum UV exposure. The data are presented in Table 4.1. The internal panel material will have aged too however, even without exposure to moisture, and might exhibit a reduced tensile strength compared to when new. As explained previously, however, variation in manufacturing means that a comparison between new and old material cannot quantitatively assess the degree of degradation of a certain mechanical property. By subtracting the tensile strength of external material from internal (and expressing as a % reduction as in Table 4.1), the influence of only the moisture exposure and an increased temperature variation can be observed. The environmental temperature variations will have affected the internal environment to a degree, as well as any heating during occupancy of the building in service.

The hydrothermal bath induced ageing behaviour, reported by Cabral-Fonseca et al. (2012), presented in Table 2.5, that fits best with this small measured decrease in performance is that conducted at 20^{o}C over 18 months. This resulted in a decrease in tensile strength of 9%. Kotani et al. (2011) showed how Fickian diffusion behaviour results in the residual strength variation attributed to hydrothermal ageing in GFRP plateauing over this period of time. – Indicating that after 18 months artificial ageing the subsequent change in properties would be negligible.

The naturally-aged material was dry for testing in the laboratory, and had been stored in the laboratory for at least six weeks. In this respect the material will have been ‘re-conditioned’. The most suitable literature sourced data against which to compare these experimental findings should therefore also observe appropriate regain. Chu et al. (2004) reported a regain in tensile strength of 33.1% of that lost by hydrothermal

ageing of pultruded GFRP at 23^{o}C for 18 months. See Table 2.4. Equation 2.8 is used to establish the re-conditioned value for strength presented in Table 4.1. It is evident that the predicted reduction in tensile strength based on the literature alone for material which has not experienced direct UV irradiation is 6.02%, which is still larger then that found from testing naturally aged material, 0.65%.

It should be reiterated that the properties of the internal panel material could have changed as a consequence of ageing in a sheltered environment. This unknown amount could result in a closer agreement if it were possible to determine the value. It appears that 18 months hydrothermal ageing, even at 20^{o}C (ambient temperature), reduces tensile strength more than that due to 17 years of natural exposure to moisture but without exposure to UV. If regain is not considered, the over prediction of degradation of strength is very large: at 8.35% over-prediction of degradation. Cabral-Fonseca et al. (2012) do not state what duration of life in service the 18-month hydrothermal programme correlates to, at any temperature of immersion conducted in the study. It would seem to represent a period longer then 17 years based on these findings.

Table 4.1 Tensile strength reduction: comparison of experimental results with literature sourced predictions

Case study experimental findings			**Literature sourced prediction based on artificial ageing experimental findings**		
Material origin	Tensile strength (MPa)	Ageing factor	% reduction in tensile strength	Ageing parameter of study	Reference
North internal	308		**9**	Due to 18 months hydrothermal aging at 20°C	Cabral-Fonseca et al. (2012)
North external	306		33.1	Regain of that lost	Chu et al. (2004)
% reduction	**0.65**	Primarily due to moisture exposure and warm/cold diurnal and annual variation (A)	**6.02**	Modified reduction	re. both of above
South internal	306				
South external	266				
% reduction	**13.07**	Due to UV, moisture exposure and warm/cold diurnal and annual variation (B)	**8.5**	Warm/cold cycles, moisutre and UV as per note 1	Carra and Carvelli (2012)
% reduction	12.42	Due to UV alone (= B - A)	**12**	Moisute and UV as per note 2	Cabral-Fonseca et al. (2012)

Note 1: Climatic chamber generates warm cycles, between 20 and 60°C that complete over 8-hour periods, and cold cycles between -20 and 20°C. These cycles are run alternately 21 times (one week) each, for a total of 8 weeks (168 cycles). The relative humidity is held at 80% during the warm cycles and 90% during the cold cycles. UV irradiation was incident at 340-400 nm wavelength, at 40 W/m^2 intensity. Lamps were switched on, then off, alternating in 12-hour intervals, throughout the duration of the test.

Note 2: Exposure cycles consisted of 4 hours UV radiation simulated with fluorescent lamps at 60°C, and 4 hours of exposure to moisture caused by constant condensation of deionized water at 50°C. The fluorescent lamps provided an irradiance of 0.77 W/m^{2}nm at 340 nm (i.e. Intensity of 262 W/m^2). Total ageing duration 4.5 months.

The exposed external material, from the south facing Visitors' Centre panels, exhibited a much larger decrease in tensile strength upon testing, of 13.1% (again taking the internal material of the south facing panels as a 'base case'). Using this as a value against which to compare accelerated testing incorporating UV exposure, moisture exposure, and cycles of temperature, shows that larger reductions are obtained after a programme of accelerated ageing incorporating multiple factors of degradation. Carra and Carvelli (2004) established a value for the reduction in tensile strength of pultruded polyester GFRP after such a programme of ageing, of 8.5%. This is a smaller reduction than that found after natural ageing over 17 years. However the accelerated ageing procedure applied in the study only lasted 2 months. (The study made no claims as to what life in natural service this programme would correspond to.) Within this period the total number of hours UV exposure was 672 hours at 40 W/m^2. The UV radiation is clearly of significant detriment to the composite's tensile strength, when combined with the other factors described.

The value derived of 8.5% reduction in tensile strength after only 672 hours irradiation at intensity 40 W/m^2 represents a severe rate of degradation. This study is again not calibrated to any duration of natural service life. Table 4.2 shows, however, the number of weeks over which a south facing façade in service in Bath, in the United Kingdom, would take to experience the same amount of irradiant energy, in the 300-400 nm part of the spectrum. Karbhari et al. (2003) state that most polymers have bond dissociation energies in the order of 290 to 400 nm wavelengths in the UV region. This range is therefore adopted for use in forming a correlation of natural exposure to artificial testing.

Table 4.2 Correlation of UV exposure in artificial ageing to that experienced over a period in service

	Experimental parameters				Equivalent life in service in Bath, UK
Reference	I (W/m^2)	t (hrs)	Energy density (MJ/m^2)	Wavelength (nm)	
Carra and Carvelli (2012)	40	672	97	350	38 week south facing façade
Cabral-Fonseca et al. (2012)	262	1500	1415	340	553 weeks south facing façade

The equivalent life in service in Table 4.2 is calculated on average solar irradiance on a south facing vertical surface, using a method as set out by Szokolay (2008). On a vertical south facing surface the incident solar insolation at the equinox (to best

represent average conditions) is 2.03 kWh/m^2/day, which corresponds to a total irradiant energy of 7.3 MJ/m^2/day. The proportion of this energy in the 290-400 nm wavelength range however is only 5% (Phillips et al. 2008), so only 0.365 MJ/m^2/day of UV in the range concerned is incident. It is noted that 553 weeks is equivalent to more than 10 years service life.

The influence of the increased intensity to create accelerated ageing by applying the UV energy over a small timescale is unknown and it is not examined further here. Table 4.2 permits a closer comparison of the studies investigating UV ageing presented in Table 4.1. The study by Cabral-Fonseca et al. (2012) imparts over fourteen times the total energy of UV irradiation to the specimens than the Carra et al. (2012) study. The reduction in tensile strength observed was 12% at the end of the ageing period. The procedure adopted had moisture exposure but not the temperature cycles incorporated into the ageing programme of Carra and Carvelli (2012). This corresponds to a 3.5% larger reduction in the tensile strength compared to the Cabral-Fonseca (2012) study. The maximum temperature achieved in both the Carra and Carvelli (2012) test and the Cabral-Fonseca et al. (2012) test was the same, 60^{o}C, however the total duration of the Cabral-Fonseca (2012) ageing was 4.5 months, more than twice as long.

It can be concluded that the inclusion of any UV irradiance whatsoever is of significant detriment to the subsequent tensile strength of GFRP, when combined with moisture exposure in accelerated ageing procedures. Similar reductions in tensile strength of specimens are achieved in much shorter ageing durations. Testing of naturally aged material from the north and south facing building panels has also confirmed UV irradiance to be of significant detriment to the subsequent tensile strength when combined with moisture exposure. With reference to the mechanisms of degradation in GFRP, it is evident that the influence of UV alone cannot be assessed by the subtraction of observed degradation due to effects including moisture and thermal variation, from combined affects such as these but also including UV. In other words, the value at the bottom of the second column of Table 4.1 is probably not accurate, and the synergistic effects of the different ageing factors are greater that the influence of each individually.

It is evident that the role UV plays in degradation is to enhance the degree to which moisture infiltration and other factors exert an effect. Cabral-Fonseca et al. (2012)

analysed polyester material using Fourier Transformed Infrared Spectroscopy (FTIR). The chromatic profile pre and post irradiation was determined. Results were reported showing evidence of a chemical change at only the surface of the material. However, spectra disclosing the existence of silica revealed that some glass fibres had become more directly exposed as a result of the UV ageing. It is known that cracking accelerates oxidation by providing increased surface area in contact with oxygen (Pochiraju et al. 2012). Combination effects of different factors enhance the processes of degradation and decomposition. This is in contrast to earlier conclusions made by Correia et al. (2006) who stated that synergistic effects of exposure to UV irradiation, moisture and temperature on the mechanical properties were insignificant.

The Visitors' Centre panel material, of south facing, external origin, is shown in Figure 3.15 to have the highest compressive modulus of all the external aged material. As explained in Chapter 3, this phenomenon was explained by an increased resin hardening with age attributed to UV exposure. As mentioned earlier in this chapter a shortage of literature has been uncovered concerning stiffness of GFRP after ageing. This is as true for compressive elastic modulus as for tensile and flexural equivalents. Some literature does present evidence of polymer resin hardening (Kotani et al. 2011), where flexural tests were conducted following ageing procedures.

It has been established by various analytical means in Chapter 3 that fibre distribution in pultruded GFRP elements is not uniform. Fibres tend to be concentrated towards the mid-depth of elements to create a resin rich surface (often attained by the presence of a surface veil) that is smooth and enhances durability protecting the fibres. It is clear then how flexure of single element GFRP specimens is more sensitive to the character of the resin rich outer layers than other tests. It is known that UV and hydrothermal ageing is of detriment to the tensile strength of GFRP, as illustrated in Table 4.1, and to the tensile modulus of pultruded polyester GFRP according to the study by Carra and Carvelli (2012). The flexural performance of specimens, however, is seen to suffer a smaller reduction with ageing, or even an increase. Carra and Carvelli (2012) showed an increase in flexural strength of 3% and an increase in flexural modulus of 20% after 2 months combined moisture-UV-freeze-thaw ageing as described in note 1 of Table 4.1. These trends are shown in Figure 2.17. Cabral-Fonseca et al. showed flexural strength to decrease as a result of hydrothermal ageing at 60^{o}C, but not by as much as

tensile and shear strength (see Table 2.5). The same study also revealed the flexural strength following UV ageing (as described in note 2 of Table 4.1) to increase by 12% (see Figure 2.7).

The finding of Qiu and Gu (2011) that elongation of GFRP at failure increased with UV radiation does not appear to fit with this theory. It is known that the elongation of pure polyester is greatly reduced by short wavelength radiation (Sasuga and Hagiwara 1987), and thus it is expected that the fibre architecture of the mats (as specimens were not pultruded) used in testing by Qiu and Gu (2011) brought about a more gradual failure influenced principally by the fibres.

The Visitors' Centre case study suggests that UV is responsible for the majority of resin hardening, though hardening is also seen to be age-dependent as well as UV-exposure dependent. The average compressive modulus exceeded the average tensile modulus of internal flange material, as well as the external material. The literature reviewed does not make the quantification of any hardening behaviour of the resin an objective, either in the enhanced modulus in compression, or the reduced limit of brittle resin fracture in tension.

The degree of flexibility in the polymer matrix of GFRP elements is of significant importance to the resulting durability, as explained above, and how UV damage accelerates other mechanisms of degradation. Owing to this, further work in correlating the limits of resin fracture established in case study testing in Chapter 3, using the method detailed in Subsection 3.2.5.2, to other measurable parameters would be valuable. If parameters such as T_g and Rockwell hardness can be established for specimens which have been aged to various extents, alongside appraisal by the method as described in Subsection 3.2.5.2 to assess the limit of brittle resin fracture (where durability is known to be in jeopardy), values which are indicative of the resin's ability to protect fibres could be quickly established.

Compston et al. (2008) have demonstrated how resin hardening is accelerated and resulting hardness is increased by UV irradiation, as illustrated in Figure 2.9. Rockwell hardness is measured in this study. Compston et al. (2008) shows that UV is known to cause hardening of polymer resins, and can be used in a controlled manner to do this on

an industrial scale. Establishing known values of T_g and Rockwell hardness corresponding to a suitable design limit of resin fracture would form vital further research.

4.2 Mondial House

Like the Severn Crossing Visitors' Centre material, the lack of 'base case' data has proved a hindrance to establishing quantifiable loss of mechanical performance. Before the influence of exposure over the service life of 30 years could be assessed, the nature of fibre architecture and issues relating to fabrication of the panel material, internally and externally, had to be established. With this accomplished the internal and external sandwich skins afforded the chance to examine the degree to which the gel coat (that comprises isophthalic resin, pigmented white, with an ultraviolet stabilizer (Brookes 2008) protected the external sandwich skin from UV related degradation of the type investigated above in section 4.1.

The glass transition temperature T_g of internal and external material was found to be almost identical, as shown in Table 3.10. It was reported by Cabral-Fonseca et al. (2012) that UV irradiation causes the T_g of polyester GFRP to rise, but only very slightly, from its initial value of 107 to 110^{o}C, as shown in Figure 2.5. The similarity of the internal and external glass transition temperatures from the case study findings cannot therefore confirm the efficacy of the UV barrier. Cabral-Fonseca et al. (2012) also reported, that a programme of hydrothermal ageing caused the T_g of polyester GFRP to fall by 16% when hydrothermally aged at 20^{o}C, to drop by 2% when aged at 40^{o}C, and to rise by 8% when aged at 60^{o}C, as shown in Table 2.5. It was seen in Section 4.1 that the ageing at 20^{o}C reproduced material of character most closely matching naturally aged material (i.e. degrading the least) where other mechanical characteristics were concerned. With this in mind it would be expected that some variation in T_g would be evident between internal and external material, attributed to the enhanced degree of weathering and moisture to which the outer sandwich skin was subjected. The overall protective action of the gel coat, which was removed as described in Subsection 3.3.2.1 prior to specimen mechanical testing, could account for the similarity of the two values of T_g. It is not to say that the glass transition temperature has not altered over the 30-year service life, but that the external material tested had experienced an environment of

limited exposure similar to that of internal material, due to the presence of the gel coat.

The mechanical properties, as determined from the case study investigation, have been ascertained, and external material compared to internal to identify any deficit. The variation observed can be accounted for by variations in the fabrication practice and quality of each sandwich skin. It would appear that the gel coat has prevented enhanced degradation of the outer sandwich skin.

The tensile elastic modulus of the internal and external sandwich skin material was determined and found to be in very close agreement, as shown in Figure 3.38. The ultimate tensile stress and shear modulus, presented in Figure 3.39 and Figure 3.41 respectively, showed a reduced performance in the internal material. However this could be accounted for through a micro-analytical investigation, which was prompted by review of existing literature (Thomason et al. 1996; Lambert et al. 2012; Schmidt et al. 2012). Undertaking microscopy and a thresholding procedure established the relative percentage of voids in the composite material cross section (see Table 3.9) and revealed the nature of the typical location and distribution. It can be noted that whilst microscopy proved very useful in establishing fabrication variation and uniformity of material (e.g. fibre size) between each of the two sandwich skins, informative data regarding degradation due to environmental or ageing factors was hindered by lack of ‘base case’ data. Comparative study of internal and external material was possible.

Figure 4.1 shows an illustrative schematic concerning four fibres within a section of GFRP element that are aligned with the direction of an applied tensile force. In this figure the tensile stiffness and strength across the marked boundary denoted by the dashed vertical red line are considered. In Subsection 2.3.1 it is explained how the amount of fibres, and their superior stiffness and strength in comparison to the polymer matrix, have a far greater influence on tensile strength and tensile elastic modulus. Equation 2.1 and Equation 2.2 are illustrative of this, despite a reduced accuracy when used to model very low fibre content GFRP such as the hand lay-up panels from Mondial House.

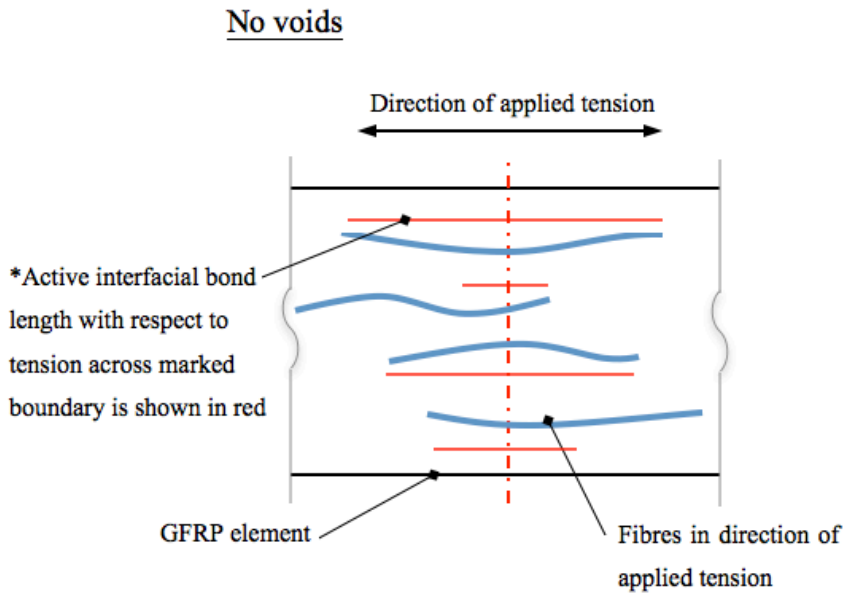

Figure 4.1 Illustrative GFRP section showing fibre length, effective interfacial bond length with respect to tension in direction shown, and absence of voids

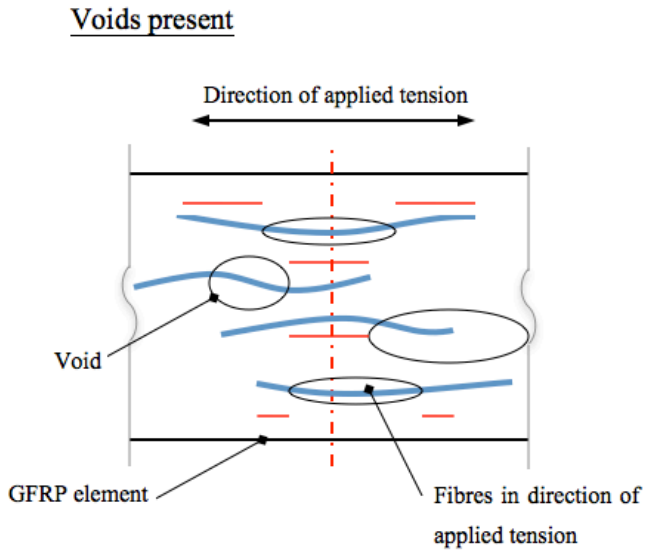

Figure 4.2 Illustrative GFRP section showing fibre length, effective interfacial bond length with respect to tension in direction shown, and voids

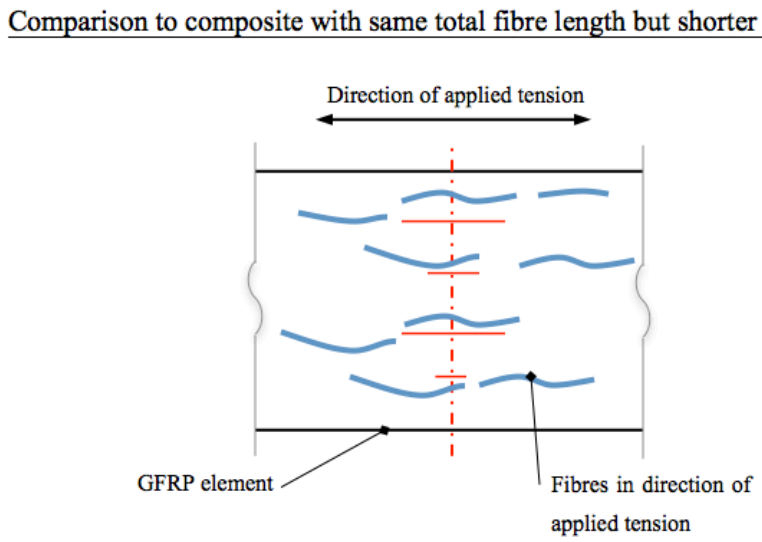

Figure 4.3 Illustrative GFRP section showing fibre length, reduced effective interfacial bond length with respect to tension in direction shown, attributed to shorter fibres, not voids

It can be seen in Figure 4.1, Figure 4.2 and Figure 4.3 that four fibres cross the dashed red boundary. In Figure 4.2 voids are shown, of random arrangement, that across the boundary considered contribute to about 10% of the cross sectional area. As the stiffness is influenced far more by the fibre fraction crossing the boundary, the voids have only a small effect on the mechanical stiffness observed. In other words, as the fibre fraction remains constant, the stiffness is largely unaffected by the presence of voids. The same could be said of tensile strength. However, the anchorage of the fibres, just like embedment length of steel reinforcement bar in concrete, must be sufficient to permit the max tensile stress to be developed in the reinforcement. In Figure 4.1 and Figure 4.2, the effective length of interfacial bond anchoring each fibre shown, against tension across the marked (dashed) boundary is shown by a continuous red line next to each fibre. It can be noted that as the effective fibre anchorage is proportional, and limited to, the shorter 'embedment' length (the red lines in Figure 4.1, Figure 4.2 and Figure 4.3). The red lines must be symmetric either side of the dashed boundary, with respect to the shorter end of the fibre. Figure 4.2 shows that the total interfacial bond length for the four fibres shown is greatly reduced by the presence of the voids (by about half in the illustrative example shown). It is hypothesised that this reduction is sufficient to account for the reduction in tensile strength observed where voids are more

frequent in internal material from the Mondial House case study investigation.

In an attempt to support this hypothesis an analogy was drawn. The increased presence of voids can be shown to have similar effect on average interfacial bond length in the composite as shorter average fibre length does. The importance of this analogy is that existing literature could be sourced pertaining to the mechanical performance of glass polymer composites as a function of fibre length (Thomason and Vlug 1996). The relevant literature in this field is predominantly concerned with thermoplastic glass composites. This is due to the implications arising in recycling and remolding of such material, where the degree to which it is mechanically reconstituted prior to melting down is of direct impact on the resulting average fibre length.

Figure 4.3 portrays an equivalent section of composite with shorter fibres. The total fibre length is the same as in Figure 4.1 and Figure 4.2. Just as before, it can be seen that the same number of fibres cross the marked boundary, though as in Figure 4.2, where voids are present, the total effective interfacial bond length concerning anchorage across that boundary is greatly reduced, to an extent where strength could be reduced.

Thomason et al. (1996) presented the results of a study investigating the influence of fibre length on the properties of glass fibre reinforced polypropylene. Strength was found to increase with increased fibre length. The trend was noted as more significant at fibre lengths below 6 mm, though still evident from the data reported up to 12 mm. Thomason and Vlug (1996) published another paper on a different part of the same study which reported experimental investigation into the influence of fibre length on tensile modulus. It was reported that laminate stiffness was virtually independent of fibre length above 0.5 mm. This paper also notes how the matrix molecular weight and fibre sizing compatibility (relating to integrity of interfacial bond) had little effect on the laminate stiffness. This analogy correlates well with case study testing results above showing good retention of stiffness despite failure observed where interfacial damage is evident, which has been observed qualitatively in microscopy images such as that shown in Figure 2.18.

The analogy adopted, expressing similarities in the influences of fibre length and void

ratio, and the supporting literature reviewed, is not sufficient to predict a quantifiable reduction in strength (or small reduction in stiffness) of the composite material. It does suggest that it is entirely possible for the voids present in the internal sandwich skins of the Mondial House panels, to reduce the tensile strength significantly, without affecting the tensile elastic modulus to the same degree. It is possible that fibres in the internal material were shorter, as well as occurring with a greater amount of voids, though the relative voids present in internal and external material was verified experimentally.

4.3 Performance of aged material

Using the ultimate stress for the aged material, and the elastic modulus as calculated from the initial linear portion of the stress strain relationship, a strain limit based on tensile failure, for both case studies can be established. For the Visitors' Centre this is 13,800 με and for Mondial House this is 5,800 με. The value for Mondial House is exceeded in testing results, owing to a departure from linear stress strain relationships seen before failure. This is thought to result from viscoelastic realignment of fibres in the chopped strand mat (CSM) reinforcement.

To appraise the strain value at which onset of brittle resin fracture occurred for the external material of the Visitors' Centre panels, and the strain value at which it occurred in Mondial House, the values for ultimate strain of the materials must be considered alongside. The strain at failure for the Visitors' Centre was found to be 13,800 με, where the strain limit for resin fracture was shown to lie between 6,000 and 9,000 με for external material. The Mondial House panel material retained 84% and 89% of flexural stiffness (internally and externally) at 8,000 με. This represents large flexibility of the resin. The strain at failure of the material, if it remained linear elastic to failure, would be 5,800 με. This implies the flexural stiffness is well preserved well into the non-linear range. This non-linear behaviour is evident in Figure 3.40.

The linear stress stain relationship exhibited by the Severn Crossing Visitors' Centre material is evident in Figure 3.13. This pultruded material is fabricated to include principle fibres that are straight, because they are held under a small amount of tension, as the element is produced. The linearity of the fibres in this material, in contrast to the random nature of the fibres in the hand lay-up panels from Mondial House is believed

to be responsible for the difference in the degree of linearity observed. At larger stresses, material that relies on fibre reinforcement that is not parallel to the direction of stress will depend an increasing amount on the resin that is suspending and binding those fibres. The resin is of lower stiffness than the fibres and at larger stresses more of the resin must be mobilized in this way to enable fibres not parallel to the tension direction to carry the stress.

It has been explained how the work undertaken in Chapter 3 filled in gaps in existing knowledge relating to durability or GFRP composite material. The phenomenon of hardening in the polymer matrix component of GFRP elements has been observed and quantified. It was identified how flexural testing of coupons captures characteristics of the resin component to an enhanced degree compared with other mechanical tests. Reference to both case study testing undertaken on naturally aged GFRP, and findings reported in the literature pertaining to testing of artificially aged material, permitted the development of a suitable methodology to quantify the hardening behaviour. The limit of brittle fracture of the resin in tension has been highlighted as a key index of when durability is in jeopardy through increased susceptibility of the fibres to environmental degradation.

By determination of the glass transition temperature for material of differing panel origins, the efficacy of a gel coat to safeguard durability has been validated. In order to do this, variation in mechanical performance that was observed had to be accounted for by fabrication and material variability. A mixture of analytical techniques including electron microscopy, together with literature-based findings was employed to achieve this.

Within this chapter the findings of Chapter 3 are discussed with reference to relevant literature presented previously in Chapter 2. Experimental results have permitted the assessment of the suitability of parameters adopted by others for accelerated artificial ageing procedures. Some findings represent a contradiction to what has been reported by others as appropriate practice for representative procedures. The temperature at which a hydrothermal bath should operate for instance, to best replicate the ageing environment, and inflict equivalent degradation on material which has not been subjected to UV, has been revealed to be much lower than that adopted by some studies

reviewed. It has been concluded that re-conditioning and the associated regain observed should be considered as a matter of course when performing accelerated ageing of composites, which is rarely the case. Literature that has claimed that 'the synergistic effects of procedures replicating UV, moisture and temperature variation are insignificant' has been contradicted. The influence of UV irradiation, when included as part of such ageing programmes with combined environmental factors, has been demonstrated to be of severe detriment to material properties and to accurately represent degradation of corresponding natural material over a 17 year design life in only 2 months. The amount of UV radiation inflicted on specimens in two literature-reported studies has been quantified. The accurate calibration between the amount of synthetic UV irradiation, and that experienced by GFRP in a natural design life, relies on determining of a factor accounting for the enhanced rate of irradiance necessary for accelerated procedures. This is identified as vital further work.

Several further issues have been encountered in Chapters 3 and 4. Those not already discussed in this section are summarized as follows. More data is needed concerning the serviceability characteristics of aged GFRP. A shortage of data was identified relating to elastic modulus of the material in tension following accelerated ageing procedures. Such data would be invaluable for use in comparing the tensile elastic modulus of naturally aged material with artificially aged, and to assess the influence of different ageing procedures adopted in more depth. This was undertaken for tensile strength in this chapter. As previously reported, studies observing the synergistic effects of ageing that replicate combined environmental factors inflict severe degradation on pultruded polyester GFRP material in a short period. Carra and Carvelli (2004) established a value for the reduction in tensile strength of pultruded polyester GFRP after such a programme of ageing, of 8.5%. Natural ageing over 17 years of GFRP of southerly facing origin yielded a reduction in tensile strength of 13%, however the accelerated ageing procedure applied in the study only lasted 2 months. The total amount of UV irradiance to which specimens are subjected in such studies is identified as being of significance, and has been quantified in this chapter. Further studies that produce synergistic effects of degradation, where the amount of each factor (UV for instance) is quantified, are required. This would enable rate dependent effects in application of degradation inducing factors to be determined. It has been shown that applying 38 weeks' worth of UV to a façade over the course of only 8 weeks, induced

almost as much reduction in tensile strength as 17 years natural service (see Table 4.1). Published studies report values for T_g and Rockwell hardness, along with values describing other mechanical properties, throughout programmes of accelerated ageing. By conducting testing of the type devised to assess the limit of brittle resin fracture for polyester matrix constituent to the GFRP in testing in Chapter 3, it is proposed that index values for T_g and Rockwell hardness could be established, relating to the critical mechanical state in the aged material when brittle fracture in the resin occurs and durability is placed in jeopardy.

Few published studies speculate as to the variation, or rate of degradation of mechanical properties, of wholly polymeric elements over a full design life. Those based on an Arrhenius relationship and drawn from data where only hydrothermal ageing is undertaken, can be shown to make significant overestimates of degradation, as shown in Figure 4.4. Chu et al. (2004) presented an Arrhenius-derived model for degradation of vinylester. Vinylester composites are considered to be of superior durability compared with those of polyester when forming GFRP elements (Pochiraju et al. 2012), and, as such, a stringent comparison is assumed. It is shown that the observed retention of tensile strength over 17 years natural ageing, using data from the Visitors' Centre case study, is 30% greater than that predicted.

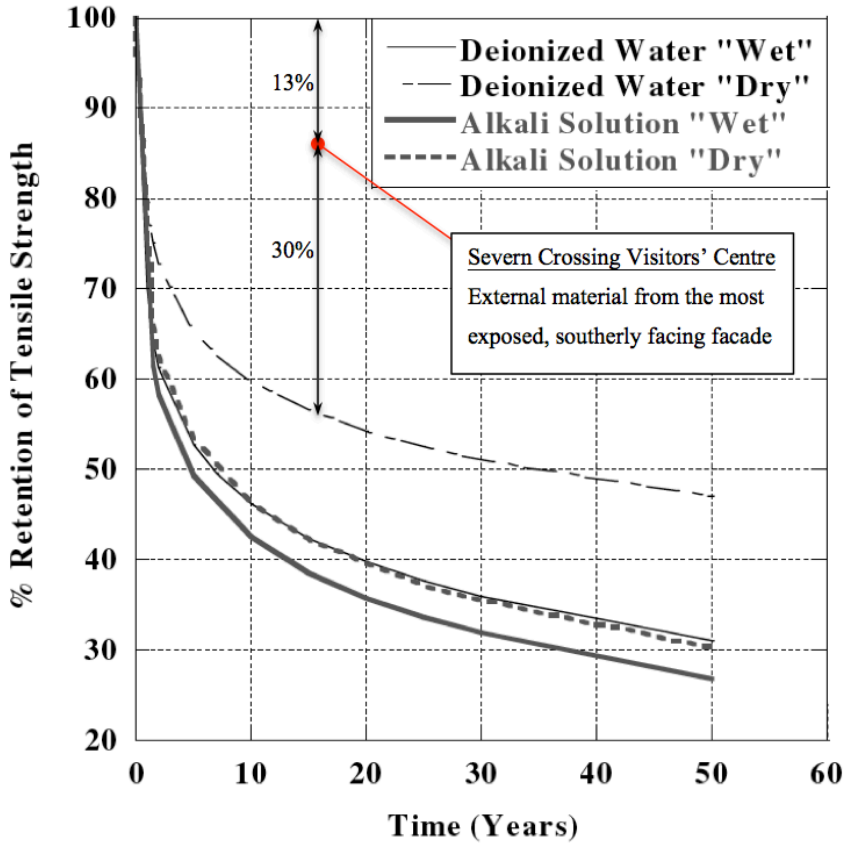

Figure 4.4 Percentage retention of tensile strength of GFRP as per Chun et al. (2004) showing relative position of experimental data point for naturally aged material

The improved retention in tensile strength observed over that predicted for superior, vinylester GFRP material, is made with respect to material that has been reconditioned and regained some of the strength lost. The study undertaken by Chu et al. adopted the use of hydrothermal ageing procedures, but as it has been demonstrated in this chapter and Chapter 3, the influence of UV exposure cannot be ignored in replicating accurate ageing characteristics. Such Arrhenius methods therefore are shown to be of very limited use in the application of predictive ageing attributed to combined effects.

The enhancement in the durability properties of GFRP by protecting the material is well documented in existing literature and has been validated by the case studies presented in Chapter 3. The profile of hypothetical polymeric facades can conform to an aesthetic fluidity that avoids sharp edges, where the type of finishes necessary to enhance durability could peel from. Facades are generally designed with shadow gaps, rain channels and a host of architectural features derived from a variety of vernacular architecture which facilitates integrity of panel boundaries suitable for finishes.

4.4 Summary and implications

In this chapter it has been revealed how voids in the composite can influence the strength and stiffness of GFRP elements. Knowledge of voids and defects are key in assessing the service life performance of a composite element exposed to the elements, because voids reduce the interfacial bonded area between the polymer matrix and the constituent fibres.

It has been established that UV exposure is of great significance regarding the mechanical deterioration of polyester unsaturated isophthalic resin of the visitors' centre panels. Whilst the rate of mechanical degradation as a consequence of UV exposure is less than that reported from accelerated laboratory studies by others, UV is a significant factor that must be addressed through the inclusion of surface veils or gel coats. Suitable design factors accounting for strength loss over a whole life in service, and for a reduction in the strain limit of brittle fracture must be observed in design.

The Mondial House hand lay-up panel material has illustrated the importance of workmanship in this form of composite manufacture. The presence of voids is suspected to influence the strength of the composite to higher degree than the stiffness. A shortage of literature relating to the influence of ageing on GFRP composites has been uncovered. However it has been reported by others, that UV can increase the stiffness of a polymer resin, either intentionally at fabrication, or during artificial ageing. The associated reduction in the limit of brittle resin fracture has not previously been documented or quantified.

Accelerated tests are not appropriate where the amount of degradation in mechanical properties is sought to correlate to a service life of natural ageing. Accelerated tests could be appropriate in cases where it is required that long term degradation is inflicted on material in over a very short timescale to assess the relative performance of different composite materials. If the materials are intended for use in an environment where they will be subjected to UV irradiation, then the accelerated ageing procedures must include UV irradiation to observe true synergistic effects. In such tests the temperature of a hydrothermal bath is a parameter that must be carefully chosen, and specimens should be reconditioned before conducting post-ageing mechanical testing.

A shortage in research concerning the performance of material that has been aged under stress has been revealed. Long-term environmental performance has been investigated in this chapter. In the next chapter long-term mechanical performance is addressed through consideration of characteristics under fatigue loading.

5 Fatigue: laboratory testing programme

The proceeding two chapters of this thesis have addressed the issue of durability of GFRP material. If industry confidence in the 'whole-life environmental performance' increases, the whole-life mechanical performance is predicted to come under greater scrutiny concerning adoption of GFRP as a construction material. Establishing pertinent material characteristics, relating to mechanical performance in fatigue, and demonstrating the existence of safe design limits for design practice is necessary to validate the ideology of polymeric facades.

By developing hypothetical prototype designs that satisfy the design conflicts revealed by a scoping exercise, key issues problematic to design have been established. An abundance of pultruded return angles, where the prying force at connections will induce stresses, at the angle root locations, in the weaker secondary fibre direction, are characteristic of suitable connection designs. These locations must endure a lifetime fatigue loading and maintain good performance. At ultimate limit state the standard practice for validation of façade schemes is 10,000 cycles, which is deemed to represent a lifetime of ultimate state loading (CWCT 1996). This chapter explores the nature of phenomena arising through fatigue loading and investigates characteristics that are vital for the informed design of polymeric façade connections. The literature review highlighted the importance of representative laboratory fatigue testing owing to the variability of pultruded GFRP elements and the complex nature of stresses in the anisotropic material.

The aim of the testing campaign presented was to establish the general behaviour and response of a suitable connection scheme. In undertaking such an exercise, the predominant type of failure/damage mechanism for the testing set-up designed has been established. It is revealed how the rate of degradation in stiffness can be measured as a means to monitor the accumulation of damage. Parameters relating to appropriate threshold design values for loading and design combination have been investigated.

5.1 Introduction

Fatigue behaviour, a characteristic of pultruded GFRP that is rarely of much

consequence to design of primary structural elements in buildings, could be of greater concern in a cladding situation (and also for application in bridges). Pultruded profile edges of prismatic GFRP units can assume forms that accommodate suitable connections. Such angled returns will require a fatigue resistance to withstand a lifetime of cyclic straining, due to the transient action of wind or occupancy loading (CWCT 1996). Fatigue testing to an equivalent degree is required to validate viable façade schemes. Much existing research focuses on fatigue when axial stresses are in the principal fibre direction (Salvia and Vincent 1996; Salvia et al. 1997; Tong 2002). However, this is not necessarily the critical stress direction in cladding connection situations. Deterministic approaches dominate, and damage is attributed to an accumulation of many cracks, unlike the damage propagation exhibited by steel (Tong 2002). By targeting behaviour in the secondary-fibre direction at angled returns, data produced will be directly transferrable to realistic connection designs.

Structural angle sections have served as the subject of this experimental investigation. Two different pultruded profiles of equal angle sections have been used to represent the edge returns found to occur in prototype designs developed in section 2.4. Component testing of representative elements has avoided the need for whole panel fabrication. Testing methodology and chosen parameters have been selected to profile how damage propagates in such an element, and how the performance of the represented connection type would endure the lifetime service of a polymeric façade. This is explained in Section 5.2.

Testing coupons of pultruded GFRP material has sought to profile the material, in terms of mechanical properties associated with fatigue. By undertaking this profiling exercise in tandem with the angle section component tests, the behaviour of the connections observed can be related to the material and design properties, as well as testing parameters. Thus the potential to apply findings to other instances where specification of GFRP material is different can be assessed. A model describing the cumulative action of successive connections, presented in the Chapter 7, draws on characteristics of connection behaviour measured by the testing reported.

The fundamental theory behind the data processing adopted to handle the large amounts of fatigue programme data is presented in Subsection 5.2.5 alongside the advantages that have proven key in presenting it in a useful form.

5.2 Methodology

5.2.1 Coupon preparation and testing procedure

Coupons for fatigue tests in tension were prepared as per previous specifications in Subsection 3.2.2.3. Monotonic tests were conducted to code of practice BS EN ISO 527 (BSi 2009). The pultruded GFRP sheet (new material) was approximately 10 mm thick and coupons were cut to width 25 mm. Coupons for monotonic (non-fatigue) tests were 'dog bone' or 'waisted' in profile to prevent failure of the aluminium tabs in the jaws of the test rig at the high loads necessary to fail the thick material. Coupons taken from the pultruded flat sheet with transverse alignment to the principal reinforcement direction were restricted to 200 mm length (the width of sheet); otherwise coupons were either 200 mm or 250 mm in length.

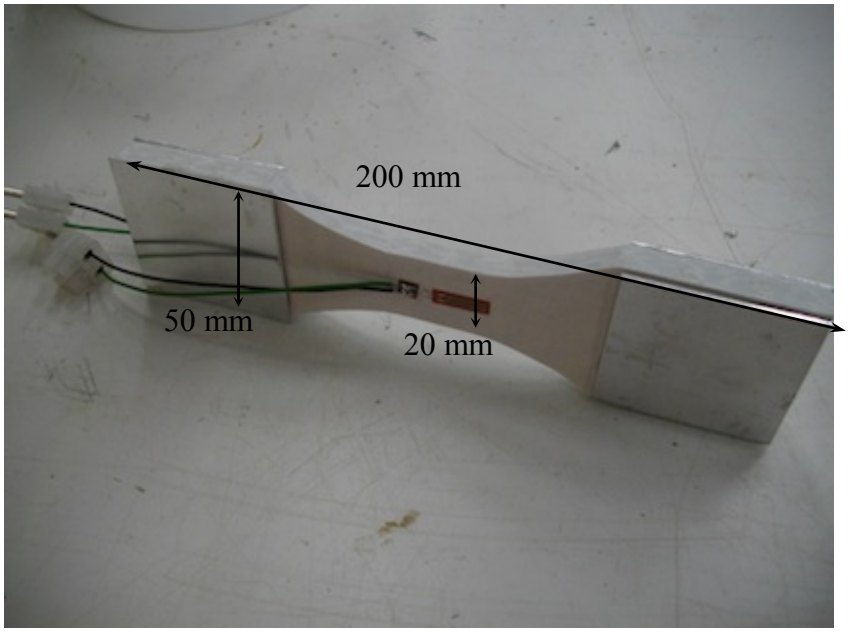

Figure 5.1 Waisted coupon of transverse alignment to principal reinforcement

Coupons for fatigue cycling were straight sided (see Figure 5.2) as the peak load necessary was lower than the monotonic maximum, and failure in the jaws was not an issue. Cycling was undertaken initially at 1 Hz for all coupons, and later 2 Hz cycling

was trialled and then adopted once results were shown to agree with 1 Hz tests undertaken. Autogenous heating and other rate-dependent mechanical consequences were not evident in the transition. The maximum number of cycles for coupons was 100,000 if the specimen was not failed by the loading. Testing was conducted under load control.

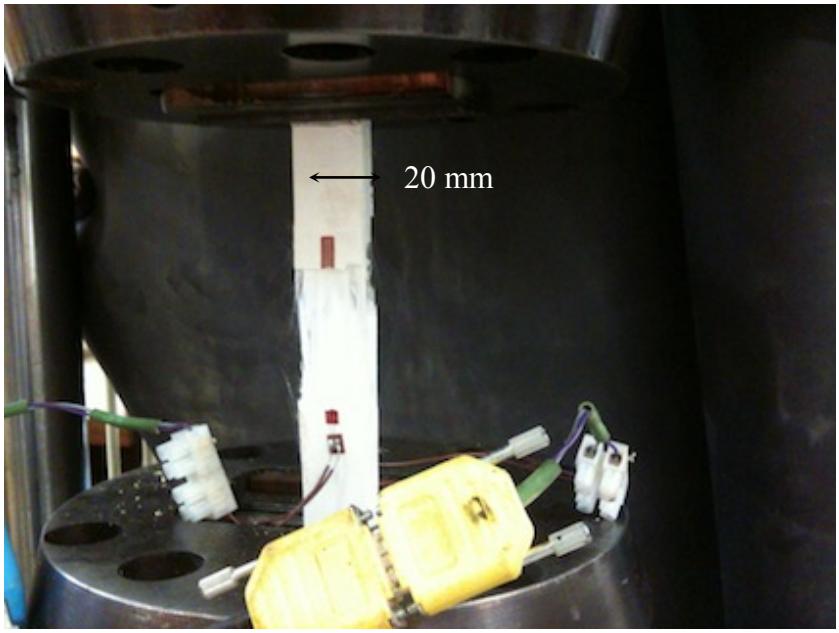

Figure 5.2 Transverse coupon failure: cycled at peak load 75% of monotonic maximum

The peak cycling load chosen (and associated stress) for each of the transverse and longitudinal coupons tested was specified as a percentage of the ultimate tensile stress. This enabled graphs of the type employed next in Subsection 5.2.2 to be constructed. The minimum load was selected to be very close to zero. A small load was necessary to avoid the material going into compression as a result 'drawback', as explained in Chapter 2. It should be noted that the data logger recorded both the imposed waveform and the specimen response with high accuracy, and the tolerancing in the driving of the rig has not increased error in the results.

The waveform chosen was sinusoidal in tension. The smoother operation of the test rig functioning under this form carries benefits of reduced noise in data. Such a waveform without sharp points is also kinder to the clamped ends of the specimens and hence chosen to mitigate slipping. A sinusoidal waveform is also how the angle sections have

been tested and reported below; by following common practice, as mentioned in Section 5.1, material data sourced elsewhere is more easily transferable.

5.2.2 Analysis of coupon test data

The number of cycles to failure, N_f, for each coupon, can be plotted against the peak value of stress in the load cycling program chosen, σ_{max}. The relationship between the variables $logN_f$ and σ_{max} is known to be linear for uni-directional reinforced composites (Harris 2003) as shown previously in Figure 2.28. The GFRP material profiles possess failure envelopes for each of longitudinal and transverse directions of stress. It was found that not all coupons failed within the maximum number of cycles (100,000) when testing was conducted as per Subsection 5.2.1. Those subjected to lower peak stress reduced in stiffness without completely fracturing during the testing. To allow these coupons to contribute to the material profile, the prospect of deriving and plotting 'stiffness reduction envelopes' was explored. The log of the number of cycles until stiffness reduced by 20%, or 50%, ie $logN_{20}$ or $logN_{50}$ could be plotted for both of longitudinal and transverse coupons. Data concerning a material stiffness fatigue limit is, in fact, more important in expressing damage accumulated, and key in assessing the behaviour of the angle section elements, and the connection represented.

It is not suggested that the amount of fatigue testing undertaken in this campaign is in any way extensive enough to carry high statistical confidence in the position of the envelopes described; the time such testing would require would fill more than an entire PhD alone. Instead what is demonstrated below is how material properties can be attained and handled so that key parameters can be extracted and applied to understanding mechanical behaviour at element and connection level.

5.2.3 Preparation of angle sections and test rig set-up

The angle section was situated in the test rig housing as shown in Figure 5.3 and Figure 5.4. The prepared specimen was secured in place by horizontal clamps and bolts, which passed through the specimen and grip the rails. The bolt-holes in the rails were drilled as low clearance and the bolt-holes in each specimen were filed out in-situ to yield as low clearance as possible and mitigate slipping and slack developing in the system. The rails were bolted securely to the fixed rig base.

In the arrangement shown in Figure 5.4 the clamped leg represents the continuous façade panel face, and the free horizontal leg, gripped at a single discrete location, represents the edge return of a pultruded panel with a discrete mechanical connection. Flange is not drilled at this location, as testing is not intended to generate data concerned with stresses around bolts in pultruded GFRP. There is existing comprehensive literature available addressing such behaviour (Turvey and Cooper 2004; Turvey and Wang 2008; Turvey 2011).

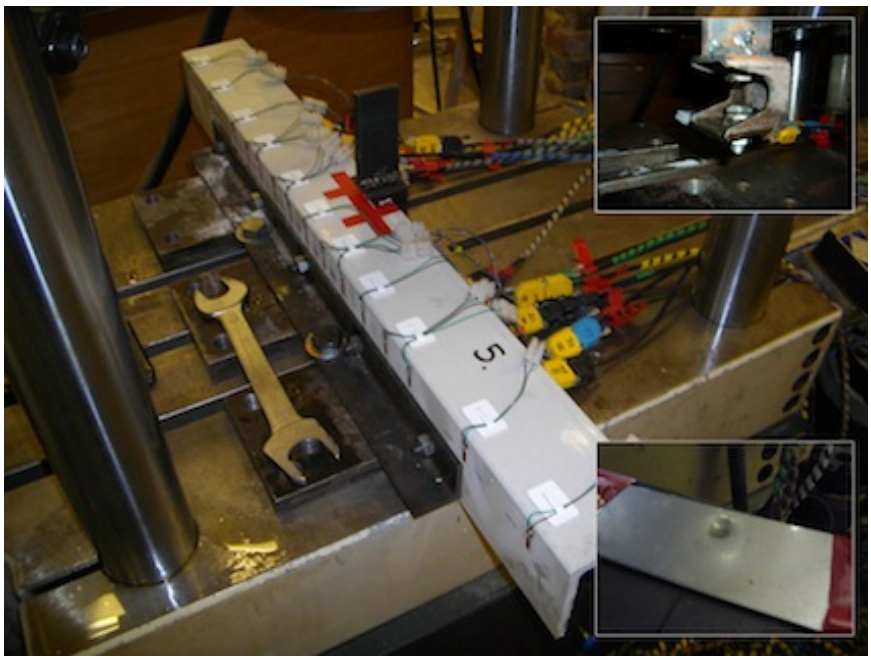

Figure 5.3 Angle section specimen sited in rig. (Crosshead and jaws moved up). Inset upper: custom welded adjustable clamp for point load application. Inset lower: protective steel tabs taped to specimen at load application point

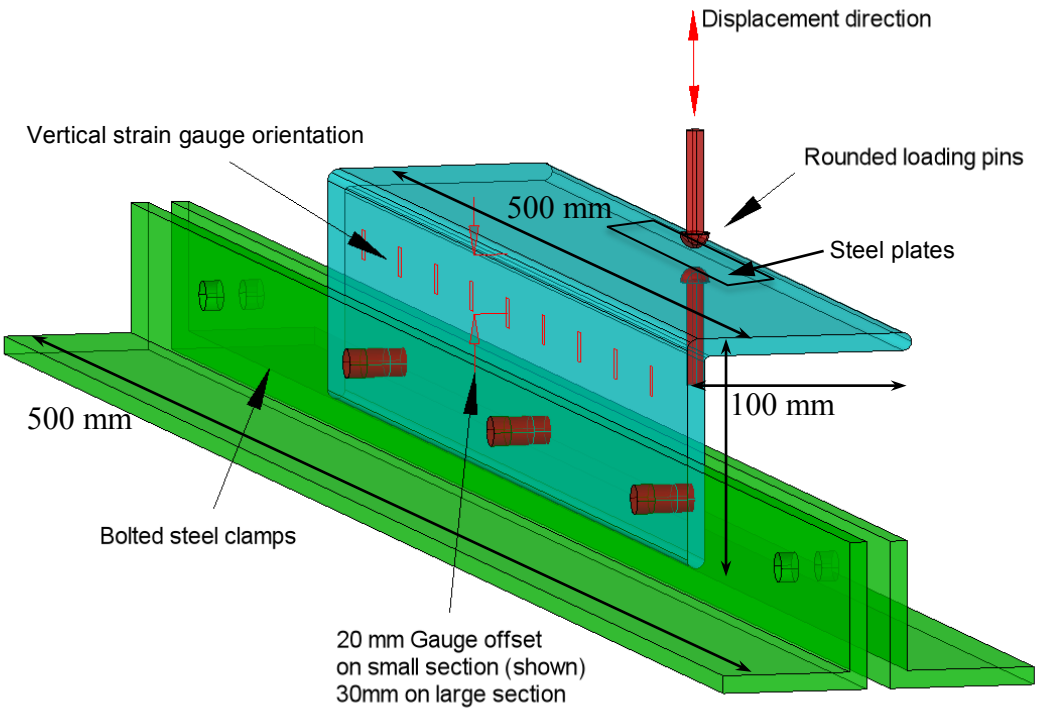

Figure 5.4 Schematic showing general arrangement of specimen bolted into rig, loading displacement direction and strain gauge orientation

The protective steel tabs at the load application point prevent localised damage in the composite. Taping to secure these using electrical tape proved the most efficient means that did not result in tabs breaking free; other tapes that could not stretch, tore away, and epoxy bonding of tabs fractured immediately upon commencement of cyclic loading. The gripper (shown inset top right in Figure 5.3) was clamped securely onto the horizontal flange and the crosshead brought down and clamped to the fin plate of the gripper. All cyclic loading commenced from a neutral displacement position at zero load. Strain gauges were attached using cyanoacrylate cement, a single component room-temperature curing adhesive.

Two different sized sections were tested (see Figure 5.5) at lengths of either 0.5 m or 1 m. These specimens were prepared and strain-gauged as shown in Figure 5.3. It can be seen in this figure that the strain gauges on a 1 m length section were not uniformly distributed along the specimen length. They were at 50 mm centres near the load application point, and 100 mm centres outside of the central region. (Exact limit specified in the results Subsection 5.3.4). The properties of the structural sections are shown in Table 5.1.

Table 5.1 Angle section design values for mechanical properties from manufacturer's literature

$E_{longitudinal}$	23	GPa
$E_{transverse}$	8.5	GPa
$\sigma_{longitudinal}$	240	MPa
$\sigma_{transverse}$	50	MPa
$V_{f\,longitudinal}$	Not available	
$V_{f\,transverse}$	Not available	

There are two further important parameters associated with strain gauge location and how the specimen is situated in the test rig. Figure 5.6 shows the gauge-offset distance from the inferred apex of the angle cross-section to the centre of the gauge. This distance was 30 mm for the larger section and 20 mm for the small section. This ratio of 30:20 was the same as that of the angle section leg thicknesses. The gripped length of flange element when clamped into the test rig rails was 60 mm for the larger section and 45 mm for the smaller section. This parameter is illustrated by Figure 5.7 and was specified to be in the same ratio as the structural angle leg lengths.

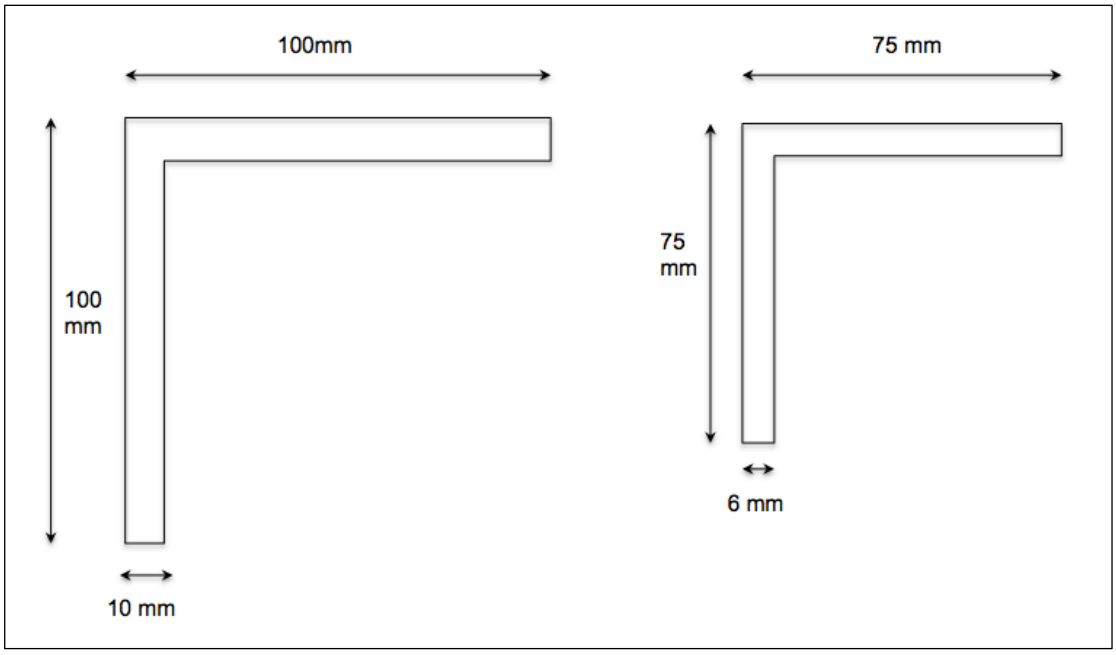

Figure 5.5 Specimen dimensions: equal angle sections (root radii not shown)

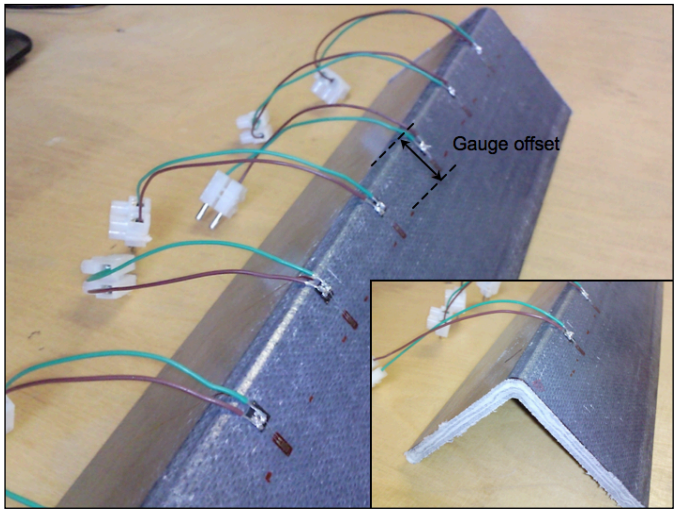

Figure 5.6 Gauge offset parameter on prepared angle section specimen

Figure 5.7 Gripped length parameter on prepared angle section specimen

The strain gauges were applied to capture the state of strain at increments along the specimen length, on the up-stand element of the section; i.e. once the stress had been transferred around the root radius. The gauges were all orientated vertically to measure the component of strain in the critical transverse direction, and how this diminishes along the specimen length. The sampling rate for data logging chosen was 10 Hz for both 1Hz and 2Hz cycling. The reasoning behind this choice is covered in Subsection 5.2.5. Essentially, over the duration of a test, the response of the specimen can be monitored, and the way the fatigue load is 'shared out' along the member length can be appreciated. The manner in which damage propagates along the element can also be

assessed, but the most fundamental, and perhaps most important quantifiable connection property established is the connection stiffness (i.e. the stiffness afforded by the integrity of the connection between the two angle section legs), and the manner in which it diminishes.

5.2.4 Defining testing parameters for angle section fatigue programme

The first decision encountered when setting out to define suitable loads (or displacements) over which to cycle, was whether to replicate realistic stresses or realistic loads. The two sizes of angle section available were both of greater thickness than would probably be necessary for the external connected structural GFRP skin of a polymeric façade. Therefore if realistic design stresses were desired, the loading required was higher than that which would be accounted for in design practice. If realistic loads were applied then strains were comparatively small. To utilize structural angles, which possess the typical angle return fibre architecture details preferred for this testing, it was decided that both options should be investigated. In fact, testing has been conducted at: realistic loads (as defined below using the plate theory concept developed in Subsection 2.4.1), realistic stresses corresponding to serviceability limit state criteria, and higher stresses to observe initiation and propagation of damage. These load/displacement parameters are also defined below.

The testing programmes undertaken can also be aggregated in a different way: load control and displacement control tests. Load control, which is the more common method for manufacturer/product developer led component validation (Harris 2003), requires failsafes to prevent rig damage should the specimen fail, and was employed for the 'realistic load' testing, where the loads were smaller. As explained in section 5.3 however, it was unfortunately not possible to impose a load control system using such low loads with the necessary control. So these, together with the high load 'realistic stress' tests (to initiate and track more damage in the specimens), were undertaken by displacement control. Displacement control is a safer way to perform fatigue tests in the laboratory, because it does not rely on programmed failsafes to limit displacement should the specimen fail. It is therefore more suitable to partner it with the higher load tests.

The decision to adopt displacement control testing can be justified on a design basis too. If a façade panel of the type shown in Figure 2.27 (as an appropriate hypothetical example) is subject to large, repeated deformations, the resulting action will be a loading that is not resisted by the stiffness of the panel or the panel mullion connection but by tension membrane action of the flexible diaphragm panel between two adjacent mullions. The reduction in stiffness at connections will occur quickly under the large loads and the resulting action at the connections will be equivalent to displacement control though a fixed angle. At ultimate limit state the standard practice for validation of façade schemes is 10,000 cycles, which is deemed to represent a lifetime of ultimate state loading (CWCT 1996).

To determine parameters for 'realistic loads', Equation 2.33 from Subsection 2.4.1 is utilised. Dimensions of panel a and b as presented in Figure 2.21 are taken to be 1.8 m (largest practicable mullion to mullion span) and 3.0 m inter-storey height respectively. p is specified as equal to zero, as it is the shear at the panel edge (the mullion reaction) that is required, and r , the y-direction vector is taken between limits y = 1 m and y = 2 m. Thus the connection load calculated is taking load for the middle third of one side of the panel, which is a realistic check accounting for lack of fit in adjacent panel-mullion connections. The uniformly distributed load on the panel, q, is taken to be 1.2 kN/m^2. This load is un-factored. Equation 2.33 becomes Equation 5.1, and the load is found to be 0.48 kN. Cycling has been conducted in the laboratory between loads ± 0.5kN for the 'realistic load' programmes of testing.

$$\int_{y=1m}^{y=2m} Q_x\Big|_{x=0}\, dy = \left[\frac{1.2\times3.0}{1.8\cdot\pi^2\left(\frac{1}{1.8^2}+\frac{1}{3.0^2}\right)}\cdot\cos\left(\frac{\pi\cdot0}{1.8}\right)\cdot\cos\left(\frac{\pi\cdot y}{3.0}\right)\right]_{y=1}^{y=2} = 0.48kN \tag{5.1}$$

Derivation of loading parameters for 'realistic strain' tests used typical design literature values for transverse moduli, E_{trans}, and ultimate strength, $\sigma_{ult\ trans}$, of the pultruded composite. E_{trans} of 15 kN/mm^2 and $\sigma_{ult\ trans}$ of 50 N/mm^2 result in a design strain of approximately 3000 με. The design values specific to some sections employed as specimens in this testing carried design stiffness in the transverse orientation, E_{trans} of

8.5 kN/mm^2, thus leading to a resulting stain limit of approximately 6000 με. Monotonic coupon testing of this material in tension established a value of E_{trans} equal to 11.1 kN/mm^2. $\sigma_{ult\ trans}$ was found to be much higher than anticipated too, at 75.2 N/mm^2. It was decided however, that a material factor of safety of 0.6 would be included to infer ultimate strain limits, which yielded 4000 με.

Appendix A reports on testing of small lengths of angle section in a 2D plane stress state imposed by monotonic loading. These specimens in a 2D plane stress state exhibited linea elastic prying behaviour to failure, at a lowest value of 4290 με. A range of testing in fatigue where the maximum transverse strain permitted was 2000, 2500 or 3000 με was adopted to cover the critical range of design strains between serviceability and ultimate limit states. 3000 με testing inflicted significant initial damage on specimens in first loading, and 4000 με testing was not undertaken. Specimens prepared and tested for 'realistic strain' testing are presented in Table 5.2 and those for 'realistic load' testing in Table 5.3.

Table 5.2 Specimen information for main 'realistic strain' tests

Specimen	Flange thickness (mm)	Flange length (mm)	Specimen Length (mm)	Max strain during cycling (με)
S1	6	75	500	3000
S2	6	75	500	2000
S3	10	100	500	3000
S4	10	100	500	2000
S5	10	100	1000	2500
S6	6	75	1000	2500

Table 5.3 Specimen information for 'realistic load' tests

Specimen	Flange thickness (mm)	Flange length (mm)	Specimen Length (mm)	Initial load during cycling (kN)
S7	6	75	500	0.5
S8	6	75	500	0.5

It has been explained above how these 'realistic strain' tests were conducted under displacement control. To determine the necessary displacement limits over which to programme the cycling of the connection, two methods were used. The first method comprised finding a theoretical load and displacement by considering the stiffness of a region of the angle section, centred under the load, responding to the imposed displacement at maximum capacity, and a region either side of this zone responding to a reduced capacity. Owing to the complex 3D nature of this problem, however, it was clear that to be confident in the values derived as fatigue testing parameters it would be necessary to determine the necessary displacements by experimental means. An initial linear ramp of load, on the connection specimen (as shown in Figure 5.3), was imposed until the maximum strain desired was detected by the central, critical strain gauge (the gauge nearest the loading point). The corresponding displacement was then noted and cycling conducted between ± limits of this value.

The initial linear ramp proved useful in establishing, as a byproduct of the exercise, the initial stiffness of the connection, in terms of force/displacement. It was decided that this would be a useful property to extract, both pre and post cycling programme, to record the degree by which the connection stiffness had diminished in absolute terms (other than in those described in Subsection 5.2.5). To further improve the credence of the stiffness values determined, the linear ramp was imposed in both positive and negative displacement directions (i.e. first down, then upward) and released/relaxed at the same rate of displacement each time. The type of graph shown in Figure 5.8 was generated; an average value of connection stiffness was determined as an average of that calculated from positive and negative displacements. The rate of displacement was 1 mm/min.

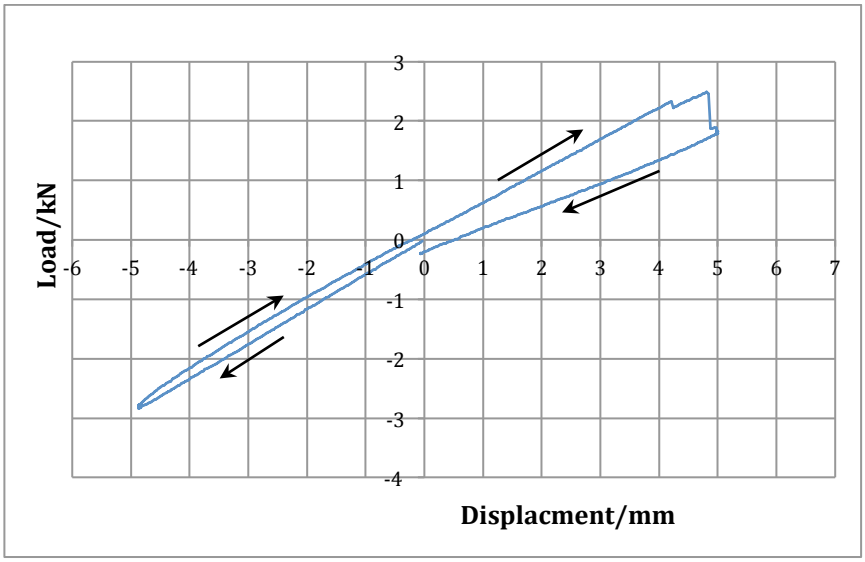

Figure 5.8 Typical response of connection to initial linear ramp (specimen S6)

5.2.5 Data processing

Data from up to 17 channels, for strain, load and stroke (displacement) had to be recorded at a sufficient sampling rate to monitor behaviour of the specimen at all parts of the load cycle, and be able to represent some form of index relating to the performance of the specimen over the entire programme of loading. Some preliminary specimens were tested under cyclic loading, to refine data capture and processing procedures. Sampling was trialled at 10 Hz, and this was shown to sufficiently capture the response of the specimen over the 1-second load cycles (see Figure 5.9).

Sampling at higher rates could improve the 'resolution' at which the behaviour of the specimen at micro-level was observed, and capture peak strains. Sampling at 25 Hz was also tested. To avoid increasing an already massive packet of test data by 2.5 times, the sampling was triggered at only the outer quartile region of the displacement cycles. This was done with a view to obtaining a higher resolution view of the important parts of the load cycle whilst not increasing the size of the data-file beyond what the analytical software employed later (e.g. Microsoft excel) could handle. The resulting output waveform can be seen in Figure 5.10. As one consequence of the preliminary angle section fatigue tests conducted, it was decided to proceed using only the 10 Hz continuous sampling approach. Sampling at 10 Hz resulted in smoother data once a suitable performance index (discussed in the section below) was derived. The influence is demonstrated by the graphs for the preliminary results presented in section 5.3.

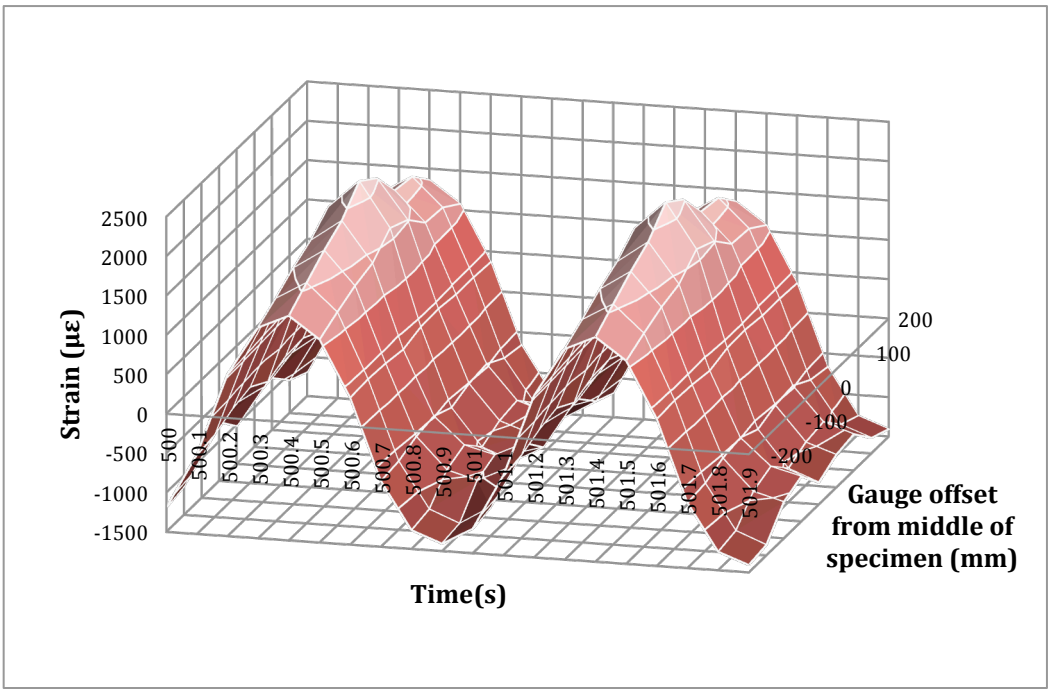

Figure 5.9 Snapshot of small time-step behaviour response of specimen when sampling at 10Hz

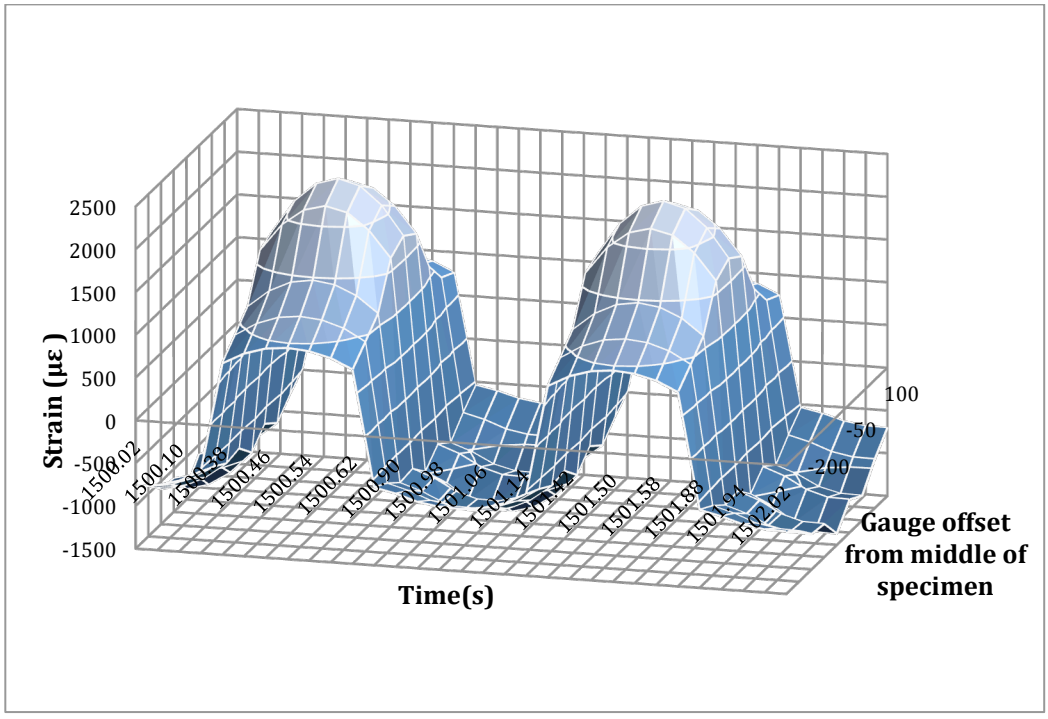

Figure 5.10 Snapshot of small time-step behaviour response of specimen when sampling was triggered in the outer quartiles of displacement at 25Hz

Whilst graphs of the type in Figure 5.9 and Figure 5.10 are useful to appreciate the response of specimens, at a micro scale, or at smaller time-steps, a more succinct index of performance was necessary to appreciate variation in the connection stiffness over the whole programme. It can be seen that in Figure 5.9 the peak appears to have been missed. The procedure adopted to monitor the performance of the composite that is explained below does not require the peak strain to be captured, and a lower frequency sampling is permitted.

The average value of the stresses, strains, loads and displacements, recorded over a specific number of cycles in a fatigue programme, is zero. Another means to produce an index that can continuously depict the performance of the connection was therefore necessary. Under displacement control the resistive load is proportional to the specimen connection stiffness. But the sinusoidal oscillations of amplitude must still be presented by some means other than an average.

The problem is analogous to one encountered in electrical engineering, where the sinusoidal voltage of a domestic AC supply oscillates between ±320 V. Within the discipline of electrical engineering the route mean square, or RMS, of the voltage is calculated and presented as an index of voltage magnitude. For the current described the RMS is 240 V, the typical domestic AC supply voltage in the UK.

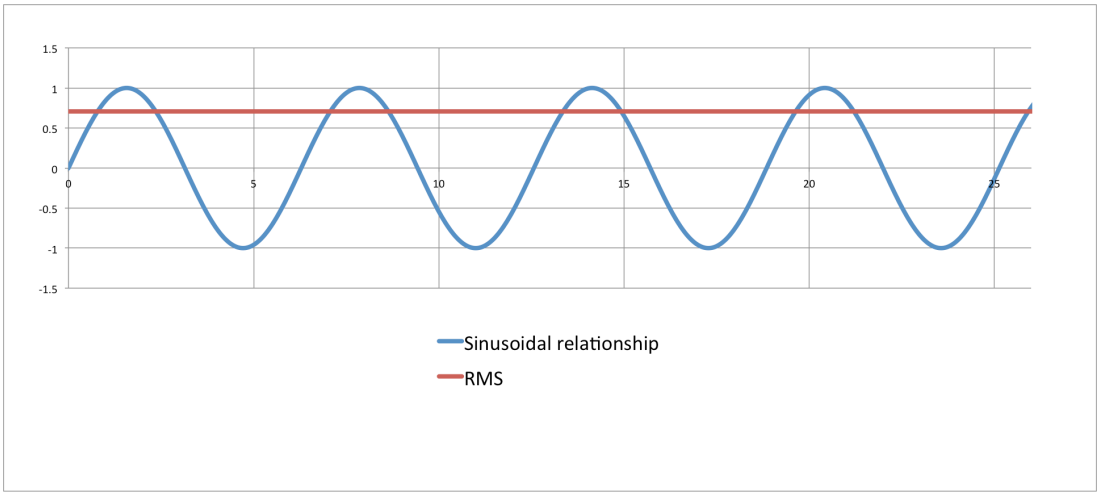

Figure 5.11 Sinusoidal relationship and associated RMS value

Applying the same procedure to the load data collected over a fatigue programme affords a continuous measure of the stiffness of the connection, and therefore, how the specimen response diminishes. A further benefit is that the procedure can reduce the amount of data by 100 times. If the RMS of loads and strains recorded over every 10 cycles (i.e. 100 data points) is assessed, the RMS load, or RMS strain at a certain strain gauge location can be presented as a continuous function of time with 100 times fewer data points. The time step, in this case, increased to 10 seconds. (Figure 5.11 shows an RMS-sinusoidal relationship over 4 seconds.) The RMS strain at each discrete gauge location along the specimen is a measure of how hard the material is working at that location. As explained in section 5.3, the relative position of the gauges relative to the location of crack occurrence, and damage in the specimen, drastically influences the response observed through the RMS strain.

The way RMS load is derived means that the degree to which the peak loads and strains are captured by the sampling is not important. The performance of the composite over the whole range of the imposed cyclic displacement is presented by a continuous index of performance, unlike that presented by data for peak loads and displacements.

Under load control, the RMS of the displacement can be assessed in the same way as the load for the previous case, and it is the inverse of this value that is proportional to the connection stiffness, and serves as an index of specimen performance.

5.2.6 Post fatigue inspection of angle section material by coupon extraction and testing

To observe the effects of the fatigue testing undertaken on the subsequent longitudinal tensile properties of the specimen, coupons were taken from two of the preliminary 'fatigued specimens', and from equivalent specimens of new material, and subjected to monotonic tension tests. Coupons were cut from specimens, aligned longitudinally with the principal fibre direction, as per Figure 5.12. Theoretically, due to the three-dimensional spread of stress in the specimen the value of stress on the upright leg of the angle is not uniform. For this reason coupons are sized such that their width is in the ratio of the length of the un-gripped portion of the flange, and the offset of the

longitudinal central axis of the coupons are in the same ratio, taking into account the thickness of the leg elements.

The coupons are extracted straight sided, as to fabricate waisted coupons would prevent the locations and ratios described above from being observed. As a consequence the ultimate stress of the material is not found (failure occurs in the jaws of the rig at the aluminium tabs), but the modulus is used as a measure to compare tensile performance.

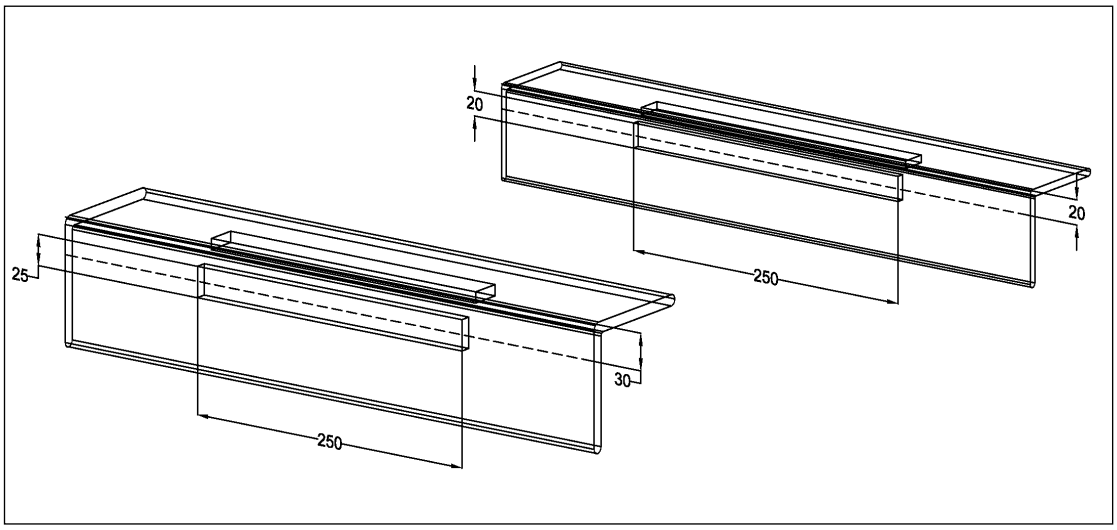

Figure 5.12 Location of coupon extraction post fatigue programme, for large (100 mm angle) and small (75 mm angle) specimen sizes, left to right. All dimensions are in mm.

5.3 Results

5.3.1 Fatigue testing of coupons in tension

To record the fatigue performance of the GFRP material in simple tension, in the secondary fibre direction, the tests described in Subsection 5.2.1 was performed and the results are presented below. It can be seen in Figure 5.13 that performing cycling of a transverse coupon at 75% of the transverse ultimate tensile strength of the coupon, caused failure within a very small number of cycles, namely fewer than 300. Fatigue testing of coupons was undertaken in load control.

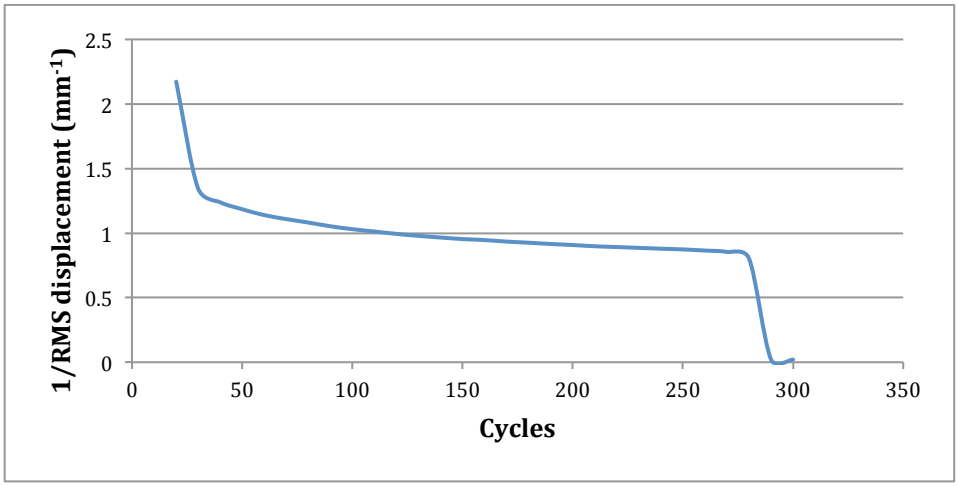

Figure 5.13 Plot for stiffness against cycles for transverse coupon at 75% of transverse material ultimate tensile strength, R = -0.2

The vertical axis in Figure 5.13 is an arbitrary measure of stiffness in the instance of load control. Under cycling to a fixed load, or peak maximum stress, σ_{max}, the RMS displacement increases until failure occurs. The inverse of the RMS displacement is proportional to the stiffness, which has been established by others as proportional to, and a good measure of, damage in the composite (Elmahi et al. 1995; Lemaitre and Desmorat 2005).

Upon inspection of the raw data this specimen was revealed to have gone into a small amount of compression at the low-tension portion of its load cycle, which was intended to have a zero load limit. The effect of the negative R-value (stress ratio) of -0.2, was hypothesised to account for the short life of the specimen. One further transverse coupon was cycled in tension in this way, where a small part of the load cycle was in compression. The plot in Figure 5.14 illustrates the fatigue life of this transverse coupon, which has a σ_{max} of 50% of the ultimate monotonic tensile strength, and an R-value of -0.2.

Material in a façade panels will experience load reversals, and the high sensitivity of the long-term mechanical performance to a negative R-value is noted.

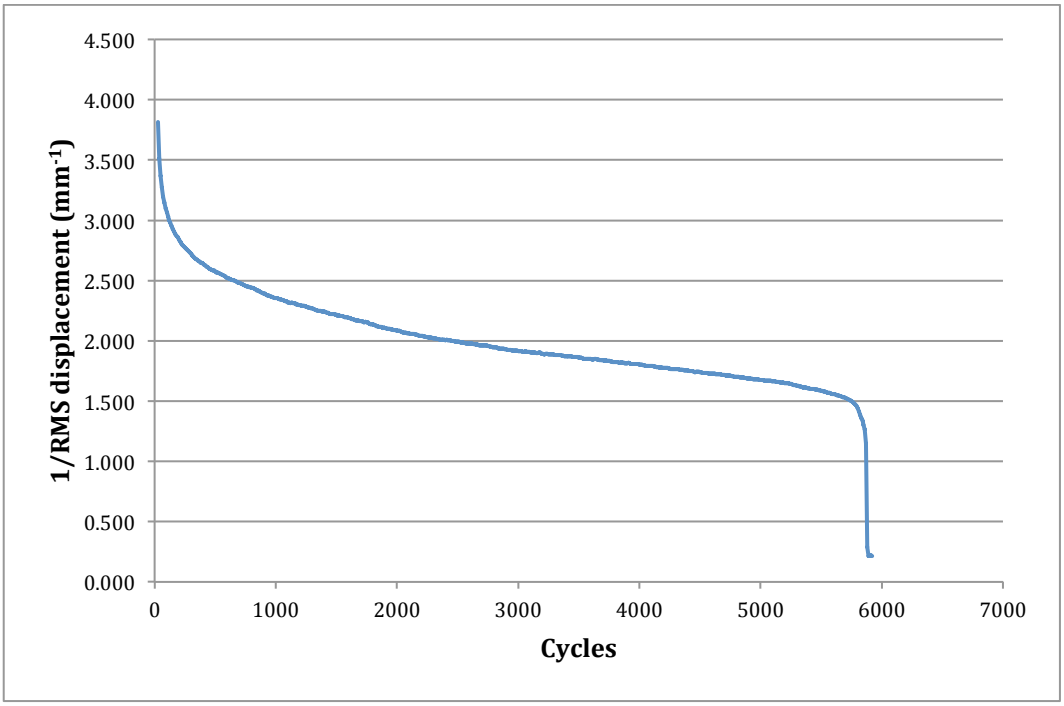

Figure 5.14 Plot for stiffness against cycles for transverse coupon at 50% of transverse material ultimate tensile strength, R = -0.2

It can be seen that approximately 5,900 load control cycles were completed before specimen failure. The stiffness was proportional too, and represented by, the inverse of the RMS displacement in the figure. It reduced initially very rapidly (over the first 500 cycles) before appearing to plateau. Failure occurred suddenly. However the stiffness reduction is seen to accelerate over approximately the last 600 cycles before failure occurred. The specimen retained 40% of its original stiffness at failure.

Coupons of transverse material were subjected to similar tests, where σ_{max} of 25%, 50% and 75% of the ultimate monotonic tensile strength was imposed, but with a stress ratio (R-value) parameter of 0.05 to ensure the coupon remained in some tension at all times. Salvia et al (1997) reported testing where an R-value of 0.1 was adopted to ensure that 'drawback' didn't occur when passing at zero stress level. All coupons lasted the full 100,000 cycles of the imposed fatigue loading. The results for retention of stiffness are shown in Table 5.4.

The findings show that the fatigue performance is very sensitive to the R-value when it becomes negative and a portion of compression is introduced into the load cycle. It is

also evident, from the tests undertaken when R is positive, that for a low σ_{max} of 25% ultimate monotonic tensile strength, stiffness is almost completely retained, however at higher σ_{max} of 50% retention, it drops significantly. Further increase in σ_{max} (to 75% ultimate monotonic tensile strength) is seen to have little effect. I.e. there is no evidence of a linear relationship.

Table 5.4 Stiffness retention of transverse coupons after 100,000 cylces in tension, R = 0.05

σ_{max} (as % of ultimate monotonic tensile strength)	% Stiffness retained
25	95
50	69
75	67

5.3.2 Preliminary angle section specimens

The two specimens subjected to testing under the title of preliminary testing were produced by a different manufacturer than pultrusions for all other subsequent testing undertaken and presented in this thesis. (Only a limited amount of this material was available at the stage of selecting testing parameters and experimenting with data capture and analysis techniques.) The section dimensions were as per Figure 5.5. The smaller 6.4 mm specimen is referred to subsequently as P1, and the larger 9.5mm specimen is referred to as P2. Specimens were both 500 mm in length and the 'gauge offset' and 'gripped portion of flange' are as defined in Subsection 5.2.3. Sampling for specimen P1 was conducted at 25Hz, triggered only in the outer quartile region of the imposed displacement. Duration of the test was 10,000 cycles at 1Hz, whereby the initial critical strain to which the material was subjected was 3,000 με. This entailed imposing a sinusoidal waveform of amplitude ±4 mm on specimen P1, and ±6 mm on specimen P2. (R = -1) These values were determined experimentally by performing an initial linear loading ramp.

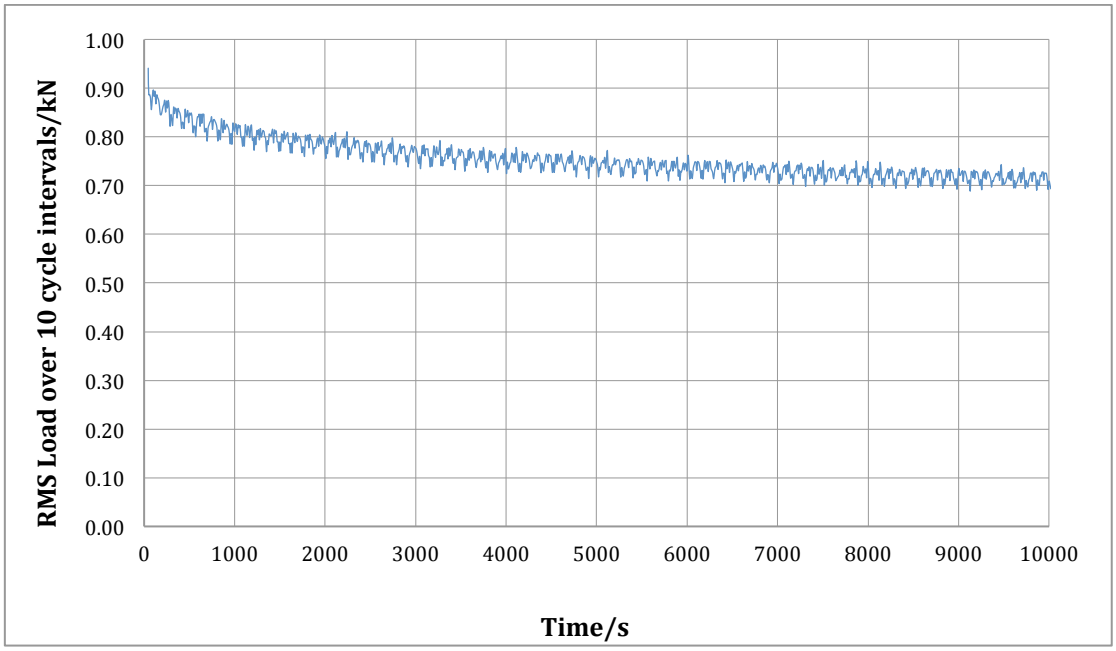

Figure 5.15 RMS load over duration of fatigue test on specimen P1

Figure 5.15 shows how the specimen P1 exhibits a reduction in load becoming more gradual over time. The profiles shown for this smaller sample present no significant evidence that could be associated with an event of abrupt fibre damage. The 'noise' witnessed in both load and strain plots for sample P1 is attributable to a combination of the nature of data logging (25 readings per second, and triggered at stroke extents) and the RMS numerical procedure:

The 10 cycles for which each RMS discrete value is calculated might contain data from an odd half wavelength of displacement. The trigger limits cause sampling to occur at 25 Hz for 0.34 seconds of positive displacement waveform and 0.34 seconds of negative displacement waveform in each cycle. With 25 Hz sampling, the number of 'time-steps' for which data is logged in the positive half of waveform and negative part of waveform is not the same in each complete cycle of results. Nor are the recorded data points at exactly the same phase position in each cycle. Instead the locations of recorded data are changing in a cycle themselves, of having more in the positive part or more in the negative part. Because the sampling is at the extents of displacement and therefore recording outer values of strain and load this effect is magnified. The effect of this can be observed in Figure 5.16, where the RMS strain profile is presented for specimen P1.

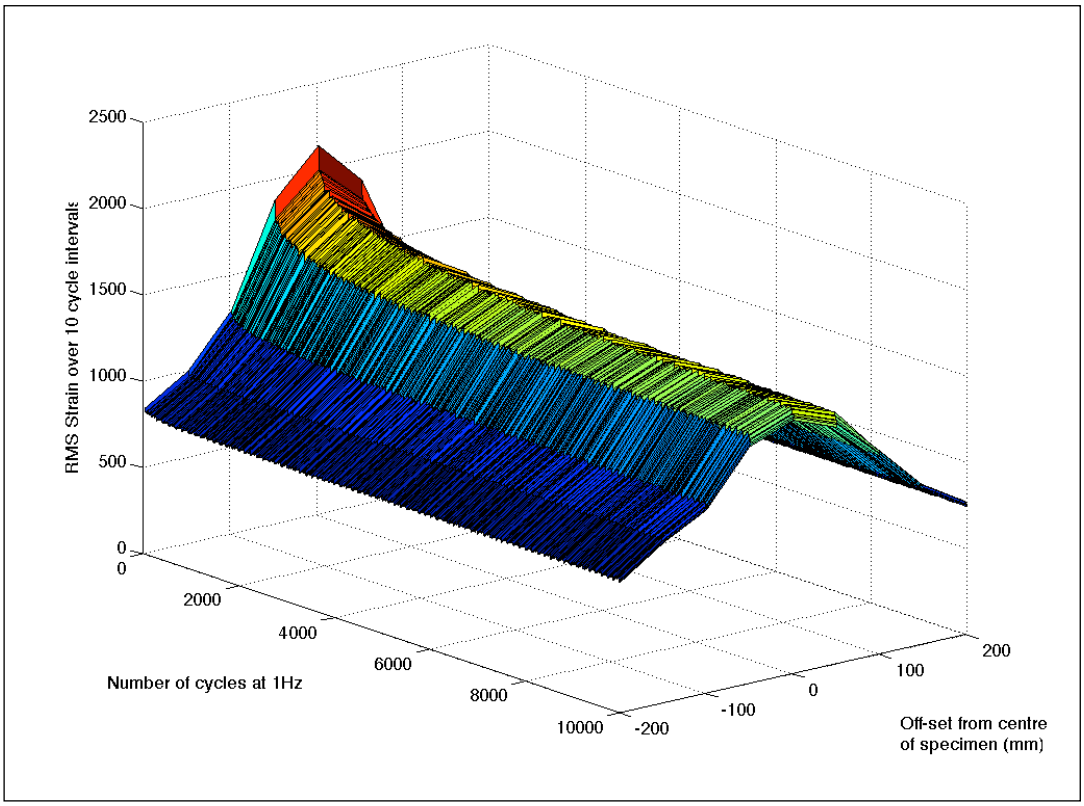

Figure 5.16 RMS strain over duration of fatigue test on specimen P1

The RMS strain is shown to diminish early on, principally within the first 2,000 cycles, as stiffness is lost near the central loaded portion of the specimen. The outer regions are shown to continue bearing as much of the load resistance over 10,000 cycles as at the start of the test, indicating the possible existence of a threshold state of stress, where if not exceeded the material stiffness is well preserved.

In Figure 5.16 the RMS strain at time t = 0 is seen to have a value of approximately 2,200. The maximum strain to which the specimen was subjected was 3,000 με. This difference is partly as a result of the RMS data processing: RMS values are typically about 0.75 of the size of the maximum strain values in a set of cycles. Where a greater difference is evident, such as for specimen P2, initial damage, inflicted in the first few cycles of loading, is responsible for the lower RMS strain when the test commences. See Figure 5.18. A similar phenomenon is observed for RMS load plots, where the RMS load at the time t = 0 appears to be much smaller (more than 0.75x smaller,) than the initial max cyclic loading.

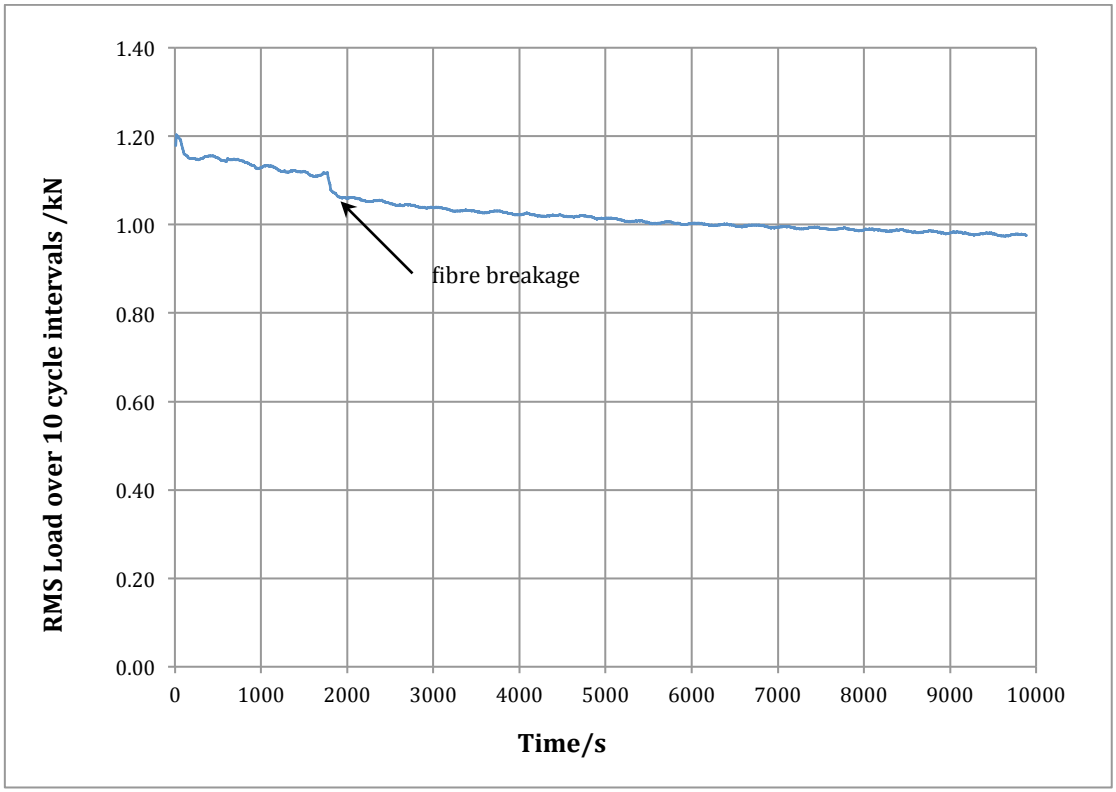

Figure 5.17 RMS load over duration of fatigue test on specimen P2

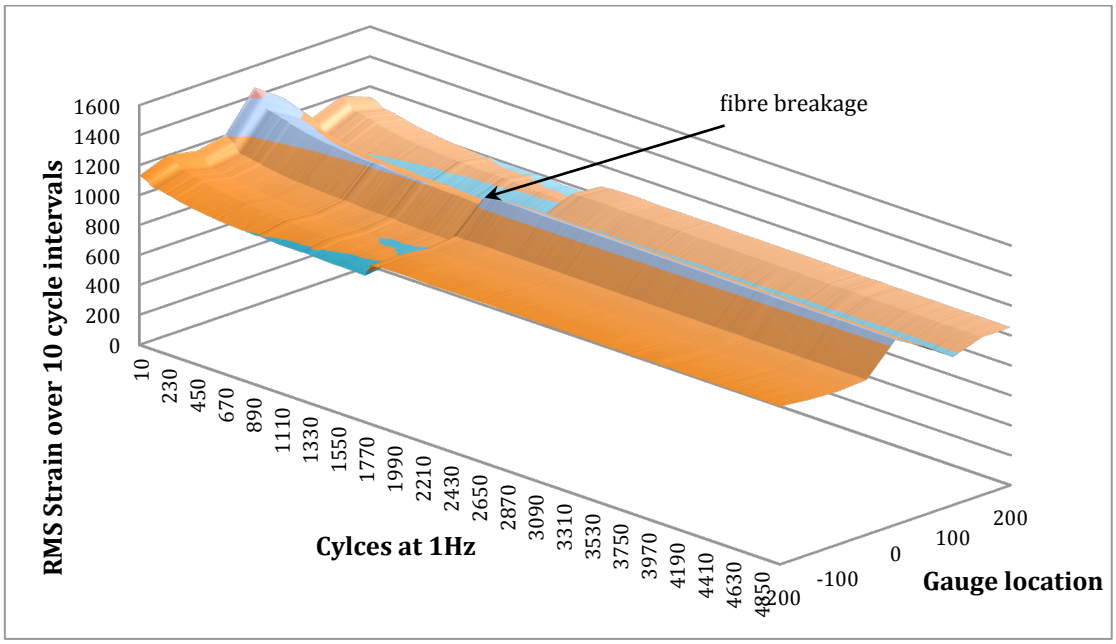

Figure 5.18 RMS strain over duration of fatigue test on specimen P2

Immediately noticeable in Figure 5.17 and Figure 5.18 is how the constant sampling rate of 10 Hz improves the smoothness of the RMS load and strain profiles plotted for P2. It should be noted that the fatigue profile presented in Figure 5.18 is truncated to

only 5,000 cycles. This is to avoid displaying results captured by two of the nine gauges that went awry in the second part of the test. Within this limit however, an event of abrupt fibre damage is witnessed, at around 1,800 cycles of loading.

The strain profile shown in Figure 5.18 points towards a more even distribution of load across the root and back flange of the specimen compared to specimen P1. This is due to the increased stiffness in longitudinal composition of this sample, without the corresponding increase in transverse element or root stiffness.

The sudden reduction in load observed in Figure 5.17, in a stroke control experiment, is evidence of an event of abrupt fibre damage (fibres being the brittle component of the composite). The corresponding increase in RMS strain, right along the specimen length, is perhaps more difficult to understand at first inspection. However a rupture in transverse fibre reinforcement at the inner root location results in a reduction in the compressive strain measured by the gauges on the back flange of the sample, and an increase in the tensile strains occurring at this location. Mathematically, this yields a result of increased RMS strain. Most surprisingly is that the crack, which could be heard as the transverse fibre component ruptured, happened right the way across the length of the specimen. The crack could be seen upon inspection post testing by prying the angle section apart, however it was not visible in photographs.

5.3.3 Post fatigue inspection of preliminary angle sections by coupon extraction and testing

The longitudinal tensile elastic modulus, *E*, from the top flange of both specimens P1 and P2, as marked in Figure 5.12, appears to have been unaffected by the transverse loading (and simultaneous longitudinal flexural loading) during the fatigue test. See Table 5.5. However, the material from the back flange, of both samples, but especially the larger one (specimen P2), seems to have reduced in longitudinal stiffness a small amount over the course of testing. The principal fibres on the ‘back’ flange of the specimen were strained to a smaller extent during the fatigue test, though the resin binding them will have experienced greater stress due to the increased transverse strain at this location (by consequence of the loading arrangement). This mechanism appears to have impinged upon the subsequent tensile performance of the composite in the

principal fibre direction, and suggests that the interfacial (fibre-resin) bond has been compromised to some degree.

Table 5.5 Influence of fatigue testing on the subsequent material primary axis tensile elastic modulus

	E (kN/mm^2)	
	P1	P2
Control	23.0	24.3
Top	23.2	25.1
Back	22.0	21.6

The pultrusion P2, stiffer in its principal direction, will have distributed the point load from the welded steel gripper over a larger region of the angle root. The two preliminary specimens tested, however, do not signal this to improve the fatigue response of the angle in terms of retention in connection stiffness. The fibre reinforcement has been shown to endure damage at the internal root location after only 1,800 cycles of the 10,000 total necessary to validate the element for whole life of service in a building façade. The frequency with which this unexpected fibre failure occurred was to be observed through the remaining tests.

Distributing the transverse strain, by adopting sections with higher longitudinal flange stiffness, appears to be of some detriment to the integrity of interfacial bond (between longitudinal fibres and resin) along a greater proportion of the specimen length at the back flange, compared to the section with thinner flanges. This is possibly evidenced by a reduced primary axis elastic modulus of specimens at this location, in subsequent tensile testing of extracted coupons. The measured reduction in principal longitudinal elastic modulus is very small, only 9%. Owing to the large value of strain adopted for the fatigue testing parameters (3,000 με), this result is considered acceptable and further testing of angle sections to investigate the drop off in connection stiffness exhibited would not include subsequent coupon extraction and tensile testing.

Sampling at 10 Hz, continuously, was deemed to be the preferred means of capturing data from the fatigue programmes. This approach represented the performance of the

composite over the whole profile of the imposed waveform cycle. Alternative means, such as assessing the stiffness in terms of a load displacement plot's gradient, at intervals in time, would not address the specimen response behaviour over all parts of the test.

5.3.4 Angle section specimens: main fatigue testing at 'realistic strains'

The 'realistic strain' loading parameters adopted above consider maximum design stresses and strains to which a polymeric façade could be designed. The largest strains selected are greater than those likely to occur in a façade. Testing at such levels of strain serves an important function in understanding both the initiation, and propagation, of damage in the connection component. Strain levels for the six specimens are presented in Table 5.6 along with specimen dimensions. Results for stiffness retention over the course of each fatigue test are also presented in the table. These values are inferred from the initial and final linear ramps conducted as described in Subsection 5.2.4. These 6 specimens are from a different pultrusion manufacturer to those tested as preliminaries. A fault in the calibration of the load cell during testing of specimens S5 and S6 meant that the results for % stiffness retained were not produced.

Table 5.6 Specimen information for main 'realistic strain' tests

Specimen	Flange thickness (mm)	Flange length (mm)	Specimen Length (mm)	Max strain during cycling (με)	% Stiffness retained
S1	6	75	500	3000	37
S2	6	75	500	2000	38
S3	10	100	500	3000	42
S4	10	100	500	2000	44
S5	10	100	1000	2500	-
S6	6	75	1000	2500	-

Figure 5.19 shows a typical load displacement graph for the final ramp. In contrast to the graph in Figure 5.8 for a typical initial linear ramp, it can be seen that post fatigue test, the connection specimen becomes stiffer at the extents of its imposed displacement. This is more noticeable for the negative displacement in Figure 5.19, which corresponds to the external angle surfaces being in tension, and inner root in compression. The specimen represented by graphs in Figure 5.8 and Figure 5.19 is specimen S6.

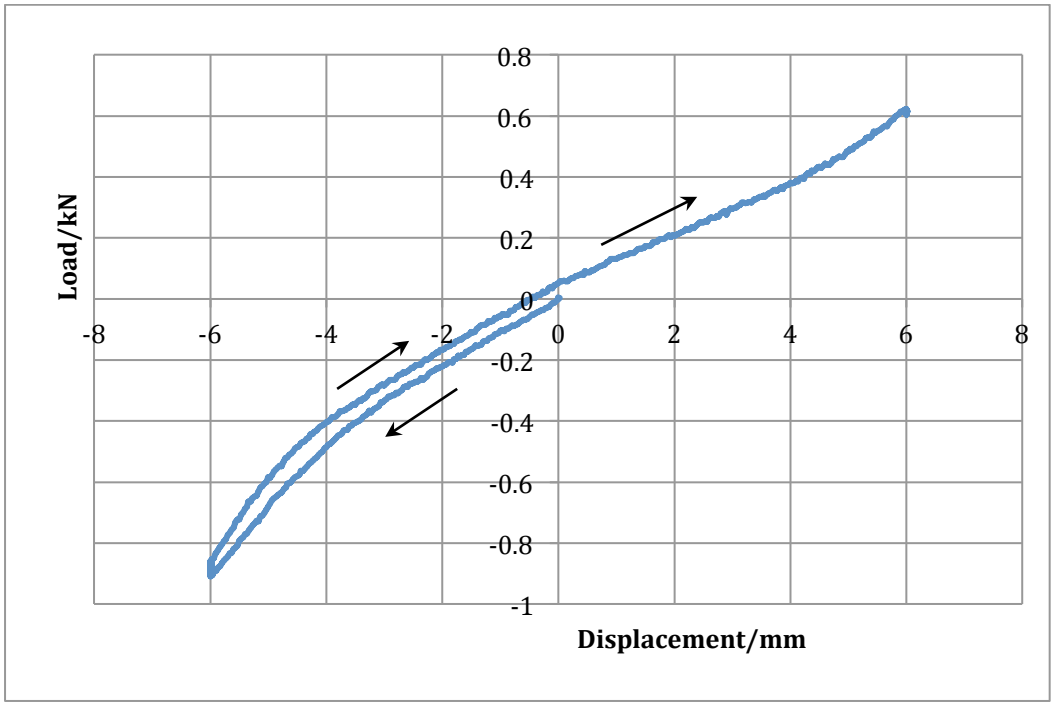

Figure 5.19 Typical response of connection to final linear ramp (specimen S6)

The graphs have implications on the type of damage imparted to the specimen by the fatigue loading. As noted above the specimen is seen to have lost more stiffness near the centre of the range of displacements imposed in cycling, exhibiting a smaller gradient in the load displacement plot near the zero load position. This highlights the importance, and benefit, of using the RMS load drop off to assess the performance of the specimen over the whole range of imposed waveform displacement. The reduction in stiffness, as related to this as an index, is expected to demonstrate better performance than when only the central linear part of the load displacement behaviour of a linear ramp is considered as presented in Table 5.6.

Comparing values in Table 5.6 for % stiffness retained does not reveal any great dependence of this variable (% stiffness retained) denoting performance on the loading parameters (chosen maximum strains) imposed. Specimen S1 and S2, which are identical in section size and length, are shown to exhibit nearly identical decreases in performance over the programme. The same is true for specimens S3 and S4. The graphs for RMS load on specimens S1-S4 are presented in Figure 5.20.

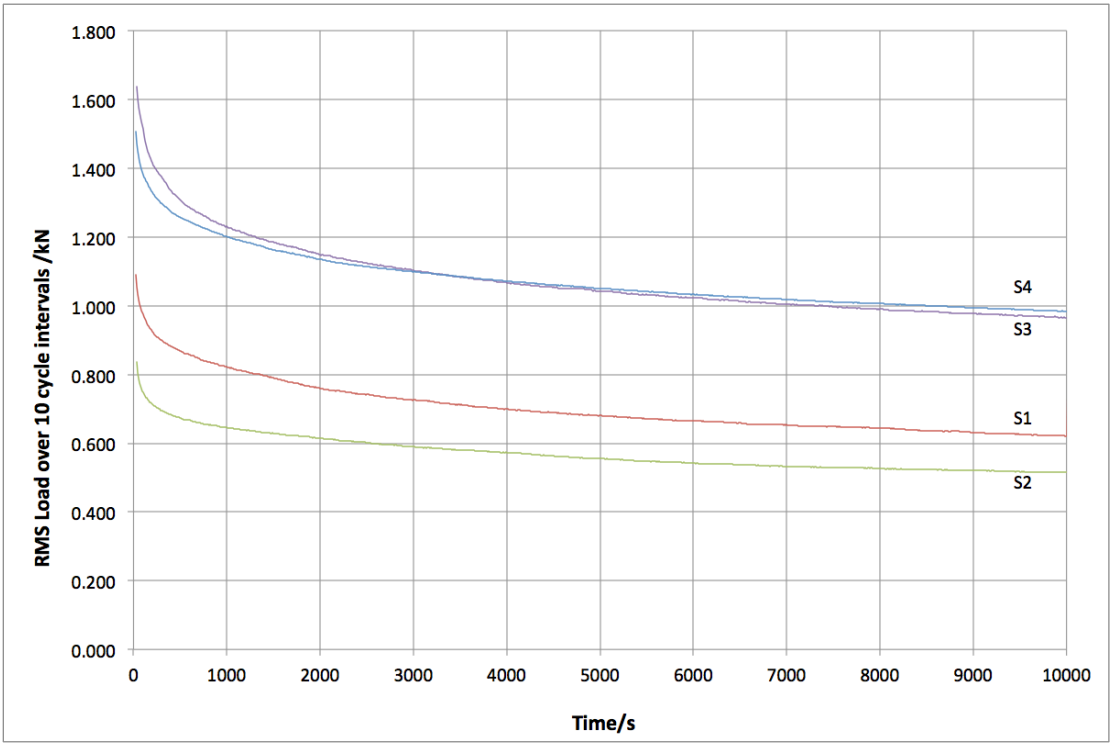

Figure 5.20 RMS load variation over fatigue programme for specimens S1-S4

The plots in Figure 5.20 appear to show specimens to retain approximately 60% of their initial stiffness, however it is known from the initial and final linear ramps conducted that closer to 40% was attained. The plots in Figure 5.20 show a rapid decline in stiffness as cycling is commenced. By the time 10 cycles have passed, and the first data point is established, the stiffness has already dropped by a considerable amount. It is this initial decrease that explains how the stiffness retention in Figure 5.20 appears to be greater than that found by the linear ramps before and after fatigue testing.

It can be seen in Figure 5.20 that the two specimens of smaller section size, S1 and S2, appear to reduce in stiffness a similar amount and follow a similar pattern of decay,

despite the maximum state of stress and strain being initially much higher for S1 (3,000 με for S1, as opposed to 2,000 με for S2)

The larger specimens, S3 and S4, behave quite differently. For these larger section size specimens, which provide a greater resistive load to the imposed displacements, specimen S3 which was subject to a higher displacement and critical strain (of 3,000 με) decays more rapidly than specimen S4, and in fact also ends up offering less resistance to the driving displacements than S4 does after 10,000 cycles. The case for the larger section specimens is perhaps more what was expected as the programme of larger displacements imposed by the waveform is of greater detriment to the conservation of stiffness.

Specimens S3 and S4 appear to commence at a close state of RMS load. This could be evidence of initial damage having been caused by the monotonic loading (conducted at 1 mm/min, to the same max strain and displacement as that observed in cycling) before the fatigue programme commenced. The load displacement graph for the initial linear ramp, for specimen S3, is shown in Figure 5.21. The sudden drop in load present at the extent of the positive displacement ramp is indeed associated with fibre breakage in the specimen. Plots describing the initial linear ramps for specimens S1-S4 all show this to some degree, though it is more pronounced on S1 and S3, where larger critical strains were imposed.

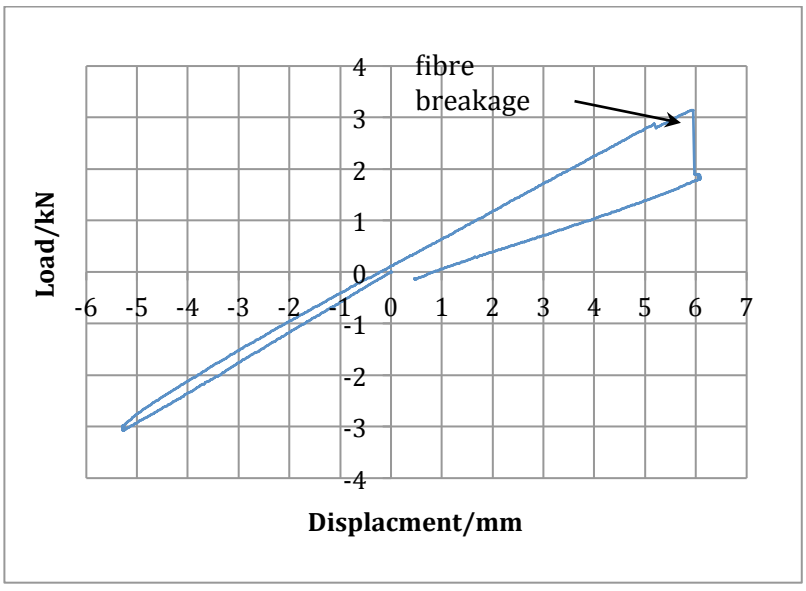

Figure 5.21 Load displacement plot for initial linear ramp of specimen S3

In contrast to the fatigue behaviour observed for specimen P1, none of the specimens S1-S4, originating from pultrusions fabricated by a different manufacturer, exhibited events of fibre failure part way through the fatigue programme. i.e. All series plotted in Figure 5.20 portrays a smooth curve indicative of a gradual decline in stiffness with progression of damage occurring at a steady rate. The continuous nature of this decay is exploited in chapter 6, where the behaviour is modelled numerically.

The graph for RMS strain presented in the following figure offers further insight into how damage propagates in a specimen. It can be appreciated in Figure 5.22 that specimen S1 endured damage during the initial linear ramp, which has resulted in a reduced RMS Strain value at the central portion of the specimen from the very first cycle.

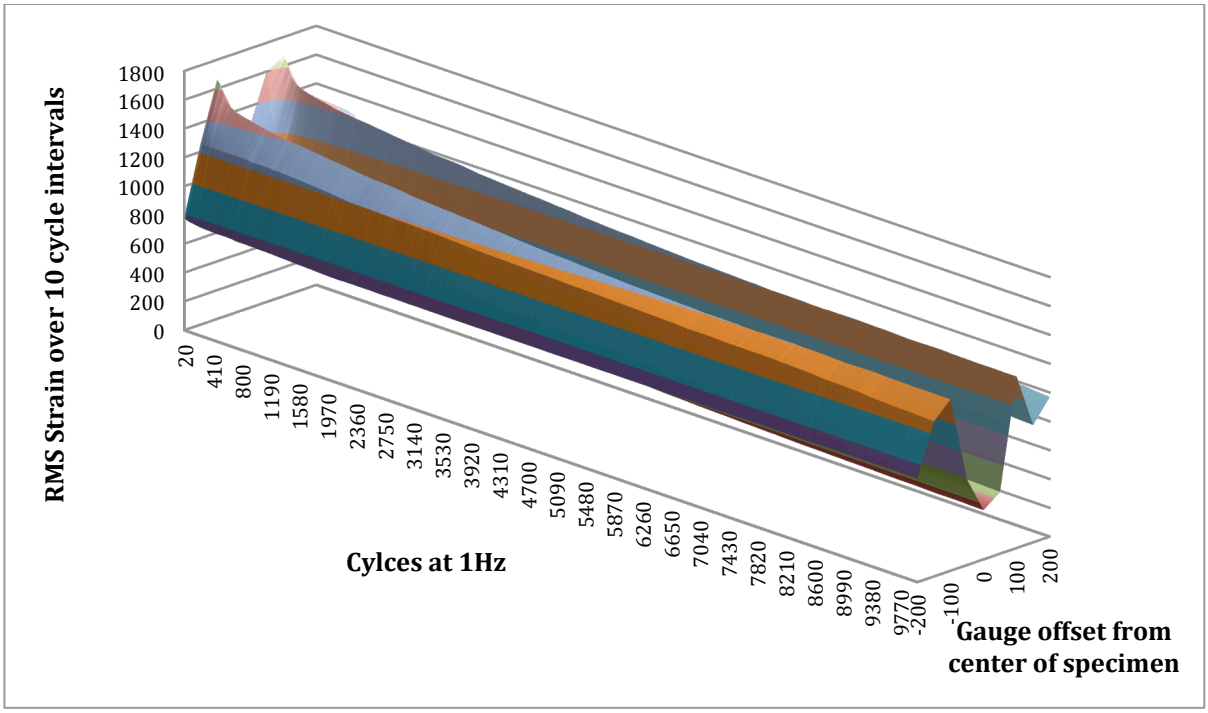

Figure 5.22 RMS Strain profile over fatigue programme for specimen S1

Compared to the RMS strain profiles observed for specimens P1 and P2, S1 in Figure 5.22 demonstrates how fibre breakage at the outer root location is represented. S1 was inspected after the test. A crack across approximately the middle third of the specimen

at the outer root location was found, as shown in Figure 5.23. Due to the relative position of this crack to the strain gauges (i.e. both located on the outer surface of the angle section) the RMS strain is reduced where the composite is not 'working as hard', i.e. where it is not resisting as much of the stress in the region of the crack. The 'trough' profile presented gets deeper, but not wider over the duration of the fatigue programme. This indicates that the cracked zone becomes weaker (or the crack gets deeper) where initiated, but does not spread any wider. This is an important finding; the behaviour is markedly different depending on fibre architecture, as this was not observed in the testing of specimens P1 and P2.

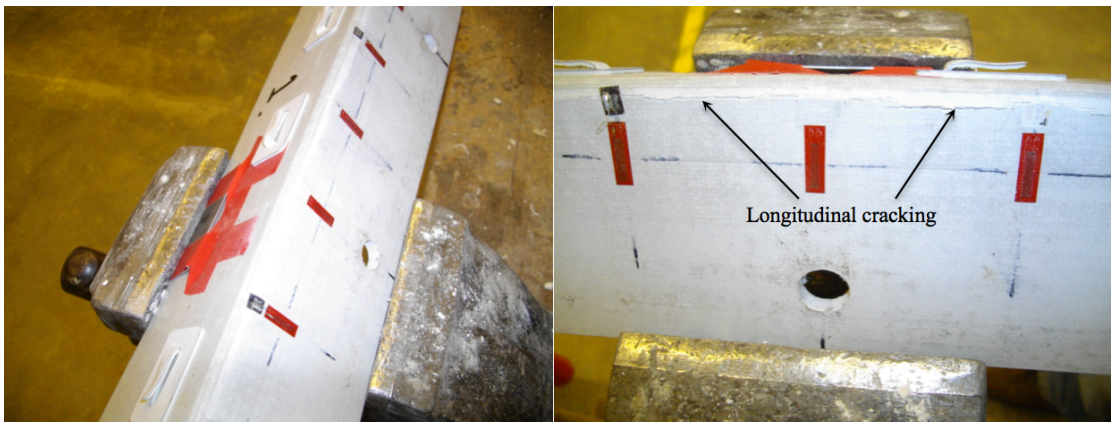

Figure 5.23 Crack on specimen S1; opened for photos using bench vice

RMS strain plots for S2-S4 exhibit the same behaviour, confirming that damage was inflicted upon each of the specimens by the initial linear ramp. Most of these plots are affected by the loss of accuracy in one or more strain gauges on the specimen (see Figure 5.24). Owing to the extent of initial damage inflicted on the specimens S1-S4, the RMS load plots in Figure 5.20 have not been used to infer percentage reductions in performance. Although a value derived from these plots would be more representative of the material performance than those in Table 5.6, for the reasons described above in this section (they would represent response to whole waveform), the influence of the initial damage is unknown and prevents accurate initial RMS strain values from being derived.

Fatigue testing undertaken at 'realistic loads' (which operate over much smaller imposed critical strains) imposed no initial damage and supplements findings from S1-S4 and P1 and P2 well. The RMS load graphs are used to examine the experimental

behaviour observed through specimens S1-S4 in greater detail in chapter 6.

Specimen S5, the set up for which is shown in Figure 5.7, was one of two specimens 1000 mm in length, tested to examine the influence of extra length in the specimen either side of the loading point. The RMS strain profile for S5 is shown in Figure 5.24, where it can be seen that problems were encountered with strain gauges, fatiguing themselves, and becoming inaccurate over the lifetime of the test. Specimen S6 tested much later on in the testing campaign timetable, suffered to a greater extent and the gauge inferred RMS strain profile for S6 is not usable. Specimen S5 provided important information relating to the response of long sections, specifically the span over which the connection loading is spread.

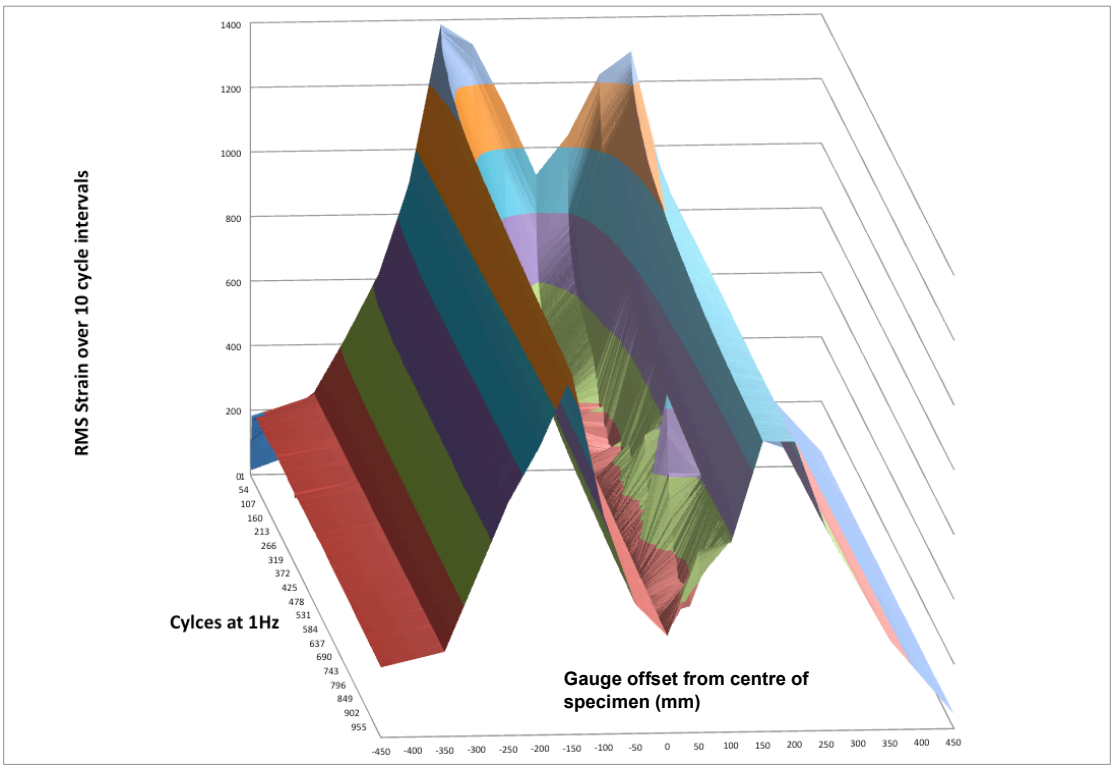

Figure 5.24 RMS strain profile over fatigue programme for specimen S5

Figure 5.24 shows that specimen S5 exhibited the same initial damage and subsequent degradation behaviour of the form previously observed for S1-S4. It can also be appreciated how the full length of the specimen is working to resist the load. This is the most important finding from the 1000 mm length specimen tests, with implications on how cumulative action from adjacent connections could manifest itself. At the state of maximum strain imposed in the cyclic loading of S5, of 2,500 με, the influence of the

imposed displacements was still just felt at the extents of a 1000 mm span.
Both longer specimens, S5 and S6, of 1000 mm length, were tested according to a max state of critical strain of 2,500 με. Unfortunately, due to a processing error in the load calibration of the test rig the data for RMS load cannot be compared against the fatigue profiles generated for specimens S1-S4.

Further testing involving more intricate plotting of RMS stress across connection specimens had to be abandoned due to poor confidence in the accuracy of the strain gauge measurements over an entire fatigue programme. Figure 5.25 shows the nature of this endeavour, and the concept will form part of the proposed further work following completion of this research project.

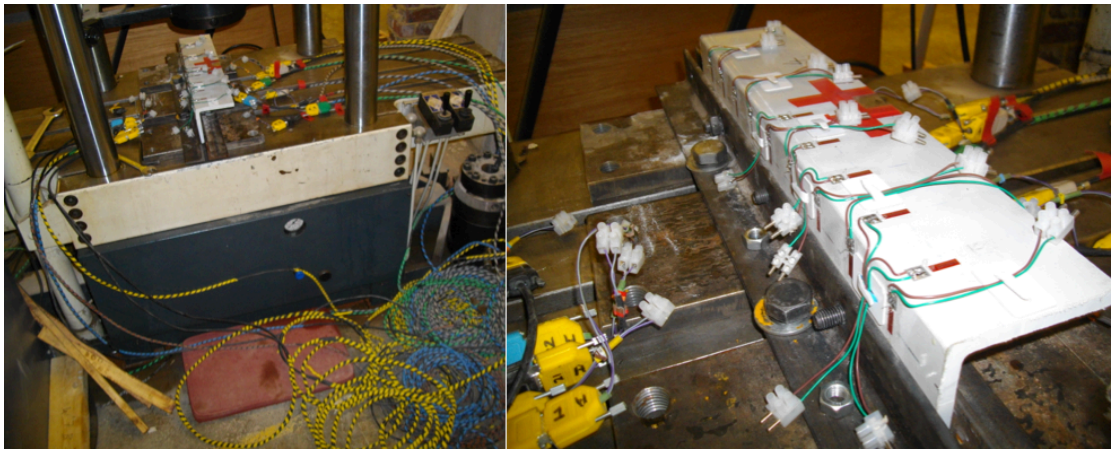

Figure 5.25 Conducting tests with more intricate use of strain gauges to plot RMS strain across greater extent of specimen was abandoned

5.3.5 Angle section specimens: fatigue testing at 'realistic loads'

Specimens S7 and S8 had identical dimensions: 75 mm leg length, 6 mm element thickness, and both 500 mm in length. Each specimen possessed a single strain gauge at the mid span (the critical location for maximum transverse strain). Specimens S7 and S8 were cycled under displacement control at 1 Hz, where the imposed waveform induced an initial maximum and minimum of + or – 0.5kN load reaction, and the maximum transverse strain was 1,100 με.

Figure 5.26 and Figure 5.27 show plots for the initial and final (after 100,000 cycle

fatigue programme of loading) linear ramps respectively, on specimen S7. It can be seen from the figures that an initial displacement of approximately 2 mm induced a connection load of 0.5 kN. The corresponding maximum transverse strain at the extent of displacement was 1,100 με.

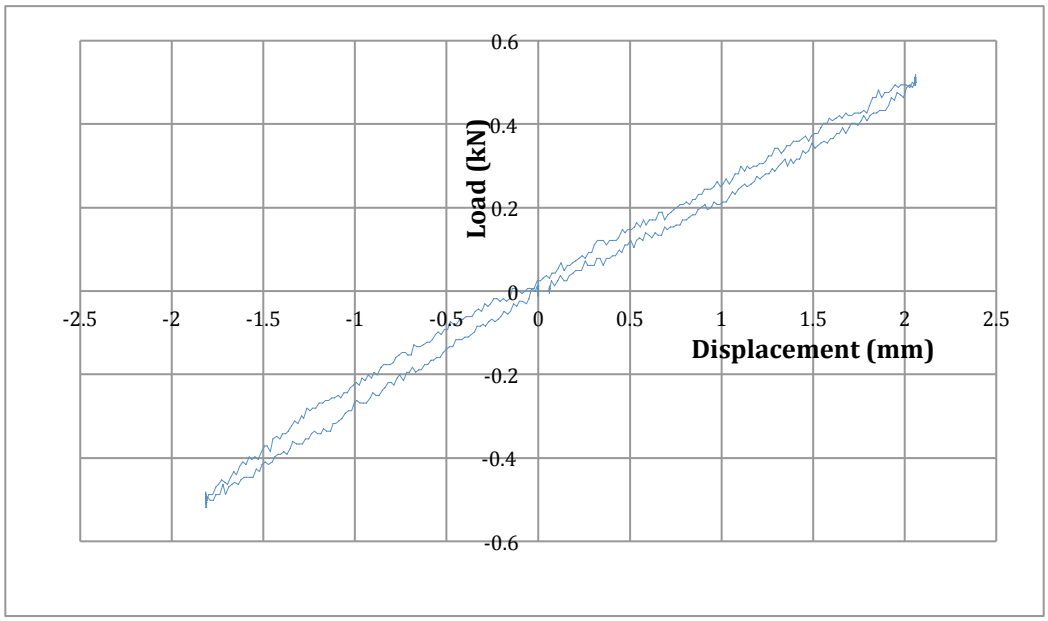

Figure 5.26 Load-displacement plot for initial linear ramp on specimen S7

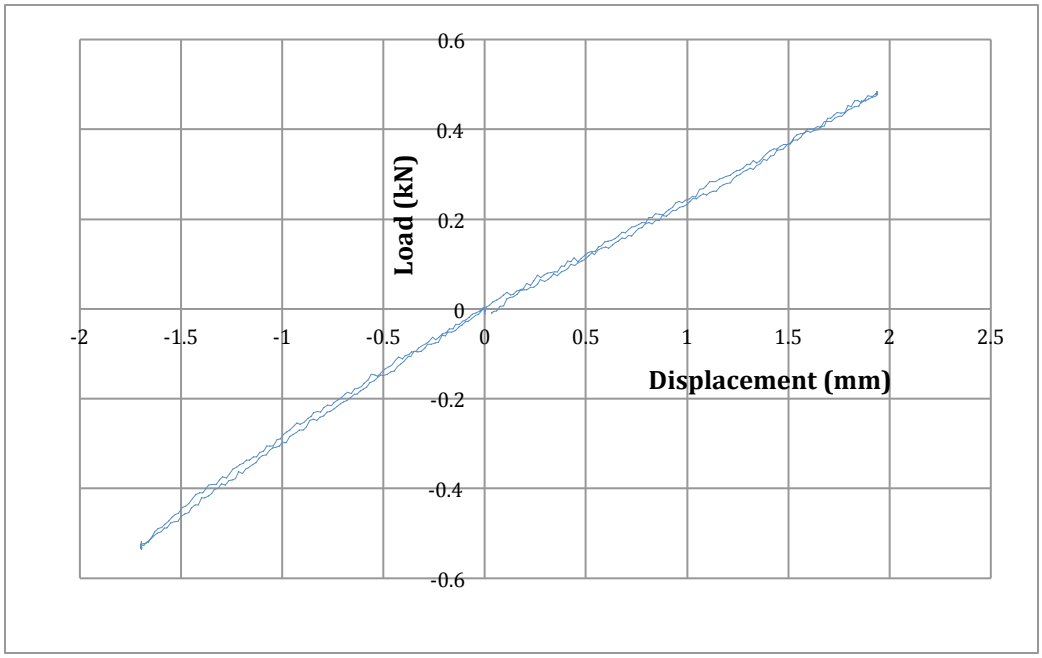

Figure 5.27 Load-displacement plot for final linear ramp on specimen S7

The connection stiffness of S7, as determined from these data, was completely retained. Values calculated as averages of stiffness in both positive and negative positions of displacement were identical before and after the cycling of the fatigue programme. Specimen S8 exhibited retention of connection stiffness of 96% over the same programme of loading. The results are summarized in Table 5.7.

It can be seen that the hysteresis evident in Figure 5.26 is not evident in Figure 5.27 after cycling. Viscoelastic response to cyclic stresses can yield this effect. Others have documented this phenomenon, though usually a small decrease in stiffness is observed (Harris 2003). A 100,000 cycle, low strain (1,100 με) fatigue programme, however, has retained full specimen stiffness.

Table 5.7 Stiffness retention of 'connection' for 'realistic load' testing as per initial and final linear ramps

Specimen	Initial maximum transverse strain imparted by the +/- 0.5kN alternating load	% Stiffness retained
S7	1,100 με	100
S8	1,100 με	96

**Note: these tests were conducted under displacement control, though as stiffness was retained, or very nearly retained, the load associated with later cycles remained very close to 0.5 kN.*

5.4 Conclusions

It has been demonstrated how some pultrusions, when subjected to fatigue cycles of maximum transverse strain of 3,000 με exhibit sudden abrupt fibre breakages which propagate along the length of the connection specimen almost in an instant. Some pultrusions however have shown markedly different behaviour, whereby initial damage inflicted to the specimen becomes more severe at the critical damaged location (damage becomes more pronounced, or cracks become deeper) but does not propagate along the

element. This suggests the existence of an important design threshold in this material. The work undertaken in this chapter can confirm this to be greater than 1,100 με but less than 2,000 με, in terms of critical transverse strain, for the fibre architecture of the pultrusions tested.

At a maximum peak transverse strain of 1,100 με full connection specimen stiffness was retained after a 100,000 cycle fatigue programme. Specimens tested to fatigue loading parameters of high stress and strain (S1-S4), have demonstrated how the stiffness, or performance, of a connection component diminishes over 10,000 cycles.

Assessing the loss of stiffness of specimens tested to fatigue loading parameters of high stress and strain (S1-S4) using initial and final linear ramps, has not revealed a great dependence on the state of initial maximum critical transverse strain in the specimen, either 2,000 με or 3,000 με, for the specimens of identical section size and length.

RMS load has served as a useful index of performance of the connection specimens, representing stiffness over the whole range of displacements from the imposed waveform. The continuous nature of the plot as a function against time has permitted further analysis techniques which enables a best fit curve to be applied to measure decay behaviour. RMS load profiles have indicated that specimens of smaller section size (S1 and S2) appear to reduce in stiffness by a similar amount and follow a similar pattern of decay, regardless of the state of initial maximum stress and strain. The larger specimens (S3 and S4) appear to be more sensitive to the state of initial maximum stress and strain; the specimen that was subject to a higher initial value of transverse strain (S3) ended up offering less resistance to the driving displacements than the one subjected to lower transverse strain (S4) did after 10,000 cycles. This case was expected; that a programme of larger displacements imposed by the waveform is of greater detriment to the conservation of stiffness.

Reduction in stiffness will always be an upper bound solution (i.e. most critical of the performance) for displacement control tests. Any ‘bedding in’, or induced slack in the test rig system set-up, will always result in smaller loads and strains recorded, and therefore a reduced inferred resulting stiffness. Such slack could occur, for instance, at

the custom welded gripper through a small amount of local damage to the steel plates. The plates mitigate this type of damage to the composite material concealed, but might deform slightly themselves over a full testing programme. The bolting arrangement through which the specimen is secured to the rails and base of the test rig was designed and built to mitigate this as far as possible. However in reality fixings can only loosen, not tighten, so again, the solution for reduction in stiffness is an upper bound one.

At the state of maximum strain imposed in the cyclic loading of S5, of 2500 με, the influence of the imposed displacements was still just felt at the extents of a 1000 mm span. This behavior must be borne in mind when considering cumulative action of adjacent connection on a façade panel. The RMS strain profiles produced have revealed the nature of damage propagation. Specimens that suffered an initial amount of damage deteriorated further by cracks (which perpendicularly bisected the direction of transverse strain) becoming deeper, but not spreading wider.

It has been highlighted that in order to accurately measure the fatigue performance of one material, a material with far greater resistance to fatigue must be used. The longevity of the strain gauges employed in this testing has exacted a limitation on the study, reducing the scope of tracking stress profiles in the specimens experimentally.

The R-value (stress ratio parameter) for fatigue cycling of tension coupons was shown to have a significant effect on the specimen performance. Results for cycles to failure, and results for stiffness loss over 10,000 cycles, are shown to be highly sensitive to even a small amount of compressive stress within the imposed waveform. There is a shortage of literature concerning studies addressing the fatigue performance of pultruded GFRP, where negative R-values are adopted for testing. Even those that go as far as examining performance of the material in flexure do not investigate the influence of negative R-values. Further work in this area will be necessary to successfully correlate material performance at coupon level to connection/element level. Coupons of material in the weaker transverse orientation, subjected to fatigue in tension where R = -0.2, reduced in stiffness by up to 60% before failure occurred, through cycling under load control at 50% of ultimate monotonic tensile strength. Other coupons cycled in tension with positive R-values reduced in stiffness by a maximum of 31%, even at σ_{max} of 75% ultimate monotonic tensile strength.

The methodology presented for the testing of angle sections is suitable for a longer duration testing campaign to validate a pultruded connection design.

5.5 Summary

The implications of these experimental findings are explored in detail in Chapter 6. They are presented together with the development of an informative design tool and design guidance developed from the testing campaign. The guidance offered is drawn from the phenomenon observed above and the characteristics notable for design purposes.

It has been demonstrated how testing can capture data, and chosen analytical means can portray the behaviour of the material. It has also been revealed where testing methods and parameters adopted are not sufficient to support a hypothesis on material behaviour and recommendations for further work have been made accordingly.

6 Fatigue behaviour of angle connections in UD-GFRP

The previous chapter demonstrated how an index of the performance of a composite connection in fatigue loading can be obtained. This chapter places these experimental findings in a theoretical context. The continuous nature of the performance index derived, and manner in which it represents the whole portion of the fatigue cycle, is exploited to enable the influence of maximum cyclic stress level to be evaluated.

6.1 Response of pultruded angles to fatigue loading of connections

The 3D specimen response is associated with an earlier onset of damage compared to the 2D plane stress response found from testing reported in Appendix A, at as low as 2000 με critical transverse strain. The 2D plane stress behaviour of the two specimens tested exhibited a linear elastic response until failure when transverse strains of 6060 με and 4290 με for each specimen were achieved. These findings are in line with the findings of El-Assal and Khashaba (2007) who assessed the fatigue performance of pultruded rods under torsional loading as well as bending. It was found that torsional fatigue programmes resulted in a strength half that compared to specimens subjected to pure bending. The torsion emanating in each longitudinal direction from a discrete connection point initiates damage at a lower transverse stress state than plane flexure. Torsion is verified to be of detriment to the interfacial bond of pultruded composites under quasi-static load cases and in dynamic/fatigue loading.

Fatigue cycles for loading of angles in a 2D plane stress state was not conducted, but the material would only experience an R-value of 0 in this case if utilising the rig described in Subsection 5.2.3. Comparison with fatigue performance of elements subjected to the 3D stress state (of the hypothetical connections) would therefore not be possible; the negative R-values (R= -1) adopted for this testing has had significant implications on the fatigue behaviour exhibited. Investigating fatigue of angles in pure flexure (pure 2D plane stress) without the associated torsion of the connection set-up, and where R=-1, would form beneficial further work. It has been observed that a reduction in stiffness of 60% under fatigue in the complex stress state (with torsion) can occur without sign of failure. Further work could test the hypothesis formed on the basis of monotonic testing results, and the work of El-Assal and Khashaba (2007), that

a threshold of damage initiation, exists at a higher state of associated critical transverse strain when torsion is not present.

The plot in Figure 5.14 shows how damage accumulates (by diminishing stiffness) with number of load cycles. It can be seen that the relationship is non-linear. The larger initial rate of damage accumulation decreases before plateauing, and then increases sharply before failure. For the loading parameters used in the test represented, the stress ratio R was -0.2. In Subsection 2.6.2 on damage accumulation, the Palmgren-Miner linear damage rule was presented: $\Delta = n/N_f$. Where Δ represents the fraction of catastrophic damage sustained after n cycles (where $n < N_f$) so that at failure $n = N_f$ and $\Delta = 1$ (Harris 2003). It has been established that this rule does not hold true for cyclic loading of negative R-values (stress ratios). It is therefore revealed that Miner's rule, illustrated by Equation 2.37, cannot be applied in instances where the stress ratio is negative. (Where the load cycle contains both compressive and tensile stress portions.)

It has been reported previously that Miner's rule is said to hold true for 'all tension' cycling and not for blocks containing differing stress ratios (e.g. tension, tension, compression, tension, or TTCT). In addition to this it has been demonstrated that it is not suitable where the R-value is negative, (such as in the fatigue testing of hypothetical connections,) because the Palmgren-Miner linear damage rule is not obeyed.

The number of coupons tested under fatigue in repeated tension in this study has not permitted verification of the type of relationship discovered by Salvia et al (1997), who established a linear relationship between applied strain and log of the number of cycles to a reduced stiffness, as shown in Figure 2.31. What has been evidenced for the pultruded material investigated, is fatigue performance that is not linear with maximum imposed load, but appears to exhibit behaviour dependent on where the maximum load falls related to discrete threshold values.

Coupons of transverse material that lasted the full 100,000 cycles of imposed fatigue loading reduced in stiffness by 5% when cycled at σ_{max} of 25% ultimate monotonic tensile strength, by 31% when cycled at σ_{max} of 50% ultimate monotonic tensile strength, and by 33% when cycled at σ_{max} of 75% ultimate monotonic tensile strength.

Further testing would be necessary to reveal the precise value ranges in σ_{max} for which damage susceptibility rapidly increases, but it appears that cycling at 50 or 75% of σ_{max} does not impart a significant difference in fatigue performance.

The state of stress and strain experienced by regions either side of a discrete mechanical connection is of importance regarding connection spacing. In the following Sections 6.2 and 6.3 the distribution of imposed load and acceptable limits are considered.

6.2 Distribution in the specimen's response to cyclic load

The distribution, or spread, of the load imposed upon the pultuded section, causes transverse strains in the secondary fibre direction that are a maximum at the location of discrete connection. The transverse RMS strain for specimen S5 is seen in Figure 5.24 to decrease to a value close to zero over the 500 mm length of section each side. Because this section experienced damage, and a stress sufficient to cause damage was induced over a large central portion of the specimen length, it is a suitable specimen subject to observe the diminishing nature of transverse stress. Modelling how the transverse stress diminishes according to this specimen will provide a safe design guideline for connection spacing to ensure a maximum permissible transverse strain is not exceeded in a polymeric façade connection of this type.

Specimen S5 was subjected to an initial maximum strain of 2,500 με. The rate at which the transverse stress diminishes is dictated by the relative longitudinal and transverse material elastic moduli, E_{long} and E_{trans}. These were found to be 33.6 and 11.1 GPa respectively, through testing of pultruded flat-sheet GFRP composite material from the same manufacturer as the angle section specimens S1-S6. It is understood that a higher longitudinal stiffness will increase the extent of the panel edge over which transverse strain acts, and a higher transverse stiffness will reduce the span over which the load acts. Equation 6.1 proposes a simple relationship that observes these trends, and is in-keeping with the experimental observation of S5. The equation describes the magnitude of transverse strain, ε_{trans}, in microstrain, at a distance, s, in millimetres, from the discrete connection point, where transverse strain at the connection is due only to that single connection, and of value ε_{conn}, in microstrain.

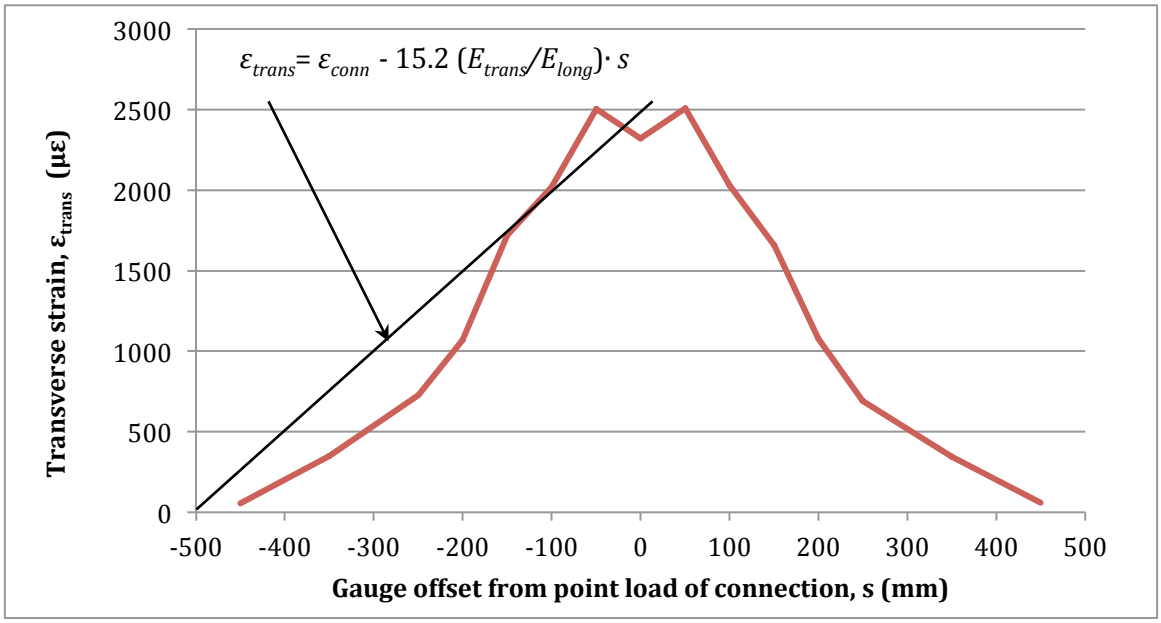

Figure 6.1 Varation in transverse strain as a function of distance from connection load, shown for specimen S5 during greatest displacement of initial linear load ramp

$$\varepsilon_{trans} = \varepsilon_{conn} - 15.2\left(\frac{E_{trans}}{E_{long}}\right) \cdot s \tag{6.1}$$

The minimum connection spacing permissible, c_{limit} , such that ε_{trans} does not exceed ε_{conn} at any point along the connected panel edge is shown by Equation 6.2.

$$c_{limit} = \frac{\varepsilon_{conn}}{15.2}\left(\frac{E_{long}}{E_{trans}}\right) \tag{6.2}$$

It is entirely possible that a connection spacing, c, of lower value than c_{limit}, may be selected. In which case the maximum transverse strain yielded, $\varepsilon_{max\ trans}$, may be calculated according to Equation 6.3. This considers the influence of adjacent connections by algebraic addition.

(6.3)

$$\varepsilon_{\max trans} = 3\varepsilon_{conn} - 15.2\left(\frac{E_{trans}}{E_{long}}\right)\cdot 2c$$

If c is smaller than $c_{lim}/2$ then $\varepsilon_{max\ trans}$ is calculated according to Equation 6.4

$$\varepsilon_{\max trans} = 5\varepsilon_{conn} - 15.2\left(\frac{E_{trans}}{E_{long}}\right)\cdot 6c \tag{6.4}$$

In summary:

if $c > c_{limit}$, $\varepsilon_{max\ trans} = \varepsilon_{conn}$

if $c_{limit}/2 < c < c_{limit}$, $\varepsilon_{max\ trans}$ is found from Equation 6.3

if $c_{limit}/3 < c < c_{limit}/2$, $\varepsilon_{max\ trans}$ is found from Equation 6.4

It should be noted that whilst these relationships are useful in ensuring that the transverse strain at connections does not exceed a desired maximum for given material properties, the strain attributed to a single discrete connection on a panel edge, ε_{conn}, must be established for the connection geometry in question. For the testing of specimens S1-S6, this can be inferred from the maximum cyclic load according to Equation 6.5.

$$\varepsilon_{conn} = 9.3\times10^{3}\left(\frac{Pl}{E_{trans}\cdot t^{2}}\right) \tag{6.5}$$

Where P is the peak load in kN, l is the offset in millimetres of the point gripper (hypothetical connection point) from the apex of the angled return and t is the section thickness in millimetres.

The load on connections will depend on the connection spacing itself. It is here that the inescapable, iterative nature of design is apparent. The equations in Section 6.2 provide a useful design starting point for a connection of the type investigated, however a safe maximum design transverse strain must be established for the composite material concerned. The value of maximum design strain chosen must consider the fatigue

performance of the section. A guideline on performing this appraisal of the pultruded GFRP composite material is outlined in Section 6.3.

6.3 Design limit for transverse strain at pultruded panel edge returns

Figure 6.2 illustrates curve fitting of plots presenting the accumulation of damage in specimens S1-S4 using a power law relationship basis. The accumulation of damage is represented by the RMS load, which is proportional to the connection stiffness. Figure 6.3 shows the same type of curve fitting procedure for specimens S1-S4, although in this plot a log law relationship is adopted as a basis for modelling the decay in connection/element stiffness.

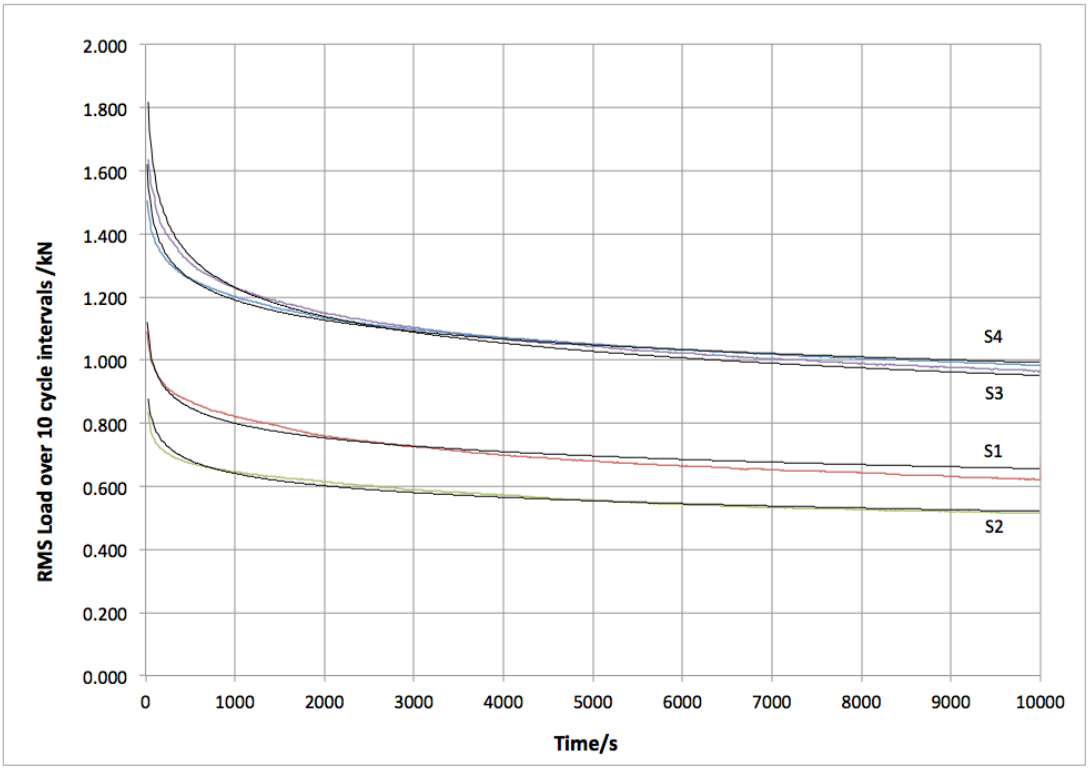

Figure 6.2 Curve fitting (in black) of RMS load profiles for S1-S4 using a power relationship

In these figures it can be observed qualitatively that a log law based relationship can more accurately model the stiffness decay profiles yielded from experiment. Statistical analysis (by method of least squares) for suitability of the best-fit lines, agrees; the average co-efficient of determination (R^2 value) evaluated is 0.930 for the log law relationships and 0.803 for the power law relationships. The form of the log law

adopted for the model as shown in Equation 6.6, and the values of the co-efficients, Φ and Ψ, for specimens S1-S4, S7 and S8 are shown in Table 6.1. The longer specimens are not included in the table, all represented were 500 mm in length.

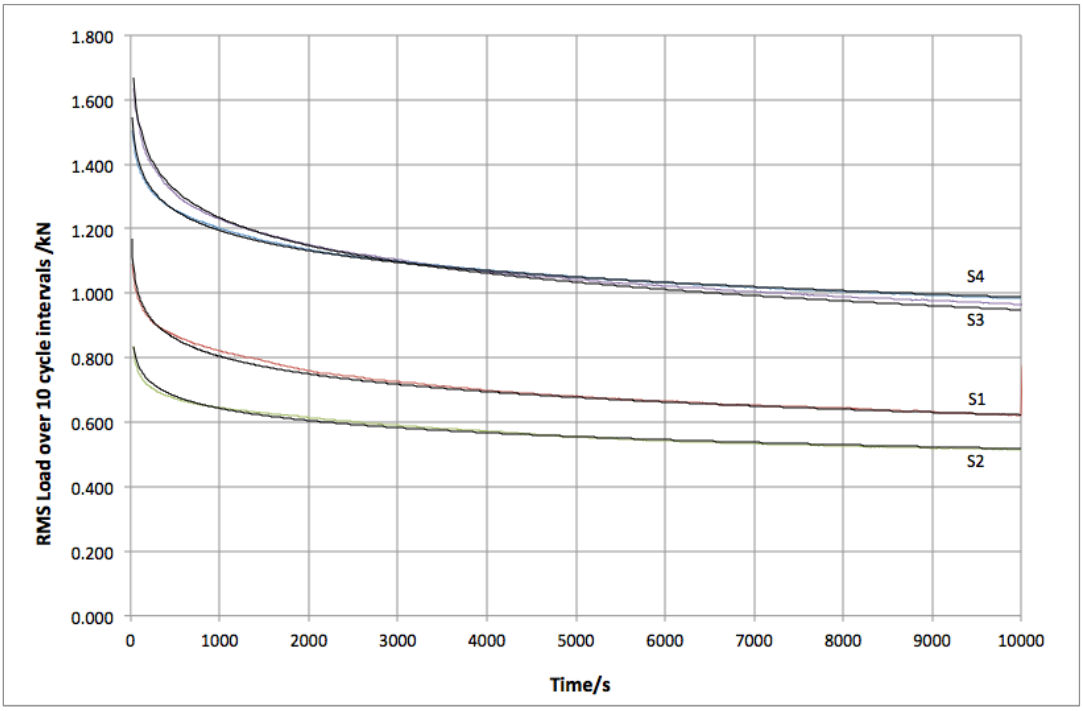

Figure 6.3 Curve fitting (in black) of RMS load profiles for S1-S4 using a log law relationship

$$RMS\ Load = \Phi - \Psi \ln(t) \tag{6.6}$$

Table 6.1 Φ and Ψ values, for specimens S1-S4, S7 and S8

Specimen	Ψ	Φ
S1	0.079	1.350
S2	0.054	1.018
S3	0.124	2.091
S4	0.090	1.814
S7 and S8	0.001	0.349

Note: Φ is a constant relating to the imposed strain, and Ψ is the coefficient of stiffness degradation.

Testing reported in Chapter 5 has revealed the existence of a threshold for flexural fatigue loading, below which damage is not initiated. The RMS load profile for the specimens S7 and S8 can be represented alongside those where damage accumulated and the performance decayed. S1, S2, S7 and S8 were all pultruded elements of the smaller section size. S3 and S4 are the elements representing hypothetical connections of larger section size. They are represented separately in terms of Φ and Ψ values, in relation to maximum imposed transverse strain in Figure 6.4.

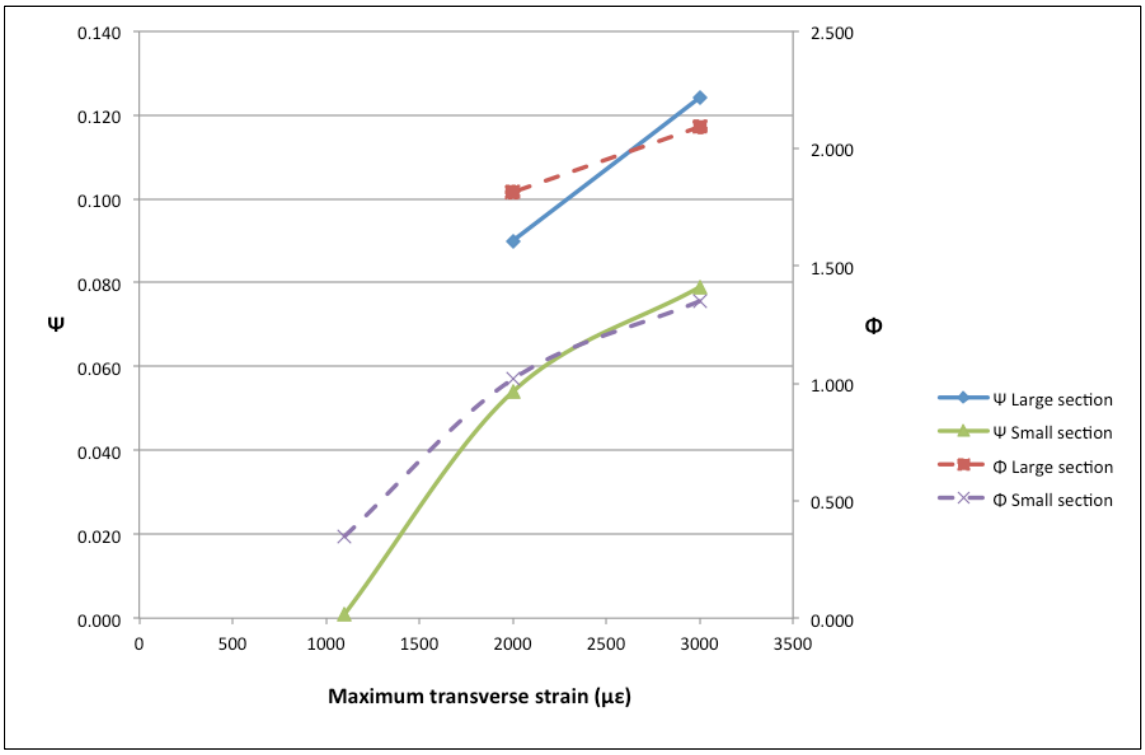

Figure 6.4 Φ and Ψ values, as a function of maximum imposed transverse strain

It is of interest whether an RMS profile for a specimen displaying no fatigue could have been produced at a higher imposed max transverse strain than the 1,100 με. In seeking to determine whether this is the case, the value Ψ, which signifies degradation in stiffness, or accumulation of damage, is examined in relation to the maximum imposed initial transverse strain. It can be seen that the green line plotted in Figure 6.4 signifies that Ψ is very sensitive to strain near the threshold of onset of damage, even under displacement control testing such as that undertaken. (The gradient of this line is much steeper near $\Psi = 0$.) The implication of this finding is that though a damage threshold exists, if exceeded, the rate at which damage propagates is very sensitive to the loading

parameters. Therefore, whilst a certain amount of damage over 10,000 cycle fatigue programme would be deemed acceptable, it is recommended that connection components are designed to retain full stiffness. There is no evidence to suggest a zero damage fatigue programme could have been achieved with any greater maximum transvers strain than that applied (of 1,100 με). The larger section size would appear to possess the same kind of limit on damage initiation if the same trend were observed. (Denoted by the blue line in Figure 6.4.)

It can also be observed in Figure 6.4 that Φ and Ψ values appear to vary with strain in the same manner. Figure 6.5 reveals, by inspection of the smaller section size denoted by the red line plot, that Ψ varies linearly with Φ. It would appear for the larger section that a Φ value of 1.2 would correlate to the threshold of damage initiation. This implies a larger state of stress and strain would be permitted by the larger sections tested. What is important however is that a threshold for damage onset does exist and can be established.

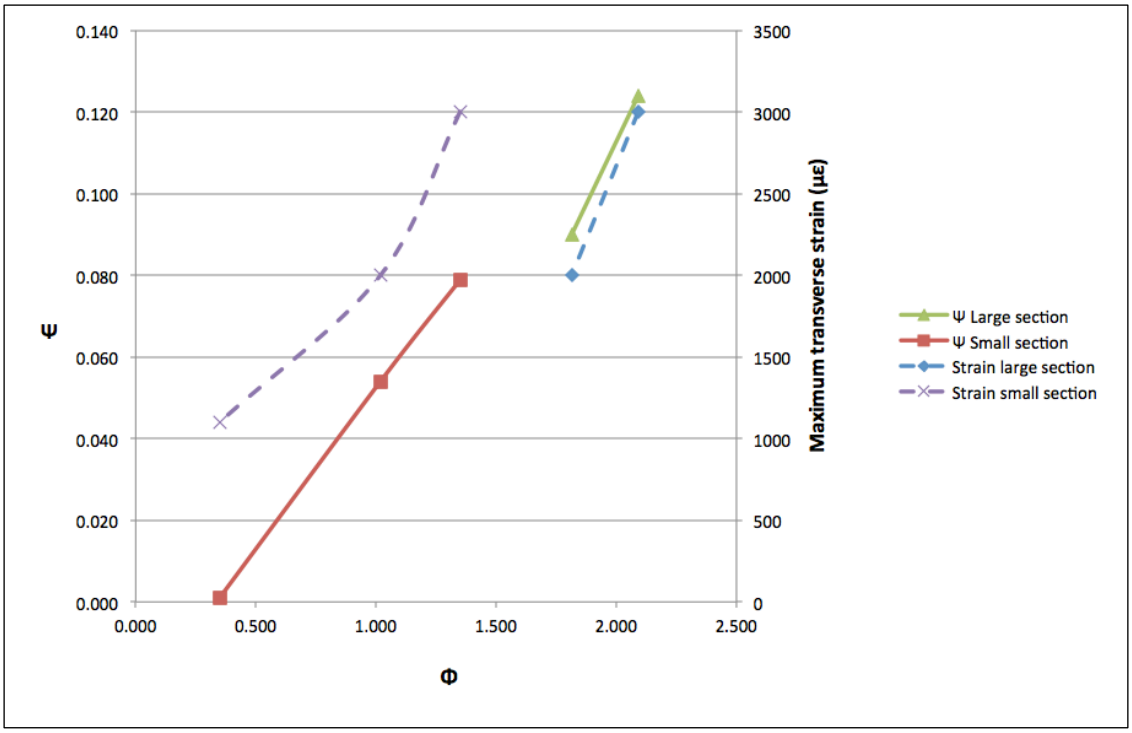

Figure 6.5 Ψ and maximum imposed transverse strain, as a function of Φ

The increased sensitivity of damage accumulation at strains near the onset of damage portrayed in Figure 6.4 is most likely attributed to the torsion in the pultruded element. El-Assal and Khashaba (2006) demonstrated a lower fatigue strength at failure where torsion was present, but also a very high sensitivity of fatigue life to the stress amplitude. See Figure 6.6.

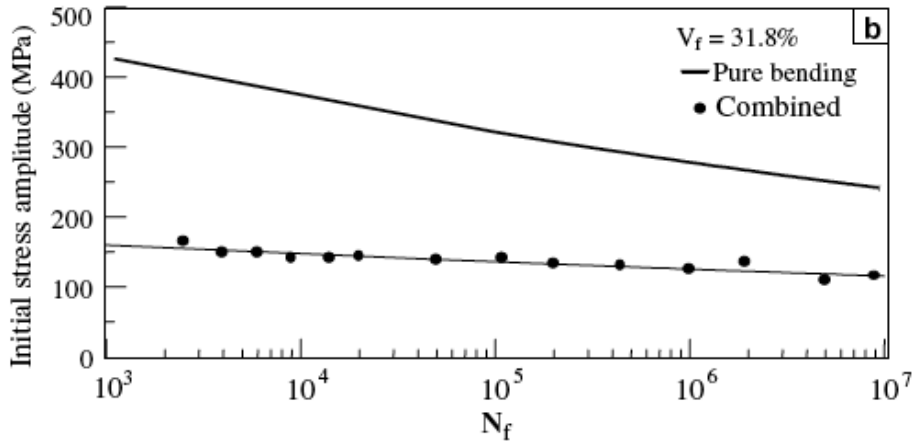

Figure 6.6 Initial stress amplitude for number of cycles to failure, for pure flexure and combined with torsion. From El-Assal and Khashaba (2007)

The testing represented in Figure 6.6 was performed under displacement control. The high sensitivity of the fatigue performance to the initial stress amplitude is evidenced by the small gradient of the line plotted, which denotes testing in combined torsion and bending.

The work of Adam et al. (1986) that investigated and modelled residual strength in composite laminates has potential to be applied to pultrusions. It is understood on the outcome of the testing reported in Chapter 5 however that it cannot apply where torsion is present. Whilst different damage mechanisms and the varying associated rates are accounted for, mechanisms relating to torsion are not. The material response to torsion has been demonstrated to be of significant impact on the fatigue life, and the rate and threshold of initiation for accumulation of damage.

Considering the sensitivity of fatigue performance to the initial stress amplitude in a fatigue programme, as observed in the testing conducted (see Figure 6.4) and in the

work of others (El-Assal and Khashaba 2007) it is recommended that a suitable design material strength factor of safety should be applied to the max permissible transverse strain at connections. For the small section hypothetical components tested, it has been demonstrated that this limit is 1,100 με, and a factor of safety inline with that commonly used in relation to absolute failure should be applied.

6.4 Summary

Experimental findings reported in Chapter 5 have been examined in relation to the work of others explored in Subsection 2.6 to establish pertinent material characteristics and offer guidance on best design practice in connection design of polymeric facades.

Data describing the performance of connection specimens under fatigue loading programmes has been correlated to a form of continuous mathematical relationship. This has permitted investigation into the sensitivity of the fatigue performance observed in relation to specimen and loading parameters. With supporting data from coupon testing and reference to the work of others, guidance on attaining sensible design limits and factors of safety for connection design has been put forward. For instance Figure 6.4 has demonstrated the existence of a threshold for transverse strain, below which no loss of connection stiffness occurs, and Section 6.2 sets out how to appraise the influence of adjacent connections in a group.

It has been identified where a shortage of literature exists, and where testing undertaken could go further to yield further useful outputs.

7 Conclusions and further work

7.1 Introduction

To permit adoption of polymeric façades as a retrofit concept, and realize the potential benefits, this thesis has furthered understanding in the key areas necessary to address a shortfall in industry required design knowledge. Initial review of topics associated with material selection and industry and manufacturing practices, and the implications of these practices, revealed the most effective forms and methods by which polymeric facades would see future application.

Development of hypothetical prototypes revealed critical issues that showed potential to greatly benefit from a programme of research. This approach also provided illustrative guidance through production of a design process flowchart of reasoning and considerations that summarises the research outputs of the review.

The implications of material selection and retrofit concept have been assessed, and the influence on attributes of building function, whole life performance, end of life options, and embodied carbon are recognized. The two critical areas reviewed in greater technical detail are durability and fatigue performance of connections in polymeric facades. Through a review of existing literature pertaining to prior relevant research in these areas, case study analysis, and laboratory testing campaigns, significant findings that fulfil both a requirement of knowledge in the construction industry, and a furthering of understanding in the field within the academic community have been attained. These research outputs are set out below together with the associated impact for each. Limitations of the study and recommendations for further work are outlined along with the benefits and motivations for its undertaking.

7.2 Research findings and implications

Case studies employing the testing of naturally aged GFRP have provided a means to assess the durability attributes of the material, and to critique models and predictions for the degradation of mechanical properties reported in literature. Characteristics and phenomena encountered through testing that were deemed to be of importance to

whole-life performance have been investigated through extended laboratory investigation.

- The tensile strength of pultruded naturally aged GFRP has shown not to reduce (or reduce by only 0.65%) over 17 years where natural exposure does not include UV irradiation.
- Where UV irradiation does occur as part of natural environmental exposure the tensile strength has shown to reduce by 13.1% over 17 years.
- Studies that have made ageing predictions based on accelerated ageing techniques and the Arrhenius relationship over-predict the degree of degradation with time. In the case examined, the over-prediction in reduction of strength is by 30% of initial strength, or even more, dependent on whether regain of mechanical properties is observed by reconditioning of specimens.

Lack of confidence in the durability of GFRP is often cited as a barrier to acceptance for application within the construction industry. These findings verify the actual performance of the material, increasing confidence in whole life performance of polymeric facades. The findings also expose the degree of inaccuracy in existing predictive ageing models. The predictive ageing techniques have also been critiqued:

- Hydrothermal ageing has been shown to be most representative of natural ageing at cooler water temperatures ($20^{o}C$).
- Accelerated ageing procedures that incorporate reconditioning, to permit regain in mechanical properties, are more appropriate.
- Accelerated ageing procedures that incorporate synergistic effects of temperature variation, moisture exposure and UV exposure are more appropriate.
- UV is of significant detriment to the tensile strength retention of both naturally and artificially aged GFRP.

The research contribution towards improving the accuracy of accelerated techniques will have significant impact in providing quicker assessment of new GFRP forms and innovations, specifically, innovations in resin type. Some pertinent characteristics of

naturally aged material have been identified. A means to quantify the behaviour exhibited, which is vital in assessing the implication of the material quality with ageing, has been developed.

- Hardening of the resin component of the GFRP has been identified as a function of ageing. The observed mechanical effects of this phenomenon have been established: a reduced limit of brittle fracture in tension, and an increased stiffness of the resin component, up until this critical strain is reached.
- Accelerated ageing techniques involving immersion in hydrothermal baths are known to increase resin plasticity. Testing of naturally aged material has shown this not to be representative. The physical mechanisms of degradation do not match.
- A procedure to quantify the extent of polymer hardening has been developed and applied as an analytical tool.

The plasticity of the polymer matrix is key in ensuring good durability of the composite material. The role in fibre protection means that degradation can accelerate once the polymer integrity is compromised. The hardening exhibited by naturally aged material is a mechanism of degradation as important as tensile strength to the whole life performance profile of polymeric façade material.

- The addition of a protective gel coat to the external surface of a façade panel has been shown to completely prevent hardening of the polymer matrix composite component during a natural ageing in service of 30 years.
- A gel coat has shown to retain mechanical properties of an outer GFRP structural skin such that the performance matches that of internal sandwich skin material after 30 years natural ageing.

Gel coats see regular application in GFRP elements fabricated by hand lay-up technique. The benefits established relating to enhanced durability, together with the potential improvements to aesthetics, justifies extending the practice to application on pultruded façade elements.

The long-term mechanical performance of GFRP elements that has been investigated within this thesis, was identified as a critical issue through a scoping exercise, drawing on review of industry, facades and manufacturing practices. It is fitting that the combined approach, researching fatigue in tandem with long-term environmental performance, or, durability, has tackled the key issues relating to whole life performance of polymeric facades.

It has been demonstrated that pultrusions from different manufacturers possess markedly different characteristics in failure and damage accumulation through fatigue loading. Mechanical testing has been devised and implemented to yield vital information about pultruded connections:

- At a maximum transverse strain of 1,100 με full connection specimen stiffness was retained after a 100,000-cycle fatigue programme.
- Specimens tested to fatigue loading parameters of high stress and strain (S1-S4) have demonstrated how the stiffness, or performance, of a connection component diminishes over 10,000 cycles.
- Testing has shown that though a threshold of damage accumulation does exist for transverse strain in fatigue loading of connections, and for direct tension fatigue loading. The rate of damage accumulation, once the limit for transverse strain in connection components is exceeded, is very sensitive to the loading parameters, and the performance quickly diminishes with increasing maximum transverse strain.

The testing campaign has pioneered the use of the RMS (Route Mean Square) procedure to present the performance of connection specimens as a continuous function throughout programmes of fatigue testing. The stiffness can be represented over the whole range of displacements from the imposed waveform using this approach.

- The RMS strain profiles produced have revealed the nature of damage propagation. Specimens that suffered an initial amount of damage deteriorated further by cracks that perpendicularly bisected the direction of transverse strain. These cracks became progressively deeper, but not wider over the duration of

the fatigue-loading programme.

- The connection specimen response, in how the load is shared out along a connected panel edge has been measured. This behaviour is key to informing good design practice when considering cumulative action of adjacent connections on a façade panel.
- The onset of damage accumulation at maximum cyclic transverse strains lower than that expected from testing reported concerning purely flexural fatigue, has evidenced a strong influence of torsion on the connection performance.

The quantitative findings presented above relate to the specific design and fibre architecture of the pultrusions tested. The absolute values in the threshold of critical transverse strain determined will only be appropriate for these pultrusions. It is recommended however, that a factor of safety to be placed on the limit of max transverse strain in design, should be in line with that considered for ultimate failure though quasi-static loading on a façade, owing to the nature of the behaviour established through this testing campaign.

7.3 Recommendations for future research

Some recommended further work is identified to be of immediate benefit to investigation undertaken throughout this project, while other more general guidance is given on the most beneficial study in the areas concerned with the aims of the project.

- The amount of UV exposure that specimens are subjected to in accelerated ageing procedures should be quantified. Research investigating the influence of rate of UV application would form vital initial study towards improving the accuracy of artificial ageing to assess durability of polymer matrix composite materials.
- To further examine the influence of UV on naturally aged material, experiment adopting a control group where wetting and drying of the material is conducted without UV irradiation.
- Further research is required where mechanical properties concerning the serviceability of GFRP elements are assessed following accelerated ageing techniques. (i.e. flexural, tensile and compressive stiffness.)

- Investigation into the relative performance of pultrusions comprising different types of resin would be of immediate benefit to industry.

It has been observed that flexural tests capture degradation behaviour associated with the quality of the resin of pultruded GFRP elements. (This is why flexural tests have formed part of the procedure developed to quantify the limit of fracture of the resin.) Considering the importance of resin plasticity regarding material durability, further work investigating the stiffness by flexural and compressive response of pultruded GFRP following accelerated ageing procedures would address a shortage of existing literature.

- Correlating the limits of resin fracture, and the processes of quantifying resin hardening developed, to other more easily measured parameters would be of significant reward. By conducting study where the assessment of polymer hardening is undertaken as described in this thesis, but with determination of T_g and Rockwell hardness in tandem, appraisal of a polymer's ability to protect fibres will be greatly facilitated.

Several further specific activities have been noted throughout the testing undertaken that would form beneficial further research in the field of durability. Two broad topics are also the two most important however.

- Research that investigates the performance of GFRP aged under conditions of mechanical stress, as well as the environmental stress. I.e. combined actions.
- Investigation into natural ageing with well documented 'base case' data for mechanical properties, but also resin chromatic profile, Rockwell hardness and T_g would be extremely beneficial further research.

The lack of controls, or 'base case' data, has restricted the number of specific conclusions that can be drawn from the vast amount of testing conducted. (Comparing aged environmentally exposed material to aged protected material has achieved this to some extent.) Activities that could extend research in durability further immediately however, include:

- Performing SEM (scanning electron microscopy) and
- DMTA (dynamic mechanical thermal analysis) on material from the Second Severn Crossing Visitors' Centre panels, where significant variation in mechanical properties was identified.

To further verify the protective qualities of protective gel coats on GFRP, these measurements, taken on panels that did not have such protection could serve to demonstrate the enhancement they afford. Variation in T_g can also be correlated to known mechanical property degradation.

The largest limitation of the study undertaken towards addressing the long term mechanical performance of connections relates to correlating basic material properties to element, or connection, behaviour. The lack of literature, and limited extent of testing, concerning the performance of pultrusions in flexural fatigue loading is responsible. Where literature reporting this type of testing does exist, the R-value is nearly always zero, and negative R-values are not investigated. To profile GFRP material of differing fibre contents, through a campaign of fatigue testing where specimens were subjected to flexure and loading adhered to negative R-values, would facilitate this objective.

A specific instance where this type of testing would yield useful comparison is in comparing the 2D angle section response to the 3D connection angle section response. Fatigue loading of the 2D, plane stress state would permit comparison with connection behaviour, quantifying the influence of torsion.

7.4 Material meets application

By revealing and quantifying the significant long-term performance characteristics of GFRP pultrusions, and demonstrating how necessary design information can be obtained, application of advanced composites in façade retrofit can be realised to yield great benefits for the built environment.

8 References

1. Adam, T., Dickson, R.F., Jones, C.J., Reiter, H., and Harris, B. (1986). A Power Law Fatigue Damage Model For Fiber-Reinforced Plastic Laminates. *Proc. Inst. Mech. Eng. Part C-J. Eng. Mech. Eng. Sci*. *200*, 155-166.
2. ASTM (2007). ASTM D7028:07e1 Standard Test Method for Glass Transition Temperature (T_g) of Polymer Matrix Composites by Dynamic Mechanical Analysis (DMA). (American Society for Testing and Materials).
3. ASTM. ASTM D 2584 – 02 Standard Test Method for Ignition Loss of Cured Reinforced Resins. (American Society for Testing and Materials).
4. Bakis, C.E., Cosenza, E., Lesko, J., and Machida, A. (2002). Fiber-reinforced polymer composites for construction - state-of-the-art review. *J. Compos. Constr*. *6*, 73.
5. Bank, L.C. (1989). Flexural And Shear Moduli Of Full-Section Fiber Reinforced Plastic (Frp) Pultruded Beams. *Journal of Testing and Evaluation 17*, 40-45.
6. Bank, L.C. (2006). Composites for construction : structural design with FRP materials. Wiley. Chichester.
7. Berketis, K., and Tzetzis, D. (2009). Long-term water immersion ageing characteristics of GFRP composites. Journal of Materials Science *44*, 3578-3588.
8. Boinard, E., Pethrick, R.A., Dalzel-Job, J., and Macfarlane, C.J. (2000). Influence of resin chemistry on water uptake and environmental ageing in glass fibre reinforced composites-polyester and vinyl ester laminates. *Journal of Materials Science 35*, 1931-1937.
9. Brookes, A.J., and Meijs, M. (2008). Cladding of Buildings, 4th Edition, Oxon: Taylor & Francis.
10. BSi British Standard (1998). BS EN 2747 Glass Fibre reinfirced plastics. Tensile test. London: BSi Publications.
11. BSi British Standard (2005). BS EN ISO 15310:2005 Reinforced plastics. Determination of the inplane shear modulus by the plate twist method. London: BSi Publications.

12. BSi British Standard (2009). Plastics - determination of tensile properties. In Test conditions for unidirectional fibre-reinforced plastic composites. London: BSi Publications.
13. Busel, J.P. (2002). FRP composites industry challenges in developing new markets, Boca Raton: Crc Press-Taylor & Francis Group.
14. Cabral-Fonseca, S., Correia, J.R., Rodrigues, M.P., and Branco, F.A. (2012). Artificial Accelerated Ageing of GFRP Pultruded Profiles Made of Polyester and Vinylester Resins: Characterisation of Physical-Chemical and Mechanical Damage. *Strain 48*, 162-173.
15. Carra, G., and Carvelli, V. (2012). Ageing of pultruded GFRP composites for building constructions exposed to combined environmental agents. In *Duracosys 2012*.
16. Cartie, D.D., and Fleck, N.A. (2003). The effect of pin reinforcement upon the through-thickness compressive strength of foam-cored sandwich panels. *Compos. Sci. Technol. 63*, 2401-2409.
17. Chandrashekhara, K. (2001). Theory of plates. Universities press, India.
18. Chu, W., Wu, L.X., and Karbhari, V.M. (2004). Durability evaluation of moderate temperature cured E-glass/vinylester systems. *Composite Structures 66*, 367-376.
19. Colin, X., Mavel, A., Marais, C., and Verdu, J. (2005). Interaction between cracking and oxidation in organic matrix composites. *Journal of Composite Materials 39*, 1371-1389.
20. Compston, P., and Dexter, D. (2008). The effect of ultraviolet (UV) light postcuring on resin hardness and interlaminar shear strength of a glass-fibre/vinylester composite. *Journal of Materials Science 43*, 5017-5019.
21. Compston, P., Schiemer, J., and Cvetanovska, A. (2008). Mechanical properties and styrene emission levels of a UV-cured glass-fibre/vinylester composite. *Composite Structures 86*, 22-26.
22. Conroy, A., Halliwell, S., and Reynolds, T. (2006). Composite recycling in the construction industry. *Composites Part a-Applied Science and Manufacturing 37*, 1216-1222.
23. Correia, J.R., Cabral-Fonseca, S., Branco, F.A., Ferreira, J.G., Eusebio, M.I., and Rodrigues, M.P. (2006). Durability of pultruded glass-fiber-reinforced polyester profiles for structural applications. *Mechanics of Composite Materials*

42, 325-338.

24. CWCT (1996) University of Bath Centre for Window and Cladding Technology. Standard for curtain walling. *Guide to good practice for facades. Test methods for curtain walling*. Bath: University of Bath, Centre for Window and Cladding Technology.
25. Domone, P., and Illston, J. (2010). Construction materials: their nature and behaviour, Spons Architecture Price Book.
26. Easby, R.C., Feih, S., Konstantis, C., Delfa, G., Miano, V.U., Elmughrabi, A., Mouritz, A.P., and Gibson, A.G. (2007). Failure model for phenolic and polyester pultrusions under load in fire. *Plastics Rubber and Composites 36*, 379-388.
27. El-Assal, A.M., and Khashaba, U.A. (2007). Fatigue analysis of unidirectional GFRP composites under combined bending and torsional loads. *Composite Structures 79*, 599-605.
28. Elmahi, A., Berthelot, J.M., and Brillaud, J. (1995). Stiffness Reduction And Energy-Release Rate Of Cross-Ply Laminates During Fatigue Tests. *Composite Structures 30*, 123-130.
29. Franke, O., and Schurmann, H. (2010). Analysis of the interaction of adjacent layers of a GFRP-laminate under fatigue loading. *International Journal of Fatigue 32*, 54-59.
30. George, S.D., Dillman, S.H., and Spe, S.P.E. (2000). Recycled fiberglass composite as a reinforcing filler in post-consumer recycled HDPE plastic lumber, Lancaster: Technomic Publ Co Inc.
31. Goodship, V. (2010) Management, recycling and reuse of waste composites, Oxford: Woodhead Publishing ; Boca Raton.
32. Gu, P., and Asaro, R.J. (2005). Structural buckling of polymer matrix composites due to reduced stiffness from fire damage. *Composite Structures 69*, 65-75.
33. Halliwell, S. (2010). FRPs - The Environmental Agenda. *Adv. Struct. Eng. 13*, 783-791.
34. Hammond, G., and Jones, C. (2008). Inventory of carbon and energy. Bath.
35. Harris, B. (2003). Fatigue in composites: science and technology of the fatigue response of fibre-reinforced plastics. Woodhead Publishing.
36. Hart-Smith, L.J. (1998). Predictions of a generalized maximum-shear-stress

failure criterion for certain fibrous composite laminates. *Compos. Sci. Technol. 58*, 1179-1208.

37. Heffernan, P.J. (2008). Canadian federal interest in FRP. *Structural Engineering International.* 12(2), 99-101
38. HMGovernment (2010). Conservation of fuel and power L2b. In The Building Regulations 2000. London: NBS.
39. Karbhari, V.M., Chin, J.W., Hunston, D., Benmokrane, B., Juska, T., Morgan, R., Lesko, J.J., Sorathia, U., and Reynaud, D. (2003). Durability gap analysis for fiber-reinforced polymer composites in civil infrastructure. *J. Compos. Constr. 7*, 238-247.
40. Khashaba, U.A. (2003). Fatigue and reliability analysis of unidirectional GFRP composites under rotating bending loads. *Journal of Composite Materials 37*, 317-331.
41. Kim, J.-K., and Mai, Y.-W. (1998). Engineered interfaces in fiber reinforced composites. Elsevier Science.
42. Kotani, M., Yamamoto, Y., Shibata, Y., and Kawada, H. (2011). Strength Prediction Method for Unidirectional GFRP after Hydrothermal Ageing. *Advanced Composite Materials 20*, 519-535.
43. Lambert, J., Chambers, A.R., Sinclair, I., and Spearing, S.M. (2012). 3D damage characterisation and the role of voids in the fatigue of wind turbine blade materials. *Compos. Sci. Technol. 72*, 337-343.
44. Lee, J., Harris, B., Almond, D.P., and Hammett, F. (1997). Fibre composite fatigue-life determination. *Composites Part a-Applied Science and Manufacturing 28*, 5-15.
45. Lemaitre, J., and Desmorat, R. (2005). Engineering damage mechanics: ductile, creep, fatigue and brittle failures, (Springer).
46. Liao, K., Schultheisz, C.R., and Hunston, D.L. (1999). Effects of environmental ageing on the properties of pultruded GFRP. *Composites Part B: Engineering 30*, 485-493.
47. Litherland, K.L., Oakley, D.R., and Proctor, B.A. (1981). The Use Of Accelerated Ageing Procedures To Predict The Long-Term Strength Of Grc Composites. *Cem. Concr. Res. 11*, 455-466.
48. Long, D., Guiqiong, J., and Tao, H. (2008). Investigation of the effect of Z-pin reinforcement on the collapse of foam-cored sandwich panels. *J. Reinf. Plast.*

Compos. *27*, 1211-1224.

49. Manning, R. (2011). One building a minute. In *CIBSE National Conference*. (London).
50. Mansour, S.H. (2000). Polymeric composites containing alumina trihydrate and silica. *J. Elastomer Plast*. *32*, 248-264.
51. McCuaig, L., Reginato, L. and Soudki, K. (2010). GFRP retrofit for facades in a Toronto School. *Construction and building materials.* 22(2), 61-69.
52. Mottram, J.T. (2011). Does performance-based design with FRP components and structures provide any new benefits and challenges? *The Structural Engineer 89*.
53. Naruse, A., Nanno, H., Kurita, M., Inohara, H., and Fukami, T. (2002). Development of all water-blown polyisocyanurate foam system for metal-faced continuous sandwich panels. *J. Cell. Plast*. *38*, 385-401.
54. Petermann, J., and Plumtree, A. (2001). A unified fatigue failure criterion for unidirectional laminates. *Composites Part a-Applied Science and Manufacturing 32*, 107-118.
55. Phillips, K.J.H., Feldman, U., and Landi, E. (2008). Ultraviolet and X-ray Spectroscopy of the Solar Atmosphere. Cambridge Univ Pr.
56. Pickering, S. (2009). End of life options for composites. In *Improving sustainable construction with FRP*. Watford: BRE.
57. Pochiraju, K.V., Tandon, G.P., and Schoeppner, G.A. (2012). Long-term durability of polymeric matrix composites, New York: Springer.
58. Proctor, B.A., Oakley, D.R., and Litherland, K.L. (1982). Developments In The Assessment And Performance Of Grc Over 10 Years. *Composites 13*, 173-179.
59. Purnell, P., Cain, J., Van Itterbeeck, P., and Lesko, J. (2008). Service life modelling of fibre composites: A unified approach. *Compos. Sci. Technol*. *68*, 3330-3336.
60. Qiu, H.W., and Gu, H. (2011). Mechanical behaviors of glass/polyester composites after UV radiation. *Journal of Composite Materials 45*, 1939-1943.
61. Ramroth, W.T., Asaro, R.J., Zhu, B., and Krysl, P. (2006). Finite element modelling of fire degraded FRP composite panels using a rate dependent constitutive model. *Composites Part a-Applied Science and Manufacturing 37*, 1015-1023.
62. Reis, E.M., and Rizkalla, S.H. (2008). Material characteristics of 3-D FRP

sandwich panels. *Constr. Build. Mater. 22*, 1009-1018.

63. Robert, M. and Benmokrane, B. (2010). Effects of ageing on bond of GFRP bars embedded in concrete. *Cement and concrete composites.* Vol.32(6), 461-467.

64. Russo, S. (2001). Creep on GFRP structural shapes. *Composites in Construction*, 303-306.

65. Sa, M.F., Gomes, A.M., Correia, J.R., and Silvestre, N. (2011). Creep behavior of pultruded GFRP elements - Part 2: Analytical study. *Composite Structures 93*, 2409-2418.

66. Salvia, M., Fiore, L., Fournier, P., and Vincent, L. (1997). Flexural fatigue behaviour of UDGFRP experimental approach. *International Journal of Fatigue 19*, 253-262.

67. Salvia, M., and Vincent, L. (1996). Modelling of flexural fatigue behaviour in UD glass-fibre-reinforced polymer. *Compos. Sci. Technol. 56*, 797-802.

68. Sasuga, T., and Hagiwara, M. (1987). Radiation Deterioration Of Several Aromatic Polymers Under Oxidative Conditions. *Polymer 28*, 1915-1921.

69. Schmidt, F., Rheinfurth, M., Horst, P., and Busse, G. (2012). Multiaxial fatigue behaviour of GFRP with evenly distributed or accumulated voids monitored by various NDT methodologies. *International Journal of Fatigue 43*, 207-216.

70. Sriramula, S., and Chryssanthopoulos, M.K. (2009). Probabilistic Models for Spatially Varying Mechanical Properties of In-Service GFRP Cladding Panels. J. *Compos. Constr. 13*, 159-167.

71. Strongwell (2009). FRP Specifications. Volume 2010.

72. Strongwell (2010). Composolite fibreglass building panel system. Volume 2010.

73. Szokolay, S.V. (2008). Introduction to architectural science: the basis of sustainable design. Architectural Press.

74. Talreja, R. (1981). Fatigue Of Composite-Materials - Damage Mechanisms And Fatigue-Life Diagrams. *Proc. R. Soc. London Ser. A-Math. Phys. Eng. Sci. 378*, 461-475.

75. Tawfik, S.Y., Asaad, J.N., and Sabaa, M.W. (2004). Studies on Polymeric Composites Containing Alumina Trihydrate and Aswan Clay Fillers. *Polymer-Plastics Technology and Engineering 43*, 57-79.

76. Thomason, J., and Vlug, M. (1996). Influence of fibre length and concentration on the properties of glass fibre-reinforced polypropylene: 1. Tensile and flexural

modulus. *Composites Part A: Applied science and manufacturing 27*, 477-484.

77. Thomason, J., Vlug, M., Schipper, G., and Krikor, H. (1996). Influence of fibre length and concentration on the properties of glass fibre-reinforced polypropylene: Part 3. Strength and strain at failure. *Composites Part A: Applied science and manufacturing 27*, 1075-1084.
78. Tolf, G., and Clarin, P. (1984). Comparison between flexural and tensile modulus of fiber composites. *Fibre Science & Technology 21*, 319-326.
79. Tong, J. (2001). Three stages of fatigue crack growth in GFRP composite laminates. *J. Eng. Mater. Technol.-Trans*. ASME *123*, 139-143.
80. Tong, J. (2002). Characteristics of fatigue crack growth in GFRP laminates. *International Journal of Fatigue 24*, 291-297.
81. Tsoi, S. (2010). Design of modern days multi-media facade. In *Advanced facade engineering and technology*, A. Lee, ed. (Hong Kong: Hong Kong Institute of Steel Construction), pp. 69-81.
82. Turvey, G.J. (2011). Experimental evaluation of bolt pull-through in pultruded glass-fibre-reinforced polymer plate. *Proceedings of the Institution of Civil Engineers-Structures and Buildings 164*, 307-319.
83. Turvey, G.J., and Cooper, C. (2004). Review of tests on bolted joints between pultruded GRP profiles. *Proceedings of the Institution of Civil Engineers-Structures and Buildings 157*, 211-233.
84. Turvey, G.J., and Wang, P. (2008). An FE analysis of the stresses in pultruded GRP single-bolt tension joints and their implications for joint design. *Computers & Structures 86*, 1014-1021.
85. Turvey, G.J., and Zhang, Y. (2007). Opening mode failure of pultruded GRP angle leg junctions. *In International conference for advanced composites in construction - ACIC 2007*, Y.p. services, ed. (Bath: York Publishing Services), pp. 389-396.
86. Vaughan, J.G., Lackey, E., Hutchcraft, E., Bennett, L., and Gordon, R.K. (2006). Some Effects of Mineral Fillers on the Electrical Characteristics of Pultruded Composites. *Composites*, 1.
87. VishayPrecisionGroup (2008). Technical Note 512-1. In Plane-Shear Measurement with Strain Gauges. Toronto: Inter Technology.
88. Wang, Y.Y., Meng, J.Y., Zhao, Q., and Qi, S.H. (2010). Accelerated Ageing Tests for Evaluations of a Durability Performance of Glass-fiber Reinforcement

Polyester Composites. *J. Mater. Sci. Technol. 26*, 572-576.

89. Wu, H.C., and Yan, A. (2011). Time-dependent deterioration of FRP bridge deck under freeze/thaw conditions. *Composites Part B-Engineering 42*, 1226-1232.

90. Yang, J.N., Lee, L.J., and Sheu, D.Y. (1992). Modulus Reduction And Fatigue Damage Of Matrix Dominated Composite Laminates. *Composite Structures 21*, 91-100.

91. Ye, B.S., Svenson, A.L., and Bank, L.C. (1995). Mass And Volume Fraction Properties Of Pultruded Glass-Fiber-Reinforced Composites. *Composites 26*, 725-731.

9 Appendices

9.1 Appendix A: Response of angle sections to monotonic loading in a plane stress state

The flexural response of the angle section connection arrangements, for which the testing methodology is described in Subsection 5.2.3, relies on a contribution from the specimen in three dimensions. Immediately beneath the load the material could be considered to be acting in a plane stress. However the regions either side of this are contributing to the loads resistance by transferring shear torsionally to the central, loaded region. (The torsional shear originates from the diminishing 2D flexural moment response as the distance from the load increases.) The strain gauge locations described in Subsection 5.2.3 record this, though to understand the 3D response more fully, the plane stress 2D response to monotonic loading can be established.

9.1.1 Introduction

In a plane stress state of loading, short lengths of pultruded GFRP angle section have been tested in flexure to reveal the ultimate strength of the fabricated element in opening mode failure. Post failure behaviour has also been demonstrated. The brittle manner of fracture, with little residual strength does not match the behaviour exhibited in testing of angles by Turvey and Zhang (2007), which is shown by the plot in Figure 9.1. This demonstrates the extent to which manufacturing variability effects measured mechanical properties of different pultrusion designs.

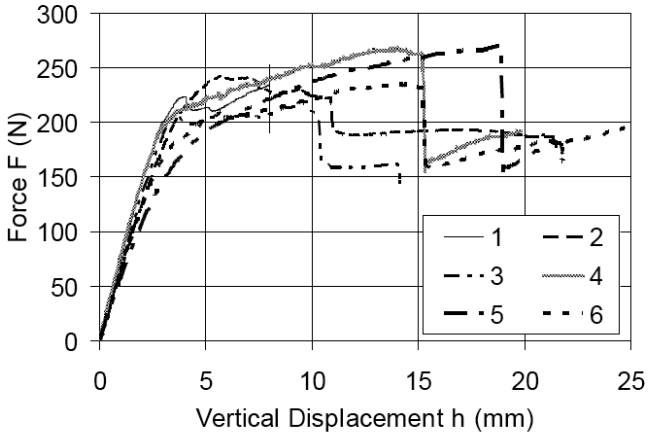

Figure 9.1 Force-displacement plots for 6 identical equal angle sections in plane-stress prying set-up for opening mode failure from Turvey and Zhang (2007)

9.1.2 Methodology

The testing reported by Turvey and Zhang (2007) adopted the use of a novel rig to impart a frictionless prying action on the specimen and measure the spread of the leg elements in tandem. The laboratory test set-up employed in this study however, and shown in Figure 9.2, used a Teflon sheet and lubricating spray to minimise friction effects. The displacement behavior was monitored only by the vertical displacement, or stroke, as recorded by the test rig's built in transducer. In order to ensure accurate stress interpretation of the load deflection data, theory considering the large angle deflections was established to determine the state of stress throughout the loading schemes implemented.

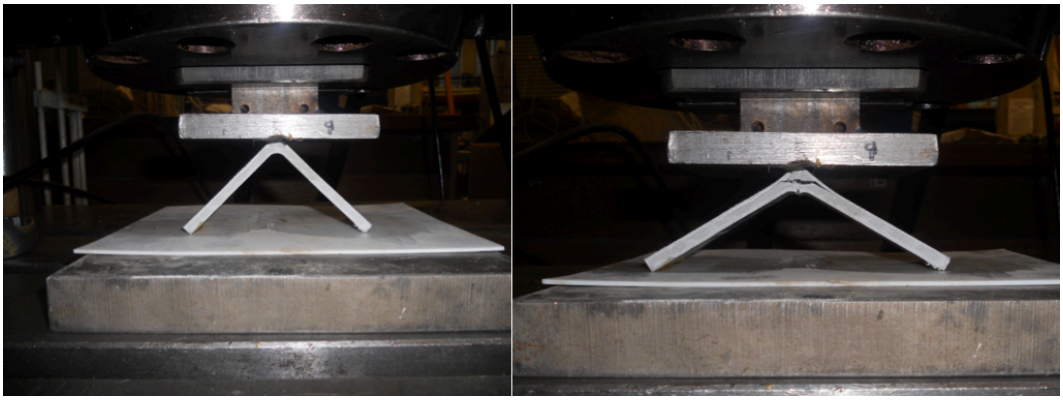

Figure 9.2 Illustration of laboratory test set-up for monotonic loading of short angle section

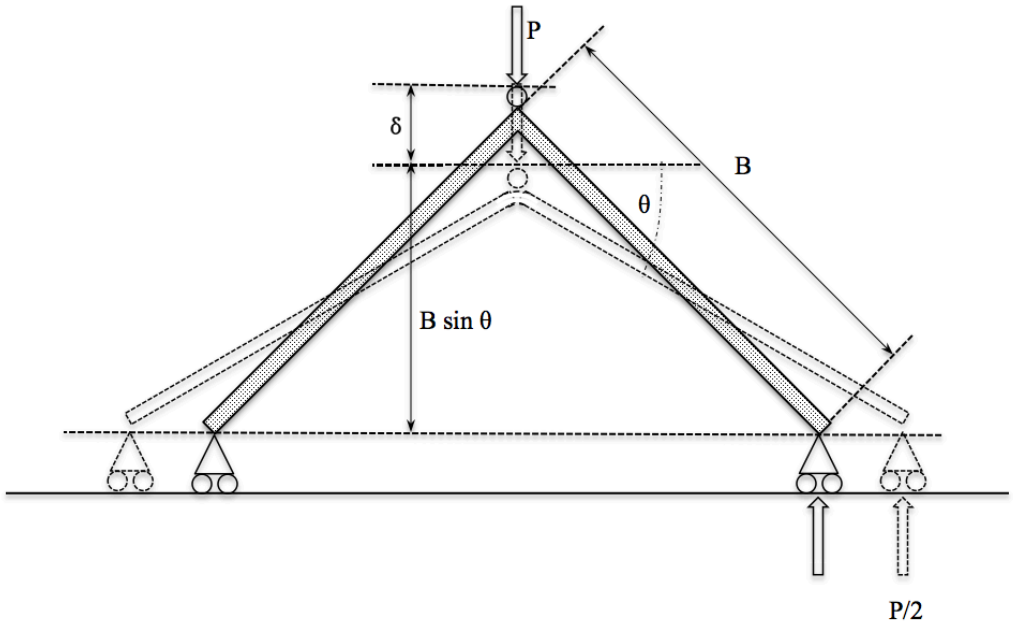

Figure 9.3 Schematic representation of critical stress derivation at angle apex

The experimental method adopted for use is illustrated in Figure 9.2. Figure 9.3 specifies variables used in derivation of the critical moment and stress at the root of the angle section. The dimension of these sections in the third (prismatic) dimension was 50 mm.

The moment at the apex (angle root), M can be expressed:

$$M = B\cos\theta \cdot \left(\frac{P}{2}\right) \tag{9.1}$$

where B is the leg length of the equal angle, and P is the applied load from the test rig in compression. θ is the varying angle the leg element of the section makes with the horizontal (which is 45^{o} when the load, P and displacement, δ are zero). By including the angle θ, as a variable, the deformed geometry is accounted for in the assessment of the moment at the root. θ can be expressed in terms of the imposed displacement, so Equation 9.1 becomes:

$$M = \left(\frac{PB}{2}\right)\cos\left[\sin^{-1}\left(\frac{1}{\sqrt{2}} - \frac{\delta}{B}\right)\right] \tag{9.2}$$

The maximum transverse bending stress at the root location can be determined, as shown in Equation 9.3, where l is the length of angle section and t is the leg element thickness.

$$\sigma = \left(\frac{3PB}{lt^2}\right)\cos\left[\sin^{-1}\left(\frac{1}{\sqrt{2}} - \frac{\delta}{B}\right)\right] \tag{9.3}$$

It should be noted that at the precise root location the element thickness is greater than t, however evaluating the stress at the innermost point, where the thickness is still t, and the tensile stress will sweep round into the root, was deemed to be an appropriate solution.

Monotonic displacement control testing to examine the quasi-static state of stress at failure was conducted under displacement control at 2 mm/min.

9.1.3 Results

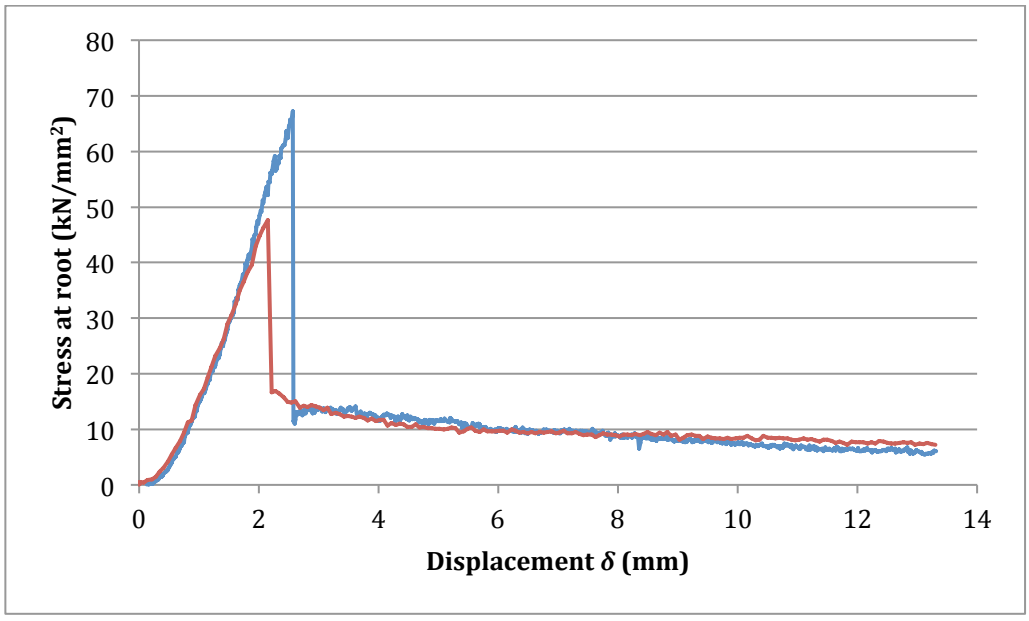

Figure 9.4 Stress-deflection plot for two identical equal angle sections in plane-stress prying set-up for opening mode failure

When tested in the rig shown in Figure 9.2, it can be seen from the plot in Figure 9.4 that the two identical specimens exhibited an almost linear elastic response up to a point at which the specimens failed in a brittle fashion, retaining very little residual strength. The strength of the two identical specimens varied by 28%. Using the tensile elastic modulus calculated by coupon testing reported above, the maximum material strains at failure were 6060 με and 4290 με for the two specimens.

The element behaviour observed in this test possess markedly different qualities to similar tests reported by Turvey and Zhang (2007), who found that there was a close agreement in maximum strength determined for each of the 18 tests conducted, in 3 sets of different lengths of the angle section adopted. Also in contrast to the results illustrated by the plot in Figure 9.4, it was reported that that the specimen response was linear elastic up to 60% of the ultimate failure load, where the response softened. A much higher degree of toughness is signified by the results from Turvey and Zhang (2007) owing to a much higher residual strength.

9.1.4 Discussion

A high degree of variation is observed for the two equal angle specimens tested in prying action under plane stress conditions. This together with the low residual strength observed conflicts with the findings of others and highlights the sensitivity of performance of pultruded angles to the manufacturing variability between fabricators/pultruders. Linear elastic behaviour to failure of a specimen at 4290 με is notable in comparison to the damage initiated in connection specimens at strains below 3000 με. The stiffness enhancement brought about by the 3D action at connections reduced the strain limit of damage in monotonic linear loading ramps, though it is shown that a significant reserve of strength remains, that is not observed in the plane stress tests above which are linear elastic to failure.

The 2D plane stress behaviour portrayed in Figure 9.4 is notably dissimilar from the 3D properties of pultruded connections tested. The 3D stress pattern, associated with the hypothetical connection arrangement adopted for testing, reduces the threshold at which damage is initiated, in both monotonic linear ramps and cyclic loading.